



Implementation of Different Types of Meshfree Technique in Computational Solid Mechanics: A Comprehensive Review Across Nano, Micro, and Macro Scales

Zummurd Al Mahmoud¹ · Babak Safaei^{1,2} · Saeid Sahmani³ · Mohammed Asmael¹ · Muhammad Atif Shahzad⁴ · Qasim Zeeshan¹ · Zhaoye Qin⁵

Received: 6 June 2023 / Accepted: 25 August 2023 / Published online: 20 September 2023

© The Author(s) under exclusive licence to International Center for Numerical Methods in Engineering (CIMNE) 2023

Abstract

This work is considered as the first comprehensive review, that covers all types of meshfree method including the traditional or developed meshless techniques that have been implemented for the purpose of investigating static analysis (bending, stability) besides dynamic analysis (free vibration, force vibration and other types of dynamic behaviors) of linear and non-linear mechanical system. The secondary methods utilized together with the meshless methods are also highlighted such as; Hamilton's principle, first-order shear deformation theory, high-order shear deformation theory, Monte Carlo, local/nonlocal theories and others. Also, some computational mechanics approaches are briefly addressed. The basic fundamental equations of meshfree methods and the error analysis are presented. Various types of schematics and structure size are discussed. Else, the implementation of composite material in solid mechanics are concisely highlighted. As a key finding, in each unique schematic in specific scale, various implemented parameters like boundary conditions, thickness to length ratio (t/l), as well as the aspect ratio have different impacts on the mechanical performance in both static and dynamic analysis. Additionally, as each meshfree method is considered unique by itself and has its own developed mathematical model, each method has different application and numerical problems to solve. Galerkin, reproducing kernel particle method, moving least square are the most common meshfree. Based on the literature, many studies mainly show interest in investigating the piezoelectric and diverse distribution of carbon nanotubes, and some in fictional graded material in different structures. This review is recommended for researchers interested in solid mechanics analysis at various scales using meshfree techniques.

✉ Babak Safaei
babak.safaei@emu.edu.tr

✉ Qasim Zeeshan
qasim.zeeshan@emu.edu.tr

✉ Zhaoye Qin
qinzy@mail.tsinghua.edu.cn

¹ Department of Mechanical Engineering,
Eastern Mediterranean University, Famagusta,
North Cyprus via Mersin 10, Turkey

² Department of Mechanical Engineering Science, University
of Johannesburg, Johannesburg 2006, Gauteng, South Africa

³ School of Science and Technology, The University
of Georgia, 0171 Tbilisi, Georgia

⁴ Department of Industrial Engineering, Faculty
of Engineering, King Abdulaziz University, Jeddah,
Saudi Arabia

⁵ State Key Laboratory of Tribology, Department
of Mechanical Engineering, Tsinghua University, Beijing,
China

1 Introduction

1.1 Meshless/Meshfree

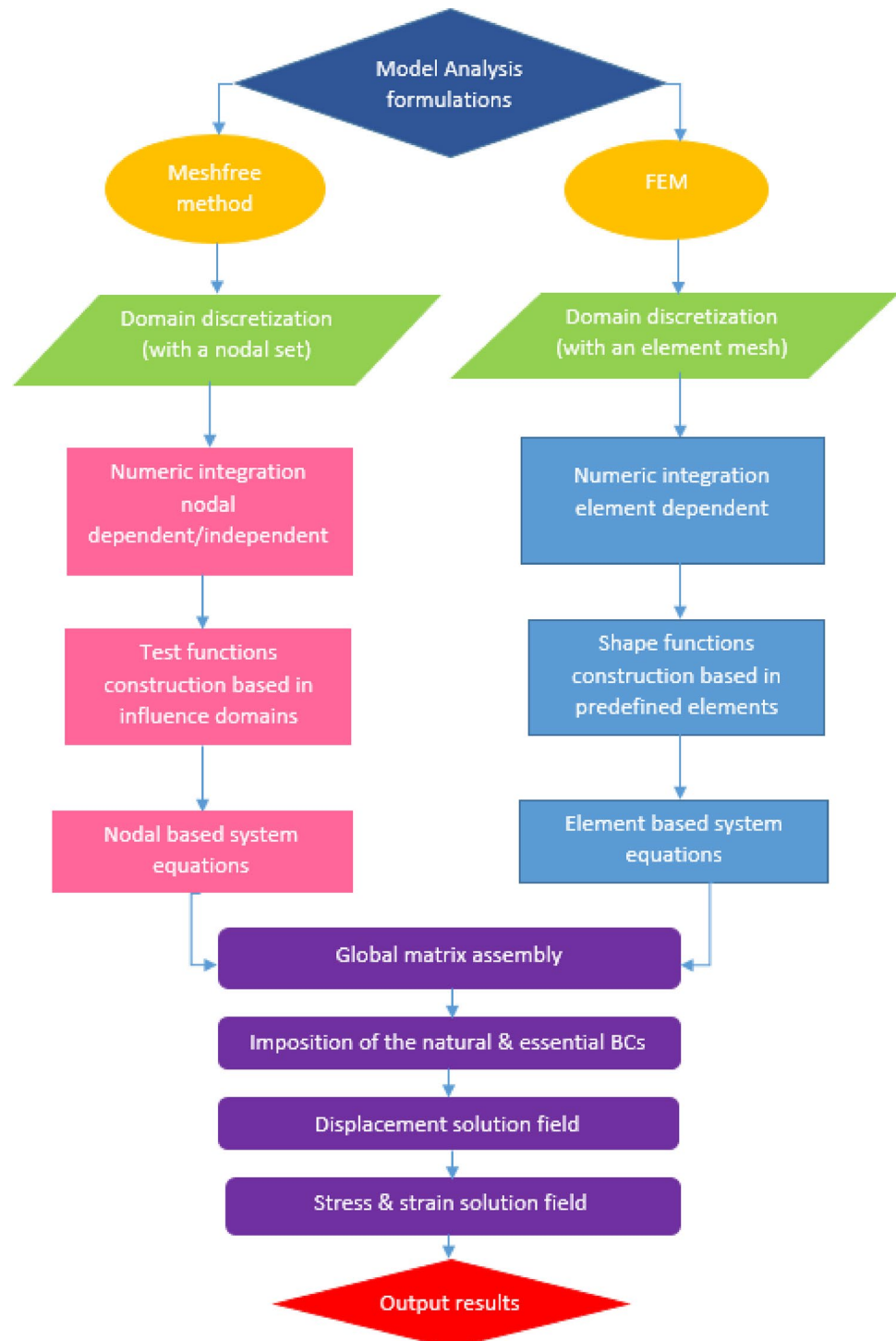
Meshless/Meshfree methods are defined as a group of numerical algorithms [1]. While they differ in how shape and test functions are created, they all possess the capacity to ease the finite element methods (FEMs) strict connectivity constraints. Belytschko [2] defined meshfree as a series of numerical techniques that are intended to overcome the re-meshing issue in many FEM simulations. In another words, it depends on the interaction of each single node with its neighbour nodes. Qiao et al. [3] presented another definition of meshfree methods as numerical methods that have absence of fixed connectivity between the discretization nodes. These methods are preferable to use in simulating impact failure, fragmentation and penetration as well as in continuum fluids and solids. Over the last two or three decades, a number of these strategies have emerged and

reached a highly developed stage. Meshfree approaches avoid employing elements to generate the approximation, in contrast to the FEM [4]. Since the superiority of the approximation is considered to be influenced by the geometric placement of nodes as well as the domain influence of each node, the placement of the nodes is rather arbitrary. Compared to the FEM, the connectivity between the nodes

that is determined by how these zones of influence overlap can be designed more freely. Figure 1 illustrates the difference between FEM analysis processing and the meshfree method analysis processing.

The basic meshfree methods and some types of developed meshfree method are illustrates in Fig. 2. Generally speaking, the most common meshfree approaches that

Fig. 1 A comparison between the formulation process of FEM and meshfree



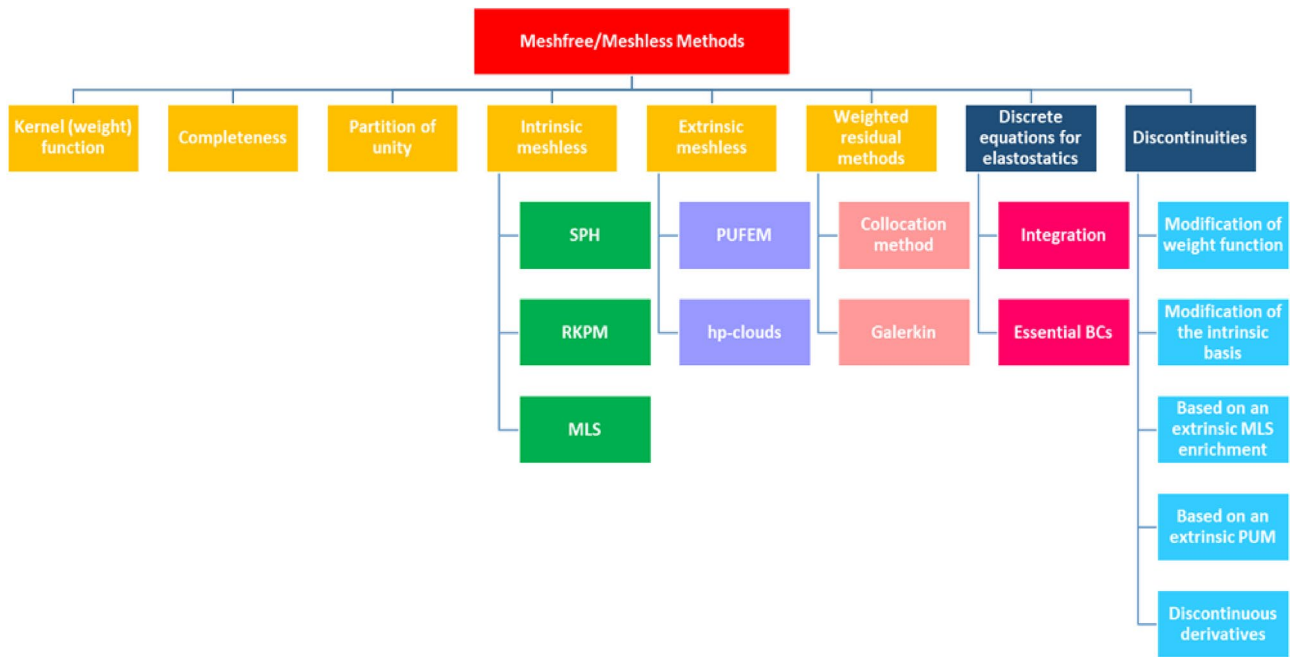


Fig. 2 Classification of meshfree methods: elementary traditional types of meshfree methods and some developed meshfree methods

have wide application are; Galerkin method [5, 6] which include element free Galerkin (EFG) as well, the particle difference method (PDM) which is categorized as a robust form meshfree technique and discretizes the governing equations (GEs) [7], Hp-meshless cloud method [8, 9], the moving least square method (MLS), which has been combined with the EFG technique [10], the reproducing kernel particle method (RKPM) [11, 12] an example of RKPM shape function of the first derivative by a tri-linear polynomial basis for microstructure dynamic shear band is shown in Fig. 3 [13], the smoothed particle hydrodynamics method (SPH) [14, 15] which have been employed to analyze the laser fusion additive manufacturing process [16]. The same method has been used recently to analyze the grinding processes [17]. There are some advanced developed meshless approaches as shown in Fig. 4, such as; the meshfree local petrov–Galerkin method (MLPG) [18, 19] it has been employed to analyze the shear loading [20] and for elastic moduli analysis of the woven fabric composite [21], the partition of unity approach meshless method [22–24], the partition of unity finite element method (PUFEM), and the diffuse approximation method (DAM) which can be utilized to generate smooth estimation of functions known at certain sets of locations and, to estimate its derivatives accurately [25], the smoothed peridynamics (SPD) which was utilized for extremely large deformation and caking problems [26], Peridynamic (PD) based elastodynamic (Peri-elastodynamics) which is a nonlocal (NLC) meshless method and a scale

independent generalized method mainly applied to visualize the ultrasonic wave and the acoustics in a plate and in nanodevice [27].

An example of a schematic of sandwich structure nanocomposites plate reinforced with carbon nanotubes (CNTs) proposed to thermoelastic dynamic analysis by the MLS meshfree method is illustrates in Fig. 5 [28]. However, it is worth to mention that the MLS meshfree methodology have the potential to transfer the NLC variables model to a local model such as the densities of the geometrically necessary dislocations (GNDs) [29].

Out of all methods of meshfree theory, the SPH as well as the material point method (MPM) are considered as the most important methods. This is because they overcome the large mesh deformation also the requirement for remeshing that are frequent towards finite element (FE) models in the Lagrangian framework, and the challenges associated with tracing history of the material in the Eulerian formulation.

Owing to the higher order smoothness of the meshless form functions and the avoidance of mesh-dependence problems, it has been demonstrated that the employment of Galerkin based approaches can reduce the need for sensitivity filtering [30, 31]. The uniqueness of meshfree methods is that their foundation is based on particle hydrodynamics and gas dynamics, and instead of relying on mesh or lines, they use nodes particles or points [32]. The key benefit of using the meshfree methods is that the issue domain does not need to be meshed. The selection of shape functions is the primary and most crucial problem in meshless approaches

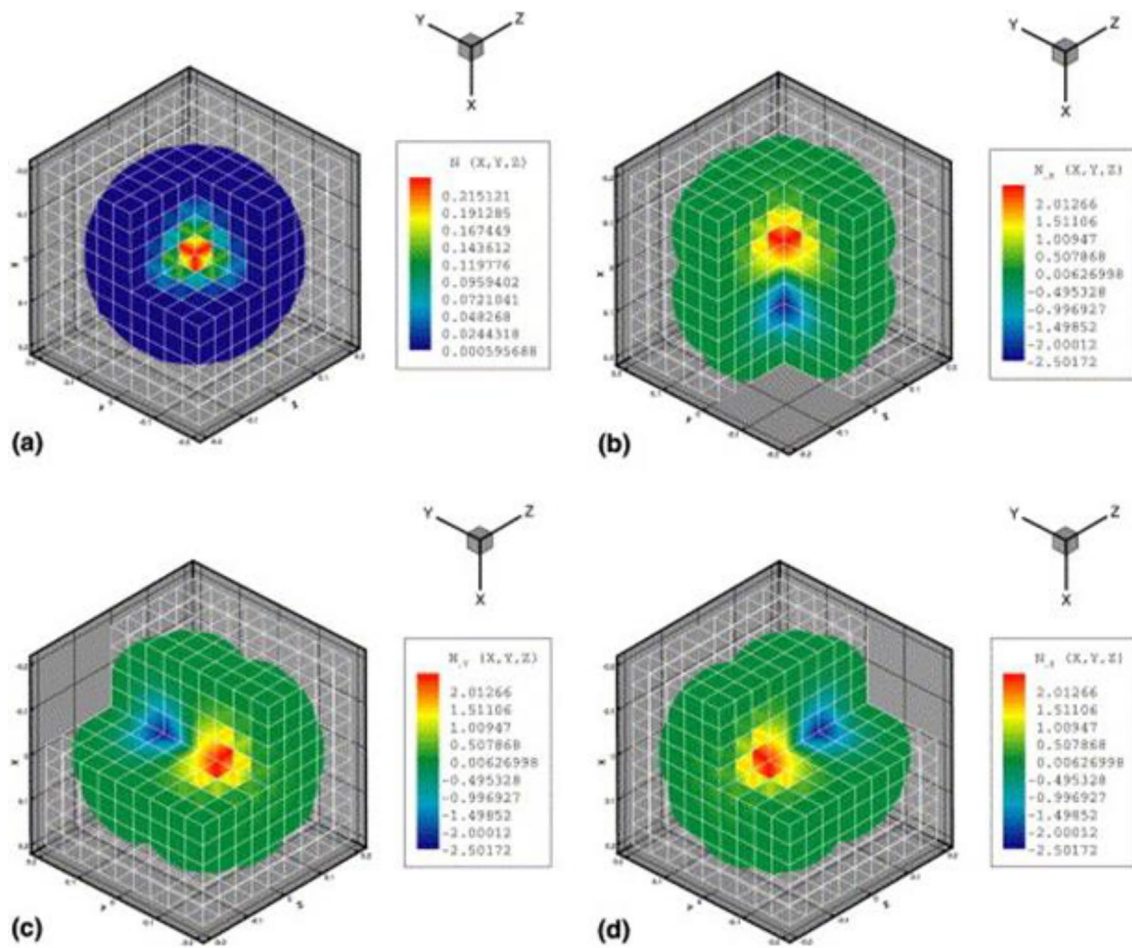


Fig. 3 A 3D of RKPM/meshfree shape function and its first derivatives generated by the polynomial basis (tri-linear) [13]

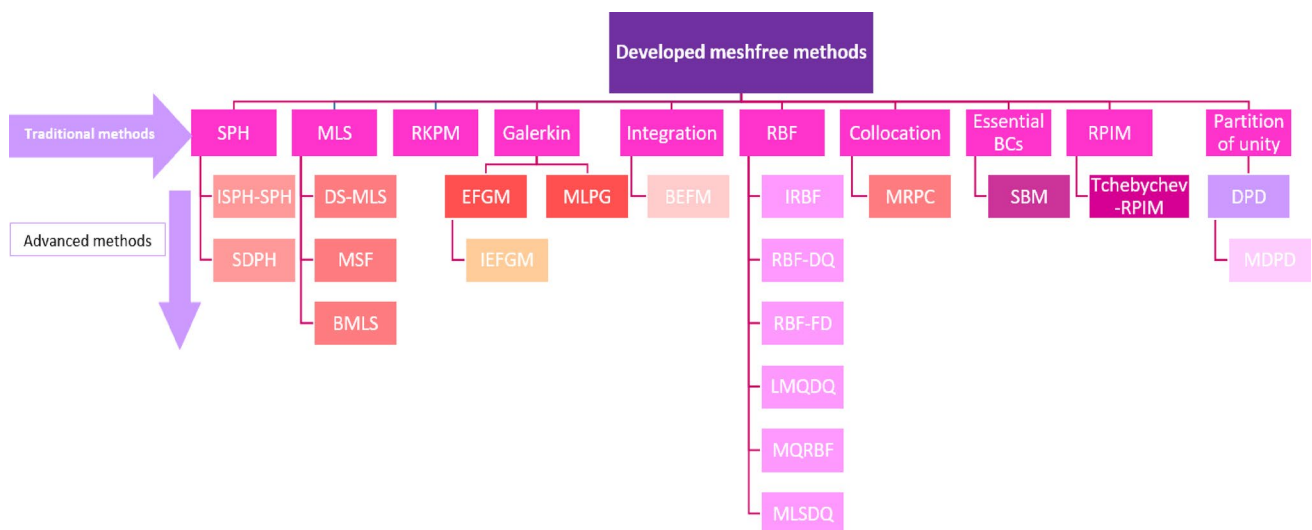


Fig. 4 Classification of Developed meshfree methods

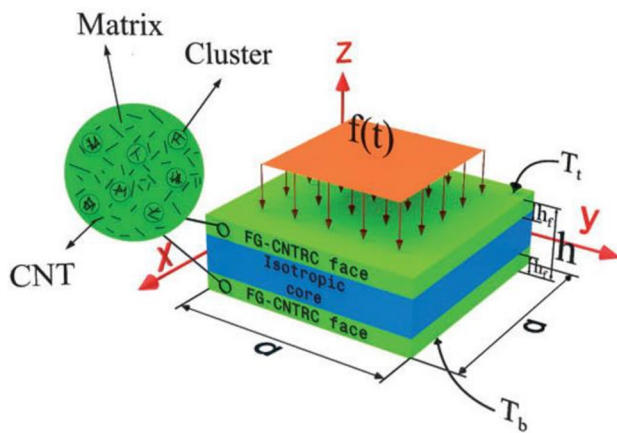


Fig. 5 The schematic of sandwich structure nanocomposites plate reinforced with CNTs and their clusters [28]

[19]. Due to the fact that most of the application of meshfree methods are in rational functions and the meshfree methods are based on Gauss quadrature, which considered as insufficient to accomplish an exact integration. Recently many studies worked on vibrational adaptively to develop the support domain size for meshless methods' shape functions. The importance of finding developed algorithms to enhance the efficiency of meshless methods is because the old techniques of meshes and other like-stabilized nodal integration may complicate the process to a bath way far off the theory of meshless.

The meshfree approach is most importantly applied in simulating plastic materials where a large deformation may occurs [33]. Additionally, 3D high complexity objects, cracks simulation, linear and nonlinear (NL) material behaviors (singularities/discontinuities), bending simulation, etc. The variety of methods in meshfree approaches have extensive applications. Ren [34] developed an explicit meshfree Galerkin formula to detect the ductile fractures throughout the finite inelastic deformation. This advanced implementation has these features: 1. Capable with thermal–mechanical coupling and stability in an adiabatic split algorithm, 2. Effective dynamics meshfree algorithm even in high speed impact, 3. Automated crack algorithm which provide the crack growth lifespan, and 4. Adopting modified forward Euler tangent algorithm for NL thermal–mechanical inelastic constitutive relation. The crack growth analysis by meshfree have been used quite often in research study as [6, 35–37]. Bui et al. [38] have developed meshfree methods to perform a transient dynamic analysis fracture variables of a functional graded crack. The novel method for the partition of unity extended meshless Galerkin method founded on moving kriging interpolation (MKI) was developed. Diverse kinds of correlation functions, including quartic polynomial, Gaussian, as well as truncated quartic polynomial, were used

to improve the MKI shape functions. The main enhancement is the removal of the correlation parameter effects that were frequently included in the MKI shape function. Lu et al. and Guan et al. [39, 40] employed the Galerkin technique for the purpose of simulating the plastic flow during the equal channel angular pressing technique (ECAP), in viscoplastic/rigid-plastic. The MPM [41] and the SPH [42] shows significant and reliability results by studying the ECAP. Furthermore, when comparing the straightforward hp-cloud technique to other meshless techniques, the fundamental boundary conditions (BCs) may be applied directly using the simple hp-cloud method since it has the Kronecker delta property [8]. Recently, the attention of researchers has been drawn to the radial point interpolation method (RPIM) and it is another meshless methodology similar to the EFG method, and have been utilized to solve various issues in the applied mechanics field [43]. For instance, Kazime et al. [44] have employed the RPIM method to accomplished an analysis for viscoplastic problem based on the Cartesian transformation method (CTM). Hu et al. [45] have performed the metal forming analysis by using the RPIM parallel point. A comprehensive review about mesh free methods which have been used in studying the fracture mechanics and cracks has been published recently [46]. Nguyen et al. [47] utilized the Galerkin radial point interpolation (GRPI) technique to investigate the crack propagation in the elastic solids. Additionally, Ha and Bobaru [48] examine the dynamic crack in brittle materials by using the meshfree PD theory. Guimatsia et al. [49] implemented the EFG method for the first time to analyze the delamination (interlaminar) and the interlaminar matrix microcracking in the composite laminates. Yaghoobi and Chorzepa [50] have performed a micropolar predynamic investigation of fracture analysis of a fiber reinforced concrete structure. Selim et al. [51] have employed Element-free IMLS-Ritz technique with the high-order shear deformation theory (HSDT), to perform a vibrational controller of functionally graded graphene nanoplates (FG-GNPs) with piezoelectric layers as presented in Fig. 6.

Recently, Behdinan et al. [52] established the MLS method to facilitate the governing thermal equation to examine the effects of graphene (Gr) and CNT on steady-state as well as transient heat transfer performances of the functionally graded (FG) nanocomposite axisymmetric cylinders under different BCs set. Furthermore, Abdollah and Boroomand [53] employed the Galerkin method to solve the problems in NLC integral models, and for inspecting the efficiency of the methods. Also, they presented some examples with smooth and non-smooth. However, Pan et al. [54] presented a review article about employing the meshfree methods in solution to image stresses of dislocations. Chen et al. [55] have published recently a review article about the developments in meshfree methods, its classes and their applications generally over the last two decade. Li and Liu

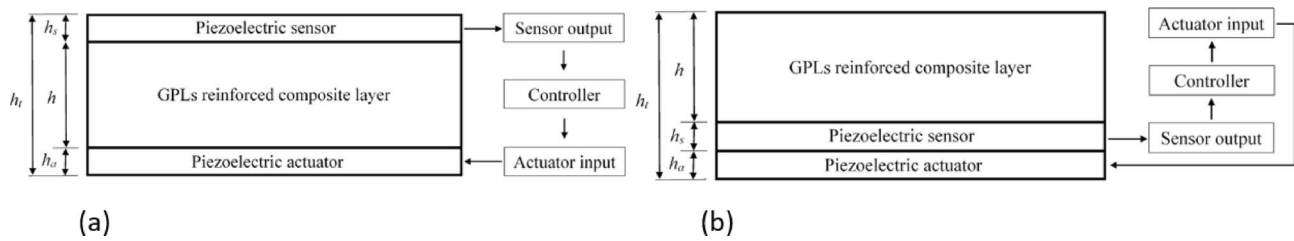


Fig. 6 The control process with 2 positions; **a** case 1 and **b** case 2 of piezoelectric sensor and actuator layers [51]

[56] have published a surveyed meshless particles methods. Also, the authors noted its role in the applied mechanics field. Also the review has covered three main methodologies and the nanoscale mechanism. A recent review paper which provides a methodological investigation into potential and the current meshless approaches for computing the partial differential equations (PDEs) that control solid mechanics difficulties has been published by Liu et al. [57]. It discusses the general phases of a node-based meshfree technique with displacements as the primary variables. Node-based interpolation methods, cell-based interpolation methods, function smoothing techniques, and MLS approximation methods are part of function approximation techniques. The special strain construction, direct differentiation, as well as the gradient smoothing, are all components of the gradient approximation. Strong-form (SF), weak form (WF), weak-strong-form (WSF), local weak form (LWF), as well as weakened weak form are all formulation approaches, a brief summary of SF, WF, WSF and LWF with a single example for each is illustrated in Fig. 7

A review focused on NL free and force vibration of shell structure and works done by meshless methods were discussed on that review [58]. Shapiro et al. [59] presented a

comprehensive discussion about CAD/CAE, highlighting the application and the classification of meshfree methods in CAD. Wu and Liu [60] presented an overview which highlights the meshfree method that were specifically applied to perform analyses for sandwich structure and laminated composites of the FG elastic/piezoelectric materials (FGEMs/FGPMs) shells as well as plates including various types of BCs. Liew et al. [61], published a review about meshfree methods that have been employed in laminated and functionally graded shells and plates specifically. Grag et al. [62] accomplished a comprehensive review which cover all theories and approaches such as; meshless, local NLC elasticity theories and etc. that have been implemented for the purpose of investigating various types of composites nanoscales structures. However, the recent development in the computational approaches that have been performed for investigating the dynamic behavior of complex structure for real time hybrid simulation (RTHS) have been studied by Betancur et al. [63]. In addition, the review highlighted that there is still a need for more studies which focused on the foremost challenges RTHS control theories such as; complex BCs, NL and uncertainties, computational efficiency as well as the multi hazard

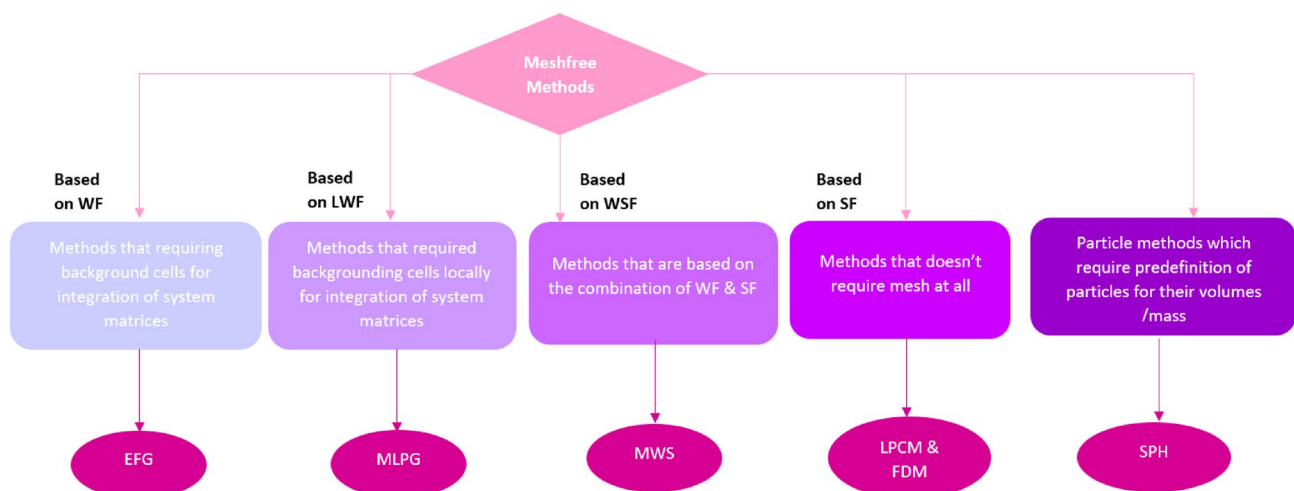


Fig. 7 A summary of comparison between WF, LWF, WSF and SF with a single example for each

engineering application. Gupta et al. [64] accomplished a comprehensive review which focused on the recent progresses in the isogeometric analysis (IGA), especially the NU rational B-splines (NURBS). Additionally a brief comparison between IGA, FEM, meshfree as well as the coupled meshfree with FEM methods has been addressed. Moreover, Gu et al. [65] performed a concurrent analysis technique for investigating the various deformation systems which needs the integration of material properties from nanoscopic to macroscopic dimensional. The radial basic function (RBF) interpolation has been employed for the purpose of determine the continuum subdomain. Where the molecular dynamic (MD) analysis was carried out for the atomic subdomain.

Meanwhile, this presented review is considered as the first of its type that covers the static analysis (bending and buckling) and dynamic analysis (free/forced vibration as well as other dynamic analysis) for all different types of structures and geometries in various scales (nano, micro, and macroscales), and summarized literature works. However, this review article is a valuable resource for researchers interested in the field of solid mechanics analysis at various scales using meshfree techniques, where the secondary methods utilized together with the meshless methods, numerical and analytical analysis are addressed.

Besides, different type of material were mentioned and the enhancement of composite distribution and the impact of various parameters on deformation, static and vibrational performance are discussed. The analyses which are considered in the scope of this comprehensive review are illustrated in Fig. 8.

1.2 Literature Methodology

The main database that has been used as in obtaining the articles in this literature review is Scopus database. The steps of selecting the articles to be studied are as followed:

As the first search cord "meshfree" OR "meshless" OR "mesh-free" OR "mesh free" has been used then AND (((("solid mechanics" OR "static analysis" OR "static" OR "dynamic analysis" OR "dynamic")) AND ("beam" OR "plate" OR "cylindrical" OR "shell" OR "sandwich" OR "cylinder"))) AND ("nano" OR "micro" OR "macro") as a search in the search cord. 573 documents emerged. Not all of the 573 documents are exactly into the scope of these review; so many some keywords were excluded. Owing to the fact that Scopus does not exclude the other alloys and metals from these search cord. The overall, documents were found by Scopus after exclude some other key words is 135, but again some documents were not relevant.

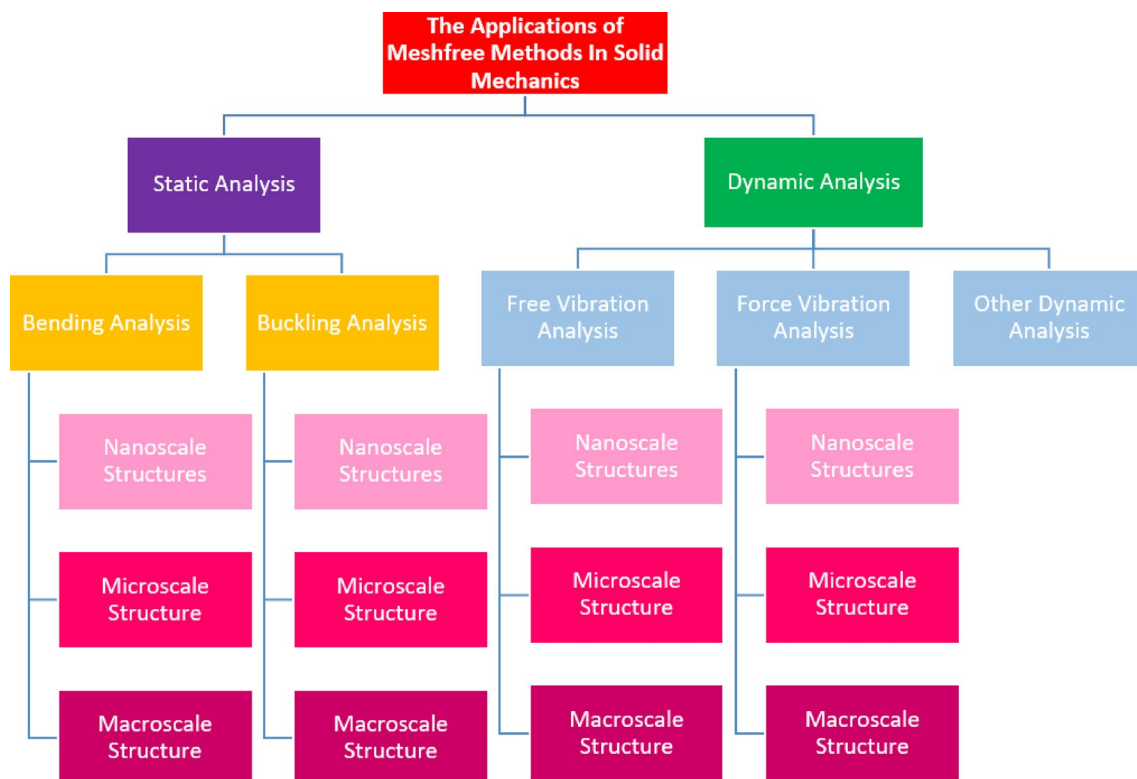


Fig. 8 The applications of meshfree methods in solid mechanics analyses and in the scope of this review

Later on, additional articles were collected from other databases such as; Google Scholar, ScienceDirect and ScienceWeb. To generate the theoretical background of the research; where the supportive articles help in emergent the contexts of the review generally.

Figure 9, shows Scopus statistics of meshfree/meshless applications in solid mechanics' analysis for different structures in nano, micro, and macro size.

The graphs show that the interests in mesh free starts at the early beginning of twenty-first century. With an upward tendency, a significant increase is shown since 2022 until today. The greatest interests were found to be in engineering areas with 40.9%, followed by 15.5% of publication in the area of mathematics. The lowest percentage of documentation was in environmental science with only 0.8%. However, the highest number of publications was recorded by China with 37 documents. Followed by 27 documents have been published in Iran. Canada has relatively fewer number of publications than USA were it recorded 12 documents and 16 documents in USA. While almost half of this number of documents have been published UK, Georgia, and India. The records show fewer numbers in Germany, and Portugal. Australia, has published the same number of documents as in KSA.

1.3 Developing and Improving the Meshfree Regular Methods

According to Seleson [66] research, the meshfree approach is a desirable discretization technique since it is simple to implement numerically, and has a low computing cost compared to other discretization techniques. In addition, this method meanwhile has some problems with accuracy and convergence. A lack of an ideal selection of quadrature points and an approximate estimate of the areas of the intersecting regions (commonly known as partial areas) among neighbor cells and a point's neighborhood are the main causes of these problems.

Among the most popular and crucial meshless techniques is the EFG approach. However, it has the drawback of poor computing efficiency when compared to the FEM. Sun et al. [67] have presented an improved element-free Galerkin method (IEFGM) in order to resolve two dimensional elastic complications that is based on the dimension splitting MLS (DS-MLS) approach as well as combining the Galerkin vibrational WF with integral coordinate transformation. The DS-MLS technique improves the speed and precision of shape function calculations by reducing the dimension as well as complication of matrix operations while resolving shape functions. Besides, the meshless approach developed from the DS-MLS approach has the ability to increase

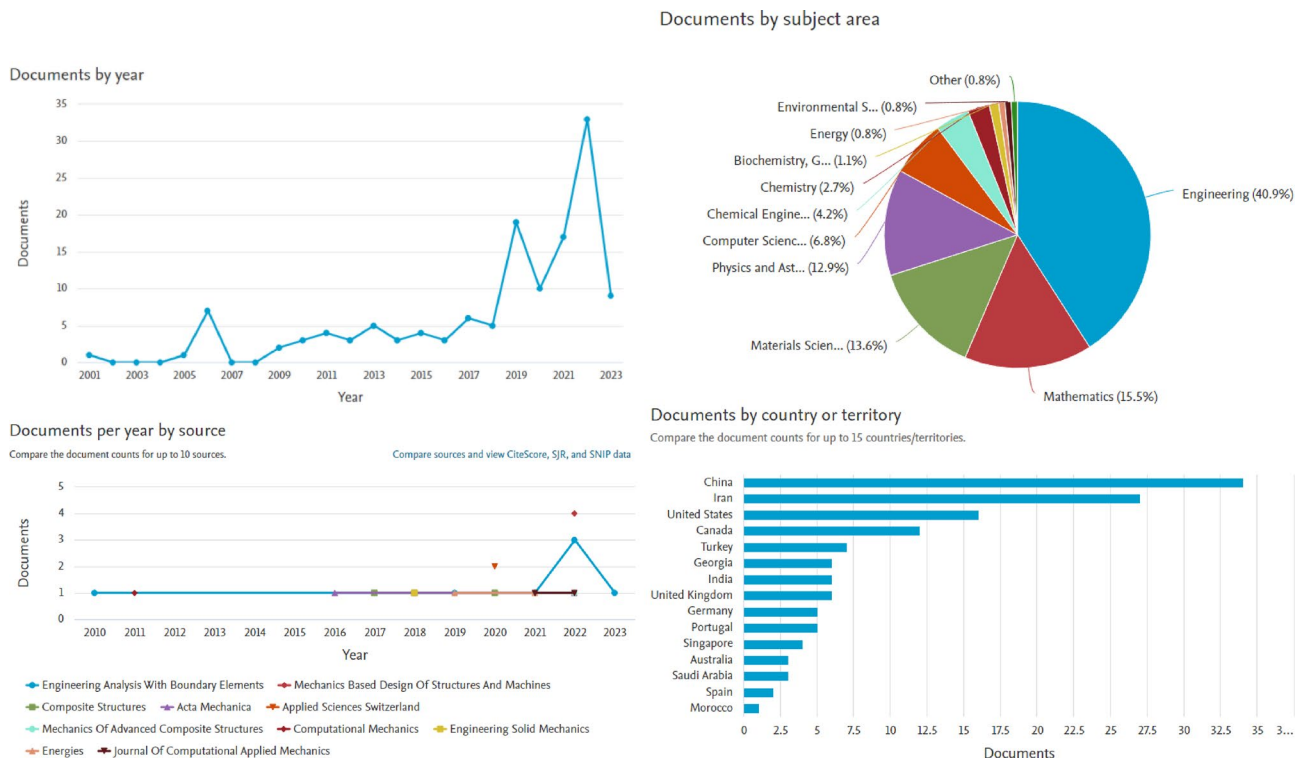


Fig. 9 Scopus statistics of meshfree/meshless applications in solid mechanics analysis for different structures in nano, micro, and macro size (2001–2023)

computational effectiveness. The IIEFGM suggested in that work can also obtain higher accuracy and uses slighter central processing unit (CPU) time than the EFG approach for some elastic issues, according to the numerical example results of the elasticity problems. Roque et al. [68] expanded the trigonometric theory for beams to include composite and sandwich plates. In addition, it demonstrated outstanding performance in free vibration (FV) analysis. For the purpose of improving some of the limitations of the global RBF approach, various authors individually indicated a local RBF method under several names such as local multiquadric-based differential quadrature (LMQDQ) technique [69], and RBF in a finite difference mode [70]. The LMQDQ has been used by, Ding et al. [71] in order to resolve 3-D incompressible Navier–Stokes (N–S) formulas in the primitive-variable format. For the first time the radial basis function based on differential quadrature (RBF-DQ) was employed to examine the FV behavior of laminated composite arbitrarily shaped plates [72]. Furthermore, Shu et al. [73] simulated the inviscid compressible flows through shock wave by using RBF-DQ. Wright and Fornberg [74] developed a method to reduce the number of stencil nodes with remaining high accuracy, by employing RBF with finite difference (RBF-FD). In this study, different models were used to test and validate the method. For the first time, the multiquadric radial basis function (MQRBF) approach was utilized to interpolate the motion equations as well as BCs to perform FV analysis of plates. Oruç [75] has developed a developed methodology based on the RBF-FD, for the purpose of solving the coupled damped Schrödinger systems in (1, 2, and 3) dimensions. Tornabene et al. [76] produced the moving least squares differential quadrature (MLSDQ) created on the RBF for solving various structural geometries made of doubly curved shells designed by composite materials as illustrates in Fig. 10 as well as Fig. 11. The first ten mode of vibration for each shape were obtained. The study concludes that with varying curvature radii while considering laminated composite materials and anisotropic lamination structures, once the structures having varied radii of curvature were incorporated, it is proved that the methodology is quite accurate compared with the semi-analytical solutions for plates, although there are some constraints must be taken. Additionally, the approach permits the application of any BCs, including both natural and essential conditions.

In a further studies the same method has been applied for the purpose of investigating the FV [77], besides static examination [78] of the functionally graded plates (FGPs) simply supported (SS) modeled by third order shear deformation theory (TSDT), the obtained outcomes were found to agree with previous analytical and numerical solutions. The Mori–Tanaka technique has been implemented in both studies for the purpose of defining the material properties. To investigates a moderate laminated thick composite sandwich

plates SS, Ferreira [79] present a formulation of the MQRBF. The author examined both stresses and displacement. High accurate results were observed and the model was compared with FEM and exact formulations. Ferreira et al. [80], developed a new meshfree method which is a finite point founded on the MQRBF, and has been employed with the third-order theory of Reddy for the purpose of analyzing and discretizing different types of plates (sandwich plate, composites laminated plates and isotropic plate). Nevertheless, the BCs interpolation has been schematically drawn out. The outcomes prove that the presented method efficient and accurate more than previous other method proposed before. Ferreira [81] has used the MQRBF again for the same structure as well as same types of plates, but in this study the FSDT and TSDT were applied. Besides, the layerwise theory was accompanied by independent rotations in each individual layer and schematically formulates the BCs interpolation. The shear correction factor is not necessary for this presented method also it combine the constitutive equation by the transverse shear stress directly calculated. The combination of layerwise with the MQRBF discretization consider as simpler yet remarkable effective numerical approach for thin and thick different types of plates (sandwich laminates and composites). For the purpose of examining Mindlin plates and Timoskenko beams for FV behavior, Ferreira and Fasshauer [82] presented a novel numerical methodology with high accuracy, by combining the pseudospectral (PS) method with collocation RBF meshfree method. Furthermore, the RKPM has been utilized to compare the natural frequency (NF) results for each type of plates with previous obtained results by Rayleigh–Ritz and by shear-deformable plate's theory established on FSDT meshfree method. The deformations of laminated composite, sandwich plates as well as shear flexible isotropic were investigated by a novel numerical scheme [83]. For producing a high accurate results, the collocation by RBF was viewed as a PS method and the layerwise theory of sandwich or laminated plate was applied. The optimum value of shape parameters variable was considered. Additionally, for studying the free behavior the harmonic solution was considered and the NF results were very close to the previous obtained results by using the Rayeigh-Ritz solution. The corresponding 3D views first eight modes of the square Mindlin/Reissner plate with clamped–clamped (CC) BCs is illustrates in Fig. 12.

However, Ho et al. [84] employed the integrated radial basis function (IRBF) and the conic programming for kinematic yield design computed homogenization of ductile and periodic composite materials. Xiang, et al. [85] employed the meshless radial point collocation (MRPC) technique founded on the thin plate spline RBF as well as the n th-order shear deformation theory for evaluating laminated composite plates FV. Besides, to determine the NF of the plates while considering different BCs, material properties,

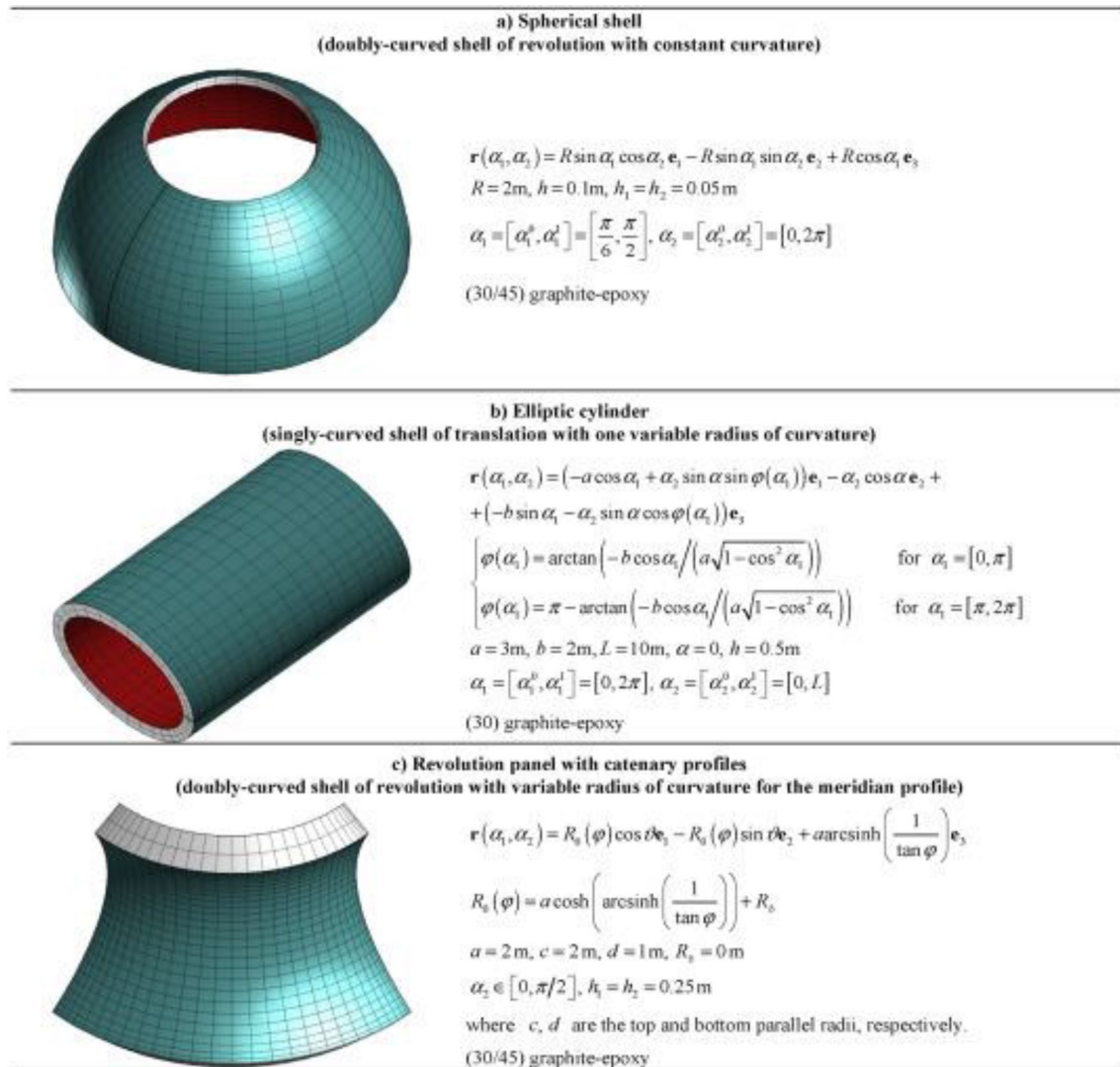


Fig. 10 The geometry of three shell structures is defined as: grid, local coordinate orientation system, and position vectors $\mathbf{r}(\alpha_1, \alpha_2)$ [76]

side-to-thickness (a/h) ratios, the zero transverse shear stress BCs on the top and bottom surfaces of the plate were satisfied by the n th-order shear deformation theory. The n th-order theory ($n=3$) was considered as a superior instance of Reddy's third-order theory. Nie et al. [86] have introduced parallel node placement technique by bubble simulation (PNPBS) applying the basic domain decomposition (DD) by the METIS software, for a random number of processors. The flowchart of the processes is presented in Fig. 13.

According to [6, 87, 88], the majority of meshfree methods rely on the MLS shape function [32–34], that neglects the Kronecker-delta property. Although absence of the Kronecker delta property tends to make treating BCs more difficult, this difficulty is usually resolved through using additional methods such as Lagrange multipliers and the Penalty method. Liew et al. [89] provided the boundary element-free method (BEFM), which is a direct meshless method

of boundary integral equation (BIE) for 2D elastodynamic difficulties. Likewise, it incorporates the improved moving least squares (IMLS) approximation with the BIE system for 2D elastodynamics in the Laplace-transformed domain. Sansour and Skatulla [90], recorded that employing the MLS approximations in a NL Cosserat continuum-based formulation has impacts for the necessary BCs enforcement as well as the rotation field updating. Furthermore, Wang and Liu [91] performed the proposed RPIM to satisfy Kronecker-delta, which leads to find the necessary BCs easily.

Rosca and Leitaó [92] stated that the governing integral equation in meshfree methods which is based on WF is derived out of the WF of elasticity local domains or over global. Besides, they offer an improvement of meshless method by using the Monte Carlo integration methodology, and considered as more efficient, simpler as well as straightforward in comparison to other local or global integration

Fig. 11 The doubly-curved surface geometry of the Ding-dong Revolution [76]

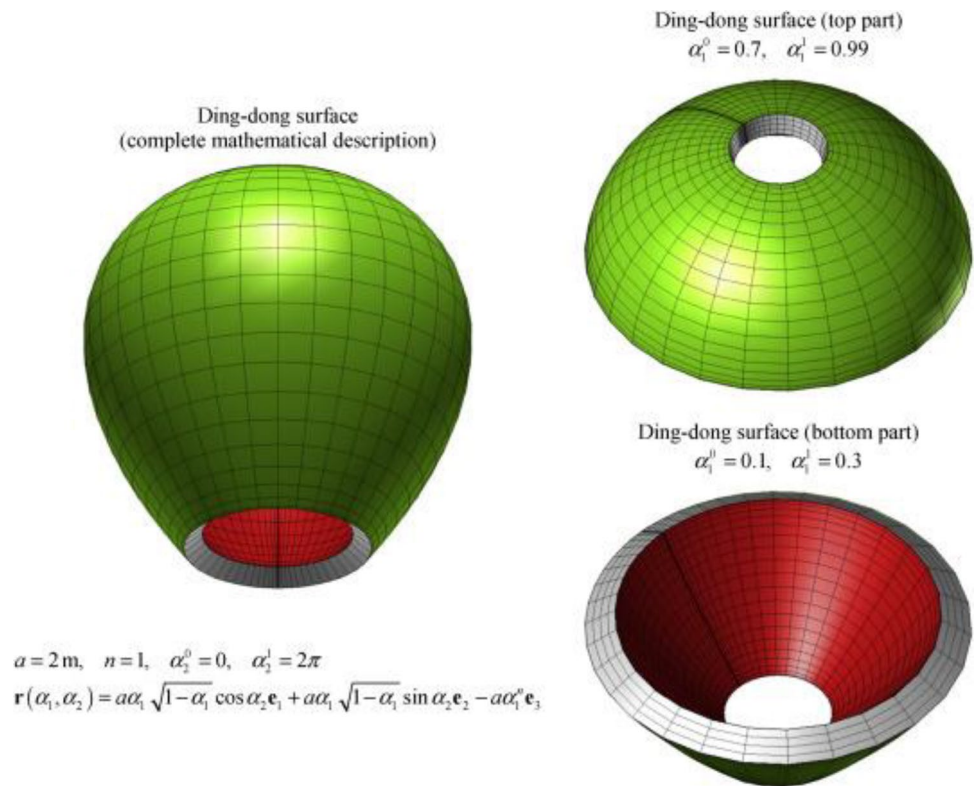
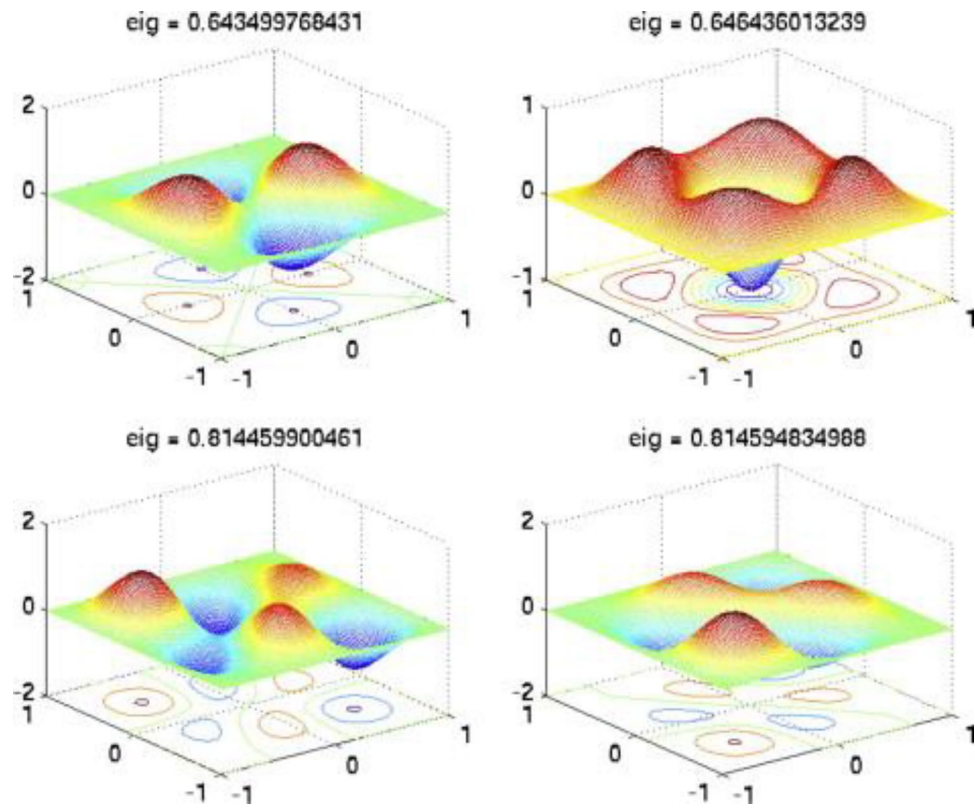


Fig. 12 The Modes (5–8) of vibration of a CCCC square Mindlin/Reissner plate with $h/a=0.01, \nu=0.3$, 3D view [83]



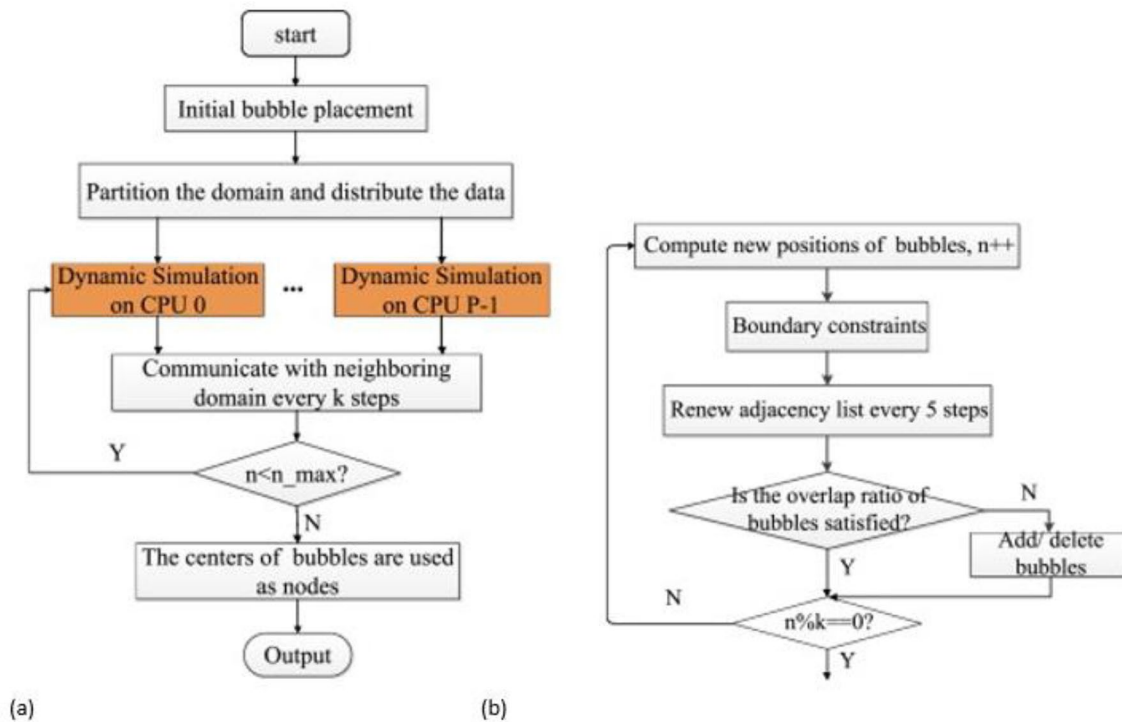


Fig. 13 The PNPBS methodology flowchart; **a** The complete process **b** dynamic simulation for each specific processor [86]

technique. Khosravifard and Hematiyan [93] stated that the most common draw back for meshfree methods are low accuracy, additional time consuming, complexity, and high CPU capacity. To overcome these problems, they modified a developed version of the CTM to treat the territory integrals in meshfree approaches. The CTM method has been used earlier to evaluated the territory integrals in the boundary element technique by [94, 95]. At the end of twentieth century, researcher's interest in developing the SPH started to increase in different mechanical engineering fields [96–98]. There were various purposes of developing the SPH method such as; seeking to solve tensile instability [99, 100], zero energy mode [101], the absence of interpolation consistency [102], and enforcing the BCs in different types of analysis [103]. However, the main drawback of SPH, is that it cannot be used to signify the rigid body motion properly as recorded by Liu et al. [12]. As a consequence of this problem, the main concept of improving the SPH is generating a corrective kernel function and remaining the initial kernel as well. To investigate the fluid-elastic structure of the incompressible fluid, Khayyer et al. [104] established an incompressible smoothed particle hydrodynamics (ISPH)-SPH meshfree technique. Liu and Liu [105], presents a review of SPH meshfree method. In addition, it highlights the recent development of the SPH, its advantages and the recent applications. Furthermore, the basic concept of KPM approximations and smoothing kernel function that have been used to

develop the SPH were reviewed. Figure 14 illustrates the schematic of two different scenarios of SPH kernel approximations in exact and not exact second order accuracy. In Fig. 14a, W which is smoothing function is not shortened by the boundary, the smoothing function integration is unity, while the integration of the smoothing function's first moment term and the surface integral are zero, while in Fig. 14b, W is condensed by the boundary, the smoothing function integration is not unity, and the surface integral and the integration of the smoothing function's first moment term are not equal to zero. Rahmat et al. [106], developed a novel three dimensional numerical model based on discrete multi physics (DMP), the MLS meshfree method, and a mass spring model (MSM).

Silling and Askari [107] have employed the PD theory to develop meshfree methods in cracks modeling. The key benefit of that method was to redefines the underlying mathematical representation of solid mechanics to ensure the identical equations hold each on or off of a discontinuity involving a crack. Besides, even in case of having a huge quantity of cracks the treating process can still be accomplished with their mutual interaction, in another words it is preventable to handle the other side of cracks separately. The conclusion of that study shows that the PD method have theoretical as well as practical advantages over other meshfree methods in fracture mechanics. As a theoretical advantages, it has the ability to determine various sets of

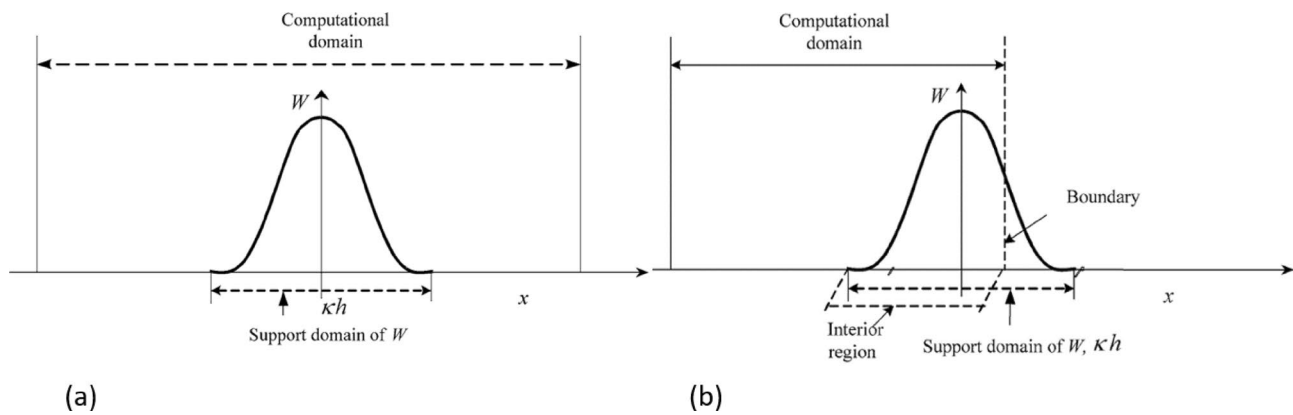


Fig. 14 The schematic depicting the intersection of the support domain and the problem domain, in which **a** the SPH kernel approximations are of second order precision. **b** The SPH kernel estimates do not have perfect second order precision [105]

continuum equations. Also, its integral equations have the potential to persist directly applicable when a discontinuity seems, which can't be guaranty by the classical theory PDEs. Furthermore, the PD approach cross over the popular issue (tensile instability) which usually shows in SPH methodology. However, the PD model is found on the interaction between pairs of nodes, which in consequence eliminate the requirement of great number of neighbor nodes to define spatial derivatives and it is counts as a practical advantages. Another significant practical fact is that the cracks emerge spontaneously as a natural consequence of the equation of motion as well as constitutive models. Amiri et al. [108] provides a model of phase-field for fracture in Kirchoff-Love thin shells that utilizes meshfree local maximum entropy (LME) approach. This technique was created to assess brittle materials and structures with complicated geometry and topology. The study includes constructing a fourth order phase-field model to be utilized with smooth approximants like IGA or LME, with a goal of boosting accuracy and efficiency while enhancing the level of convergence. Zhang et al. [109], work is considered as the first study that incorporate HSDT with an meshfree approaches for the purpose of examining a FV response of CNT reinforced FGPs. Selson and Littlewood [110] presented a Conjunction work in meshfree PD simulations. In 3D, they estimated numerical partial volumes utilizing a recursive subdivision and sampling technique. For the purpose of avoiding the numerical estimation of the singular integrals in the boundary element technique and to eliminate the singularity of the fundamental solutions, Fu et al. [111] developed singular boundary method (SBM) which is defined as meshfree technique by claiming the conception of origin intensity factors. The developed schematics are shown in Fig. 15 as well as Fig. 16. Additionally, due to the fact that the SBM avoids the singularity in the fundamental solution, Lin et al. [112] employed the SBM to investigate the linear elastic half plane

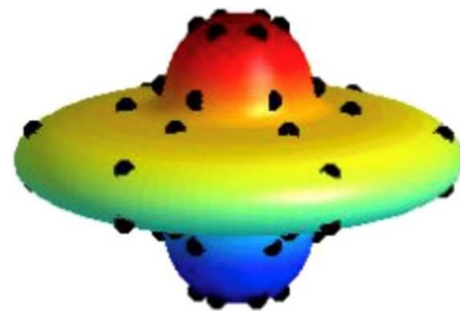
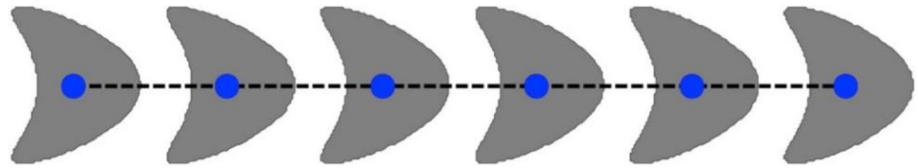


Fig. 15 The top-shaped axisymmetric schematic structure [111]

with cavities of buried under incident P and SV waves for the purpose of verifying the seismic response.

An investigation of the application of an undisturbed influence functions with a finite support for enhancing the accuracy as well as convergence of the mathematical solutions in PD was also conducted. Liu et al. [113] presented a review which focused on boundary element method (BEM) and its application in improving various types of methods such as the symmetric Galerkin formulations and the boundary meshfree methods. The MLPG meshfree method has been implemented with the MD method to perform a multi-scale simulation. Additionally, both multiple time steps and multiple length scales were performed in the mathematical cases. The obtained results demonstrated that the suggested method is optimum in reducing the computational cost and decreasing the reflection of phonons [114]. Tang et al. [115] applied the MLPG to analyze the materials with strain-gradient effects. Since there is no FEM having the ability to solve the strain gradient theory (SGT) formulation, the nodal rotational degree of freedom (DOF) nodal were not considered. The results show that superior results to mixed FE procedures or primal of MLPG were obtained in fourth-order elliptic problems. However, the redefined SGT has

Fig. 16 The periodic with one line scatterers schematic structure [111]



been employed by, Limkatanyu et al. [116] to investigate the beam bulk material nanoscale effect in a study which focused on examining the bending, stability and FV of a nanobeam structure substrate moderate model. Besides, the free energy of the surface has been obtained by utilizing the Gurtin–Murdoch surface elasticity theory. Yvonnet et al. [117] demonstrated a new meshfree natural element method (NEM) expansion. A visibility requirement was incorporated in this methodology, and designated the constrained natural element method (C-NEM), for the sake of selecting natural neighbors for computing the shape functions. The particular shape functions were computed using an adjusted, limited Voronoi diagram. A few of the obstacles associated with this method in non-convex domains were averted. In addition, the study of problems requiring fractures or discontinuities became simpler. Unlike other meshfree approaches, the introduction of essential BCs is relatively easy since the NEM satisfies the Kronecker delta features. Bessa et al. [118] developed a connection between the meshless state-based PD approach and further meshless approaches, specifically MLS reproducing RKPM. It has been determined that discretizing state-based PD immediately yields to estimate the derivatives produced by RKPM. Nevertheless, state based PD has achieved similar results at a considerably less computational cost. In response to the results; an update to the method was provided, in which the constraints of the utilization of BCs as well as the application of non-uniform (NU) grids were modified by employing RKPM. The PD NLC meshfree method was employed for comparing the empirical findings of carbon fiber reinforced polymeric-halloysite nanotubes (CFRP/HNT) laminates under in-plane shear and flexural loads, where the PD analysis prove that the halloysite nanotubes (HNT) obstruct the cracks growth [119].

To investigate the complex phenomena spall fracture that is caused by the shock wave, Ren et al. [120] have developed and employed the RKPM method with multiscale micromechanics theory that has been suggested by Wright and Ramesh [121]. Furthermore, Mishra et al. [122] developed a closed-form mathematical expression called multibody dissipative particle dynamics (MDPD) for simulating a complex wall analytically. MDPD is an adjusted version of the particle-based meshfree methodology dissipative particle dynamics (DPD). Based on unlimited advantages of meshfree method, it has various application in biomedical and pharmaceutical fields. For example, Imai et al. [123]

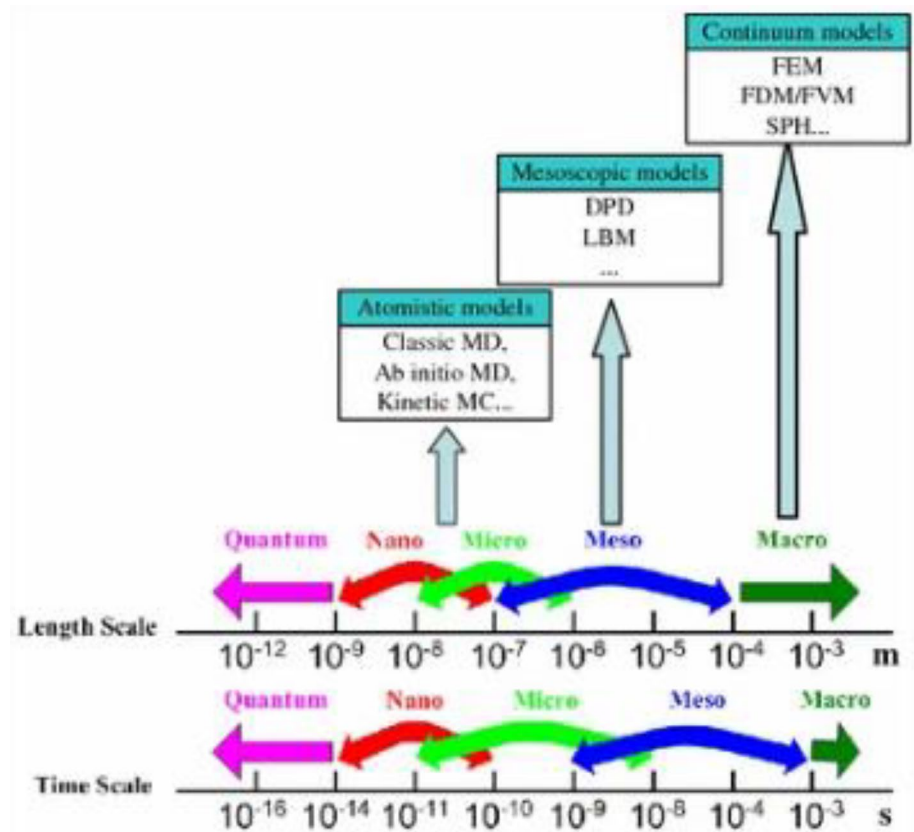
recorded that BEM is the highest rigorous process for Stokes flow, and it is exclusively beneficial for infinite flow complications. The semi-implicit method (MPS) and DPD were extensively utilized as well for cellular flow difficulties. Also, the meshfree methods have applications in food industry [124]. Liu et al. [125] presented a review of DPD, and it included the formulations, methodology, implementation procedures, some related numerical aspects and applications in different fields. Figure 17 illustrates the different time and length scale corresponding computational methods, and it is observed that for each single length scale, different method must be adequate.

Where the boundary moving least square (BMLS) satisfy the BCs easier, it has a benefits over other traditional meshfree methods in solving higher dimensional problems. It has been applied to solve two dimension elasticity problems [126]. Chen et al. [127] have combined the smoothed discrete particle hydrodynamics (SDPH) and FVM as shown in Fig. 18, in order to achieve higher effective performance in solving a multiphase flow difficulties of gas-particle. The Ritz-Galerkin discretization has been employed with Kirchhoff–love hypothesis, equilibrium configurations and the kinematics of the shell for generating the mathematical modeling of the thin shell [128]. Some of the unique numerical examples that have been examined are presented in Fig. 19. Moreover, Thai et al. [129] have employed the Galerkin-WF meshfree technique for bending and stability analyses as well as vibrational analysis models for functional graded material (FGM) sandwich isotropic plates to generate the discrete formulas of the system. This study focused on applying the generalized shear deformation theory for FGM for static and dynamic examination, based on the IGA approaches.

Recently, Faghidian et al. [130] reproduced an effective meshfree numerical method with a sequence of solutions for kinetics as well as kinematics field parameters. However, the mixture stress gradient theory of elasticity and the stress gradient theory through a stationary variation basis were performed for FG nanobar in tension. Figure 20 shows 3D schematic of the variance of an axial nondimensional (ND) displacement for a FG nanobar \bar{u} exposing linear axial loading against ND abscissa \bar{x} .

A study by Chen et al. [131] focused on investigating the application of RKPM for NL structures with large deformation analysis considering elasto-plastic and hyperelastic materials, the computational results revealed that RKPM

Fig. 17 The differentiation in time and length scale corresponding computational methods [125]



manages severe material distortion more efficiently compared with FEM owing to smoother shape functions then, as a consequence, gives results with greater accuracy subjected to huge deformation. Contrary to traditional FEM, nodal spacing NU in RKPM does not result in an irregular mesh shape, which greatly reduces the correctness of solution. Whenever NL RKPM is applied to virtually incompressible hyperelasticity and perfect plasticity circumstances, no volumetric locking is seen. The basics of MLS method and its developed formation and interpolations were presented by Breitkopf et al. [132]. Žur and Faghidian [133] developed a novel numerical meshless theory for unified gradient elasticity theory of torsion in nanobar. The presented meshless technique was founded on the principle of Reissner stationary vibrational. Likewise, unconventional series solutions for kinetic and kinematic field variables were discussed. An outstanding agreement between the meshfree technique and the exact solution was detected. Figure 21 illustrates a torsional performance of the unified gradient elastic bar as influenced by NLC besides gradient characteristic characteristics at the nanoscale. In a further study, for the rigorous investigation of the dynamic properties of elastic nanobeams, the mixture unified gradient theory of elasticity has been utilized by Faghidian et al. [134]. A coherent vibrational framework was created, and the dynamic equilibrium boundary-value problem was recognized with the appropriate shape of the

extra non-standard BCs. Besides, the elastic nanobeams' FV and wave dispersion response were investigated analytically. Additionally, the demonstrated augmented elasticity theory has shown to be effective in achieving the softening and stiffening responses of nanobeams. A novel arithmetic benchmark for dynamic modelling of elastic nanobeams has been discovered. The developed MUGEM offers a realistic solution to addressing nano-scale structure dynamics in pioneering MEMS/ Nanoelectromechanical systems (NEMS).

Sladek et al. [135] implemented the micro-dilatation theory to develop a novel meshfree method for porous elastic material which is known as the MLPG. Additionally, the MLS was employed to define the spatial variation of displacement and micro-dilatation. In a recent study, Kwak et al. [136] presented a novel meshfree method for the annular plates and cylindrical shells of ply drop-off laminated conical in which the FV analysis has been investigated. The conceptual framework of FV examination was founded on FSDT, then the field functions were estimated using an innovative meshless Tchebychev-RPIM approach. In addition, the shape function was founded on Gaussian radial functions and Tchebychev polynomials. The GEs as well as BCs for ply drop-off laminated composite shell substructures were developed. Implementing an artificial spring approach generalizes the boundary and

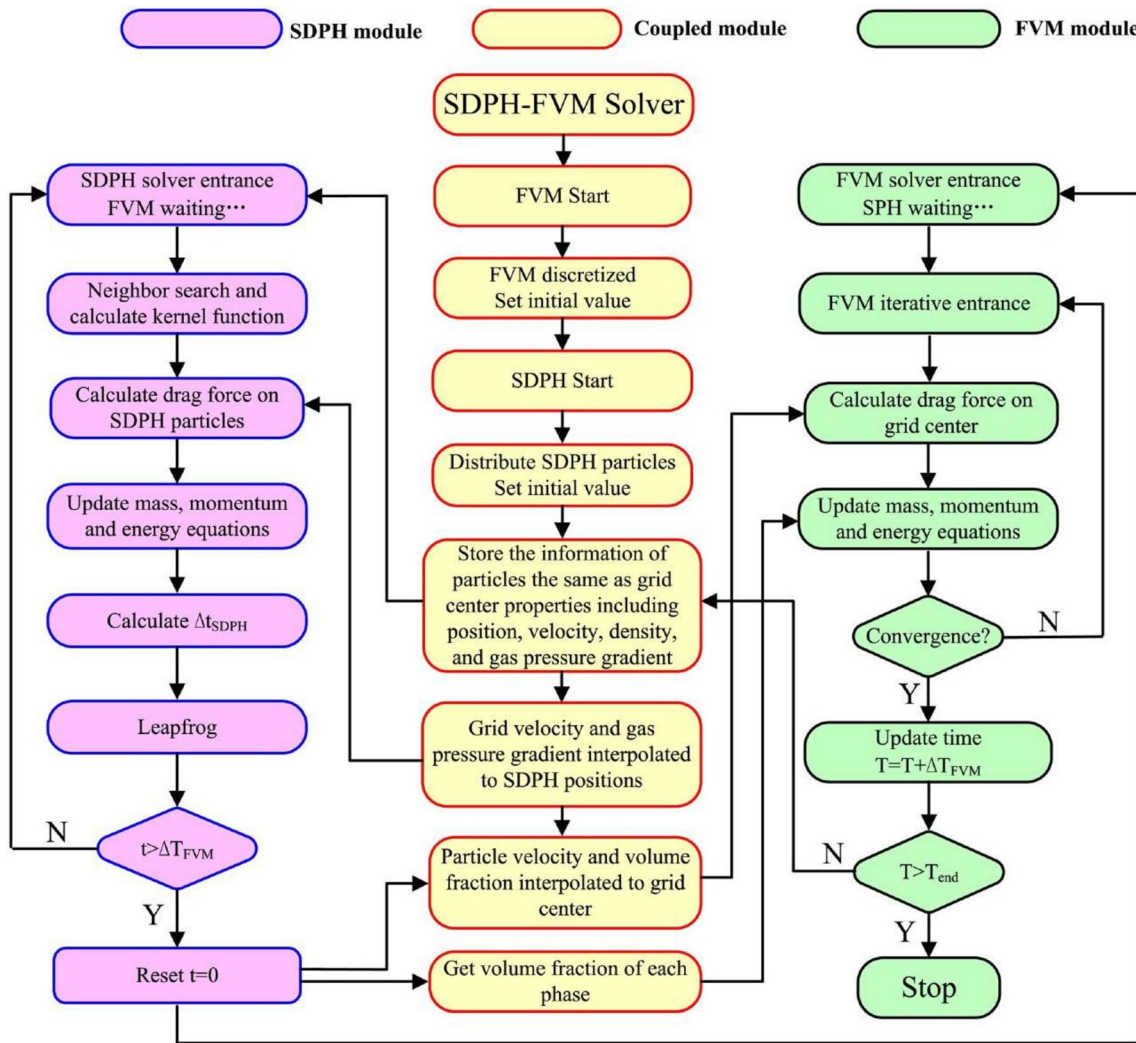


Fig. 18 SDPH and FVM combination algorithm [127]

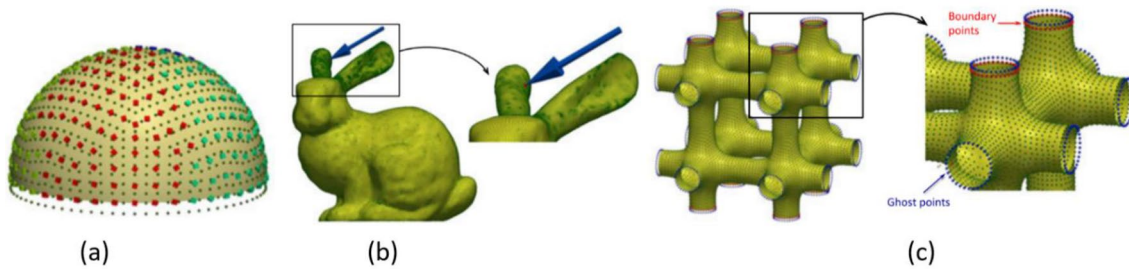


Fig. 19 The Pinched hemisphere **b** bunny **c** connected pipes [128]

continuous conditions, and the type of BCs determined by the spring stiffness values. A schematic of the ply drop-off laminated conical shell is illustrates in Fig. 22. And Fig. 23 illustrates the geometry of the combined region.

1.4 Mathematical Modeling

In this section the basic formula of traditional meshfree method are presented. The following equation of meshfree

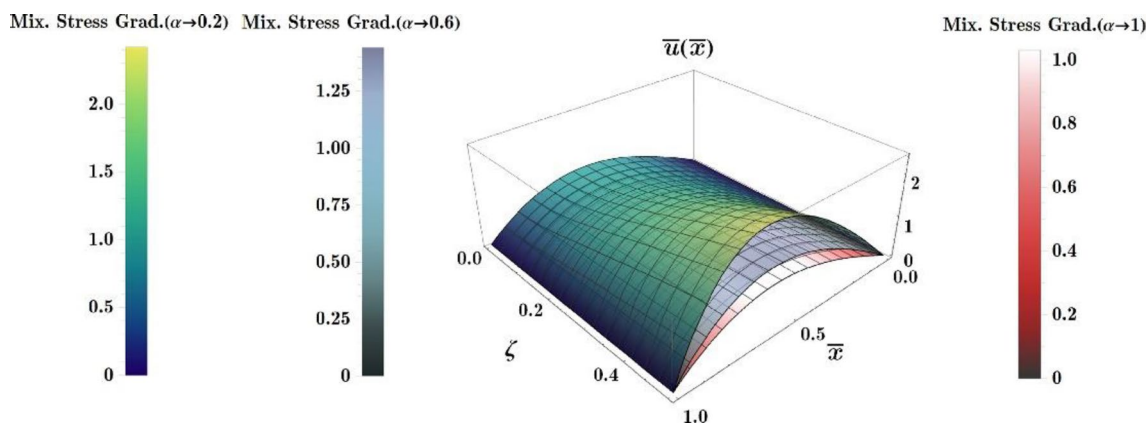
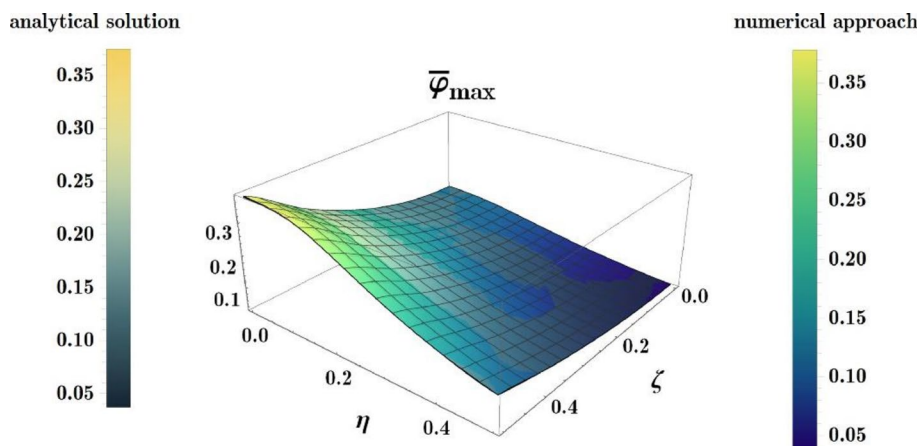


Fig. 20 The FG nanobar is exposed to axial linear loading with fixed–fixed BCs \bar{u} Vs. \bar{x} and ζ for fixed $\alpha=0.2, 0.6, 1.0$ [130]

Fig. 21 The torsional rotation of the regularly loaded fixed end nanobar in 3D [133]



estimation for a scalar function u in terms of the material (Lagrangian) coordinates has the basic approximations [1]:

$$u(x, t) = \sum_{I \in \mathcal{I}} \Phi_I(x) u_I(t) \tag{1}$$

where: the shape function $\Phi_I: \Omega \rightarrow \mathbb{R}$, the nodal values at particle I located at position x_I u_I , and the set of nodes I for which $\Phi_I(x) \neq 0$ is ℓ

The general formula of SPH is defined as following equation [137]:

$$u^h(x) = \int_{\Omega} w(x - y, h) u(y) d\Omega_y \tag{2}$$

Although the continuous form of SPH is second order complete, it can be simply exposed that the discrete SPH form is given by [1]:

$$u^h(x) = \sum_I^N w(x - x_I) u_I \Delta V_I \tag{3}$$

where the RKPM is developed from the continuous SPH approximation, but the $C(x, y)$ correction function is

presented into the approximation so as to rise the order of completeness of the approximation [12].

$$u^h(x) = \int_{\Omega_y}^0 C(x, y) w(x - y) u(y) d\Omega_y \tag{4}$$

where $K(x, y) = C(x, y) w(x - y)$ with $C(x, y)$ is defined such that the approximation is n th order consistent \mathbf{p} .

Numerical integration must be used to assess this continuous statement. In the RKPM, a discrete variation of the RKPM is obtained through this stage.

$$\begin{aligned} u^h(x) &= \int_{\Omega_y}^0 C(x, y) w(x - y) u(y) d\Omega_y \\ &= \sum_I^N C(x - x_I) w(x - x_I) u_I \Delta V_I \\ &= \mathbf{p}^T(x) [\mathbf{M}(x)]^{-1} \sum_I^N \mathbf{p}(x_I) w(x - x_I) u_I \Delta V_I \end{aligned} \tag{5}$$

For MLS approximation; $u^h: \Omega \rightarrow \mathbb{R}$ of the function $u: \Omega \rightarrow \mathbb{R}$ is posed as a polynomial of order m but with *non-constant* (NC) coefficients. The local approximation around a point $\bar{x} \in \Omega$, evaluated at a point $x \in \Omega$ is given by

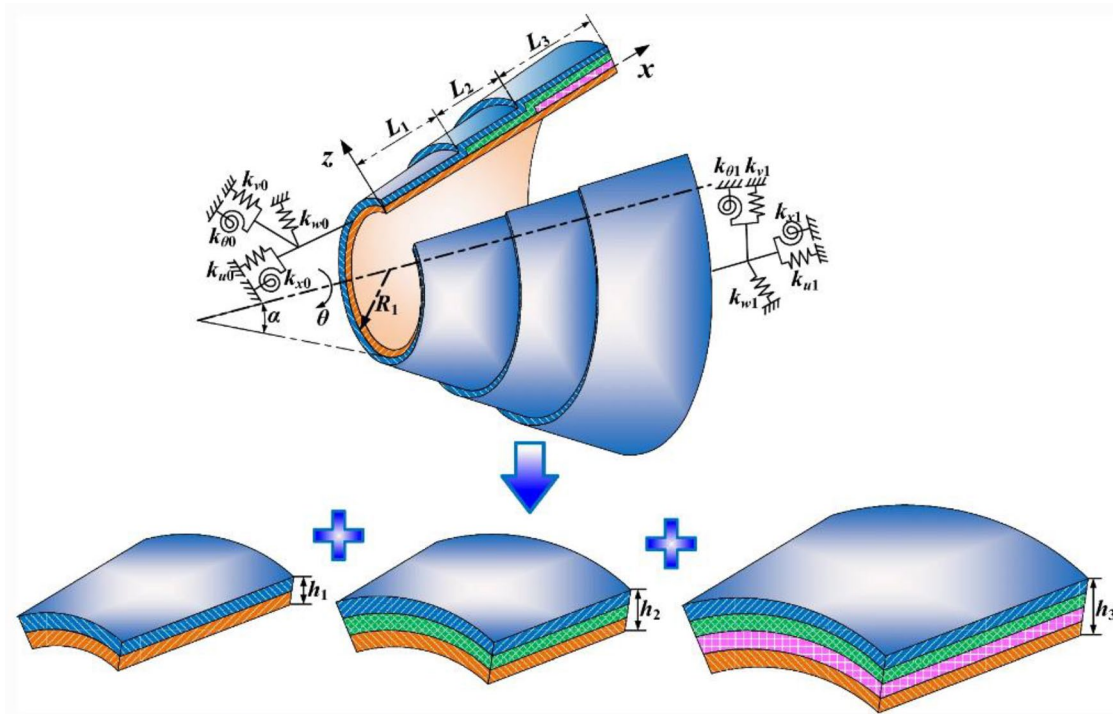
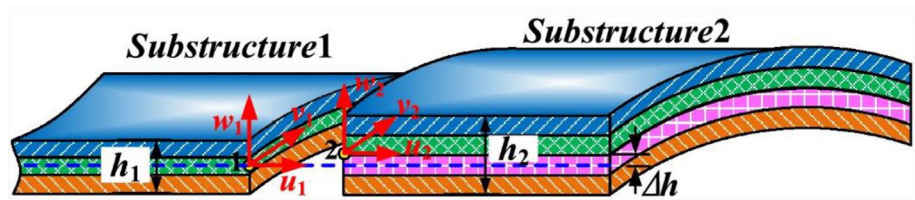


Fig. 22 Schematic of the ply drop-off laminated conical shell [136]

Fig. 23 The geometry of combined region [136]



$$u_L^h(x, \bar{x}) = p^T(x) a(\bar{x}) \tag{6}$$

where $p(x)$ is a complete polynomial of order m , and $a(x)$ contains NC coefficients which depends on x .

The formula of PUFEM is define as [24]:

$$u^h(x) = \sum_{I=1}^N \varphi_I^0(x) \sum_{j=1}^1 p_j(x) v_{jI} = \sum_{I=1}^N \varphi_I^0(x) p^T(x) V_I \tag{7}$$

where coefficients v_{jI} are nodal unknowns and $\varphi_I^0(x)$ is the shape function based on the Lagrange polynomials.

The approximation in the hp-clouds method can be enhanced by adding the different partitions of unity and written as follow at any point of $x \in \Omega$ [138, 139]

$$u^h(x) = \sum_{I=1}^N \varphi_I^m(x) u_I + \sum_{I=1}^M \varphi_I^k(x) = \sum_{j=1}^1 p_j(x) v_{jI} \tag{8}$$

While the $\varphi_I^m(x)$ and the $\varphi_I^k(x)$ both are meshless shape functions of the orders m and k respectively.

A set of test functions Ψ are chosen and the system of equations is determined by sitting ε^h

Orthogonal to set of functions for Weighted residual (WR) methods

$$\int_{\Omega} \Psi \varepsilon^h d\Omega = 0 \text{ or } \int_{\Omega} \Psi (\mathcal{L}u^h(x)) d\Omega = 0 \tag{9}$$

$$\int_{\Omega} \Psi \left[\mathcal{L} \left(\sum_{I=1}^N \Phi_I(x) u_I - f(x) \right) \right] d\Omega = 0 \tag{10}$$

Usually, the collocation method formula is not use as it is; for better illustration the formula of elastic foundation (EF) with the governing equation of a string is in assist. And by choosing a specific parameter of $a=0.01$, $c=1$ and $f=-1$ for boundary points $\times 1$ and $\times 2$ the familiar equation can be written as follow:

$$(-a \sum_{I=1}^N \Phi_{1,xx}(x_j) + c \sum_{I=1}^N \Phi_I(x_j))u_I + f = 0, J = 2, \dots, N-1 \tag{11}$$

The exact solution of Galerkin method is given by:

$$u(x) = 1 - \cosh(mx) - (1 - \cosh(m)) \frac{\sinh(mx)}{\sinh(m)}, m = \left(\frac{c}{a}\right)^{\frac{1}{2}} \tag{12}$$

The general formula of the Discrete equation for elastostatics is given by:

$$\int_{\Omega}^1 \varepsilon(u) : C : \varepsilon(\delta u) d\Omega = \int_{\Gamma}^1 \bar{t} \cdot \delta u d\Gamma + \int_{\Omega}^1 b \cdot v d\Omega \tag{13}$$

The integration is evaluated only for the direct nodal integral which defined as integration point as well:

$$\int_{\Omega}^1 f(x) d\Omega = \sum_{J \in \mathcal{L}} f(X_J) V_J \tag{14}$$

where adding additional stress points to the nodes is enhancing avoiding the instabilities due to rank deficiency, so the stress point integration is written as follow [2]:

$$\int_{\Omega}^1 f(x) d\Omega = \sum_{J \in \mathcal{L}} f(X_J) V_J^N + \sum_{J \in \mathcal{L}^s} f(X_J) V_J^S \tag{15}$$

For the support-based integration for the background mesh or cell structure over performing Gaussian quadrature

$$\int_{\Omega}^1 f(x) d\Omega = \sum_J f(\xi_J) w_J \det J^{\xi}(\xi) \tag{16}$$

where ξ is local coordinates and $\det J^{\xi}(\xi)$ is the determinant of the Jacobian.

For modification of the intrinsic basis such as EFGM which can be defined based on crack kinematics, the Westergaard solution is introduced into the basis P [140]:

$$P^T(x) = [1, X, Y, \sqrt{r} \sin\left(\frac{\theta}{2}\right), \sqrt{r} \cos\left(\frac{\theta}{2}\right), \sqrt{r} \sin\left(\frac{\theta}{2}\right) \sin(\theta), \sqrt{r} \cos\left(\frac{\theta}{2}\right) \sin(\theta)] \tag{17}$$

Approaches founded on an extrinsic MLS enrichment to model cracks in meshfree techniques is to introduce the analytical

$$u^h(X, t) = \sum_J P(X_J)^T a(X, t) + \sum_{K=1}^{n_c} (k_1^K Q_1^K(X_I) + k_1^K Q_{II}^K(X_I)) \tag{18}$$

For methods based on an extrinsic PU enhanced XFEM

$$u^h(x) = \sum_{I \in \mathcal{L}} \Phi_I(x) u_I + \sum_{J \in \mathcal{L}^c} \Phi_J(x) H(x) a_J + \sum_{K \in \mathcal{L}^f} \Phi_K(x) \tag{19}$$

$$\sum_{\alpha=1}^4 b_K^{\alpha} B_{\alpha}(x) \tag{20}$$

Typically, the solutions for PDEs with discontinuous coefficients have discontinuous derivatives along the discontinuity, and the discontinuous derivatives is given by;

$$u^h(x) = \sum_I \Phi_I(x) u_I + b \Psi(x - x_a) \tag{21}$$

1.5 Error Estimation

Concerning finding the best values for the variables involved in the approximation of the error, some studies have worked on improving meshfree methods for the purpose of studying the error function. For example, Gavete et al. [141] employed the EFG approach in combination with several selection strategies of the MLS approximations, for different structures such as plate, rod, and beam. Lu and Chen [142] have provided a great summary of adaptive Galerkin meshfree techniques. Chung Belytschko [143] presented an error estimator established on residuals that compares the variation between an improved stress field and raw EFG field, similar to conventional ZZ error estimator in FEM. Durat and Oden [144], have employed the a hp-adaptive approach to accomplish an a posteriori error estimator, using a dual meshfree technique, global stringent constraints on the energy are found in [145]. But, Krongauzr and Belytschko [146] have established a posteriori approximation error for meshless algorithms for refining the corrected derivative adaptively. Bordas and Duflot [147–149] have worked on some studies which focused on error measuring for the extended FEMs which are considered for further developing in error estimation in meshfree/meshless methods with intrinsic. Moreover, h-adaptively is more easily incorporated into meshfree methods than mesh-based approaches because of their absence of involved meshing. Hence, a meshless framework makes it conceptually simpler to construct p-and r-adaptively. While, a local error estimator, or at the very least an indication, is required to drive the adaptively. Some other studies that have worked on error estimation were published such as, Combe [150] who worked on adapting approach for the EFGM, the RKPM adaptation by [151], as well as the error approximation of EFG which been considered by Gavete et al. [141]. Zhang et al. [152] implemented RPIM method combined with suitable implicit time integration to perform transient wave propagation investigation by the dispersion analysis for different structure and geometries. The dispersion error of the numerical findings was extensively examined through a dispersion analysis. Furthermore, it has been determined that the RPIM with sufficient support domains of quadrature points is capable of producing nearly no spatial dispersion errors that are significantly less than those resulting from the conventional FE methods having the same node scatterings. Therefore, monotonically enhancing the computation precision of the arithmetical outcomes by employing reducing

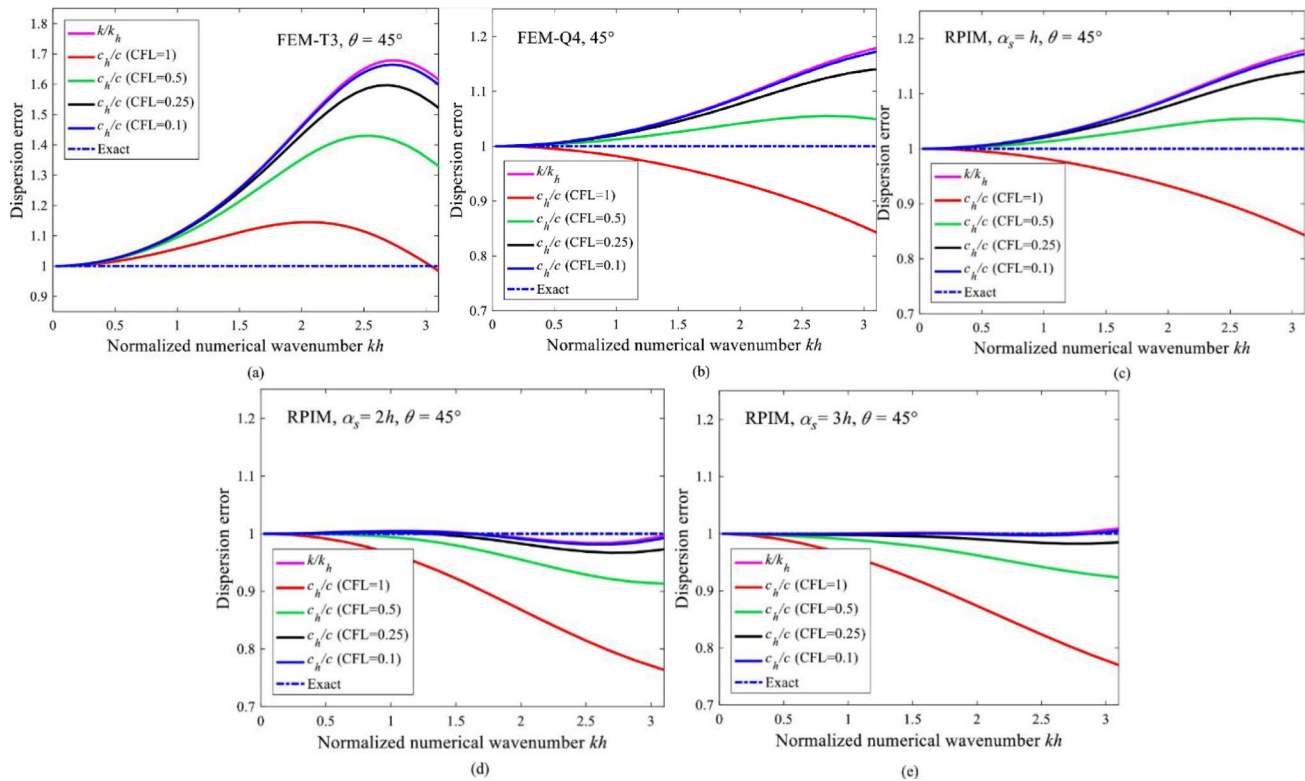


Fig. 24 The overall dispersion error obtained along the wave propagation angle $\theta=45^\circ$. Vs. the normalized numerical wave number kh for several methods: **a** FEM-T3; **b** FEM-Q4; **c** RPIM with $\alpha_s=h$; **d** RPIM with $\alpha_s=2h$; **e** RPIM with $\alpha_s=3h$ [152]

time steps was guaranteed. Figure 24 illustrates the graphs of the overall dispersion errors from several numerical techniques. It shows that several unique CFL numbers as well as wave propagation angles were taken into consideration owing to clearly as well as comprehensively evaluate the dispersion properties.

Rabcuk and Belytschko [153] employed the posterior error estimation for the adaptive refinement for 2D and 3D structures. Bayona et al. [154] described how to anticipate an error of a solution via RBF-FD approach with a one (constant) shape parameter value. This was founded on analytical formulas developed for the local estimated inaccuracy of RBF-FD equations. Because error indication is reliably, and the possibility of estimating the optimal form parameters accurately, which reduces the solution error to the minimal value, has been demonstrated. Furthermore, Duan et al. [155] investigated the error of displacement and established an analysis of different structure after developing a mesh-free method through the consistency of the derivatives of nodal shape functions in meshfree Galerkin methods, and a novel framework was proposed. Additionally, the presented three-point integration scheme employed background triangle elements, of which the smoothed (corrected) nodal derivatives at quadrature sites were computed via a discrete divergence consistency (DDC) for quadratic approximations,

which consist of the MLS approach with the quadratic basis. It also reveals that the corrected nodal derivatives satisfy the differentiation of the approximation consistency (DAC) for quadratic approximations, hence the proposed methodology is known as the quadratically consistent three-point (QC3) integration scheme since it fulfills both the quadratic DAC and the quadratic DDC. Hou et al. [156] provide error analysis based on the vibration analysis results of a strain gradient plate model to examine the error ratio among analytic solution, MLS approximation, and MKI for the model with varied small-scale parameters. Fu et al. [157] have presented a developed BPM by using the Laplace transformation theory, to perform a numerical modeling of the time fraction diffusion equations. Although the recursive composite multiple reciprocity technique (RC-MRM) was employed in purpose of converting the inhomogeneous problem to higher-order homogenous. The error variation of LTBPM is illustrates in Fig. 25. This example demonstrates that the suggested LTBPM performs efficiently for 3D fractional diffusion equations. Correspondingly, all final errors have a high probability of reducing rapidly and subsequently when M boundary increases it will increase as well. Although the turning points of error curves were controlled by the accuracy of NILT input data. Besides, it implies that the final inaccuracy is primarily owing to the Stehfest numerical inverse Laplace

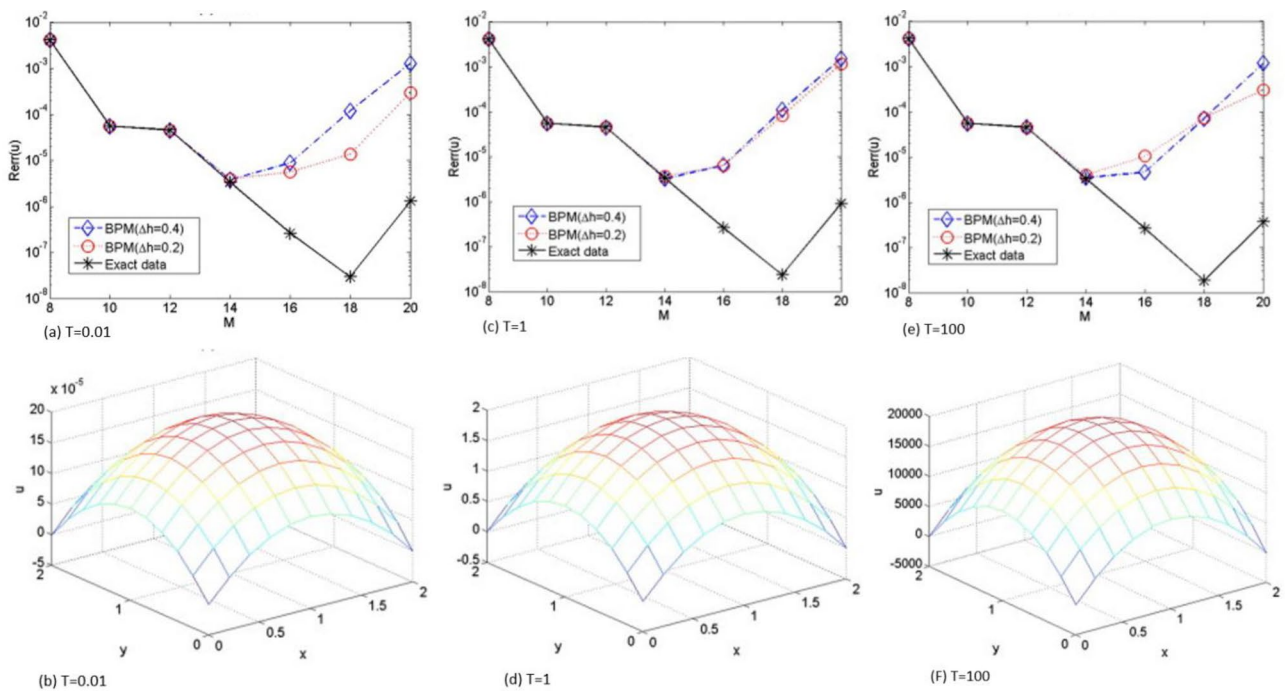


Fig. 25 LTBPM error variations with respect to M on different time instants **a** $T=0.01$, **c** $T=1$, **e** $T=100$; and LTBPM solution at $z=1$ cross section on different time instants **b** $T=0.01$, **d** $T=1$, **f** $T=100$ [157]

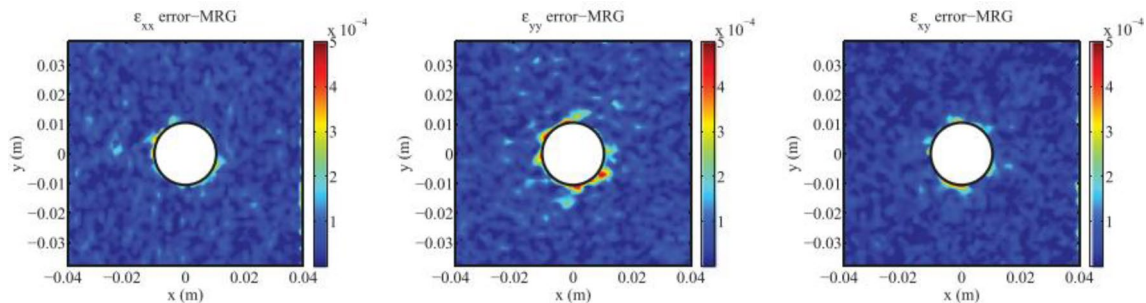


Fig. 26 The respective absolute error of the MRG, the strain and absolute error contours for nodal noise level of 1×10^{-2} pixels and loading angle of $\beta=45^\circ$. And the domain is assumed to span 1600×1600 pixels [158]

transform instead of the BPM computation. Iliopoulos and Michopoulos [158] have performed an absolute error distributions calculations for random grid method (MRG) and traditional meshless method. Figure 26 shows the respective absolute error of the MRG.

As recorded by Wu et al. [159] in a proposed study of modeling and analyzing different composite solid structure (pressure vessel, cantilever beam and unite cell) by implementing an immersed meshfree method based on Galerkin method, it was proved that the optimal error estimate in the energy norm is satisfied by the non-conforming Galerkin method in problems such as elasticity interface. Additionally, the author proved that this method can be used in estimating the error in micro and macroscales. Dehghan and Najafi

[160] implemented the RBF high order mesh free method with other high order methods for numerical solution of a non-classical one-dimensional two-phase Stefan problem. A comparison between the methods results and error analysis were performed. In a short communication article presented by, Roque et al. [161] the examination of the error for the obtained fundamental frequency (FF) after employing the MQRBF combined with HSDT to investigates the FV behavior of the FGPs was accomplished. In overall, the relative error is minimal and decreases as the number of points/side increases. In certain circumstances, the error is contrary to this trend, which was previously discovered and discussed in many articles. Furthermore, when compared to exact results previously published, the error is less than 1% for

each case in the evolution of ND frequency with the number of nodes for a/h ratios of a SS plate. The ND frequency has been compared to the available exact results. The number of nodes in a regular grid was modified and investigate several exponents p . The plate is rather thick, having $a/h = 5$ and the errors = 0.4%. Ferreira [162] implemented the root mean square (RMS) error, after employing the MQRBF as well as the inverse MQRBF approaches to examine the static behavior of laminated composite beams (isotropic, symmetric and orthotropic) under uniform bending load. The CC and the SS BCs were considered. Furthermore, the isotropic three point bending beam was considered to evaluate the method. An excellent performance was observed by validating the results.

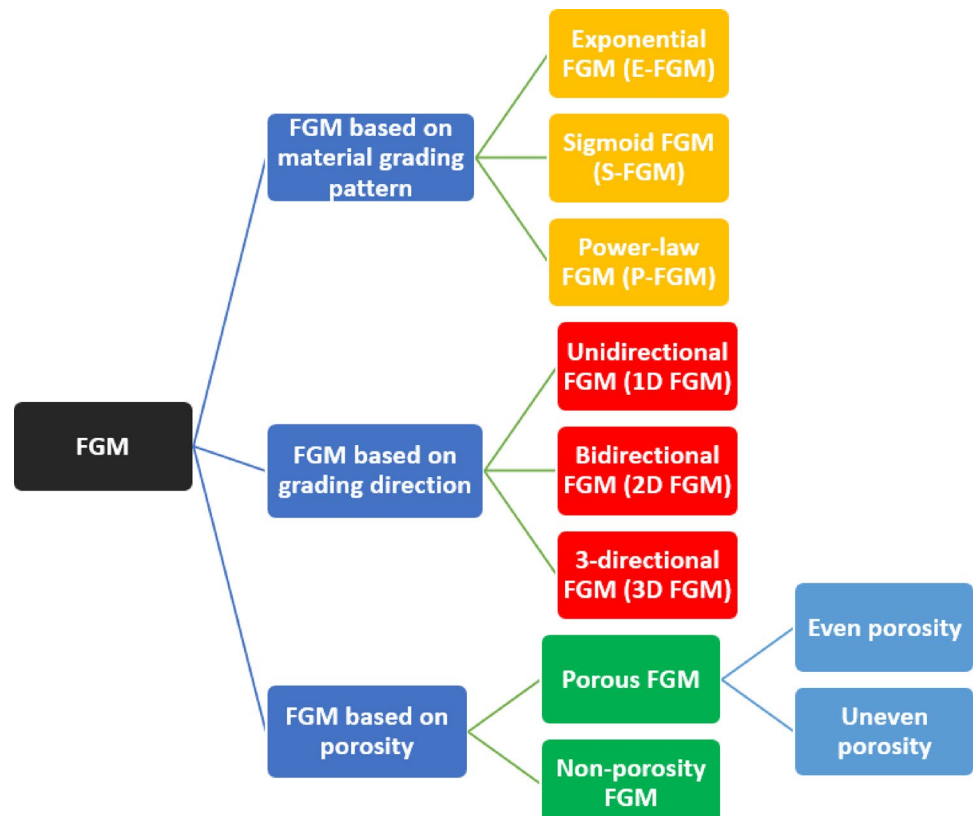
1.6 The Implementations of FGM and Other Composite Materials in Solid Mechanics Structures

For the high importance and advantages of the FG composite material, the researcher shows high interests into it in various engineering complex structure from MEMS to bridge and the various classification of FGM are illustrated in Fig. 27. As an examples, Civalek [163] employed the DSC to discretized the BCs and the GEs for the purpose of studying the statically bending behavior of a composite laminated thick symmetric cross-ply. Besides, for presenting the

singular convolution algorithm both the Lagrange delta sequence (LDS) kernel as well as Regularized Shannon's delta (RSD) kernel. Nian et al. [164] proposed an innovative nature inspired functionally graded lattice filled protection structure (FGLPS) for the purpose on enhancing the structural energy absorption characterizations subjected to ship impact load. The novel structure proved to be highly efficient in reducing the prolong impact time and the peck impact force as well as play a prominent protecting role. Furthermore, Mellal et al. [165] employed the HSDT and generate the equation of motion by using the Hamilton's principle (HP), for the purpose of examining the buckling and the FV behaviors of perfect/imperfect FG beams with an EF. Also, the Navier's method has been utilized for solving the system analytically.

Hadji et al. [166] developed a novel NLC hyperbolic shear deformation beam theory (HSDBT) for the purpose of examining the FV response of a porous FG nanobeam. Also, the equation of motion has been defined by using the HP. Mercan et al. [167] performed a FV study for a FG cylindrical shells that founded on love shell theory by utilizing the DSC method which guaranties an accurate NF results. In a novel study focusing on a laminated conical shell problem, Civalek [168] study the FV behavior of a laminated conical shells by employing the DSC methodology and the governing equation has been formulated by utilizing the Love's first approximation classical thin shell theory. Furthermore,

Fig. 27 The various classification of FGM

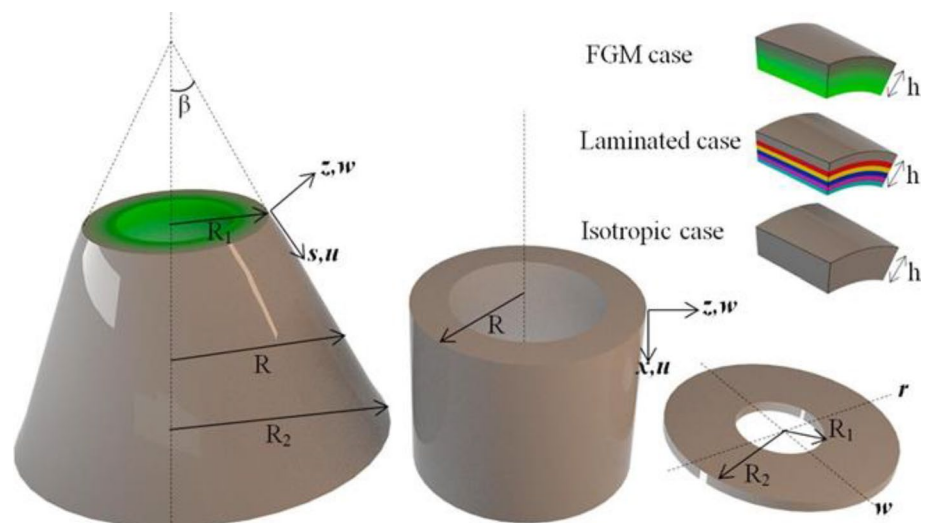


the same author has employed the same methodologies as well as for the purpose of determining the FV analysis but this time for a composite orthotropic laminated conical as well as a single isotropic conical shells [169]. Likewise, Vinh et al. [170] investigates the bending and FV behavior of a FG sandwich various plates structure. The analysis has been performed by developing a new superior first order mixed plate element (IMQ4). The parabolic distribution shear stresses has been assumed and it enhance the transverse shear stresses due to the fact that it satisfy the free condition of the transverse shear stresses at lower and upper plates' surfaces. Besides, the FSDT has been combined with the mixed FE formulation for the purpose of generating the fundamental equations of the novel element. A further study has been established by, Hadji et al. [171] which focused on examining the FV of a beam structure made of CNTRC subjected to different BCs. Besides, for generating a new refined beam method, the HP combined with trigonometric shear deformation theory (TrSDT) were employed for the purpose of developing the equation of motion and the outcome equation has been defined analytically. Additionally, the presented developed model has the ability to address the shear deformation effect as well as dealing with three unknowns just like the FSDT for Timoshenko beam with eliminating the shear correction factor. Also, the authors addressed that the CNTRC beam can be analyzed analytically under various BCs. Moreover recently the HP has been employed combined with NLC elasticity to study the FV of the FG nanoplates by, Hadji et al. [172] followed by an analytical solution for the obtained equation. Rizov [173] accomplished a delamination analysis under NL creep behavior of beam made of FGM by employing the Ramberg–Osgood stress strain relation. Ersoy et al. [174] employed the DSC as well as the harmonic differential quadratic method (HDQ) approaches for analyzing the FV of curved structural

components and annular plates as shown in Fig. 28. Besides, the governing equation of motion has been generated based on HSDT, FGM, laminated and isotropic material properties were considered. The obtained results shows that the shells' accuracy and convergence significantly affected by number of grids in the circumferential directions. Also, for capturing the demanded accuracy with high efficiency for shells; the author recommended using 11 grids in the circumferential direction. Additionally a good agreement has been observed between the obtained results and previous published data.

Avcar et al. [175] studied the enhancement of the deviation of exponent of volume fraction (VF) of CNTs on the NF of CNTRC in beam structure under various BCs. The equations of motion were found based on HP and TSDT followed by analytically solution. Furthermore, a recent comprehensive review has been published by, Alibar et al. [176] which aimed to investigate the vibrational behavior of various nanocomposites structures affected by porosity as well as CNT distribution and VF. Besides, the FGM reinforced CNTs were addressed. Moreover, Nuhu and Safaei [177] accomplished an inclusive review about analyzing the vibrational behavior of nano/microscale assemblies made of composite materials in various engineering systems such as nano actuators, biosensors, as well as electromechanical by implementing the NLC/nonclassical continuum theories of elasticity. Chakraborty et al. [178] accomplished a review paper which aimed to cover the enhancement of CNT on panel's and plates' vibrational behavior and stability. Figure 29 illustrates a pie chart of the covered literature which shows a comparison between FG-CRTRC, RD-CNTRC and 3-phase composites. Kim et al. [179] used various types of fillers such as; CNT/silver nanowire (AgNW) and others in a ternary systems for a stretchable Polydimethylsiloxane (PDMS) composite electrodes, for the purpose of examining the electromechanical behaviors. It has been observed

Fig. 28 The annular plates and curved shells schematics with various materials [174]



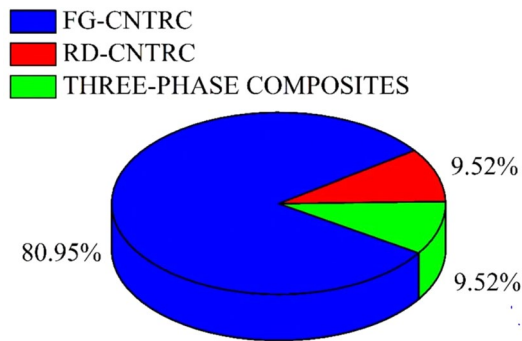


Fig. 29 A representation of the research interests in CNTRC concerning stability dynamic response and vibration characterizations in percentage [178]

that high mechanical reliability can be obtained with significant rupture strain under tensile deformation. Another remarkable outcome of tensile was that when the AgNW networks disconnected on the outer layer of the composite, it result in a fifty percent rise in resistance under extreme tensile strain. Additionally, a gradual rise in the resistance combined with remaining the electromechanical stability has been observed under large elongation values.

Jankowski et al. [180], employed the NSGT combined with Reddy HSDT for the purpose of studying the dynamic response of a smart nanobeam founded on NEMS and made of a sandwich functionally graded porous (FGP) with piezoelectric layers in various length, affected by nonlocal parameters. The results outcomes shows a diversion between FV resulted from classical and NLC approaches. Kurpa et al. [181] employed the R-function method combined with Rayleigh–Ritz approach for the purpose of investigating the FV of a sandwich plate structure made of FGM as a face layer and a core made of ceramic with various porosity distribution. Pajand and Masoodi [182] accomplished an analytical analysis for the purpose of investigation the NF as well as stability load of a curved beam columns made of FGM and considering semi-rigid connectors. In a novel study, Pajand et al. [183] investigated the static analysis of a FG non-prismatic sandwich curved beam structures. While the Ritz methodology and the total potential energy were employed to define the governing equations, although the Reddy and Timoshenko beam theories were utilized to develop the formulation. The obtained results shows that the Shear impacts were observed to be significantly greater in FG curved sandwich beams with high curve as well as low slenderness ratios. Moreover, the cross sectional type, taper ratio, and the gradient index were also found to have a substantial impact on static performances. Fantuzzi et al. [184] performed a FV analysis for various arbitrary designed FG-CNT reinforced plates, the mapping technique has been accomplished via NURBS and the FSDT has been employed

to determine the mechanical performance of the structure. Besides, the governing equation strong form has been solved by implementing the generalized differential quadrature method (GDQM). Arefi et al. [185] employed the sinusoidal shear deformation theory (SSDT) as well as the NLC elasticity theory for the purpose of analyzing the FV performance of a nanoplate made of FG polymer composite and reinforced with GNPs and based on Pasternak foundation. I Arefi et al. [186] work, the same methods were employed and the same Pasternak foundation has been utilized for the purpose of investigating the bending behavior of a multi-layered curved nanocomposite beams made of FG polymer composite and reinforced with GNPs and a shear layer has been embedded on the top of foundation. Also, several patterns dispersal of nanoplatelets were considered. Tornabene et al. [187] employed the FSDT and the GDQM for FV analysis of a laminated nanocomposite shells (conical and cylindrical) and plates in which each layer is generated as a three-phase composite that include CNT/fiber/polymer and the CNTs has been added to the polymer matrix. Tornabene et al. [188] investigated the enhancement of CNT agglomeration on the FV of the layered composite doubly curved panels and shells. Different CNT exponential dispersals as well as numerous laminations schemes along the structure thickness. The theoretical and numerical models has been performed by utilizing the Carrera’s unified formulations (CUF) and HSDT and the GDQM respectively. The authors published a further study by implementing the same methods but the aim of this study was to investigate the enhancement of CNT agglomeration on the linear static behavior of the same mentioned structures [189]. Sobhani and Safaei [190] employed the harmonic differential quadrature method (HDQ) to examine the FV of cylindrical shells structure made of the reduced Gr oxide nanocomposite (rGON) where the Halpin–Tsai (HT) homogenization technique has been utilized (which is a developed method that is used to determine the composites reinforced by nano/micro-particles) [191]. Besides, the HP, the general shell theory combined with the FSDT were employed to determine the main formulas. Additionally, the following distributions of the FG types of the reduced Gr oxide; UD, FGA, FGV, FGO and the FGX. The enhancement of various distribution on the NF compared with the pure polymer has been considered.

1.7 Computational Methods in Mechanics

The meshfree techniques can also be classified into numerical and analytical methods and some of these methods were classified according to, Liu [57] such as strain constructed PIM (SC-PIM), smoothed PIM (S-PIM), etc. which consist as L/NL elliptic PDEs. Also, as a NL hyperbolic PDEs SPH, MWS and LRPIM. In addition some other computational meshfree were mentioned by, Xiao et al. [192] such as;

discontinuous deformation analysis (DDA), material point method (MPM), as well as the discrete element method (DEM). Although there are many other analytical methods which are in used to analyze solid mechanics and fluid mechanics such as; FEM, finite difference method (FDM), (BEM), Finite volume method (FVM), smoothed FEM (SFEM), and eXtended FEM (XFEM) [192]. Besides, the most communal difficulties that faces the progress in computational mechanics software's are summarized in Fig. 30. Also, Fig. 31, illustrates the various types of programming languages implemented in analyzing computational mechanics with it is s advantages as well as it is shortcoming [192]. It is worth to mention that the SFEM methodologies consist as a group of methods developed by combining the standard FEM with some meshfree approaches which leads to have higher accuracy and greater convergence rates than regular FEM [193]. Safaei et al. [194] utilized the unit cell methodology (UCM) to define the entire impact of various parameter on the FV of a honeycomb sandwich structure(HCSS). In addition the representative volume element (RVE) approach has been employed. The main objective of that study was to examine the stress state, modal as well as the FV analyses of the HCSS under various BCs. Besides examining the impact of various material and structure properties on the NF of (HCSS). The results were validated with analytical and arithmetical previous published data. In a further study proposed also by, Safaei et al. [195] in which the authors

analysis the HCSS as a core of a beam under static as well as harmonic loads and compare its behavior with the normal hexagonal shape sandwich as a beam core by implementing the FEA. The obtained results shows that using carbon fiber instead of metal as a skin layers for the sandwich beam have more advantages such as; higher stiffness and lighter weight. Besides, the sandwich beam strength can be enhanced by the ply angle alignment as well as layers quantity. In the other hand, the NF increased due to the rise in core thickness as well as rising the skin layers, in another words increasing the height of the core will influence the NF and the shear stress. The most popular meshfree methods and meshbased methods which are utilized in the computational mechanics are illustrated in Fig. 32.

Sheikh and Behdinin [196] presented a comprehensive review for the implementation of significant discrete scale as well as multiscale computational techniques for analyzing composite materials. Various types of composites materials were discussed such as; metal/polymer based composites, CFRP, nanocomposites and etc. also various characterizations were presented such as; fracture and failure analysis, dynamic and FV. Ramteke and Panda [197], published an inclusive review which concentrates on linear/NL analysis of various porous graded (PG) structures', it is computational modelling as well as the experimental challenges. The review has covered vibration, linear/NL static and the transient deflection, although the stress parameters

Fig. 30 The most communal difficulties that faces the progress in computational mechanics software's [192]



Fig. 31 The various types of programming languages implemented in analyzing computational mechanics with its advantages as well as its shortcoming [192]

	Advantages	Shortcomings
C/C++	<ul style="list-style-type: none"> Oriented-Object Scalability 	<ul style="list-style-type: none"> Pointer Garbage Collection
Fortran	<ul style="list-style-type: none"> Performance Parallel Scientific Computing Complex 	<ul style="list-style-type: none"> Hard Package Readability
Python	<ul style="list-style-type: none"> Library Communities 	<ul style="list-style-type: none"> Memory Footprint
MATLAB	<ul style="list-style-type: none"> Productive Interactivity Matrix Simulink 	<ul style="list-style-type: none"> Slow Paid Portability

were considered. Another comprehensive review has been published by, Gierden et al. [198] where the authors were interested in the FE-Fast Fourier transformation (FE-FFT) methods based on the 2-scale methodology, which have been utilized for computational mimic of macroscopic material performance and the microstructure evolution. Geers et al. [199] presented a review which focused on investigating the developed multi-scale computational homogenized methods. The review covers various issues such as first order homogenization in solving mechanical systems, thin structure beams as well as shells as shown in Fig. 33, thermal problems and others. Cueto et al. [200] published an inclusive review about the natural neighbor Galerkin methodologies (NEM) which cover the explanation of Laplace and Sibson in fluid and in solid mechanics. In addition, the authors, highlighted some drawback of meshfree method such as; handling of secondary variables, imposing the essential BCs. Lorong et al. [201] evaluated and highlighted the most recent innovations in computational mechanics' involvement in the computer modelling of machining and blanking. Besides, the contribution of computational mechanics which has been developed at a very global scale entitled macroscopic scale, while it required an illustration of the deformations of the part. Furthermore, the FD can be considered as a good alternative for solving homogenization issues in heterogeneous multi scale methodology [202]. Rafiei et al. [203] presented analytical simulations for a double skin composite wall shear strength and the resulted outputs were validated. In an

earlier study, Rafiei et al. [204] developed FE model for the purpose of mimic the performance of a unique composite shear wall system subjected to in-plane loading. Artioli et al. [205] employed the high-order virtual element approach for the purpose of solving the homogenization problem in NL composites with long fiber. Nevertheless, the same method has been implemented by, Marino et al. [206] to investigate the homogenization of polycrystalline materials.

However, the self-consistent clustering analysis (SCA) has been utilized by [207, 208] to investigate the NL mechanical and damage behaviors of a braided woven composites. Civalek and Akgöz [209] investigated the FV of a microscale annular sector as well as sector shaped graphene with an EF (Winkler-Pasternak) by implementing the NLC elasticity method. The numerical solution was found by employing the DSC. Also, the thin plate theory has been employed combined with 8 nodes curvilinear element in order of converting the governing equation of motion to a computational region. Besides, various BCs set and NLC parameters were considered. In an earlier work, Civalek [210] employed the DSC for the purpose of examining the FV as well as buckling behavior of a various structure of composite plates. Although the computational domain has been mapped through employing the geometric mapping transformation with a 4 nodes element. The validation results prove that the DSC is an accurate simple algorithm for analyzing the mentioned system. The same author utilized the same method in a further study [211] to investigate

Fig. 32 The meshfree methods and meshbased methods utilized in the computational mechanics

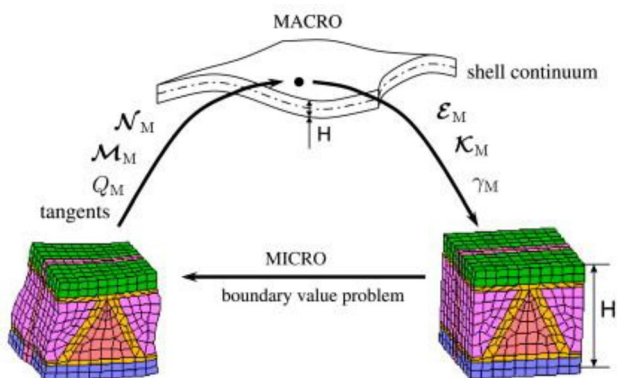
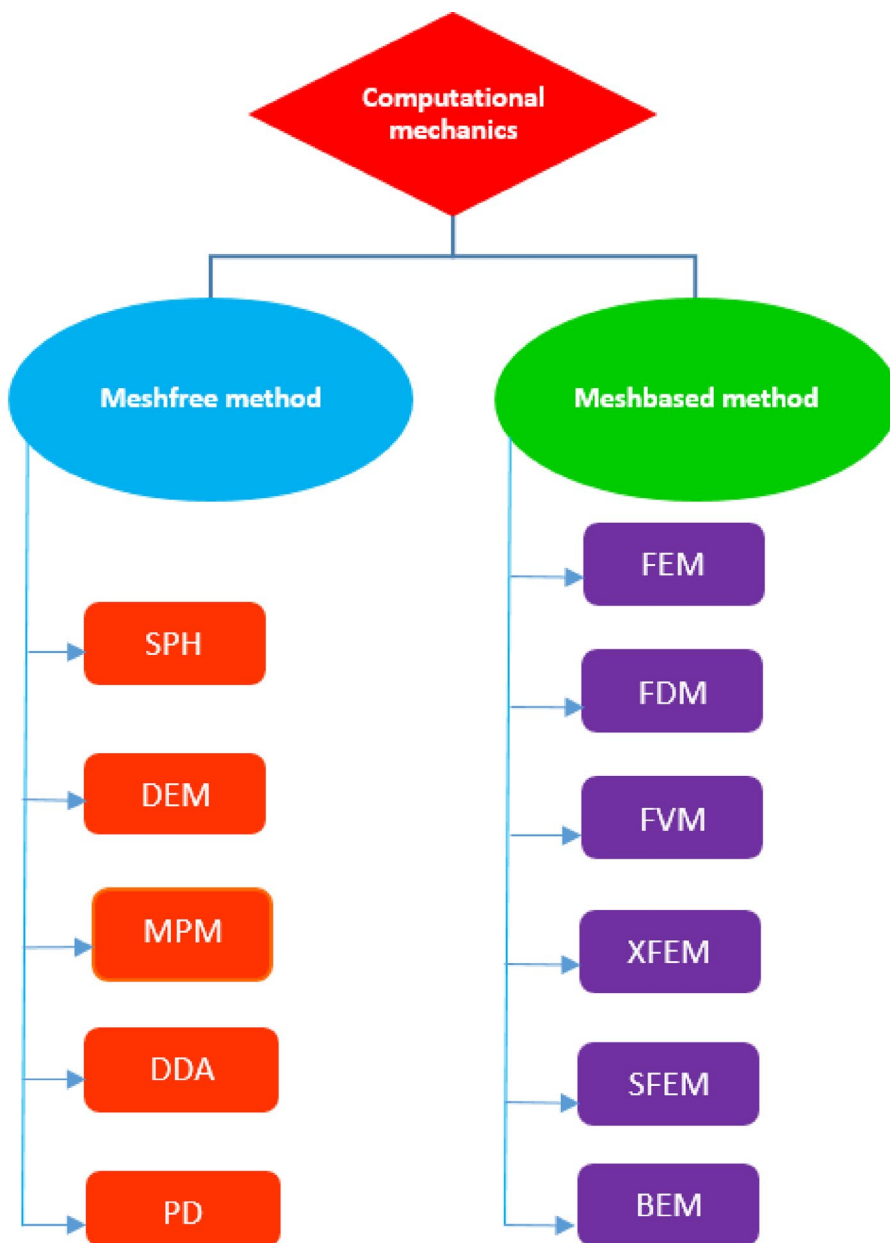


Fig. 33 Schematic of a shell in 2-scale homogenization problem by thickness representative volume element (RVE) [199]

the FV of a straight-sided quadrilateral plates where the geometrical transformation has been employed for the purpose of converting the BCs and the GEs to a square computational domain. By validating the results a remarkable accuracy and convergence were obtained compared to exact and numerical solutions. The HDQ has been employed in an earlier study by, Civalek and Ülke [212] for the purpose of examining the linear bending behavior of a circular plates both analytical and numerical solutions were presented. Also, the error-grid numbers relationship has been calculated by HDQ, FE, DQ and FD. Civalek [213], employed the HDQ in a novel study for the purpose of investigating the NL of a thin isotropic plates with a rectangular geometry based on Winkler-Pasternak EF subjected to different types of dynamic loads. The

obtained results prove that the Pasterank parameter (G), has less effect on the plate displacement than the Winkler parameter K . Besides, a reduction in the plate deflection has been observed due to the increasing in G . The modified strain gradient elasticity theory (MSGT) has been implemented by Akgöz and Civalek [214] for the purpose of studying the buckling behavior of a protein microtubules, and the Matlab code has been generated based on the MSGT. Various mode numbers, lengths, and material parameters were chosen to examine the enhancement of scale effect and material parameters on the buckling performance. Jalaei et al. [215]

employed the Navier's and inverse laplace transform methodologies for the purpose of solving the GEs which obtained by Hamilton's variation in a study focused on investigating the transient response of porosity-dependent viscoelastic FG nanobeam subjected to a dynamic load in a magnetic fields as shown in Fig. 34. Besides, the Kelvin-Voigt visco constitutive model was implemented to examine the model's internal damping effect. Additionally the effect of thickness stretching has been studied through the implementation of nonlocal strain gradient theory (NSGT).

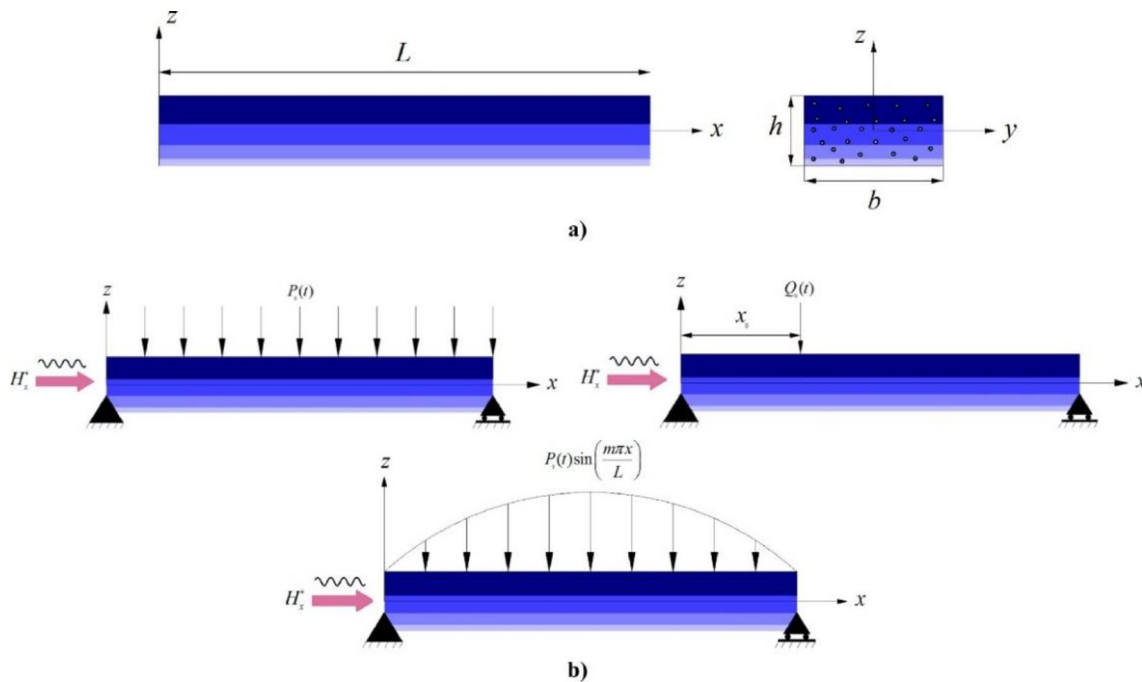


Fig. 34 The schematic of **A** the nanobeam made of visco-imperfect FG, **B** The porous FG in nanobeam under dynamic loading excitation and magnetic field [215]

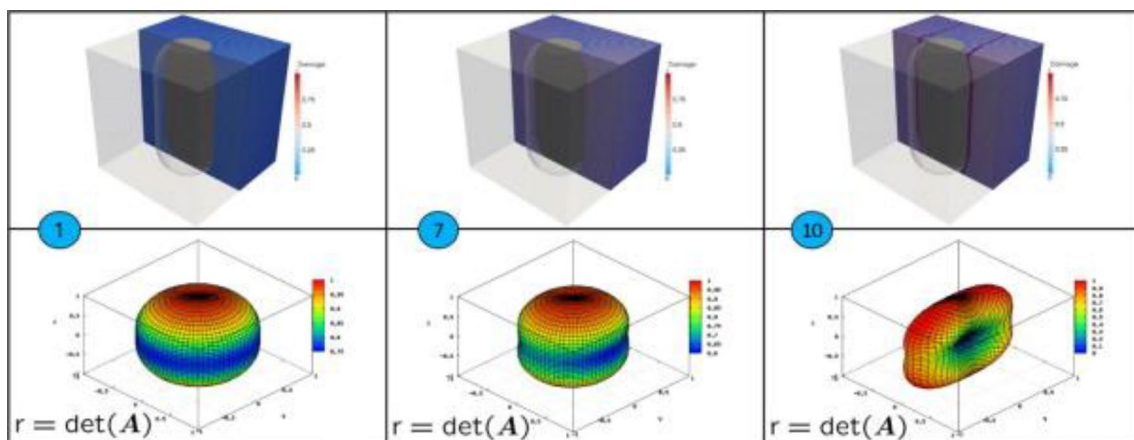


Fig. 35 The onset macroscopic failure detection through acoustic tensor [216]

For the purpose of detecting the macroscopic failure through acoustic tensor in macroscale as illustrated in Fig. 35, Spahn et al. [216] employed the FEM combined with FFT- for micro formulation. The macroscopic destruction behavior has been predicted using NL material properties generated by microscopic physical phenomena on a smaller length scale. Additionally, for computational simulation of periodic microstructures recently the FFT-based method has been demonstrated to be a quick and accurate tool [198].

Recently, Numanoğlu et al. [217] investigated the FV, thermomechanical and size dependent of a nanobeam. HP has been implemented based on the Timoshenko beam theory to obtain the size dependent dynamic formulas, then combined with the stress formula of the NLC elasticity approach. While the eigenvalue problem has been solved by FE and separation of variables total methodology. Also, the local NLC stiffness as well as mass matrices were generated through the WR approach of finite element analysis (FEA). Suchde et al. [218] accomplished a review about point cloud generation (PCG) and its implementations in meshfree methodologies. Various approaches and software employed for PCG in meshless, although the initial territory discretization processes for the time dependent issues has been addressed. Additionally, a car model has been presented and analyzed followed by generating a mesh with a node density similar to Gmsh FE mesh generator. Figure 36, illustrates the generated mesh with PCG that created by vertices of mesh. Safaei et al. [219] employed the FEA to investigate the CBL and bending of a sandwich beam made of carbon foam as a core and the outer face sheets made of carbon fiber under thermal as well as axial compression loads. Also, the heat distribution along the sandwich layers has been examined. The author of that study recommended using the aerogel instead of fiberglass as an insulation in electronics and aerospace industries based on

their unique obtained results. Balokhonov et al. [220] suggested an approach for digital modelling of a 3D structure of materials with reinforced particles of complex irregular shapes which has been identified experimentally, which implied that the scale invariance of natural mechanical disintegration. The particles were distributed at random across the matrix and coating computational domains to construct two-phase structures of metal-matrix composites (MMCs) as well as coatings of varying spatial sizes. Nevertheless, where resilient coatings and composites material are becoming gradually more important in various industrial applications which are considered as main application of tungsten carbide (WC) nanoparticles, Asmael and Memarzadeh [221] presented a comprehensive review that focused on the latest accomplishments as well as challenges facing the electrochemical machining of WC. Fallahi et al. [222], employed a high order 1D computationally effective model founded based on the framework of CUF for the purpose of studying the enhancement of fibers orientation path on the mechanical performance (stability and FV) and to analyze the variable angles in tow panels statically. However, many researchers shows interesting in studying the mechanical properties of various composite materials by implementing the MD approaches [223–231]. Pajand et al. [232] studied the NL performance of FG sandwich shells as well as plates by implementing the equivalent single layers method (ESL) with rule of mixture methodology. The investigation has been accomplished by FEA and numerically, where in FEA for structural discretization has been obtained through employing a triangular shell element, and for justifying the locking problems the mixed interpolation of the Tensorial components methodology (MITC). It has been demonstrated that an extension of the unstable part of the equilibrium path as well as a drop in buckling load cause by decreasing the core E. besides, the load capacity in FG-sandwich shell and beam of two FG faces sheets with a homogenous core is

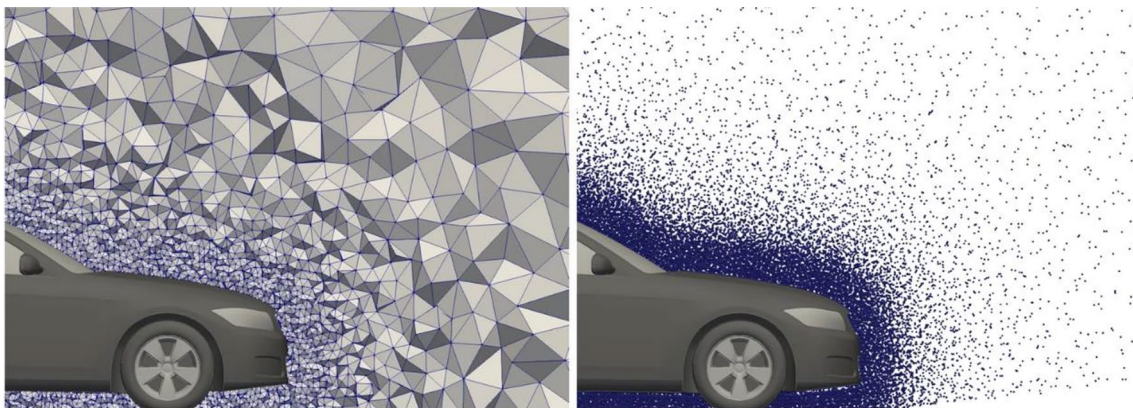


Fig. 36 The PCG around the car utilizing the Gmsh. A mesh wedge left side and the associated segment of the point cloud made up of mesh nodes right side, and the point cloud merely shows the points behind the displayed mesh slice [218]

lower than that of with FG core and homogenous face sheets. Also, the buckling load has been observed to decrease by raising the power index (n), owing to the conversion of material properties as of ceramic toward metal. Milić et al. [233] proposed a NL geometric IGA framework for a shell structure created of a composite laminates counting piezoelectric layers considered by the electro-mechanical coupling. While the Mindline-Reissner theory which include the transvers shear impact has been implemented for the kinematics of the shell. For structural discretization the NURBS, ACSHELL9 and the Shell91 (Ansys) finite elements were utilized. Milić et al. [234] employed the same approach again to investigate the same structure but in this article only NURBS has been employed to develop the formulation of the IGA shell and the Greville's points has been utilized for defining the normal vectors of the surface. Also, in this article the Mindline-Reissner theory was combined with FSDT for the purpose of maintain the level of arithmetical determination in an adequate realm.

1.8 Boundary Conditions in Solid Mechanics

There are various classifications of BCs sets that vary based on the structure aimed to investigate such as; SS, FF, CC, SF, CF, and CS these BCs can be used in beams structure. While in case of analyzing plates the BCs vary to SSSS, CCCC, CF, CF, SFSF, SCSC and FFFF. In this review the majority of mentioned studies from literature considered studying the enhancement of various BCs on buckling, bending and vibrational behaviors. Also in the studies which were interest in piezoelectric material the enhancement of BCs on electrical load has been considered. Where implementing essential BCs is an important challenge in meshless approaches. Since meshless interpolation is unable to evaluate the Kronecker delta property, and therefore enforcement of prescribed values is more difficult than using the FEM [235]. However, the authors purposed a comprehensive overview designated techniques for enforcing essential BCs in Galerkin methods. Moreover, some studies such [236], finds that in various BCs sets the estimated deflection by the designed model was always slighter than the classical approaches. To eliminate the shear locking, the CS model supposed to be applied for the thin plates [237]. The obtained results in [238] shows that there is a relationship between the enhancement of BCs with the and type of distribution of reinforcements in various structures. More significant results of the effect of BCs is presented in Tables 1, 2, 3, 4, 5, 6, 7, 8, 9 and 10. Liu and Karamanlidis [239], stated that when the chosen shape functions fulfil the Kronecker-delta characteristic therefore the essential BCs might be directly satisfied. Lei et al. [240] stated that the Kronecker delta property is not accessible through the shape function; so the authors implemented the transformation method [131], for the purpose

of enforcing the essential BCs. In that study the following sets of BCs were investigated with UD, FG-O, FG-X; SSSS, SCSC, SFSF, SSSF, CCCC and CCCF. The full transformation methodology has been presented by [241], in order to implement the essential BCs. Also, the Lagrange multipliers has been utilized to implement the essential BCs [242]. The implementation of crucial BCs in meshfree computation requires extensive CPU time owing to the loss of Kronecker delta characteristics within meshfree shape functions, Chen and Wang [243] developed a novel BCs treatments in meshless computation of contact difficulties. However, the maximum buckling load effected values were recorded in CCCC. In a novel investigation of high order plate theory, Neves et al. [244] employed the principle of displacements under CUF for the purpose of defining the BCs as well as the explicit governing equations. Wang et al. [245] employed the penalty methodology to apply the essential BCs. While the equation of motion and the BCs were obtained by employing the HP by [246]. Karami and Malekzadeh [247] focused on employing the DQM to investigate the FV of a quadrilateral thin plate various BCs were examined. It has been noticed from the results that adding a clamped BC cause an increase in the NF of all nodes in rhombic plates. Also, in trapezoidal plate the CCCC recorded higher NF values than SSSS. Furthermore, the challenge of enforcement of BCs for systems with governing differential equations as well as at least two BCs at the boundary point is one of the main difficulties in the classical utilization of DQM. Several strategies were suggested for handling this challenge. Bert et al. [248], proposed two established approximate techniques for the purpose of solving dynamic problems in structures the first methodology is a developer of complementary energy approach, and the second methodology was the δ technique which eventually emerged as the DQM. Jang et al. [249], established a static analysis (bending and stability) of different structures subjected to different BCs by utilizing the DQM. The results were compared with previous results which was obtained numerically by Galerkin. Moreover, the CCCC as well as the SSSS for the first time were subjected to thin skew plates by, Wang et al. [250] by using the DQM as well as the oblique references axes were employed.

In a recent study, Noroozi et al. [251] the obtained results shows that by applying the CCCC higher NF values were recorded than SSSS. Liew et al. [252] stated that, generally, plates having clamped ends possess a larger load carrying capacity, unless when the BCs contain a free edge (e.g., SSFC). Furthermore, the dimensionless (DL) axial compression obtained by utilizing the clamped BCs was almost doubled the DL axial compression obtained by utilizing the simply supported [253]. Artan and Batra [254] employed the initial values methodology for the purpose of examining the FV of a strain gradient beam by utilizing three different sets of BCs through considering the higher ordered

Table 1 Classification of Meshfree methods for Static bending analysis (nanoscale)

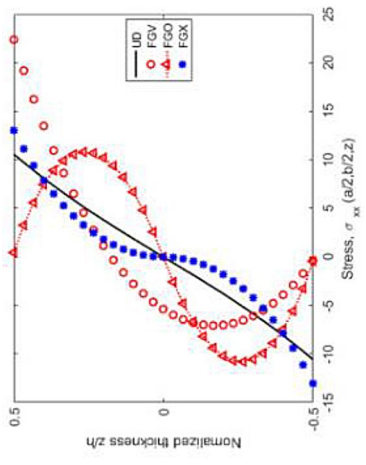
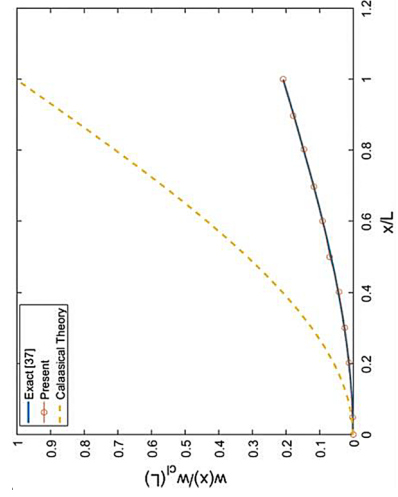
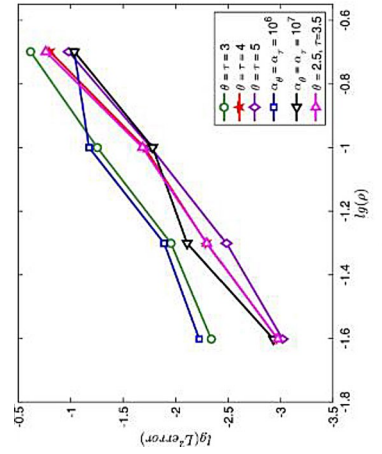
Meshfree method	Structure	Bending Analysis	Aim	Results	Output	Refs
MKI	-Nano Plate	- Uniform load	-Examine the behaviors of FG CNTRC nanoplate		<ul style="list-style-type: none"> -The presented model have high reliability and stability in different analysis -Decreasing in NF and increasing in displacement well led to stiffness-softening mechanisms -The maximum and minimum central deflections were gained for the FGX and FGO patterns, correspondingly -Anti symmetric axial stress recorded by FG-V -A symmetry axial stress has been recorded by FG-X, FG-O and UD 	[270]
Galerkin	-Beam	-Bending, torsion and indentation	-Analyzing a strain gradient of micro and nano scale beams		<ul style="list-style-type: none"> -The bending rigidity of the classical beam found to be lower than that of the strain gradient beam, implying that using classical beam theory effects remarkably on error in the obtained results 	[271]
EFG	-Plate	-Deflection Under uniform loading	-Analysis of different shapes of plates -Estimation of errors of EFG in plate bending problems		<ul style="list-style-type: none"> -The key factors enhance the convergence of EFG are: Nodal spacing, penalty factors, weight functions, number of monomial basis functions 	[5]

Table 1 (continued)

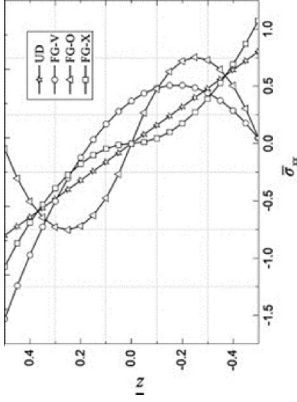
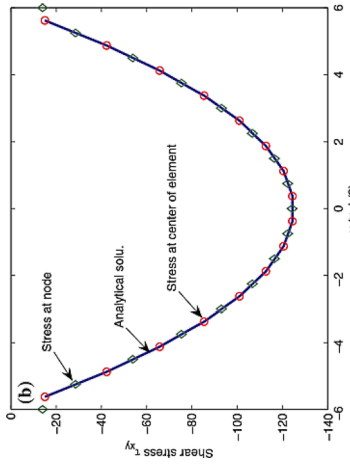
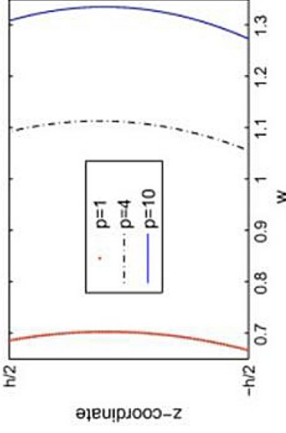
Meshfree method	Structure	Bending Analysis	Aim	Results	Output	Refs
Element-free kp-Ritz (EFkp-Ritz)	-Plate	-Different set of transverse load	-To prevent shear locking effect for very thin plates and full static analysis		<ul style="list-style-type: none"> -Different CNT scattering patterns considerably influence the NL behavior of CNTRC plates -Several types of CNTRC plates respond NL to change in BC, plate aspect, w/t ratio, and CNT content by volume -In FG-X CNTRC and FG-O and UD the central axial stress = zero 	[272]
SFEM (Galerkin)	-Rod -Beam -Plate	-Elasticity -Strain smoothing	-Fully analysis of stability, vibration and shear		<ul style="list-style-type: none"> -SFEM results are more accurate than FEM results -Domain discretization of SFEM is more flexible than FEM -The analytical solutions and the numerical solution shows to be identical 	[273]
RBF	-Plate	-Bi-Sinusoidal load	-Develop a HSDT that takes extensibility in the thickness direction into account when modeling FGPs		<ul style="list-style-type: none"> -Effect of $\epsilon_{zz} \neq 0$ exhibited importance in thicker plates and for a thinner FGPs, the σ_{zz} must be considered in the formulation -@21² grid σ_{zz} reached 1.4917 -It has been noticed that @ Grid = 17² there were no further changes in w and σ_{zz} values -A superior solution for FGM plates was guaranteed with $\epsilon_{zz} \neq 0$ the implementation of RBF collocation with HSDT provides 	[244]

Table 1 (continued)

Meshfree method	Structure	Bending Analysis	Aim	Results	Output	Refs
RBF RBF-FD	-Beam	-Uniform load	-Investigates the Timoshenko nano-beam by meshless and NLC elasticity theory		<ul style="list-style-type: none"> - Multi-quadrics RBF have been employed - Significant results were obtained by using global collocation method (GCM) - Local and NLC equation for uniform loading are almost identical - Relative error < 6% - The convergence at $\mu = 5$ observed to be excellent and smooth 	[274]
MLS	-Cylinder	-Pressure	-Analyzing nano-composite cylinder under thermal and mechanical loading		<ul style="list-style-type: none"> - Mechanical loading have higher effect on hoop stress and radial displacement than thermal loading - CNT volume has higher effect than CNT waviness on thermo-elastic dynamic behavior - The propagation speed decrease with increasing temperature environment - Both displacement and stress were observed to increase by increasing temperature environment 	[275]

Table 1 (continued)

Meshfree method	Structure	Bending Analysis	Aim	Results	Output	Refs
MLS	-Cylinder	-External and internal pressure	-Static analysis of FG-SWCNT		<ul style="list-style-type: none"> -The maximum value of hoop stress recorded for FG-V type considered as the lowest maximum compared with other types -The hoop stress in FG-V type decrease by rising the VF of CNT -Both radial displacement and hoop stress can be increase by reducing the cylinder thickness -Reducing the cylinder thickness have a remarkable impact on hoop stress distribution trends -Both CNT distribution and wall thickness effect on defining the maximum hoop stress location 	[276]
RBF	-Beam	-Transvers load	-Bending analysis by RBF and modified coupled stress theory for laminated composite Timoshenko beam SS		<ul style="list-style-type: none"> -Signiant accurate results were obtained -The length scale parameter control the changes in both rotational magnitudes and deflection of the beam -The Navier and numerical solutions were illustrated for $l=0, h/2, h$ -Good stability was obtained by numerical solution although in very thin beams 	[277]

Table 1 (continued)

Meshfree method	Structure	Bending Analysis	Aim	Results	Output	Refs
MLS	-Plate	-Uniform load	-Investigates the electro-mechanical response		-Electrical input may trigger in higher plates deflection than mechanical loads, and ZnO NWs provide higher deflection compared to GaN NWs	[278]

BCs. Zhao et al. [255] examined the vibrational behavior of thick rectangular plates made of FGP (Al/Al₂O₃) as shown in Fig. 37 analytically with arbitrary BCs. The obtained results shows that the plates with CCCC BCs recorded higher ND frequency parameters (FPs) that plates with SSSS BCs in all examined modes.

Zhao et al. [256] found that the square palates' made of aluminum/alumina and subjected to CCCC in all modes recorded significantly higher values of critical buckling temperature than the same plates' subjected to SSSS. Chen et al. [257] stated that the FGM plates under various types of edges when it is subjected to CCCC BCs it recorded greater buckling load factors than those subjected to SSSS BCs can be obtained. Ahmadi [258], observed that the NFs obtained by CC multiple-nanobeam system (MNBS) BCs were similar to NFs obtained by free-free (FF) MNBS BCs. Else, the author observed that increasing the Winkler stiffness *k* the NF of the clamped chain of triple-nanobeam system (TNBS). Pradhan et al.[259] observed that the FG cylindrical shells subjected to CC and FF BCs recorder greater values of NF than those subjected to a SS BCs. Additionally, Ansari and Darvizeh [260] stated that among all BCs alternatives, the clamped FGM shell exhibits the largest NF. Barati et al. [261] implemented an advanced four variables plate theory in a novel study for the purpose of investigating the FG piezoelectric plates' with porosity vibrational as well as the electro-thermal-mechanical performance. The results of that study shows that the DL frequency in different thermal atmospheres in (uniform, linear and nonlinear) temperature rises obtained by applying the CCCC BCs is much greater than the values obtained by applying the SSSS BCs. Besides, changing only one condition in each BCs sets to clamp can also enhance the DL frequencies. On the other hand, [262] found that the greatest fundamental frequencies (FFs)for all values of lamination angle φ were obtained by applying the SSSS BCs. Also, it has been reported that the electromechanical coupling values obtained by plates subjected to SSSS BCs is higher than the values obtained by plates subjected to CCCC. This results were found based to the fact that the CCCC allows to have more constraints which leads to have smaller range of displacement as well as rotations for nodes [51].

Natsuki and Natsuki [263] explore the enhancement of BCs and resonant frequency on the elastic modulus (*E*) of a nanowires made of CNT based on EF and subjected to a clamped BCs as illustrated in Fig. 38. The authors stated that the clamped length highly influenced the vibrational frequency reliance with an *E*, especially if $E > 1.0\text{TPa}$. In addition, owing to the calculation errors between *E* as well as vibrational frequency; the impact of the clamped BCs on predicting the *E* cannot be neglected. Wang et al. [264] employed the Adomian decomposition methodology combined with the modal analysis to proposed an iterative

Table 2 Classification of Meshfree methods for Static bending analysis (microscale)

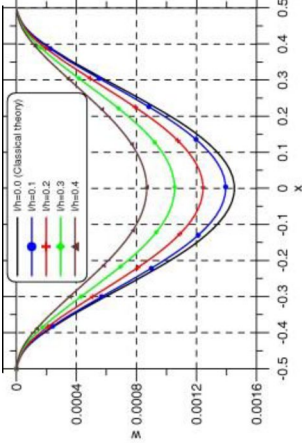
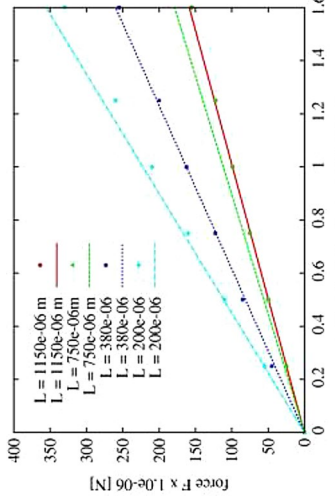
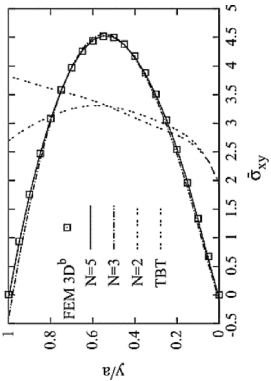
Meshfree method	Structure	Bending Analysis	Aim	Results	Output	Ref
Method of fundamental solution (MFS)	–Plate	–Deflection	–Static analysis for developed new model of Kirchhoff plate (arbitrary shapes)		<p>–Higher deflection and lower bending moment were recorded in elliptical micro-plates than rectangular shapes in SS BCs @ fixed material volume</p> <p>–@ BCs CC the rectangular micro-plates always have higher values of bending moment than elliptical plates, while the opposite is true for deflection</p> <p>–The amount of deflection that have been obtained by the classical theory is greater than the proposed theory @ all set of BCs</p>	[236]
MLS	–Beam –Sheet	–Deflection	–Modelling elastic scale effects for different micro structure by strain gradient		<p>–The results obtained from 1D and 3D micro space were almost identical</p> <p>–The transversal contraction can be neglected</p> <p>–The results for sheet analysis were similar with beam analysis</p> <p>–For large deflection in sheet, the ratio of normalized magnitude between various scaling levels were variable</p> <p>–Sheet bending results in a curvature</p>	[283]
RPF	–Beam	–Surface loading –Sinusoidal surface loading	–To study the static response of beams made of FGMs		<p>–As a suitable approximation order is utilized, 3D displacement and stress components can be estimated accurately</p> <p>–The σ_{xy} inaccurately predicted via TBT or second order theory as presented by its variation along the y-axis @ $x=0$ and $z=b/2$</p>	[284]

Table 3 Classification of Meshfree methods for Static bending analysis (macroscale)

Meshfree method	Structure	Bending Analysis	Aim	Results	Output	Refs.
Radial and polynomial basis functions	-Plate	-Pure bending mode	- FV and Static analyses for various plates		<ul style="list-style-type: none"> -Reducing the error by adding more nodes owing to the abnormality of nodal distribution -The nodal integration was applied to solve eigen equation and discrete equilibrium equation -By the mentioned formula shear locking were avoid, applicable for complex domains, and significantly stability and accuracy for extremely distributed nodes -The maximum normalized deflection = 1.015 @ approximately 120 nodes in irregular nodal distribution -To eliminate the shear locking, the CS model supposed to be applied for the thin plates -Additional stiffening effects on the structural rigidity and triggers shear locking were obtained through the shear strain smoothing 	[237]
IEFGM-(DS-MLS)	-Plate -Beam	-Stress -Displacement -Absolute error	-Improving the EGM for computational calculation and elasticity prospective		<ul style="list-style-type: none"> -Greatest accuracy solution than normal EFG method -Less CPU time 	[67]

Table 3 (continued)

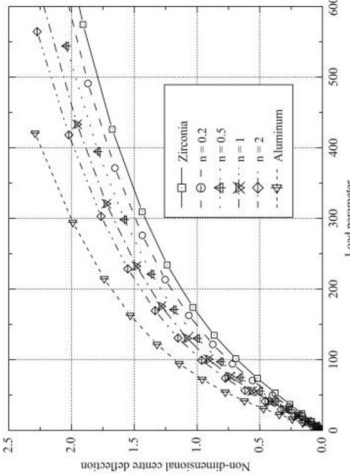
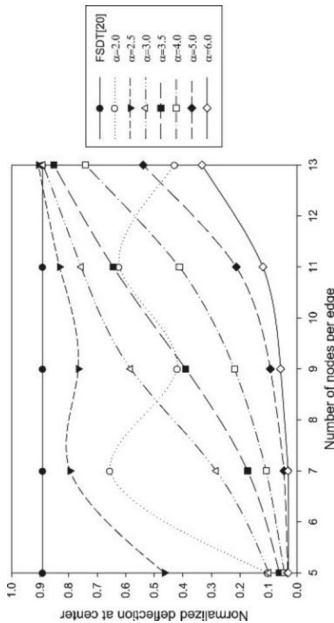
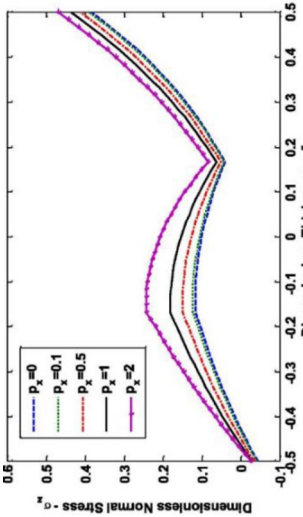
Meshfree method	Structure	Bending Analysis	Aim	Results	Output	Refs.
RKPM	-Cylindrical Shell	-Uniform radial pressure	-Analyze NL response exposing mechanical and thermal load and to evaluate the bending stiffness		<p>-The DNI has been utilized to exclude shear and membrane locking</p> <p>-It has been observed that by increasing the load the central displacement has grow</p> <p>-The panels displacement which corresponds to small exponent is significantly lower than that of panels corresponds to great VF exponent</p>	[304]
MKI	-Plate	-Uniform load	-Analyzing the mechanical behavior of FGP		<p>- When different sets of nodes employed, the scaling factor affects the normalized deflection at the center of the FG plate</p> <p>-As the gradient index increases the deflection magnitude increase</p> <p>-The results accuracy declines when $2.0 < \alpha < 3.5$. For $\alpha > 4.0$</p> <p>- The central deflection meets to literature solutions achieved by implementing the FSDT</p>	[305]
SSPH	-Beam	-Uniform load	-Investigates the bending behavior of various 2 directional FG-beam sandwich structures		<p>-As the gradation exponent in x-direction rise up the Max. Normal stress on the outer surface of the structure with all thickness ratio except ratio 1-8-1 will increase. While it decrease @ the top surface of 1-8-1</p> <p>-@ the top and bottom external surface of the structure $\tau = 0.0$</p> <p>-@ a point between the core (1D FG) and the top skin (2D FG) a quick drop in shear stress is observed</p>	[306]

Table 3 (continued)

Meshfree method	Structure	Bending Analysis	Aim	Results	Output	Refs.
MLS Galerkin	-Plate	-Out plane uniform load	-Investigate stiffened circular plates by FSDT and meshfree		-Higher deflection values were recorded by the flat plate than the stiffened plate, due to the constraint effect	[307]
MORBF	-Beam	-NL bending	-Investigates the FGP for NL bending		-The lowest deflection values were recorded @ CC BC under UDL with $n=0$ - α the porosity VF has a remarkable impact on the NL bending behavior -As increase the central deflection of the FGP beam will increase too @ fixed values of n (power law index)	[238]

(a) Deflection u_3 versus load P for C-C FGP beam under UDL ($n=0$)

Table 4 Classification of Meshfree methods for Static buckling analysis (nanoscale)

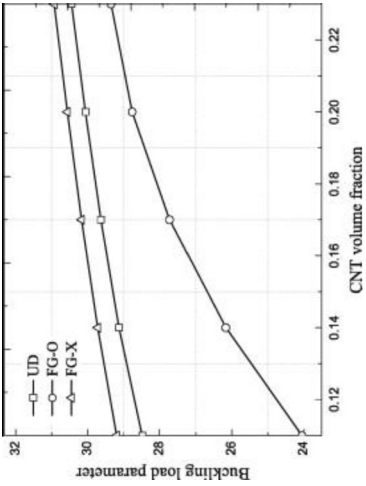
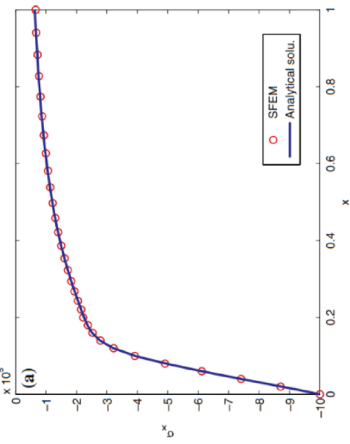
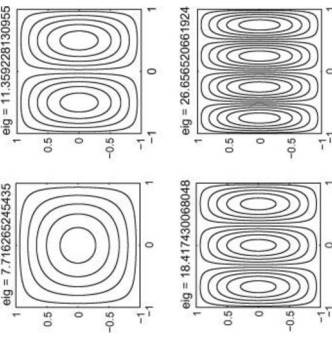
Meshfree method	Structure	Buckling Analysis	Aim	Results	Output	Refs.
kp-Ritz	-Plate	-Uniaxial compressive pressure	-Buckling investigation of (FG-CNTRC) exposing numerous in-plane mechanical loads,		<ul style="list-style-type: none"> -The BC and buckling strength of CNTRC plates significantly affected by ΔT, loading, plates aspect ratio w/t ratio and volume % of CNT -The buckling load parameters has greater values at greater VF of CNT since the CNTRC plates' stiffness is bigger at a higher CNT VF values -The greatest buckling load values were recorded in FG-X plates 	[240]
SFEM (Galerkin)[193]	-Rod -Beam -Plate	-Stability -Tensile load -Pressure load	-Fully analysis of stability, vibration and shear		<ul style="list-style-type: none"> -SFEM results compared to FEM results seems matching -Domain discretization of SFEM is more flexible than FEM -All computed stresses and displacements were in good settlement with the analytical results 	[273]
RBF	-Plate	-Buckling load linearized	-Develop a HSDT that takes extensibility in the thickness direction into account when modeling FGPs		<ul style="list-style-type: none"> -Outcome of $\epsilon_{zz} \neq 0$ exhibited importance in thicker plates. Also, for a thinner FGPs, the σ_{zz} must permanently considered in the formulation 	[244]

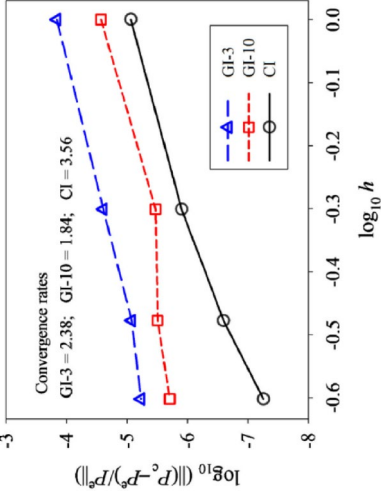
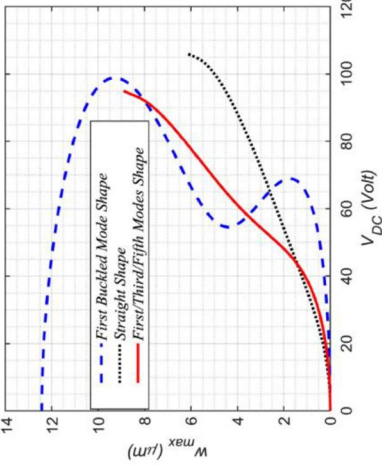
Table 4 (continued)

Meshfree method	Structure	Buckling Analysis	Aim	Results	Output	Refs.
RBF RBF-FD	-Beam	-Uniform load	-Investigates the Timoshenko nano-beam by meshless and NLC elasticity theory		<ul style="list-style-type: none"> - Multi-quadrics RBF have been employed - A local collocation method has been employed - Relative error < 3% - At $a/h = 10$ and 20 excellent convergence has been obtained - At $a/h = 100$ the problem size effects the convergence 	[274]
MLS	-Plate	-Uniaxial compression	-Investigates the buckling and the thermal vibrational of the FG-CNTRC		<ul style="list-style-type: none"> - Decreasing the t/b will decrease the CBL - The greatest buckling load value was recorded in FG-X distribution - The smallest buckling load value was recorded in FG-O distribution - As ν_f rise up to 0.17 the CBL will increase - Under uniaxial load condition, increasing the length-to-width (l/w) ratio will cause a reduction in CBL 	[245]
RPIM	-Plate	-In plane edge load	-Investigates FV and buckling behavior of FG-GPLRC		<ul style="list-style-type: none"> - Increasing cut-out size for all the shapes of the cut-out, will lead to reduce CBL - A reduction in CBL parameter means that the system stiffness reduce as well, and it is caused by increasing the size of the cut-outs 	[251]

Table 5 Classification of Meshfree methods for Static buckling analysis (microscale)

Meshfree method	Structure	Buckling Analysis	Aim	Results	Output	Ref
Kp-Ritz	-Plates	-Uniaxial biaxial compression load	-Investigates the postbuckling behavior for laminated composite plates		-Diverse types of laminated composites plates were examined (cross-ply, isotropic plat, angle ply) -The linear/NL eigenvalue were analyzed -The results for both postbuckling and buckling were identical with previous published data for FEM -The computed displacement found to be in acceptable agreement with the series solution -A snap-through instability has been observed by applying the SSSC and SSSC	[252]
MK	-Cylindrical	-Axial compression	-Analyzing the postbuckling and axial NLB reactions of the random checkerboard composites structure by developing the MK meshfree method of microshell		-The importance of the stiffening property corresponding to the rotation gradient tensor expands with increasing GNPs VF -By decreasing the l/w aspect ratio for GNPs reinforcements for a specific value of GNPs VF, the role of couple stress size relying on the CBL as well as critical shortening of an axially compressed cylindrical microshell turns to be significantly important -The snap-through phenomena is detected when the postbuckling routes were traced -The stability of a microshells under axial compressive load increase as the CBL enhances by the increased in GNPs' volume fraction	[253]
RKPM	-Cylindrical	-Axial compression	-Postbuckling analysis of CNTR-FG		-The postbuckling behavior may slightly effected by the changing in the BCs of the unloaded edges -An observation of sudden decreasing changes in the postbuckling strength by changing the BCs from CC to supported on the loaded curved edges -The postbuckling response significantly affected by the BCs	[326]

Table 5 (continued)

Meshfree method	Structure	Buckling Analysis	Aim	Results	Output	Ref
Galerkin MLS RKPM	–Plate	–Buckling load	–Investigates the FV and buckling responses of thin plate strain gradient	 <p>Convergence rates $GI-3 = 2.38$; $GI-10 = 1.84$; $CI = 3.56$</p>	<ul style="list-style-type: none"> –As the internal scale parameter l the CBLs will increase –The critical loads improve with enhancing the boundary constraint increases –The Classical BC higher impact than high order on the CBLs –GI-10 accuracies much greater than the GI-2 –CI considered as the greatest accurate methodology and it demonstrates the superiority of CI with smoothed gradients 	[327]
Galerkin	–Beam	–Compressive axial load	–Examine the effect on incorporating the impact of the snap-through buckling in an electrostatic shallow arched. Besides, investigate the displacement performance		<ul style="list-style-type: none"> –The proposed curved beam design's continuous snap-through instability resulted in a magnitude greater displacement over a parallel-plate actuator with equivalent geometrical dimensions and equal operating conditions –Only the first and fifth modes of the predicted first three symmetric buckling modes to delineate the first curvature of the shallow arch microbeam had significant effects on the micro-actuator performances –The straight profile exhibited a incessant deflection toward the minor stationary electrode and supreme deflection of $6 \mu m$ 	[246]

model for the purpose of investigating the forced vibration behavior of a NU beam with NL BCs (hardening NL spring boundary). It has been observed that, the degree of nonlinearity reflected in the vibration response differs with varied base excitation amplitudes with the fixed NL supported spring parameters. Besides, the beam VA and its period remained within a particular boundary stiffness range varied with the extent of boundary nonlinearity under the same base motion excitation. While the excitation frequency as well as the amplitude were defined, the vibration status can be modified by modifying the NL spring property. However, that study solution can be considered as an initial step for further studies of investigating the vibrational performance of NU beams with various NL BCs subjected to diverse excitations.

2 Static Analysis

2.1 Bending Analysis

2.1.1 Bending Analysis in Nanoscale

Significant reliable bending results of impact of the embedding nanofillers and stress responses as well as to static electromechanical deflection of the SMP were obtained. The examined structure of FG nanocomposite porous plates under static electromechanical load is shown in Fig. 39 [265]. Safaei et al. [266] have applied the EMT's approach with HSDT combined with a MLS meshfree method and the meshless for of strain to investigate mechanical loading (static bending) and thermal gradient of the PNSPs with the FG CNT porous core of clusters/polymer nanocomposite layers.

By applying three different uniform case load 0, 500, 100 kPa to study the central deflection performance for the PNSP with square geometry and SS, subjected to a thermal gradient load on. The result shows that intensified deflection is caused by the direction of the moment at $T_b > T_t$. In addition, by applying a thermal gradient loads the mechanical deflections observed to be moderated specifically when $T_b < T_t$ as shown in Fig. 40. Besides, Fig. 41 illustrates the unique sandwich plate structure reinforced CNT.

Dastjerdi and Aghadavoudi [267] investigated the deflection and the stress distribution in sandwich plates presented in Fig. 42 by the first-order shear deformation theory (FSDT) founded on meshfree method and the MLS meshfree approach has been employed for approximating the displacement field. Remarkable results were recorded at CNT VF = 5% and six vacancy defects in the CNT configuration caused a rise in the sandwich plate deflection up to 41.67%.

For analyzing the bending performance of the FG nanoplates with diverse geometries, the nonlocal strain gradient

meshfree method (NSGM) based on NSGT and HSDT were employed. Additionally, moving kringing (MK) meshfree method was employed to resolved the deflection [268]. It has been observed from the obtained results that the displacements decreased when length to thickness ratio (l/t) increased. For the increased in n , strain gradient parameter and the NLC parameter the displacement increase and decrease. Chinh et al. [269] employed the point interpolation (PI) meshfree method which is a combined of RBF with the polynomial basic function (PBF). For the purpose on analyzing the static behavior for a sandwich beam structure with a porous core that has vary mechanical properties through the depth direction, and with a FG face sheets as illustrates in Fig. 43. The obtained results shows that the 1–8–1 beam with a higher soft-core ratio softens and has more defections than the 1–2–1 beam. Besides, as the power low index (k) goes up, the beams deflection decreases. The reason for this is due to the fact that the effective elastic modulus of FGMs improves as k rises. Additionally, by analyzing the effects of the porosity coefficient (e_0) on the DL transverse displacement at the mid-span of thick beams ($L/h = 5$) and thin beams ($L/h = 20$) for three types of BCs SS, clamped-hinged (CH), and CC. It has been observed that the displacement is greatest for SS beam and least for the CC beam.

2.2 Bending Analysis in Microscale

The mechanical load has been applied to the CNTR-FG cylindrical panels and caused a large deflection; for studying this deformation through geometrically NL analysis, Zhang et al. [279] applied the Kp-Ritz approach. CNTs were considered as classified in the thickness direction of the cylindrical panel, as well as effective material characteristics were evaluated using an Eshelby–Mori–Tanaka-based micromechanical model. The formulation relies on the FSDT. The RKPM approximates the two-dimensional displacement field. To enhance computational effectiveness and to prevent shear and membrane locking, the stabilized conforming nodal integration scheme has been implemented to evaluate bending stiffness of the system. Additionally, the direct nodal integration (DNI) methodology was used to determine the membrane and shear terms. It is observed from Fig. 44 that when CNT is increased by volume, the ND central deflections decrease. This phenomenon was observed also at different types of CNT panels.

Thai et al. [280] accomplished a bending analysis of FG isotropic microplates exposed to sinusoidal distributed transverse load and a homogeneous square microplate SS exposed to sinusoidal dispersed load. In both cases results were validated and compared to insure the chosen method reliability. The results show that the meshfree method guaranty a remarkable reliability of the fundamental sizes for support domain. Besides, rising the material l/t led to

Table 6 Classification of Meshfree methods for Static buckling analysis (macroscale)

Meshfree method	Structure	Buckling Analysis	Aim	Results	Output	Ref
RKPM	-Plate -Beam	Tension	-Developing accelerated, convergent and stable nodal integration for RKPM	<p>(d)</p>	<p>-Owing to the implicit gradient construction, significant efficiency is accomplished, and the method's complication is comparable to that of DNI</p> <p>-The ideal convergence for nodal integration was demonstrated to require both stabilization and vibrational consistent integration</p> <p>-Provides stable solutions for huge deformation issues</p> <p>-As contrasted to the experimental data, the spurious modes in the unstabilized nodal integrations produce very poor performance</p>	[332]
Galerkin	-Plate	-Compression	-Providing a suggestion for an FSDT meshfree methodology to examine buckling and FV of rectangular stiffened plates		<p>-The critical stress obtained 196.59 kPa @ plate thickness 1.5 m</p> <p>-The critical stress obtained 456.7 kPa @ plate thickness 3 m</p>	[333]
RKPM		-Uniaxial compression -Pure shear loading	-FV and stability analyses of shear-deformable plates		<p>-Absence of shear and membrane locking</p> <p>-A generic particle is impacted with other particles inside its area of influence during numerical implementations; typically, the values should be sufficiently high to prevent singularity of the stiffness matrices</p> <p>-Maximum shear buckling factor $K_s = 9.5$ and recorded @ aspect ratio = 1</p> <p>-By raising the value of t/b the buckling load intensity factor will decrease</p>	[334]

Table 6 (continued)

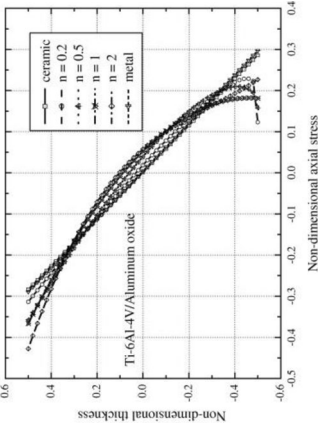
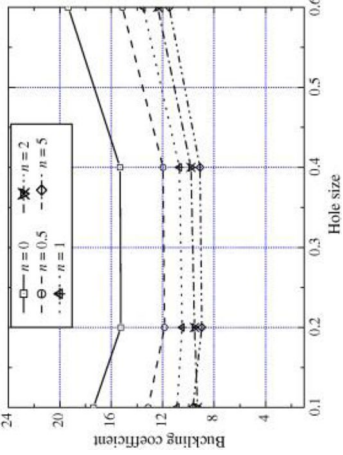
Meshfree method	Structure	Buckling Analysis	Aim	Results	Output	Ref
Kp-Ritz	-Plates	-Axial stress -Mechanical load	-Study the NL behavior subjected mechanical and thermal load		<p>The stabilized compatible nodal integration technique was employed for the purpose of calculating the bending stiffness</p> <p>The shear locking was eliminated</p> <p>A noticeable influence on the displacement has been noticed caused by the VF exponent in plates exposing thermal and mechanical load</p> <p>The VF exponent highly influence defining the distribution of the axial stress close to the top and bottom surfaces</p> <p>A compressive stress has been observed on the plates' top surface, while a tensile stress on the bottom surface</p> <p>The lowest tensile stress has noticed on the plates with $n = 0.2$</p> <p>Plates made of metal or ceramic recorded the highest tensile stress values</p>	[355]
Kp-Ritz	-Plates	-Uniaxial mechanical and thermal load	-Analyzing different geometries of FGPs ceramic-metal		<p>Shear locking were avoided</p> <p>The hole size and VF exponent have a major impact on a plate's buckling load and buckling mode</p> <p>The BCs have influence on buckling mode</p> <p>When the VF exponent rises, the buckling load decreases, while if it decreases the first mode's CBL initially decreases; and the buckling load initiates to escalate when the hole size rises further</p> <p>The range of the VF exponent (0-5)</p> <p>The range of width of the square hole size a_y/a (0.1-0.6)</p>	[256]

Table 6 (continued)

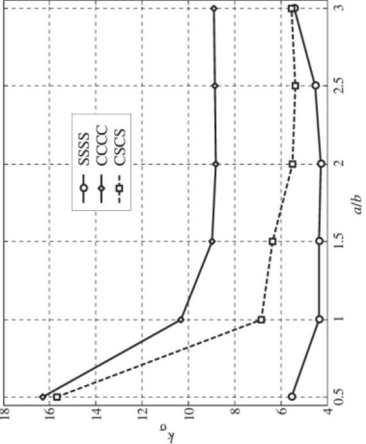
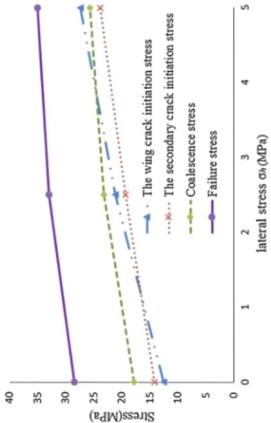
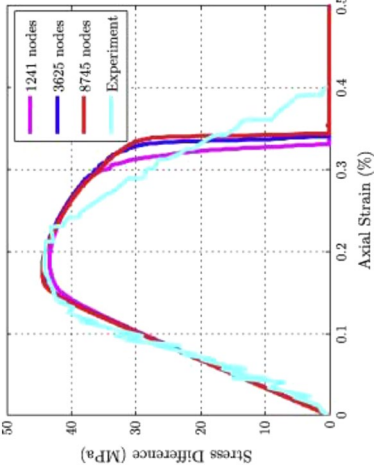
Meshfree method	Structure	Buckling Analysis	Aim	Results	Output	Ref
RBF	-Plates	-Pin load -Partial uniform load -Parabolic load	-Investigates the buckling behavior of FGM rectangular plates under various load case	 <p>The graph shows the buckling load factor K versus the aspect ratio a/b for three boundary conditions: SSSS (solid line with circles), CCCC (dashed line with squares), and CSCS (dotted line with triangles). The x-axis ranges from 0.5 to 3, and the y-axis ranges from 4 to 18. SSSS and CCCC show a sharp increase in K as a/b increases, while CSCS shows a more gradual increase.</p>	<p>-The buckling load factors for SSSS BCs were smaller than for CCCC BCs</p> <p>-The stress must be uniformly distributed @ a point where there the edge size is smaller than the distance from the edge</p> <p>-The present ND stresses σ_{xx}^0/σ_0 far away from the midpoint of the edge is much more smaller than the stress close to the midpoint of the edge</p>	[257]
GPD	-3D solid	-Uniaxial and biaxial compression	-Simulating the initiation, propagation and combination of 3D preexisting pungent and embedded flaws -Study the failure process	 <p>The graph plots Stress (MPa) on the y-axis (0 to 40) against lateral stress σ_x (MPa) on the x-axis (0 to 5). It shows the progression of stress from crack initiation to failure. Key points include: wing crack initiation stress (blue dashed line), secondary crack initiation stress (red dotted line), coalescence stress (green dash-dot line), and failure stress (purple solid line).</p>	<p>-The wing cracks growth length in the specimen exposed to biaxial compression is shorter than wing cracks exposed to uniaxial compression</p> <p>-@ lateral stress > 2.5 MPa, the wing cracks were started after the second cracks</p> <p>-Increasing the lateral stress will increase the failure stress and coalescence stress</p> <p>-Numerical and experimental results were in good agreements</p>	[336]
Galerkin (nodally regularized)	-Cylinder	-Uniaxial compression	-Analyzing the large deformation of 3D fragmentation concrete structures	 <p>The graph shows Stress Difference (MPa) on the y-axis (0 to 50) versus Axial Strain (%) on the x-axis (0 to 0.5). It compares experimental results (cyan line) with three numerical models: 1241 nodes (purple line), 3625 nodes (blue line), and 8745 nodes (red line). The numerical models show a peak in stress difference around 0.25 axial strain, followed by a sharp drop, which closely matches the experimental data.</p>	<p>-The positive value of stress-strain with different discretization indicates the compression and the legend denotes the number of nodes in the discretization</p> <p>-A well correlation between the study results of the stress-strain responses and the stress-strain response obtained experimentally in earlier studies</p> <p>-Absence of remarkable mesh sensitivity within the 2 level of the smoothing algorithm</p>	[337]

Table 7 Classification of Meshfree methods for free vibration analysis (nanoscale)

Meshfree method	Structure	Dynamic Analysis	Aim	Results	Output	Refs.
EFG	-Cylindrical	-Mode shapes -NF	-Investigates the enhancement of nanotube curvature on the overall elastic characteristics of the nano-structured composite cylinder		<ul style="list-style-type: none"> -The sensitivity of frequency response (FR) and the effective moduli reduced by increasing the waviness -The effective reinforcement of the nano-composites is remarkably decrease by the waviness -The impact of various parameters on NF were studied -The first (FPs) shows to increase by increasing the thickness 	[360]
SFEM (Galerkin)	-Rod -Beam -Plate	-FV	-Fully analysis of stability, vibration and shear		<ul style="list-style-type: none"> -The arithmetical results were in good agreements with exact solution results 	[273]
GCM	-Plate	-FV	-Determine the FGPs sandwich plate's FV		<ul style="list-style-type: none"> -The impact of dissimilar layers thickness ratios and a/h, material properties and BCs on NF of the sandwich plate structure were observed -The nth-order shear deformation theory are applied 	[361]
RBF	-Plate	-FV	-Develop a HSDT that takes extensibility in the thickness direction into account when modeling FGPs		<ul style="list-style-type: none"> -When $\epsilon_{zz} \neq 0$, excellent correlation with exact theories is obtained. For all values, convergence solutions are that were obtained -The CUF virtual displacements stand for the purpose of deriving the explicit GEs and BCs -Radial basis functions were combined to resolve the static and eigen-problems 	[244]

Table 7 (continued)

Meshfree method	Structure	Dynamic Analysis	Aim	Results	Output	Refs.
MLS	-Plate	-FV	-Analyze multifunctional smart sandwich plate (MSSP) by advanced and reliable technique with Reddy's TSDT		<ul style="list-style-type: none"> -σ_{zz} is insignificant compared to σ_{xx} and σ_{yy}. -Deflections were minor in contrast to the thickness of MSSP when a linear analysis was performed -There is no slip @ the interfaces of the core and piezoelectric layers. This signifies that the layers were all fully connected -Reddy's HSDT was employed to model all of the layers. As a result, no additional continuity demand is required for the layer interface -The NF can be enhanced by adding more voids along the FG symmetric pattern 	[362]
RKPM	-Cylinder	-FV	-Investigate the influence of particles dispersion and domain size on the convergence behavior		<ul style="list-style-type: none"> -The enhancement of different BCs set on the frequency was examined -The effects of lamination scheme and the cylindrical curvature on frequency were studied -The max. frequency occurs @ $\varphi = 35^\circ$ in symmetric scheme, and @ $\varphi = 45^\circ$ for the anti-symmetric scheme -The BC SSS recorded the highest FFs @ any φ 	[262]
Kp-Ritz	-Sheet/ Plate	-NL vibration	-To present numerical solution and mathematical modeling to Gr sheets		<ul style="list-style-type: none"> -@SSS, CSCS and CCCC BC's @ all side length by increasing the amplitude the NL frequency increase -As an overall the highest amount of ND frequencies was recorded @ SSS -As an overall the lowest amount of ND frequencies was recorded @ CCC -The ND frequency amplitude became more flat when the aspect ratio increase -A reduction in ND frequency amplitude was obtained due to the increase in the aspect ratio 	[363]

Table 7 (continued)

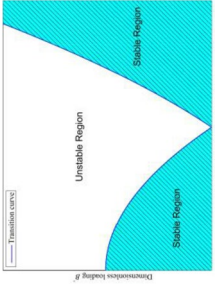
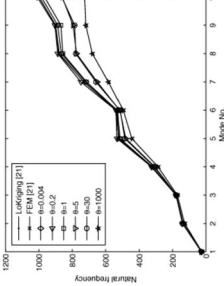
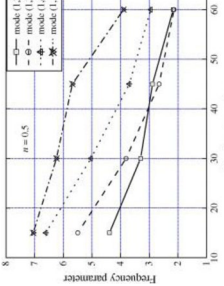
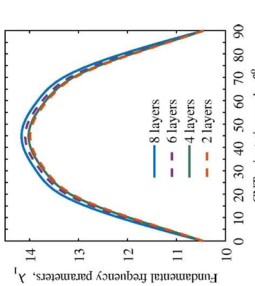
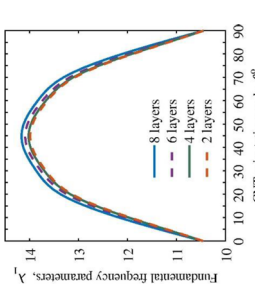
Meshfree method	Structure	Dynamic Analysis	Aim	Results	Output	Refs.
Galerkin	-Plate	-FV	-Dynamic stability analysis (linear/NL)	 	<ul style="list-style-type: none"> -As the VF in CNTs increase the vibrational amplitude will reduce -The size of stability areas grows as the volume percentage of CNTs increases -The SWCNT distribution patterns have a considerable impact on the size of stability regions 	[315]
MKI and Galerkin	-Beam	-FV	-Develop a vibration analysis under multi load cases by combining 2 meshfree methods	 	<ul style="list-style-type: none"> -The numerical damping effect reduces the accuracy of the current procedure when the time-step is considered excessively large -Even @ large number of time steps the current method provide a steady dynamic response -A good agreement of NF results with previous published results were obtained -The vibrations mode highly effect by the BC's and thickness -The change of magnitude of the frequencies is due to VF exponent -The VF exponents have slight impact on the mode shapes excluding the sequence of some higher modes 	[364]
Kp-Ritz	-Shell	-FV	-Analyzing a FGPs metal and ceramic conical shell panels		<ul style="list-style-type: none"> -Increasing the number of laminated layer lead to slightly decrease the FF -In all types of CNT distribution, increasing the orientation angel of the CNT enhance the FF 	[109]

Table 7 (continued)

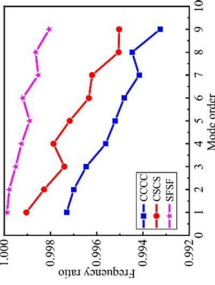
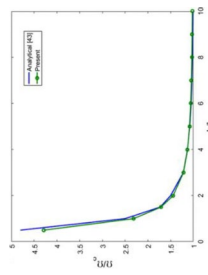
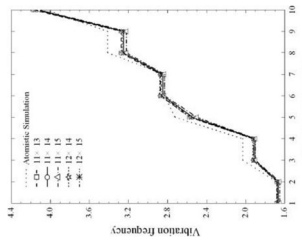
Meshfree method	Structure	Dynamic Analysis	Aim	Results	Output	Refs.
MKI	-Plates	-FV	-Analyzing the vibration of SGPs		<ul style="list-style-type: none"> -The natural frequencies estimated by classical plate model were higher than those of by NST -It is noticed that @ ultrahigh-order mode shapes roughly low NF were recorded -The MKI method has significant precision and good stability in continuum shape functions -Subjecting the structure to a weak BCs leads to reduce the difference between the SGPs' frequency and CP model 	[156]
Galerkin	-Beam	-FV	-Analyzing a strain gradient of micro and nano scale beams		<ul style="list-style-type: none"> -The NF increased due to improve the material's size dependence -The NF was greater than for the classical beam with 2.5 times @ $l/t=1$ 	[271]
MK	-Tube	-FV	-Analyzing the SWCNTs under different restrictions		<ul style="list-style-type: none"> -Increasing the diameter led to reduce the variation in the NF -The mechanical characteristic of the SWCNT converted to graphite sheet as long as the tube diameter continuously increased and this is similarly applicable for the free frequencies -The SWCNTs mechanical properties transform to graphite sheet as a consequence of increasing tube diameter; this phenomena is similarly valid to free frequencies -The numerical accuracy of the obtained results can be enhanced significantly by utilizing a suitable ratio of meshless nodes among circumferential and longitudinal directions 	[366]

Table 7 (continued)

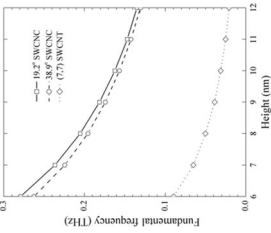
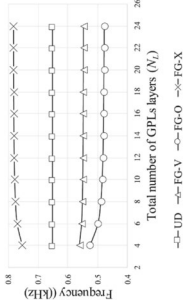
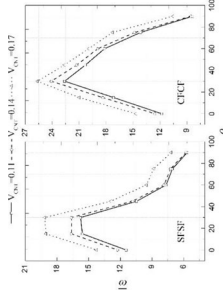
Meshfree method	Structure	Dynamic Analysis	Aim	Results	Output	Refs.
MKI	-Beam	-FV	-Investigate the cantilevered SWCNC resonators potential		<ul style="list-style-type: none"> -Increasing the length of carbon nano-structure will decrease the FF -@ ultra-high level the fundamental frequencies were observed -The SWCNC resonators considered as more promising in mass detection application owing to greater value of resonant frequencies than equivalent SWCNC resonators -As λ (geometrical parameter) increase the mechanical resonators will dramatically decrease, frequencies will shift in both SWCNT and SWCNC -The most sensitive part in the cantilever beam is the free end -The equivalent SWCNTs have much more lower FFs than the 2 types of SWCNCs with apex angles of 19.2° as well as 38.9° 	[367]
IML-S-Ritz	-Plate	-FV	-Investigates the active vibration control of FG multilayer		<ul style="list-style-type: none"> -Increasing N_L of FG patterns will enhance the FF -Changing the total number of GPLs layer will not cause any changes in the FFs in UD pattern -It has been observed that the N_L after it reached the critical point; it will not cause any further rise in the FFs in all kinds of FG patterns (it can be neglected) 	[51]
Kp-Ritz	-Cylinder	-FV	-Frequency parametric analysis		<ul style="list-style-type: none"> -An initially fast increase in (FFs) were observed due to the lamination angle increase -Increasing the rotational speed further leads to decrease the parametric frequency -The sensitivity of parametric frequency through changing number of layers reduce with increasing the lamination angle 	[368]

Table 7 (continued)

Meshfree method	Structure	Dynamic Analysis	Aim	Results	Output	Refs.
MLS	-Plate	-FV	-Investigates the buckling and the thermal vibrational of the FG-CNTRC		<ul style="list-style-type: none"> -In regular and irregular CNTRC the natural frequencies were enhanced by t/b and VF -The regular plates have different mode shapes than the irregular plates of CNTRC 	[245]
MLS	-Cylinder	-FV	-Investigates the resonance and the FV of the nanocomposites cylinder		<ul style="list-style-type: none"> -In cylinder with wavy or straight CNT the increasing the CNTs aspect ratio led to enhance the (FPs) -In cylinder with straight CNT increasing the VF led to enhance the (FPs) -The CF cylinder have lower value of NF than CC cylinder -A reduction of VA in both types of cylinder -IN cylinders made of CNTRC and w=0 the maximum amplitudes were recorded 	[340]
RPIM	-Plate	-FV	-Investigates the buckling and FV behavior of FG-GPLRC		<ul style="list-style-type: none"> -@ low values cut-out size for all the and different sets of BCs will decrease the (FPs) -A general increase in the (FPs) were observed @ high cut-out size and it is more clear @ CCCC than SSSS -A minor raise in the weight fraction of GPLs results in an enormous rise in buckling load as well as in frequency characteristics 	[251]
MLS	-Beam	-FV	-Investigates the vibrational behavior of strain gradient nanobeam		<ul style="list-style-type: none"> -The reducing in length and the increasing in mode order will cause increase in the NF difference between that predicted by the strain gradient elastic beam and the classical beam -The SWCNT NF significantly effect by the stiffness with boundary spring range (0.1 – 1000N/m) -Increasing the stiffness boundary spring > 1000 N/m has minor effects on NF 	[369]

Table 7 (continued)

Meshfree method	Structure	Dynamic Analysis	Aim	Results	Output	Refs.
RBF	-Beam	-FV	-Investigates the dynamic response of 2D FG nanobeam		<p>-The NLC impact has a greater impact on the NF with FF and CC BCs than with SS, CF and CS BCs</p> <p>-When the n increase and NLC parameter increase; the NF reduce</p>	[370]
MLS	-Plate	-FV	-Investigates the electro-mechanical response for the advanced composite plates reinforced by piezoelectric ZnO NW and GaN NW		<p>-Since rectangular plates act like beams, square plates have significantly greater NF values than rectangular plates. Furthermore, raising the thickness dramatically raises NFs through raising the stiffness of smart plates</p> <p>-The FFs of bimorph plates observed to increase by raising the volume fraction</p>	[278]

reduction in the normalized displacement value. In addition, this study recommends a selection of $\alpha = 2.6$ in order to yield accurate results and, less bound values in contrast with analytical solution. Nevertheless, by examining and validating the results of the isotropic microplates it has been observed that for all cases of $l/h \neq 0$, the analytical TSDT model were essentially smaller than the ND displacements from the IGA- refined plate theory (RPT) model, though the displacements of these models have nearly identical results. Utilizing the same RPT model, the presented outcomes founded on moving Kriging integration meshfree technique were to some degree closer to the reference value as validated and compared. Roque et al. [281], accomplished a bending analysis for micro isotropic plates SS by using a meshfree method with a modified couple stress theory (CST), founded on FSDT of plates. The improved CST includes only one length scale parameter, which simplifies the theory owing to the fact that the single scale value is easier to establish experimentally. The FSDT bending equations were developed using a meshless approach that utilized collocation with RBF. The numerical methodology was demonstrated to be simple to apply and to produce accurate results that were in outstanding agreement with the analytical solutions. Sahmani and Safaei [282] investigated the NL bending performance of the micro/nano-beam subjected to distributed load, made of a bi-directional functionally graded material (BDFGM). The pseudo-arclength continuation method (P-ALCM) combined with GDQM applied to define the NLC strain gradient load-deflection responses of NL bending. The results observed that the bending stiffness decrease by enhancing the lateral as well as the axial material characteristics gradient indices; due to this to execute the required maximum deflection value it is necessary to applied lateral load. Figure 45. Illustrates the NLC strain gradient uniform lateral load- maximum deflection responses related to NL bending.

2.3 Bending Analysis in Macroscale

Li et al. [285] analysis of the shear bending in large deformation stated that, in any numerical simulating of strain localization under large deformation, the meshfree techniques can be used whether the structure is 2D or 3D. Gong et al. [30] reported an investigation of varied loading circumstances and compliance reduction under stress limitations using the EFG approach with Gaussian integration. The design variables are the densities at the particles, and the meshless shape functions were used to interpolate the densities just at computational Gauss points. In order to enhance the density field's smoothness and exclude the checkerboard problem, Li et al. [286] employed the SPH to optimize linear structures (cantilever plate, CC beam, and Messerschmitt-Bölkow-Blohm (MBB)) under various load

Table 8 Classification of Meshfree methods for free vibration analysis (microscale)

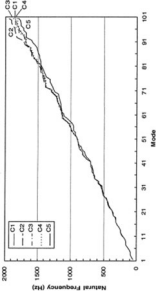
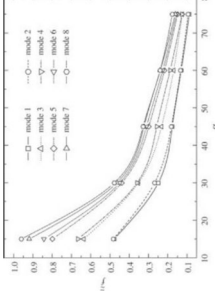
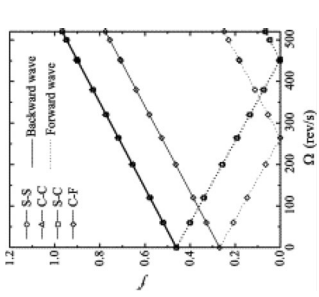
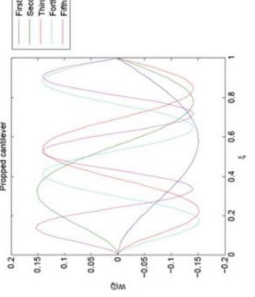
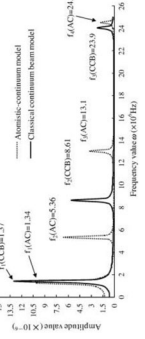
Meshfree method	Structure	Dynamic Analysis	Aim	Results	Output	Refs.
GEM	-Plate	-FV	-Analyze the damped sandwich plate and developed an iteration method for solving the eigenvalue		-Significantly efficient to apply the GEM to sandwich plate structures while obtaining accurate evaluation of modal damping and natural frequencies over a wide frequency range	[374]
Kp-Ritz	-Conical shell panels	-FV	-Identify the vibrational response		-The 1D and 2D Kp-Ritz technique is considered higher robust than the conventional Ritz technique because it avoid the necessity of Eigen equations in each case of BC being reformulated	[375]
RKPM	-Shell	-FV	-Analysis the rotating cylindrical shells vibration		-The developed formula consider the impact of Coriolis and centrifugal forces, and the initial hoop tension caused by the rotational motion	[376]
RPIM	-Beam	-Free transverse vibration	-Analyzing the impact of the size effect on flap wise vibrational behavior of rotary micro beam		-The ND frequency increased by increasing the length and the hub radius of the micro beam	[377]
MLS Developed method	-Cylinder	-FV	-Study the vibrational characterization and dynamic response of the long microtubules		-@ high frequency the length of micro beam has higher effect	[378]
					-For the FFs the hub radial has higher impact	
					- Angular velocity influenced the NDNF annihilates	
					-Curved and straight microtubules have different vibration characterization, different NF and different vibration models	
					-The vibrational behavior is significantly affected by the BCs @ both ends with curved configurations	

Table 8 (continued)

Meshfree method	Structure	Dynamic Analysis	Aim	Results	Output	Refs.
Galerkin MLS Kernel	–Plate	–FV	–Investigates the FV and buckling behaviors of thin plate strain gradient		<ul style="list-style-type: none"> –As the internal scale parameter / rise as a consequence the NF will increase –The NF improve with enhancing the boundary constraint increases –The Classical BC higher impact than high order on the fundamental NF 	[327]

situations. The findings demonstrated that, the superposition of the topologies achieved by exposing a single load condition and the optimized topology for several load instances are not equal. Moreover, SPH solution provides a more logical optimal topology than the EFG approach by using the FEM solution as a reference. Figure 46 illustrates the various topologies.

Krysl and Belytscko [242] have studied the EFG on different shapes of Kirchhoff thin plates. Findings from this analysis demonstrates that Mindlin-Reissner theory or techniques like discrete Kirchhoff theory are not necessary. The usage of a quadratic polynomial basis satisfies the consistency requirements. A baseline mesh for numerical integration is provided using a subdivision technique resembling finite elements. Lagrange multipliers impose the necessary BCs. It is demonstrated that random grid geometries, CC and SS BCs, as well as orderly and disorderly grids, may all be used to attain excellent accuracy. The optimal support, according to numerical research is around 3.9 node spacing's. Also high-order quadrature is essential [287]. The thin plate bending issue has been resolved using the MLPG method. The method adopts a local symmetric WL and the MLS approximation to interpolate the solution parameters. On regularly formed domains (generally, spheres in three-dimensional applications) in addition to their boundaries, all integrals can be efficiently evaluated. The penalty technique was performed for enforcing the important BCs. For the purpose of demonstrating how the MLPG technique is implemented and performed, several numerical examples were looked into. The outcomes of numerical examples demonstrated that given CC and SS edge conditions, excellent accuracy can be attained for arbitrary nodal distributions. As the MLS approximation-based original solution from the current technique is of C2 type, no additional post processing is necessary to calculate the strain and stress [288]. According to Liu [289], high efficiency in analyzing static deflection of plate structure with complex shapes have been achieved by applying the EFG with MLS. The EFG method combined with HSDT has been utilized to investigate the static deflection of thin and thick laminated composite plates. Results shows that TSDT gave superior accurate outcomes than the classical or FSDT and there is no necessity for shear correction factor. In addition, for shear correction factor $K = 56$, the solutions obtained from FSDT were quite close to those of TSDT and ELS [290]. Dastjerdi et al. [265] have developed meshfree method combined with Reddy's TSDT of plates, for solving the electromechanical governing coupled equation of smart multidisciplinary plate (SMP) subjected to static loads.

Peng et al. [291] accomplished the bending examination of a folded laminated plates through applying the FSDT meshfree technique. Liew et al. [292] has performed a bending analysis by using the EFG method to investigate

Table 9 Classification of Meshfree methods for free vibration analysis (macroscale)

Meshfree method	Structure	Dynamic Analysis	Aim	Results	Output	Refs.
EFG with Kriging interpo	-Plate	-NF -Eigenvalue	-Vibrational analysis of different composites laminates plate structure (square, elliptical and square)		<ul style="list-style-type: none"> -Maximum NF at stiffness ratio = 1 -The domain's irregularly nodal distributions have no discernible impact on the frequency solutions -The irregular nodal distribution in the domain has no noticeable impact on frequency -By comparing ξ values of EFG, Ritz, DSC, and other of three-ply for 6 modes almost the values were identical -@ 506 nodes mode 6 the maximum ξ_1 was recorded = 96.588 -Increasing the stiffness ratio (E_1/E_2) will cause a reduction in DL frequency 	[404]
RPI	-Plate	-FV	-Static and FV analyses of isotropic and composite plates		<ul style="list-style-type: none"> -The heights recorded error value was less than 2% at an irregularity factor = 0.4 -There is no significant effect of nodal distributions' irregularity on the solution -adding more nodes will reduce the irregularity 	[237]
Galerkin	-Plate	-FV	-Analyzing stiffened and unstiffened corrugated plates		<ul style="list-style-type: none"> -Sinusoidally and trapezoidally corrugated plates were investigated -Drive the equivalent elastic properties of the trapezoidally of the plates -After defining the stiffeners' displacement field in terms of the plate's displacements, the stiffness matrix of the structure was derived by superimposing the plate's and stiffeners' strain energies 	[405]
Galerkin	-Plate	-FV	-Providing a suggestion for an FSDT mesh-free method to analyze buckling and FV of rectangular stiffened plates		<ul style="list-style-type: none"> -The critical stress obtained 196.59 kPa @ plate thickness 1.5 m -The critical stress obtained 456.7 kPa @ plate thickness 3 m -$N_c = 2$ can provide acceptable results for most plate difficulties -The range of d_{max} is 2-4 	[333]

Table 9 (continued)

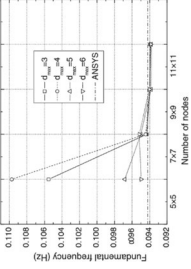
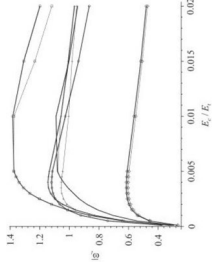
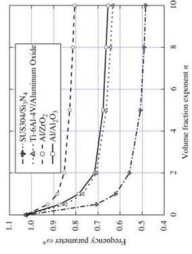
Meshfree method	Structure	Dynamic Analysis	Aim	Results	Output	Refs.
Galerkin	-Plate	-FV	-With the FSDT mesh-free approach, FV analysis of folded plate structures		<ul style="list-style-type: none"> -The mass matrices and stiffness of the stiffened and unstiffened flat plates were first modified to avoid the direct superposition failure -The mass matrices and stiffness of the composite structure were obtained through superimposing the mass matrices and stiffness of the stiffened and unstiffened flat plates were obtained using the meshless approach -The highest value of frequency and ND frequencies in all different structure were recorded in mode 5 -A smaller sized support accomplished weak convergence specifications compared with those accomplished through large sized support 	[406]
GEM	-Plate	-FV	-To analyze the FV for plates (panels) with delamination unidirectional sandwich panels		<ul style="list-style-type: none"> -The influence of the delaminated area on the dynamic characteristics grows as the length of the debonded area increases -The impacted modes are determined by the position of the debonded region -In moderately flexible cores the NF increased as a consequence of increasing of the core moduli 	[407]
Kp-Ritz	-Plate	-FV	-Investigate the FV of FGPs in 2 different plates geometry		<ul style="list-style-type: none"> -The transverse shear effect and rotary inertia were examined by applying the FSD theory -The VF exponent (0-5) remarkably enhance the frequency -The impact of l/t on frequency considered as independent of VF -@ skew angles $\Theta > 30^\circ$ in skew plates the trend of frequency increment speed up -There is no evidence that the shear correction coefficients has impact on frequency in case of $a/h \geq 10$ -At a volume fraction = (0-2), a prominent drop in frequency has been observed although the curves flattered after volume fraction > 5 	[408]

Table 9 (continued)

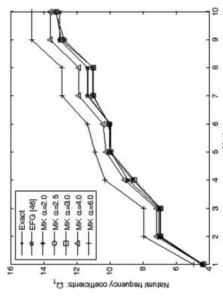
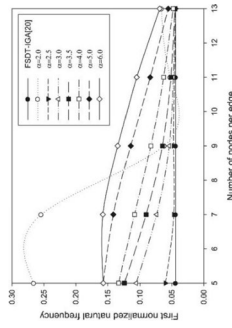
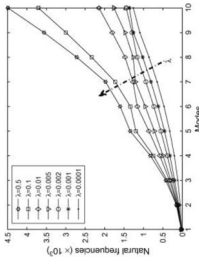
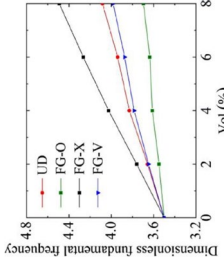
Meshfree method	Structure	Dynamic Analysis	Aim	Results	Output	Refs.
MKI	-Plate	-FV	-Develop a novel meshless technique for analyzing various types of classical Kirchhoff's plates		<ul style="list-style-type: none"> -The proposed method shows to have high efficient in imposing the essential BC's and absence of further treatment approaches -The scaling factor and the correlation parameter have an influence on frequencies and on the CPU-time -The MK method have a superior advantage over the MLS method 	[409]
MKI	-Plate	-FV	-Analyzing the mechanical behavior of FGPs		<ul style="list-style-type: none"> - @ $\alpha = 3.0$ the best results were obtained -The greatest accurate results were achieved @ $2.5 \leq \alpha \leq 3.5$ - The accuracy dropped @ $\alpha = 2.0$, and if $\alpha \geq 4.0$ -Increasing number of nodes leads to have better agreement with previous published data obtained by FSDT 	[305]
RPIM	-Beam	-FV	-Investigates the NF and the transvers response		<ul style="list-style-type: none"> -Increasing the core stiffness will enhance the NF to increase 	[410]
MLS and Ritz	-Plate	-FV	-FV analysis of multiscale FGR-PMMA		<ul style="list-style-type: none"> -The meshless method was employed to investigate the macroscale structure -Increasing the VF of Gr will increase the essential frequency -The distribution of Gr control the FG-GRC plates frequency -The plates with FG-X distribution recorded the uppermost frequency -Remarkable, the stiffness of the FG-GRC improved by the Gr distributed close to top and bottom of the laminated plates and the opposite is correct for the Gr distributes close to mid-plane 	[411]

Table 9 (continued)

Meshfree method	Structure	Dynamic Analysis	Aim	Results	Output	Refs.
MLS Galerkin	-Plate	-FV	-Investigate stiffened circular plates by FSDT and meshfree		-By comparing the results with FEM model the error found to be very small almost negligible -For enforcement of the essential BCs the RKPM was employed - Significant computational stability was achieved @ $d_{max} \geq 3$ -In all cases the highest values of frequencies were recorded @ mode 4	[307]

the SMA beam pseudoelastic’s behavior. The EFG formula has been developed by introducing the MLS shape function parallel with continuum tangent stiffness tensors to an equilibrium equation that is considerable in WF. The load versus deflection resulted by bending test is illustrated in Fig. 47. A nearly identical load–deflection response in the three different nodal arrangements is observed, which leads to expose the major advantage of the meshless techniques over FEM that is, a highly smoothed and continuous discretization field caused by the weight function. As a consequence of this unique and required discretization, a reduction in demanding modal preparation and more accurate solution in small node sets or in extremely irregular nodal arrangement will be revealed.

Dastjerdi et al. [293] have applied the MLS with FSDT to scrutinize the static performances of the nanoclay-reinforced plates with piezoelectric layer as shown in Fig. 48. The static behavior is improved by applying the exfoliated morphology with nanoclay. In addition, it is observed that the plate’s deflections have reduced by increasing the input voltage owing to the mechanical loading, although a further increase may cause a reverse deflection. Likewise increasing the nanocomposites layer thickness will lead to decrease in the deflection.

The EFG method was employed to analyze arithmetical modeling of the size effects with the gradient elasticity formulation. The bending analysis for cantilever beam CC from one end were performed, and the load was subjected to the other free end. The results of this analysis shows that by decreasing the displacement, the stiffness ratio decreases as well but the strain ratio will increase [294]. Ferreira et al. [295] employed the RBF collocation with two higher order Zig-Zag theories for analyzing laminated plates made of three layers as shown in Fig. 49. Furthermore, the Taylor expansion up to fourth-order has been employed for the equivalent single layer (ESL) method. Figure 49 illustrates the procedure of assembling ESL approach on a k layer. After obtaining the results and validated with HSDT theories, is shows clearly that for normal and transverse shear stresses, transverse displacements and all values of a/h ratios; the FSDT is not efficient for utilizing the thick laminates. Besides, applying the SINUS-ZZ theory is more significant than z^3 -ZZ theory for thicker plates.

Ferreira et al. [296] implemented the SSDT besides the RBF collocation, aiming to analyze the laminated spherical shells geometry illustrates in Fig. 50. Besides, the CUF was employed on behalf of obtaining BCs and the equation of motion. The obtained results presented by the different set of nodal were compared with results obtained previously by FSDT, HSDT and the results shows to be almost identical.

Ferreira et al. [297], in a novel study employed the trigonometric shear deformation theory used for displaying a discretized symmetric composite sandwich plates via the

Table 10 Classification of Meshfree methods for force vibration analysis (nanoscale)

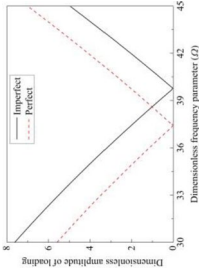
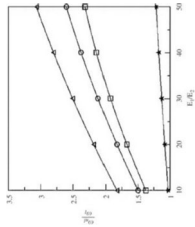
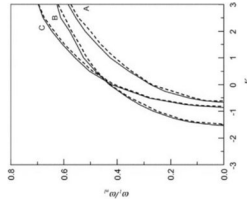
Meshfree method	Structure	Dynamic Analysis	Aim	Results	Output	Refs.
Galerkin	–Plate	–Dynamic stability (in-plane load harmonic)	–Dynamic stability analysis (linear/NL)		–As the VF in CNTs increase the vibrational amplitude will reduce –The size of stability areas grows as the volume percentage of CNTs increases –The SWCNT distribution patterns have a considerable impact on the size of stability regions	[315]
GEM	–Plate	–NL vibration (loaded by initial stress)	–Investigate NL vibrations behavior of a two-layered cross-ply plate with EF		–Foundation stiffness, initial stress, E_1/E_2 and vibrational amplitude enhance the frequency behavior of the NL vibration –The extensional stress and the pure bending stress in the plane of the plate combined generates the initial stress –Increasing the E_1/E_2 will increase the coupling between bending and extension and increase the frequency ratio	[415]
GEM	–Plate	–NU stress	–Investigate NL behavior of laminated plates		–@ great amplitude values the plates observed to be enhanced by the HSDT –For plate made of two layer the impact of Young's modulus in thickness direction on the frequency ratio is remarkable –The buckling coefficient of 4 layered antisymmetric and symmetric cross-ply plates were larger than those obtained by 2 layered plate –The FSDT obtained higher results than HSDT	[416]

Table 10 (continued)

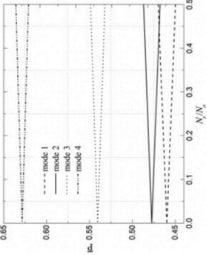
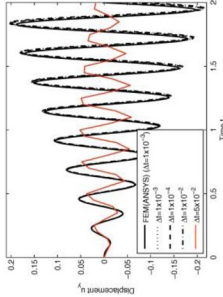
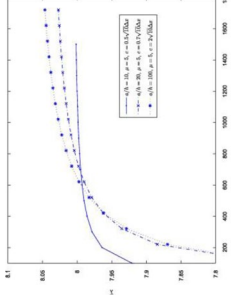
Meshfree method	Structure	Dynamic Analysis	Aim	Results	Output	Refs.
Kp-Ritz	-Cylindrical panels	-Static and periodic axial force)	-Analyze CNTR-FG cylindrical panels under dynamic stability		<ul style="list-style-type: none"> -Formulate a of Mathieu–Hill equations -Analyzing the instability sections -The effect of VF of CNT, radius-to-thickness ratio and edge-to-radius ratio -The instability regions of modes 1 and 2 overlap in UD and FG-V when $N_s/N_0 > 0.35$ -The change in CNT VF has no significant effect on the responses, nonetheless as the CNT VF increases, correspondingly rises the value of the ND (FFPs) -The greatest overlap area observed in FG-X panel and the smallest in FG-V 	[417]
MKI and Galerkin	-Beam	-Forced vibration	-Develop a vibration analysis under multi load cases by combining 2 meshfree methods		<ul style="list-style-type: none"> -When applying harmonic load and the results compared to the FEM solution, it demonstrates that when a very coarse set of 5×5 nodes is employed, a considerable error may occur, however all other nodal densities can produce acceptable agreements even with a coarse set of 11×5 nodes 	[364]
RBF RBF-FD	-Beam	-Uniform load	-Investigates the Timoshenko nanobeam by meshless and NLC elasticity theory		<ul style="list-style-type: none"> -Too large time step leads to reduce the methods' accuracy -Multi-quadrics RBF have been employed -Significant results were obtained by GCM -A superior results were obtained with relative error $< 0.5\%$ -Various shape parameters have been used for different a/h -Remarkable results were obtained 	[274]

Table 10 (continued)

Meshfree method	Structure	Dynamic Analysis	Aim	Results	Output	Refs.
IML-S-Ritz	-Plate	-Impact	-Study the impact analysis of FG-GPLs reinforced composites plate with the Winkler-Pasternak foundation		<ul style="list-style-type: none"> -Increasing the DL Winkler and Pasternak modulus parameters reduces the resultant center deflection time history -Raising any of the DL Winkler or Pasternak modulus parameters induces lower displacement as compared to plates without EF, and enhancing both leads to a combined decrease in central deflection time profile -The consequence of adjusting the DL Winkler and Pasternak modulus parameters on the contact force time histories is scarcely noticeable and there is no discernible difference -A minor disparity between results has been observed 	[418]

MQRBF. The aim of this method was to employ the trigonometric functions over the entire thickness direction, permitting for zero transverse shear stresses at the bottom also the top of plate surface. A numerical analysis was done for three different types of plates subjected to different loading conditions; square sandwich plates made of three layers subjected to uniform load, square cross-ply laminated plate made of four layers $[0^\circ/90^\circ/90^\circ/0^\circ]$ exposed to a sinusoidal load, as well as a thick square isotropic plate subjected to uniform load. All obtained outcomes of in-plane displacement, shear and normal stresses, were compared with previous work published by the same author, exact results, FEM results and shows a good agreement. Besides, the results prove that using these methods guarantee excellent solution for the composite plates. Neves et al.[298] implemented the quasi-three dimensional SSDT with developed employment of CUF and the base of collocation RBF for addressing the thickness stretching matter on static analysis response of FGM plates. A novel algebraic model was proposed, the bending analysis was performed on isotropic FGPs and square plate with sandwich structure filled with FGM core, and 91 mathematical layer were considered, a sinusoidal load was applied for both types of plates. The obtained results shows good agreement with previous available results found by other meshfree methods and FEM. Furthermore, the author stated that it is necessary to consider the σ_{zz} in the formulation. Ferreira et al. [299], employed the MQRBF parallel with the TSDT (for beam and plate), to analyze the static bending of beam structure and plate structure with different geometrical characterization. The BCs interpolation for beam and plate for SS and CC supported were obtained based on the MQ interpolation. The beams (symmetric laminated composite, orthotropic and isotropic) all were subjected to a uniform load and both CC and SS BCs. Where the plate made of four layers with the same thickness oriented at $[0^\circ/90^\circ/90^\circ/0^\circ]$, was exposed to sinusoidal load (perpendicular pressure), and the BCs were set as SS. By validating the results it is observed that this method has high accuracy for composite laminates. Additionally, accurate prediction of transverse displacement, normal stresses and transverse stresses were accomplished. In a novel study published by, Neves et al. [300] the collocation RBF according to a SSDT for plates was employed, for examining the bending analysis of the FGM square plate. The development of displacement besides stresses throughout the thickness direction for different values of the exponent k was demonstrated via a 21×21 grid. A considerable modification in the transverse displacement and in the normal stress were observed by considering $\epsilon_{zz} \neq 0$. Ferreira et al. [301] studied the static bending deformation of a square sandwich plate made of three layers SS subjected to uniform load, and a square cross-ply laminated made of three layer $[0^\circ/90^\circ/0^\circ]$ SS exposed to sinusoidal load. The analysis was established

Fig. 37 A thick rectangular plates made of FGP with various porosity models [255]

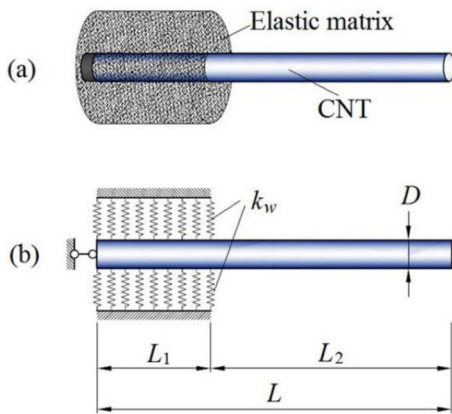
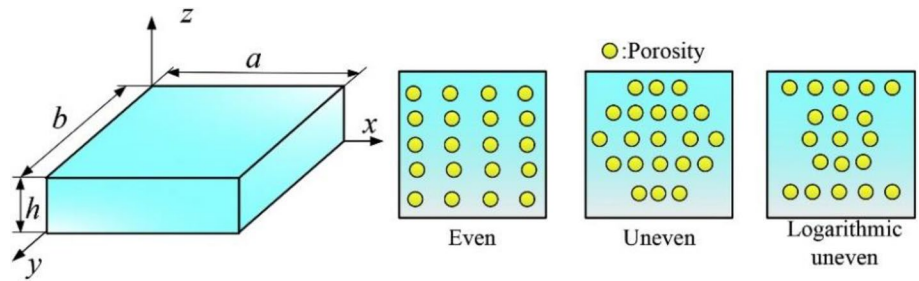


Fig. 38 The nanowires made of CNT based on EF subjected to a clamped BCs [263]

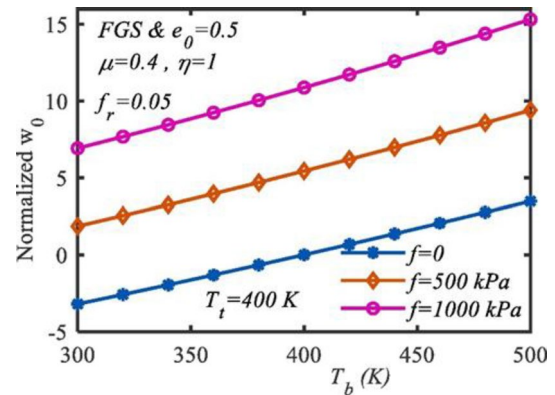


Fig. 40 The relation between central normalized deflections versus the bottom surface temperature in square SS PNSP under different uniform load case [266]

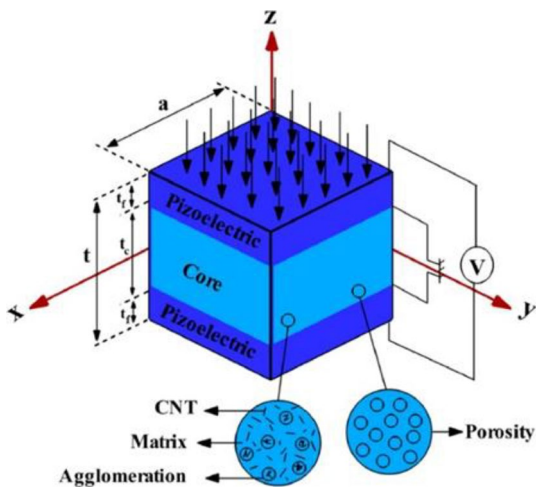


Fig. 39 Structures of the proposed FG nanocomposite porous plate bonded with 2 piezoceramic layers under static electromechanical inputs [265]

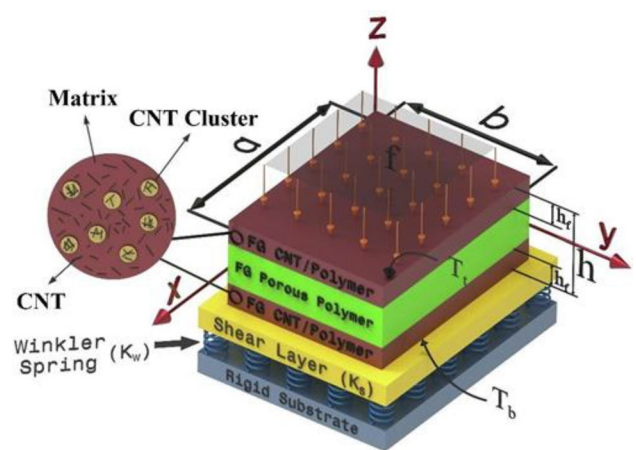


Fig. 41 Sandwich plate structure with a FG porous core with 2 nanocomposite as an outer layers reinforced with CNTs and their clusters [266]

by employing the meshfree MQRBF combined with the layerwise deformation theory. The Kansa's unsymmetric collocation method has been implemented to predict the BCs by RBF. By comparing and validating the results it is proved that this method is highly significant and it is not required to use the shear correction factor. Ferreira et al.

[302] implemented the RBF meshfree technique founded on the layerwise deformation theory for the purpose of investigating the bending performance of laminated composite spherical shell that has a layer orientations as $[0^\circ/90^\circ/0^\circ]$ and $[0^\circ/90^\circ/90^\circ/0^\circ]$. The spherical shell was SS, under sinusoidal vertical pressure. The results were compared with layerwise analytical, HSDTs and FEM and found to be in

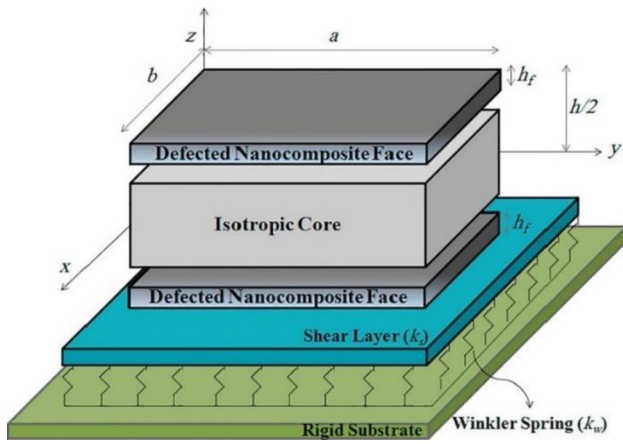


Fig. 42 The sandwich plate schematic with 2 defected CNT/polymer face sheets resting on two-parameter EF [267]

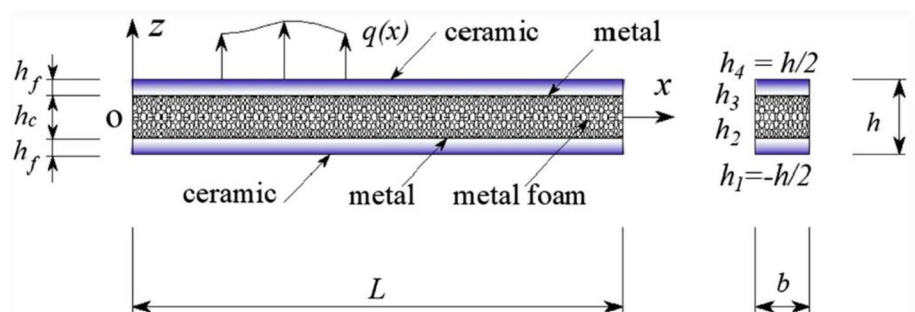
good agreement. Ferreira et al. [303] employed the collocation RBF method and the HSDT, for the purpose of investigating the static deformation of the SS FGPs with square geometry. The cross-validation technique has been applied for choosing the optimum values of the shape parameters in the RBF. Moreover, for assuming the effectual properties of FGM the Mori–Tanaka homogenization approach has been considered. In a recent study.

2.4 Static Analysis Buckling

2.4.1 Buckling Analysis in Nanoscale

The MLS has been applied in parallel with the modified Halpin–Tsai approach and Reddy’s TSDT, for examining the mechanical buckling for multifunctional smart sandwich plates (MFSSP) that contains a Gr nanocomposite and porous layers with two active piezoelectric layers as displayed in Fig. 51. The outcomes shows that the MFSSP’s mechanical buckling response improves significantly as the Gr VF increases. Moreover, embedding extra pores in the core layer enhance the MFSSP’s thermal stability behavior, without significantly lowering their mechanical stability responses [308].

Fig. 43 Schematic of porous sandwich beam with its coordinate and geometrical parameters [269]



To study the buckling behavior of single walled carbon nanocones (SWCNCs), Yan et al. [309] has applied a meshfree computational framework originated from the MKI. Figure 52 demonstrates the relationship between the average energy per atom relative to the compression ratios in various kinds of CNCs with identical geometrical parameters. A significant energy jump emerges at each energy curve, which corresponds to CNC buckling. A fascinating fact is that the essential axial compression displacements of all types of CNCs were recorded as 0.22 nm. Besides, consequently the corresponding axial compression ratio rises as a function of $(1/\cos\theta_i)$. Where in CNC the θ_i considered as the apex angle of i th types.

The electrostatic and buckling analysis of a thin beam have been examined by using different set of uniformly distributed load and BCs (pinned–pinned, fixed–fixed, fixed–free, and fixed–pinned) using the local point interpolation method (LPIM) method. The results show that at fixed–fixed, the critical the highest value of buckling load λ was at four different nodes [310]. A novel active sandwich plate have been developed and analyzed by Dastjerdi et al. [311] where a porous CNTRC core was implemented in a sandwich structure within two piezoelectric layers. FG patterns of CNT

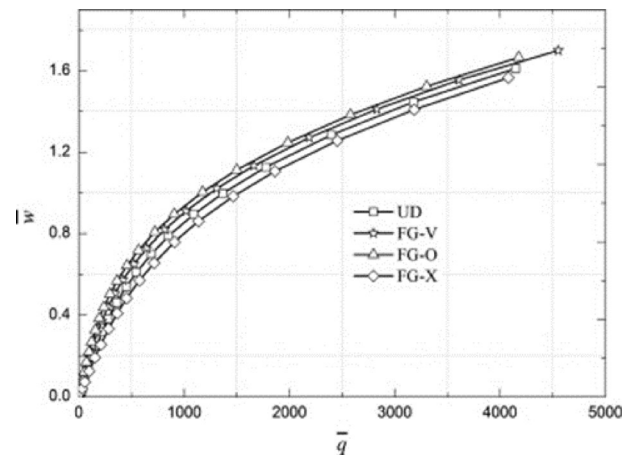


Fig. 44 The Variation in the ND central deflection with load @ fully CC BC for CNTR-FG cylindrical panels exposed uniformly distributed radial pressure @ $h=0.004$ [279]

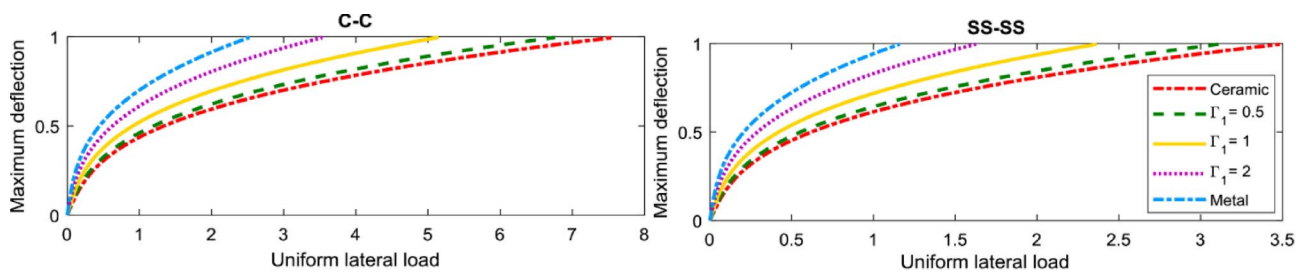


Fig. 45 The NLC strain gradient uniform lateral load- maximum deflection behavior related to NL bending for CC and SS BCs [282]

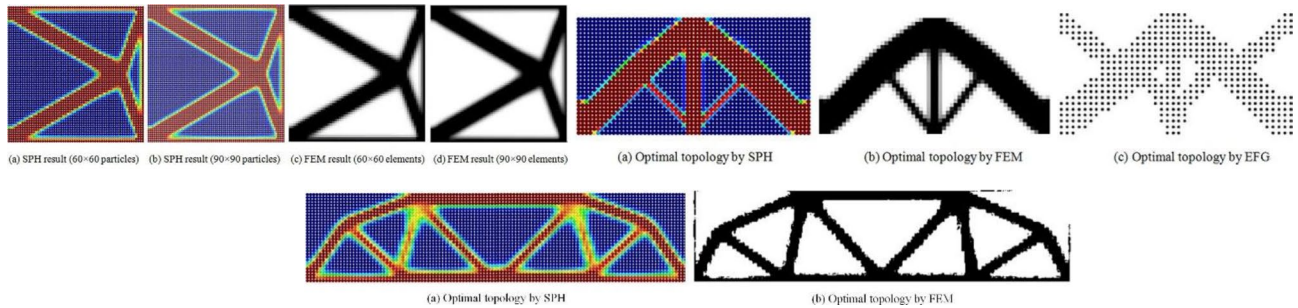


Fig. 46 a The cantilever plate topologies derived from various discretization's, b Optimal topology of the beam with C-C BCs c $F1=2, F2=1$ for multiple loading case and c Optimal topology of MBB beam for multiple loading cases (c) [286]

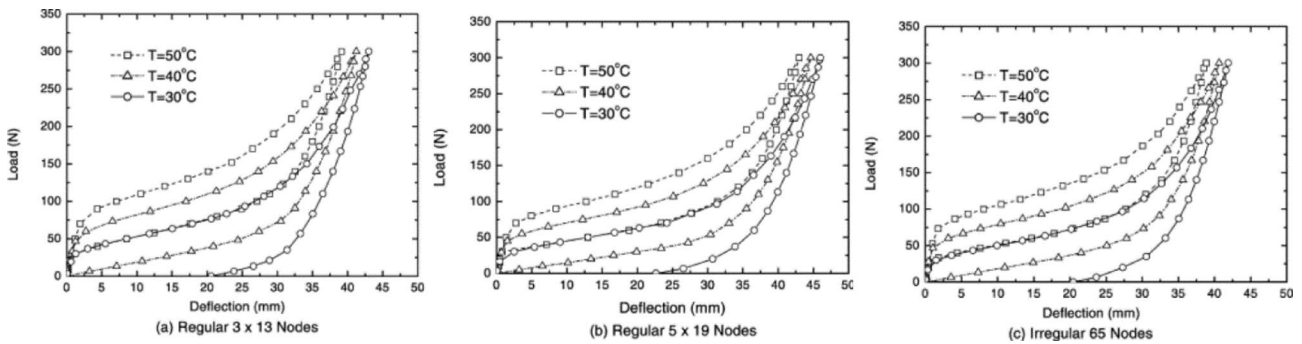


Fig. 47 The load versus deflection results from bending test [292]

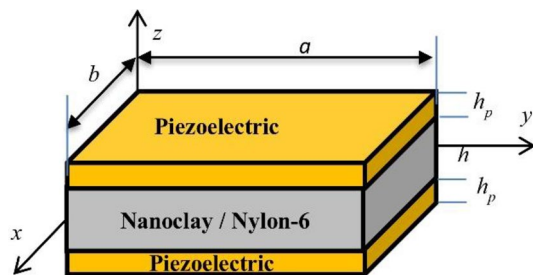


Fig. 48 The nanocomposite plate schematic structure [293]

dispersal and porosity dispersal were investigated for the core layer. The suggested active multidisciplinary sandwich plate (AMSP) thermal as well as mechanical buckling resistances were highlighted. The governing Eigen value equations of the buckling evaluation for AMSP were found using Reddy's TSDT. Using a meshfree solution devised, the critical buckling resistance values of AMSP were derived from the GEs. In a comprehensive study framework, the impacts of porosity, CNT, and geometric dimensions on the buckling resistance of AMSPs were examined. Additionally, a remarkable increase in buckling resistance have been achieved by using the CNTs as a reinforcement in the core layer. Figure 53 presents the schematic of the sandwich

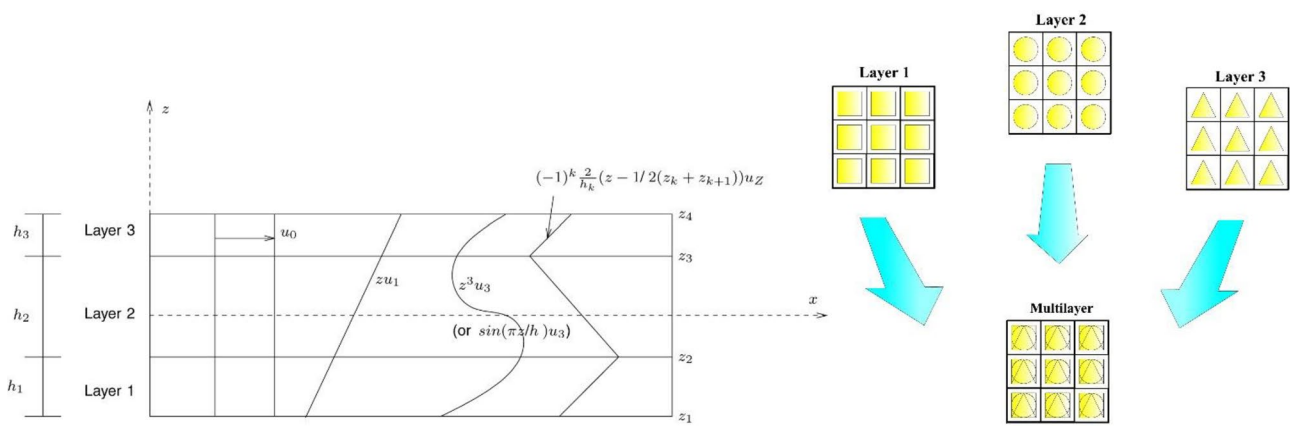
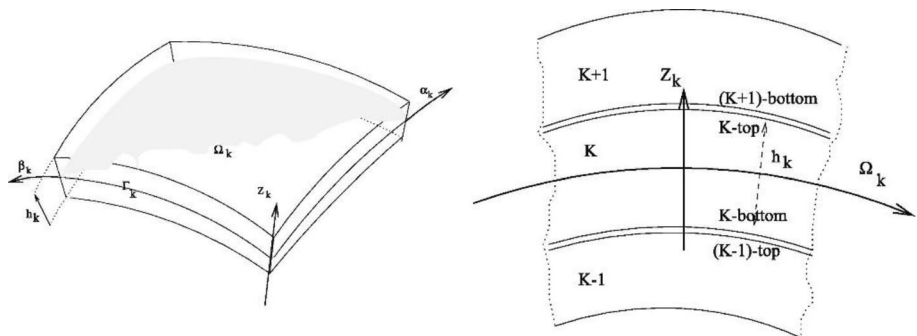


Fig. 49 The arrangement of the ZZ assumption for the three-layered laminate and the ESL approach assembly process [295]

Fig. 50 The geometry and notations for the doubly curved multilayered shell [296]



structure of the piezoelectric layer under the biaxial buckling load.

The MLS approach has been employed to generate an interpolation function in order to carry out numerical forming of SWCNTs which guaranty a spontaneously satisfaction of the high order continuity, and that it is using the displacement as the only nodal degree of freedom. Besides their bending buckling response were numerically simulated [312]. The (15, 0) CNT of 12.78 nm contour's subjected to axial compressive strain within buckling is shown in Fig. 54. Prior to buckling, there are two minor compression zones near the tube's ends. Figure 54a. As an outcome, two snap buckles formed in the two compression zones Fig. 54b. The maximal axial compressive strain was indicated as a significant inducer of kinking besides can thus be utilized as a criterion of bending buckling. Furthermore by comparing the buckling bending angles that found by MLS and by the atomistic simulation both methods gave identical values and only at very high bending angles a slight difference in the average energy per atoms has been observed between both methods. Moreover the obtained results prove that this method can be utilized to determine the mechanical deformation of SWCNTs accurately. Also, a true displayed of bending buckling can be defined.

Liew et al. [313] have used the Galerkin approach founded on the FSDT to study stability analysis for unstiffened/stiffened of orthotropic plates (trapezoidal corrugated plate) thin and thick plates by applying elastic buckling. A uniaxial in-plane compression in y-direction was considered. The results were validated and the error was calculated. Safaei et al. [314] investigated the thermal besides mechanical buckling of light-weight polymeric nano-composite sandwich plates structure as shown if Fig. 55. The MLS meshfree method was employed to facilitate the governed buckling equations. While implementing the FSDT and TSDT for determining the sandwich plates total energy functions. It has been observed that the thermal and mechanical buckling response were enhanced by adding the CNTs into the outer layers. Besides, the critical mechanical loads were reduced by porosity, although it enhanced the thermal buckling.

Rafiee et al. [315] investigated the square plates (piezoelectric to CNTRC) to define the effect of applied voltage (Vs_0), and the thickness ration (h_p/h) on buckling temperature ($T_{cr} = \Delta T_{cr} + T_0$) subjected to a uniform temperature rise ($Vc^* = 0.12$). Furthermore, Kiani [316] performed an axial buckling analysis of magnetic affected stocky nanowires carrying electric current by using Galerkin-RKPM meshfree method. To examine the compressive critical

buckling load (CBL) of doubled nanowires in magnetic field, Kiani [317] applied the RKPM meshless method and the assumed mode method (AMM) and significant results were obtained. Additionally, the four coupled equations of the CBL have been solved through RKPM. Shahmohammadi et al. [318], employed the Galerkin method for solving the extended NL differential equilibrium system equation and the compatibility equation of the doubly curved imperfect shallow shells comprised of FG-CNTRC as shown in Fig. 56, and subjected to lateral and in plane loads. Ipek et al. [319] investigated the stability behavior of a nanoplate made of FG-CNT based on Winkler EF as shown in Fig. 57, subjected to a compressive load in an elastic as well as thermal atmospheres through employing FSDT for plate. Followed by implementing the Galerkin for solving the critical biaxial compressive loads and various CNT distribution were considered and investigated.

2.4.2 Buckling Analysis in Microscale

Thai et al. [280] presented a buckling examination of FG isotropic as well as sandwich microplates founded on refined FSDT and MCST. The Galerkin-WF generates a discrete system equation; these equations were solved by MKI mesh-free method. The same standard of selecting the BCs in FEM were used due to the fact that the MKI method satisfies the function of Kroncker delta. The first six mode shapes of isotropic FG circular microplates fully CC under buckling analysis by $n = 10$, $h/R = 0.1$ and $l/h = 1$ are presented in Fig. 58.

The ND CBL parameter observed to dramatically decrease; due to the increasing in thickness-to-radius ratio. On the contrary, as n levels increase, the ND CBL parameter rises as well. Furthermore, once material l/t increases, the ND CBL parameter increase. Additionally, the CBL variate from the current size-dependent model ($l/h = 1$) and the

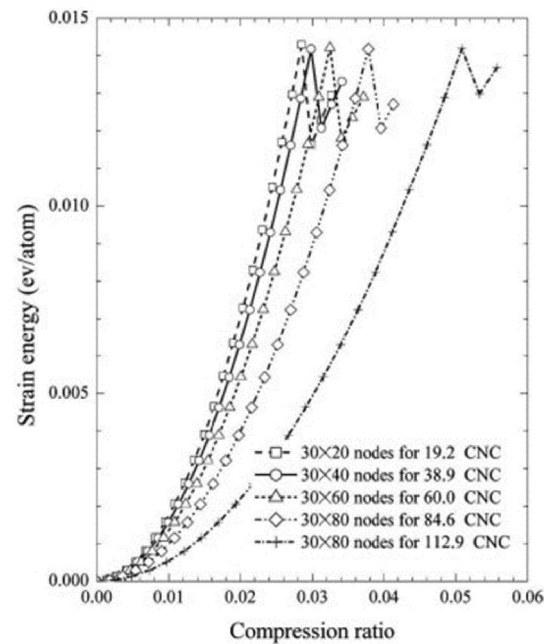


Fig. 52 The average strain energy/atom Vs. compressive ratio for CNCs with identical side edge length of 7.48 nm. [309]

traditional model is essential, although the variation reduce as the thickness of the microplate increases.

For stability analysis for the random checkerboard composite cylindrical microshells, Yang et al. [253] have developed the MKI for size dependent shell model shown in Fig. 59, which includes rotational gradient tensor. The snap-through phenomena observed by tracking the post-buckling paths. The importance of the stiffening property corresponding to the rotation gradient tensor expands with increasing the VF of GNPs. Likewise, for a given value of GNPs VF, decreasing the l/w proportion of GNPs reinforcements increases the significance of couple stress size

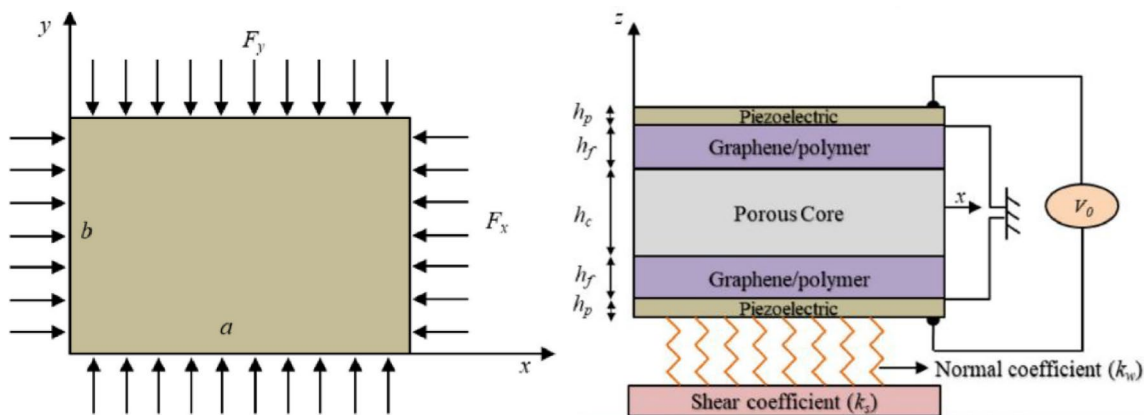


Fig. 51 The MFSSP's Schematic including 2 piezoelectric layers, 2 Gr/polymer nanocomposite layers and 1 porous core resting on a two-coefficient (k_s and k_w) basis and exposed to mechanical loads (F_x and F_y) and electrical input (V_0) [308]

dependability in the CBL as well as critical shortening of an axially compressed cylindrical microshell. The same schematic have been employed in a further study [320], to investigate the NL stability analysis for a microshell with random reinforcements exposed to a collective load (axial and lateral). The Kriging meshfree based numerical strategy has been implemented for enforcing the essential BCs the nodes. Besides, satisfying the Kronecker delta by employing the correct MK shape function. The obtained results show that, considering adding the lateral compressive load for the collective loading condition with axial compression dominance it was obvious that the region of snap-through expertise developed largely as well as the corresponding minimum load shifts to induced more deflection, yet a smaller shortening. Moreover, for specific VF values as well as specific particular area of graphene nanofillers (GNFs), merging of axial or lateral compressive load will cause a reduction in the critical stability values loads of collective compressed of the microshells roles of microscale-dependent gradient tensors. Figure 60, illustrates the shortening behavior of unsystematically reinforced nanocomposite shell subjected to a domination lateral load condition.

Alshenawy et al. [321] applied the MK meshfree approach combined with the 3D strain gradient continuum mechanics to investigate the stability response of the thermos-electro-mechanical loaded FG piezoelectric with microshell cylindrical structure as shown in Fig. 61. The MK method has the ability to showcase the transition buckling mode containing various gradient tensors with microsize-dependent. Three different micro-strain gradient tensors were investigated. The obtained outcomes of the second NL stability under compression show that the stiffening character was significantly greater than the first one as shown in Fig. 62. However, the electric actuation role can be neglected by shifting to the postbuckling territory. Lower values for stiffening character of the 3D mechanical/electrical bifurcation load gradient

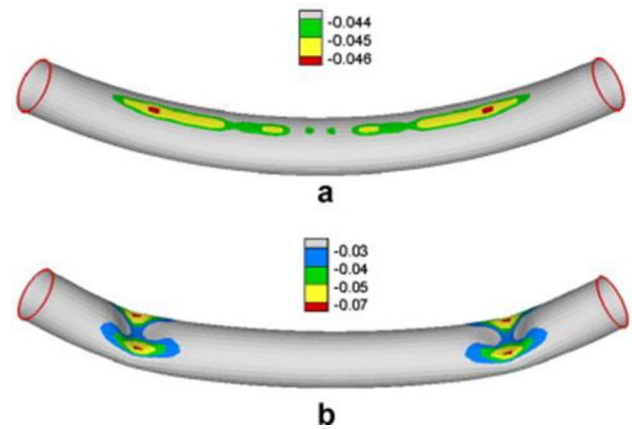


Fig. 54 The (15, 0) CNT of 12.78 nm contour's subjected to axial compressive strain within buckling: **a** configuration just before buckling; **b** the final buckling pattern [312]

tensor compared with the values obtained for the first post-buckling load.

Sahmani and Safaei [282] investigated the size-dependent postbuckling performance of the micro/nano-beam subjected to axial compressive load, made of BDFGM. The P-ALCM combined with GDQM were employed to define the NLC strain gradient postbuckling configuration. The results determined that the nonlocality decreases CBL despite enhancing the impact of strain gradient size. The axial compressive load–deflection for several NLC parameter values and CC and SS BCs is presented in Fig. 63. Furthermore, at deeper into the postbuckling regime, the NLC size impact rises, resulting in a larger gap between curves. Nevertheless, a reverse observation completed on strain gradient size reliance. These expectations were identical for both CC and SS BCs. In a recent research published by, Yuan et al. [322] and focused on analyzing the NL buckling (NLB) of the hydrostatic pressurized FG composite with conical microshells

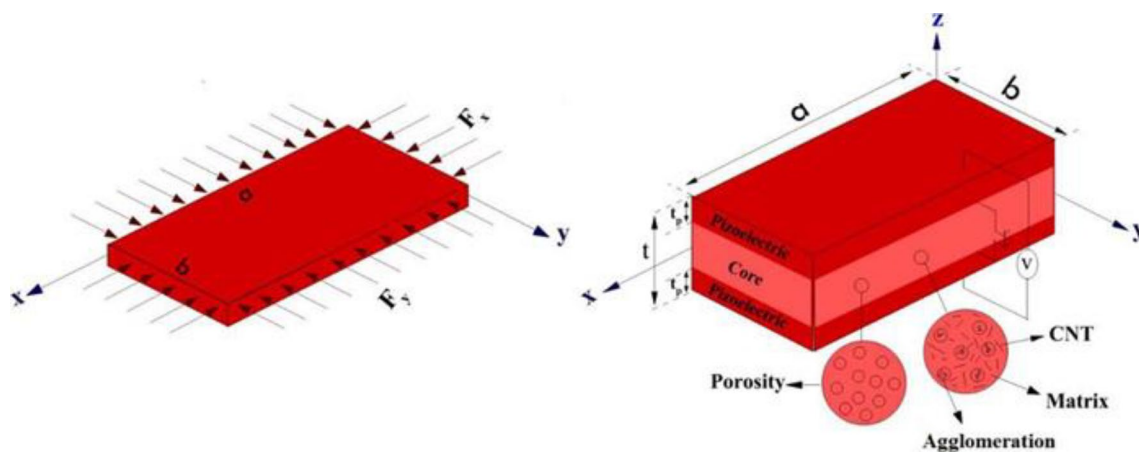


Fig. 53 The schematic of the AMSP subjected to a biaxial buckling loads [311]

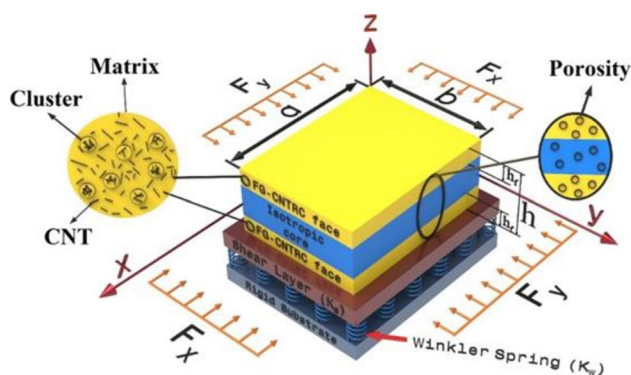


Fig. 55 Porous sandwich plate reinforced with randomly-oriented CNTs and clusters in between two outer nanocomposite layers [314]

structure. The GDQM of discretization pattern combined with Galerkin technique were applied to define the size-dependent NL problem and different types of homogenization scheme were investigated. The outcome shows that the impact of the material property gradient index over the NL critical buckling pressure is observed to decrease for a FG composite conical microshell with a larger semi-vertex angle. Furthermore, it has been discovered that the coupled stress size reliance is more essential in NLB. Figure 64 illustrates the difference of the improved couple stress-based critical buckling pressure of FG composite conical microshells with ratio of R_1/h resulted from several minor scale parameters. In both types of BCs, it has been observed that the NLB behavior with low ratio of R_1/h highly effected by the couple stress size reliance. The NL lateral buckling of a cylindrical microshell has been numerically investigated based on the TSDT of a deformable shell model and modified SGT in continuum mechanics [323]. Additionally, the arithmetical solution designed for the microstructural-dependent NL has been conducted utilizing MK meshless approach, which is capable of accurately adapting the critical BCs.

The buckling analysis of an electro-thermomechanical NL stability made by FG piezoelectric with cylindrical panels shape, subjected to compression load with SS and CC

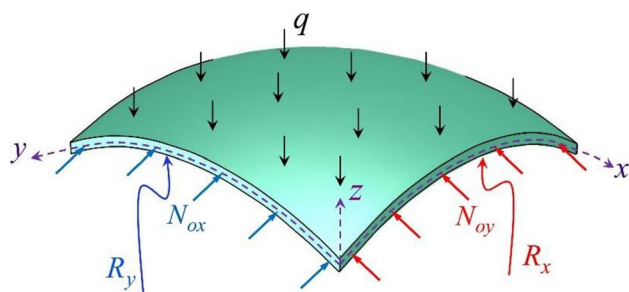


Fig. 56 Schematic of a FG-CNTRC doubly-curved shell [318]

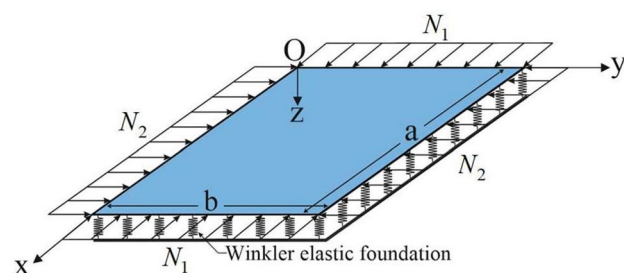


Fig. 57 The schematic of a nanoplate made of FG-CNT based on Winkler EF [319]

BCs has been performed [324]. The existence of the buckling mode transition in the microstructure was predicted by employing the MK meshfree method. Hence, the implementation of MK method in this article was considered as one of its types. The panel models with MK meshfree method base and various arrangement of nodes established on the Chebyshev, ordinary uniform and unordinary patterns are shown in Fig. 65. It is found that when the microsize-dependent gradient tensors were considered, the first and second bifurcation loads, in addition to the first and second minimal postbuckling loads, increase concurrently. Furthermore, due to the size dependency, the lowest NLB loads related to the first and second buckling modes were shifted toward a less panel deflection besides a greater panel shortening. Furthermore, taking into account the microscale size dependencies, the micropanel end shortening associated to the first and second bifurcation loads rises. Furthermore, the first and second loads, along with the lowest postbuckling loads, decrease as the property gradient index increases, resulting in a higher VF of PZT-5H phase when compared to PZT-4. The property gradient index value, in contrast, has a minor effect on both first and second critical shortenings in addition to shell deflections at the first and second minimal NLB points.

Liu et al. [325] employed the MK method for the purpose of solving the size dependency problem. The study's objective was to inspect the postbuckling as well as the NLB of a cylindrical microsized shells comprised of checkboard arbitrarily reinforced nanocomposites under combined load (lateral and axial compression). The SS and the CC BCs were taken into account in this study. The eccentric load-shortening behavior of arbitrarily reinforced microshells subjected to lateral dominated load encountered with nanofillers with diverse aspect ratios ($l = 40 \mu\text{m}$, $V_{\text{GPL}} = 1.5\%$) is illustrated in Fig. 66. It is shown that the stability of coupled compressed composite microshells rises by increasing the aspect ratio of nanoscale reinforcements. This outcome was achieved since the plane-type of shape allied with the GNFs creates the significant surface area specification in enhanced reinforcing of the resin matrix. An example of

Fig. 58 The results of the first six mode shapes of isotropic FG circular microplates fully CC under buckling analysis by $n=10$, $h/R=0.1$ and $l/h=1$ [280]

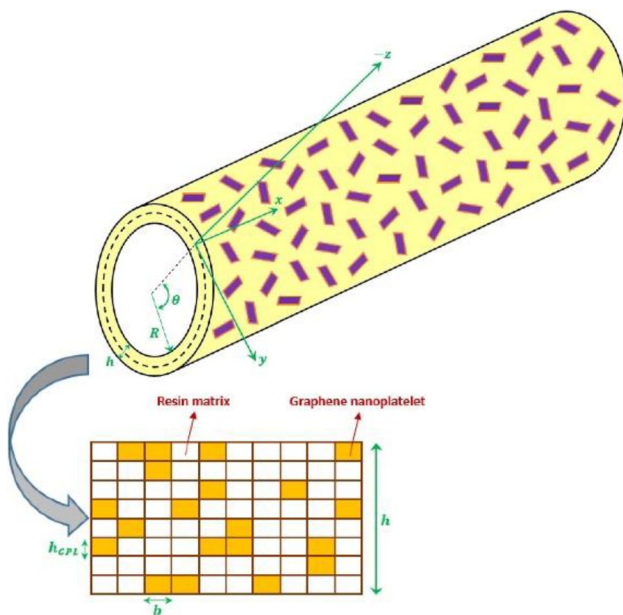
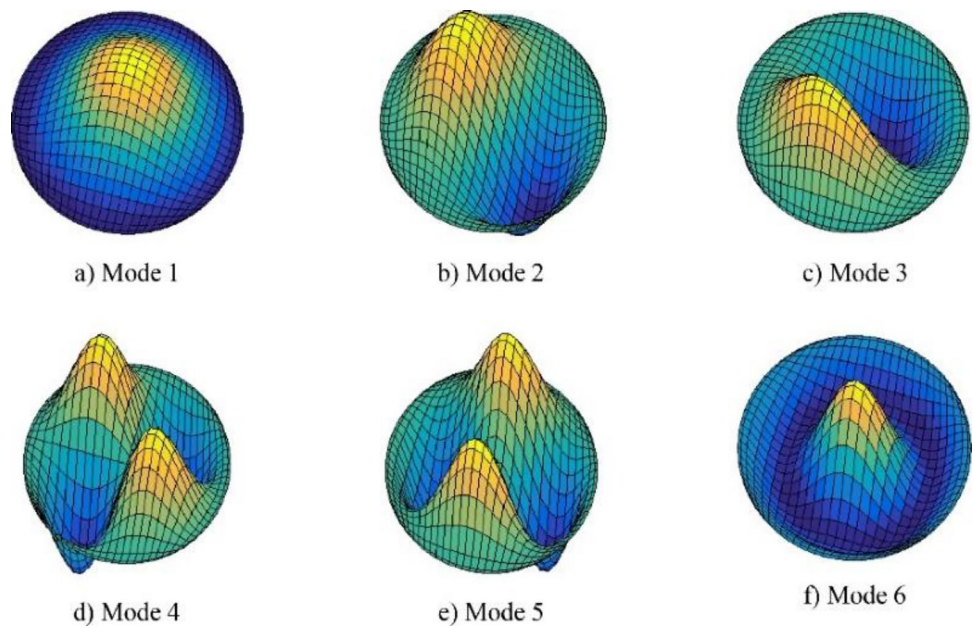


Fig. 59 The schematic of a cylindrical microshell with GNPs reinforcement distributed in checkerboard random pattern [253]

investigating the postbuckling in a flowchart has been presented by, Liew et al. [252] and shown in Fig. 67.

2.4.3 Buckling Analysis in Macroscale

The stability behavior of the discretely thick plates having different geometries as presented in Fig. 68 have been investigated by using the hp-cloud method combined with Mindlin's theory. The analysis has been accomplished by applying

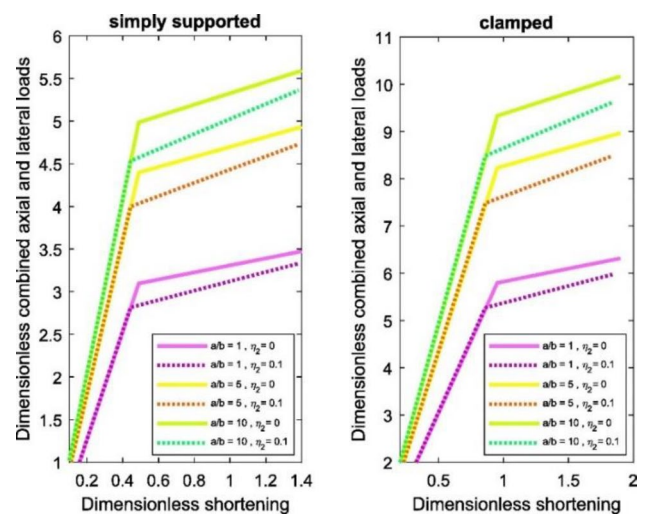


Fig. 60 The shortening behavior of randomly reinforced nanocomposite shell subjected to domination lateral load condition with nano-fillers with several aspect ratios ($l_0=l_1=l_2=40\mu\text{m}$, $V_{GPL}=1.5\%$) [320]

pure shear load, uniaxial and biaxial in-plane compressive. Findings from this analysis reveal that the local buckling is found to be coefficients with point supports and intermediate. Moreover, the hexagonal and quadrilateral plates have 25 scattered nodes, triangular plates have 15 or 25 scattered nodes, circular plates have 13 scattered nodes and the semi-circular plates have 9 scattered nodes [8].

The RBF method has been used by, Liew et al. [328] to investigate thick plates (trapezoidal and skew) subjected to a NU load in buckling analysis. The discrete system equations were solved to find the initial stresses pre-buckling. The

Fig. 61 The schematic of piezo-electric microshell thermo-electromechanical loaded FG and Chebyshev, the regular uniform and irregular the 3D nodal arrangements patterns for the MKM-based shell models [321]

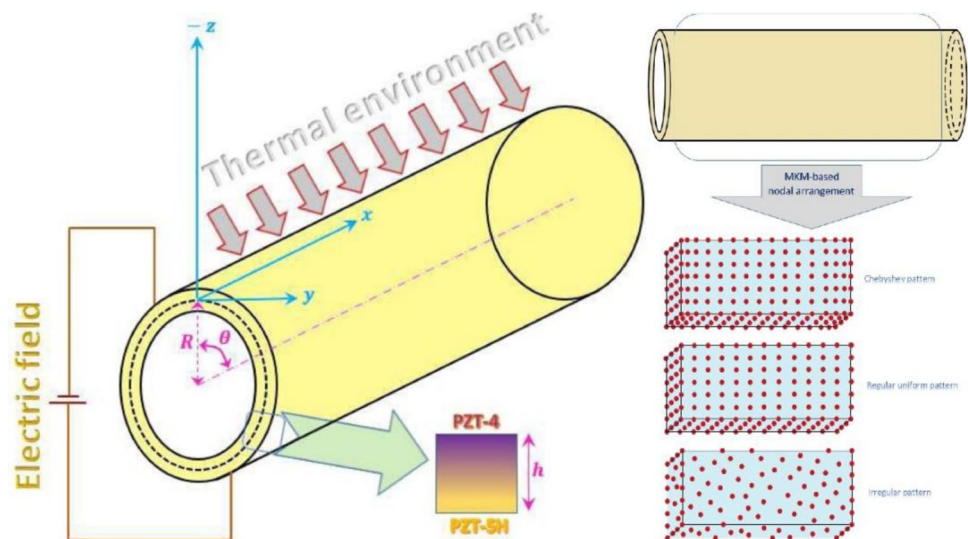
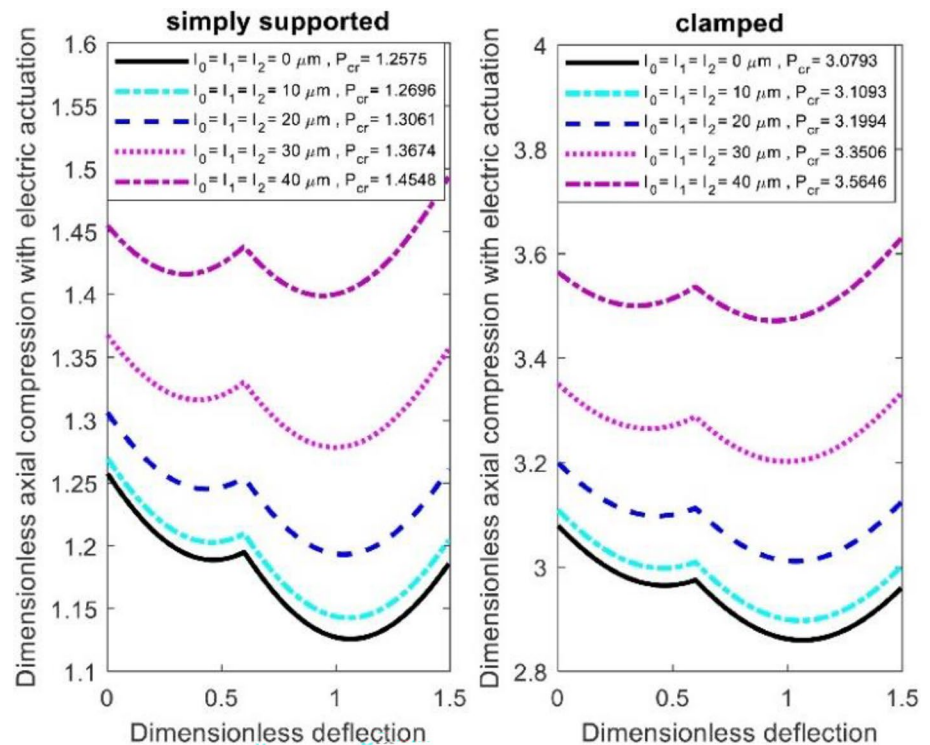


Fig. 62 The 3D mechanical/electrical load–deflection graphs of FG piezoelectric microshells with and without the micro-strain gradient tensors @ ($V_0 = -500$ v, $\Delta T = 0^\circ\text{C}$, $\eta = 0.5$) [321]



RBF proved to be efficient in buckling analysis in these circumstances. Liu [329] employed the RPIM to analyze shear deformable laminated plates subjected to numerous BCs for static buckling. The displacement and CBLs were determined using the TSDT. The results shows that the critical buckling stresses of the three unique plate models grow as the modulus ratio (E_1/E_2) increases. Additionally, it has been noted that as E_1/E_2 rises, and the error concerned between CBLs expected with classic laminated plate theory (CLPT) as well

as TSDT expand. The RKPM method has been employed to investigate the large deformation problems NL elastic materials under different case load (plain strain compression and tension and axisymmetric compression) [131]. The buckling analysis for square shape with a hole, subjected to uniaxial tension was examined. A reduction in the maximum strain value in the numerical model and an increase in the reaction force will cause an increase in the internal length parameter value. As a consequence, the stiffness ratio will reduce but the strain

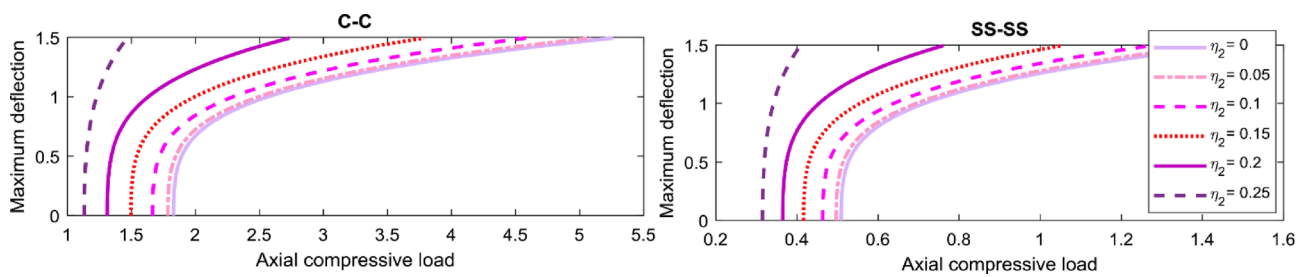


Fig. 63 The axial compressive load–deflection for different NLC parameter values; CC and SS BCs [282]

ratio will rise [294]. Ferreira et al. [295] employed the RBF collocation with two higher order Zig-Zag models to mimic laminated plates and four layer $[0^\circ/90^\circ/90^\circ/0^\circ]$ as well as three layer $[0^\circ/90^\circ/0^\circ]$ square cross-ply laminates SS and CC supported. Both uni-axial and bi-axial buckling load were applied. Figure 69 illustrates the first four buckling modes for bi-axial buckling load SS laminated plate of three layer $[0^\circ/90^\circ/0^\circ]$ for SINUS-ZZ formulation. The obtained results shows that for all various grids the results obtained with applying CC BCs were higher than those obtained with SS.

Ferreira et al. [330] examined the stability of elastic plates (isotropic plates and cross-ply laminated plates) under uni-axially and bi-axially buckling load hence; the eigenvalues were considered as the buckling loads. The BCs were set as SS. The analysis was established by using the collocation RBF and TSDT of Reddy. It has been observed that results obtained by uniaxial load were much greater than those obtained by bia-axially load Fig. 70 presents the mode shapes

of $(45/-45/-45/45)$ laminates for uniaxial loading, with several a/h ratios, and $N = 15$. Excellent agreement was obtained by comparing the results with previous methods.

Kumar et al. [331] employed the MQRBF for discretizing the governing differential equations (GDEs), after proposing a novel inverse hyperbolic HSST (IHSSST) so as to analyze the stability of porous FGM plate on the base as shown in Fig. 71. While, three different types of porosity dispersal were taken into consideration. By investigating the enhancement of number of nodes, and span to thickness ratio (a/h) of the FGM-4 plate on the buckling load parameter subjected to biaxial loading were $a = b = 1$ and $n = 0.5$. It has been observed that increasing a/h leads to decrease the buckling load parameters wither in 1, 2, and 3 dimension. As an overall observation the maximum value of buckling load parameters in all different values of a/h were recorded at node distribution 7×7 .

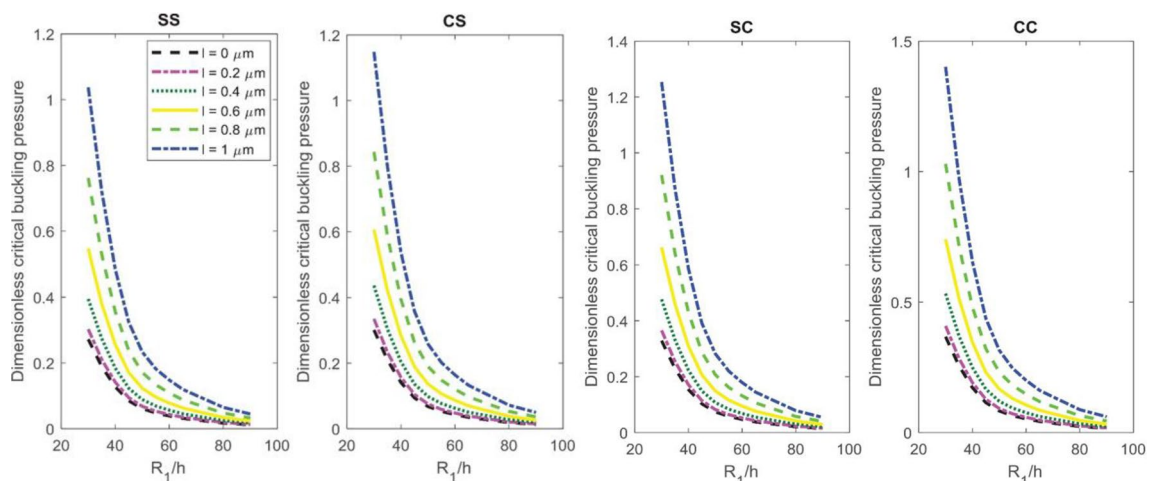


Fig. 64 The difference of the improved couple stress-based critical buckling pressure of FG composite conical microshells with ratio of R_1/h resulted from several minor scale parameters [322]

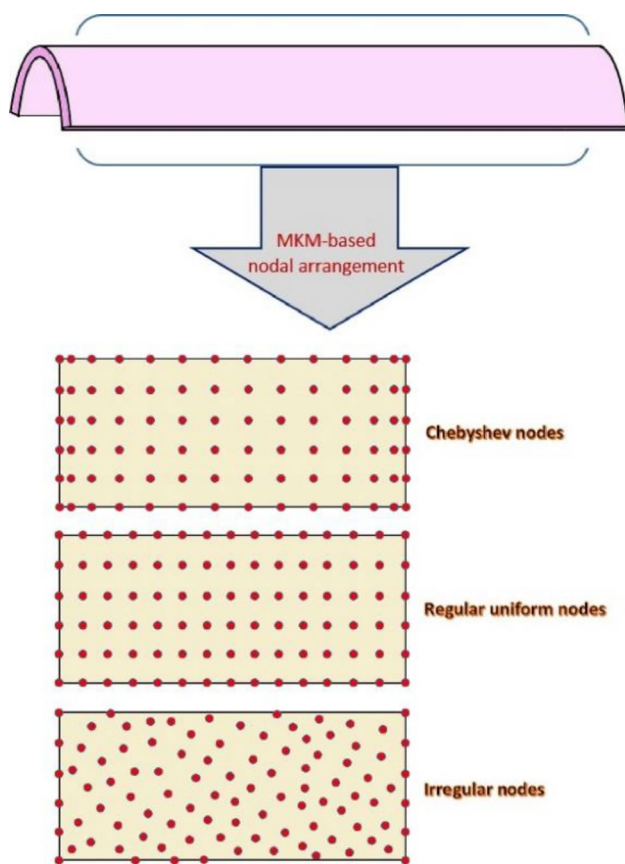
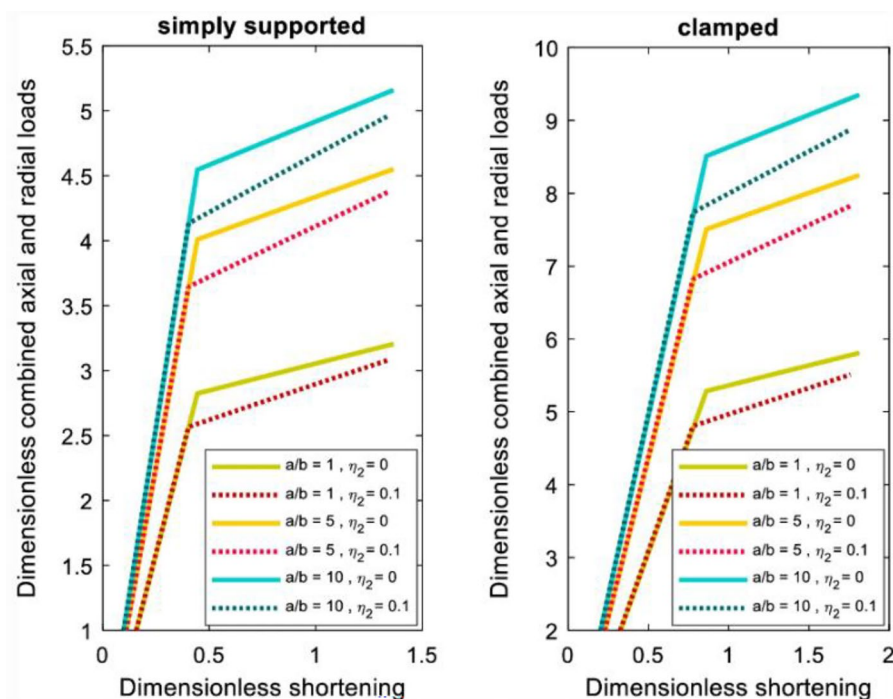


Fig. 65 The panel models with MK meshfree method based and various arrangement of nodal established on the Chebyshev, regular uniform and irregular patterns [324]

Fig. 66 The eccentric load-shortening behavior of arbitrarily reinforced microsized shells subjected to lateral dominated load having nanofillers with diverse aspect ratios ($l=40\mu\text{m}$, $V_{\text{GPL}}=1.5\%$) [325]



3 Dynamic Analysis

3.1 Free Vibration

3.1.1 Free Vibration in Nanoscale

A FV investigation for several CNT reinforced composites (CNTRC) plates in thermal atmosphere was conducted using the EFkp-Ritz technique. The analysis was run to evaluate NL vibration, and dynamic buckling. The outcomes illustrates that the fundamental ND NF's greatest and smallest values have been determined for CNTRC plates with CCCC and SFSF BCs. In addition, the maximum and minimum values of ND fundamental NF were observed for CNTRC plates with CCCC and SFSF BCs correspondingly, for various forms of CNTRC plates with varying BCs [338]. Furthermore, the dynamic vibrational analysis of nanocomposites plates reinforced using wavy CNT by employing the MLS method have been performed [339]. The MLS method has been used to examine the resonance as well as the FV of a finite length FG nanocomposites cylindrical reinforced with a wavy CNT [340]. The analysis shows that the vibrational behavior is highly influenced by the waviness of the CNTRC in cylindrical structure. As observed from Fig. 72, the lowest values of speed in radial vibration and the greatest values of amplitudes were shown in the first mode of resonance, considering the fact that the frequency of loading is improved during the second and third modes of resonance. Furthermore, cylinders with wavy CNTs exhibit greater amplitude and lower

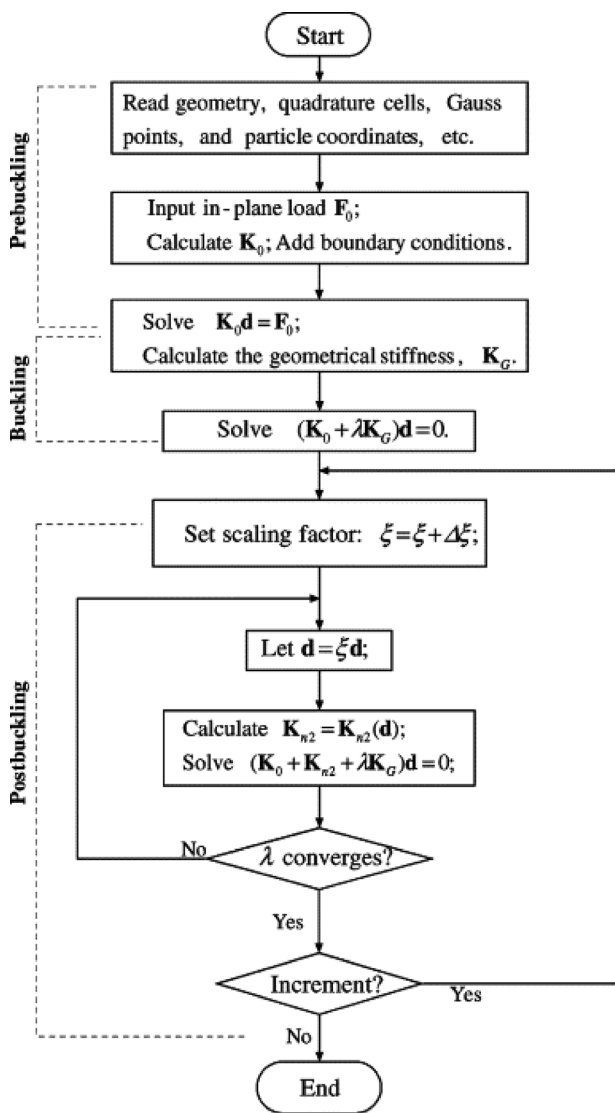


Fig. 67 The postbuckling analysis flowchart in a plate [252]

speed compared to cylinders with straight nanotubes. In addition, when CNT volume increase, the vibration amplitude will reduce, while it speeds for straight and wavy CNTRC cylinders in the all resonance modes.

Thai et al. [270] employed the MKI meshfree for the purpose of investigating the FV of nanoplate with and without hole. The obtained results show that, in the plate with complicated hole the frequencies rise with an increase in the l/t as well as the value of V^*_{CNT} . Additionally, the FGX and FGO patterns gave the major besides the minor values of ND natural frequencies, correspondingly. Also, the highest frequency values were recorded. Ansari et al. [341] employed the Galerkin for examining the NL FV for the frictional viscoelastic nanobeams. To determine the FV performance of a single layered graphene sheet (SLGS), Zhang et al. [342] applied the Kp-Ritz technique combined with the

NLC continuum model as an element-free computational framework (EFCF). In addition, the Eringen NLC constitutive equation joint with the classical plate theory were combined by the NLC continuum model, and it revealed to have the capability of accounting for the small scale effect. Furthermore, the Kp-Ritz method proved to be efficient for solving SGLGS vibration of NLC continuum model. Figure 73 illustrate the first eight vibration mode shapes of CCCC BCs for SLGS.

Ghayoumizadeh et al. [343] has applied the local integral equations (LIEs) founded on the MLPG technique to investigate the displacement field as well as finite length FG nanocomposite reinforced by CNT's elastic wave propagation under a transient dynamic analysis. The arrangements of the aligned CNTs was deduce to differ as three types of FG dispersion along with the uniform distribution (UD) throughout the radial direction of axisymmetric reinforced cylindrical composites. A unit step function was employed to examine the function in the LWF that led to local integral equations (LIEs). The examined territory was separated into smaller sub-domains with a circular shape. Ejabati and Fallah [344] implemented the meshfree finite volume method (MFVM) so as to investigate the enhancement of air drag on dynamic analysis for the moving nanoparticles. The GEs were integrated over control volumes (CVs) boundaries and approximated by Gauss quadrature methods. A comprehensive analysis was carried out to validate the possible applicability of the MFVM to solve problems in the nanoscale state when compared to exact solution methodologies. Besides, the MLS method has been utilized to estimate the unknown field variables. Dastjerdi et al. [345] have investigated the aspect ratio and the impact of CNT waviness on the vibrational performance by applying the MLS meshfree method and the FSDT for a sandwich plate made of a pure polymeric core and the outer layer made of two CNT/polymer. Also, the Winkler spring has been used on the foundation as shown in Figs. 74 and 75.

The MLS method was employed with TSDT for the purpose of resolve the couples governing eigenvalue equations of the smart multifunctional sandwich plates proposed in Fig. 74. The results of this study shows that the implanting of pores inside the core will improve the NF of the plate owing to the significant decrease in the weight of the structure, as shown in Fig. 76 [346].

An essential study for vibration analysis of structure with nanoscale was established by Kiani [347] were he employed the RKPM meshfree technique to examine the FV of nanorod as shown in Fig. 77 with two different set of BCs (fixed-fixed and fixed-free). The AMM model was execute to check the precision of the RKPM methodology. The attained natural frequencies by the models were similar. Furthermore, the fluctuation of FFs relative to the support

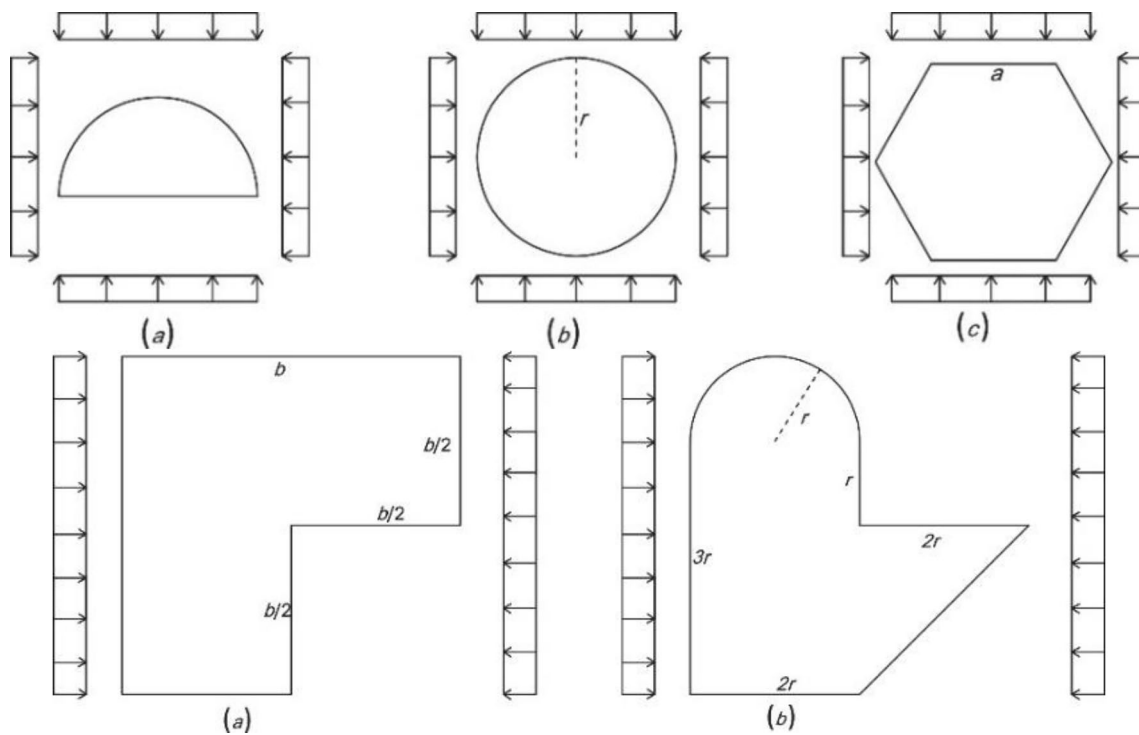
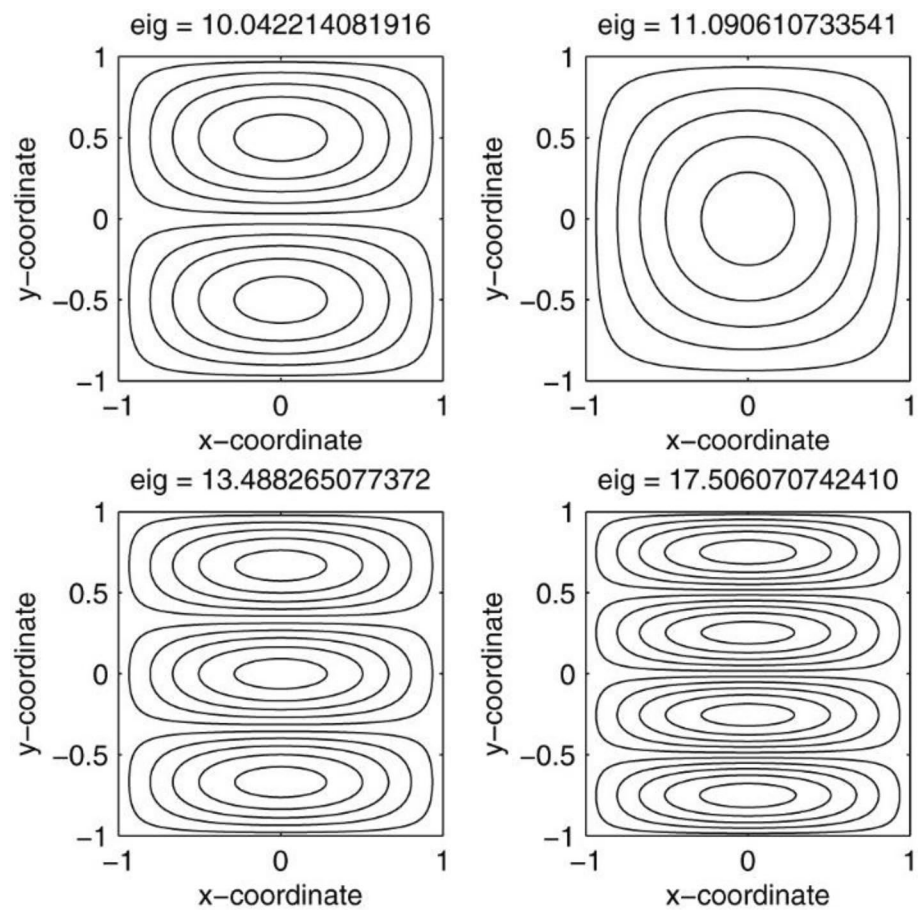


Fig. 68 Different geometry shapes of thick plates [8]

Fig. 69 The first four buckling modes for bi-axial buckling load of three-layer $[0^\circ/90^\circ/0^\circ]$ SS laminated plate for SINUS-ZZ formulation [295]



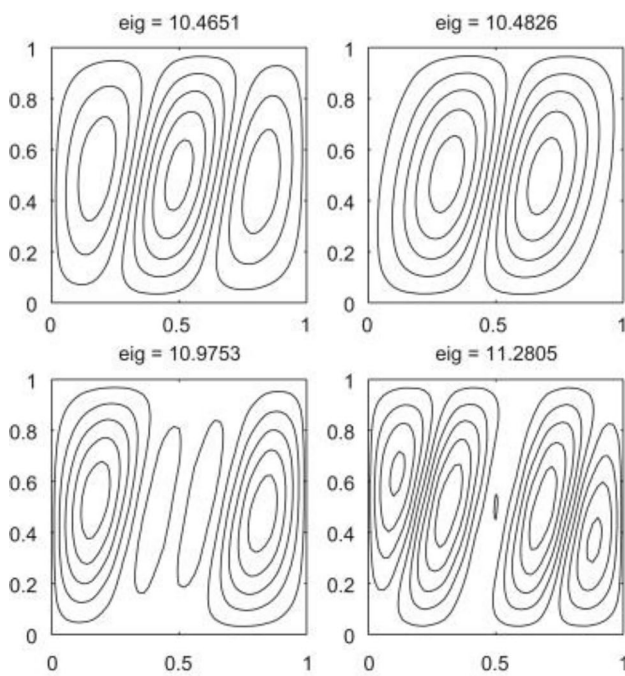


Fig. 70 The mode shapes of (45/−45/−45/45) laminates for uniaxial loading, using various a/h ratios, and $N = 15$ [330]

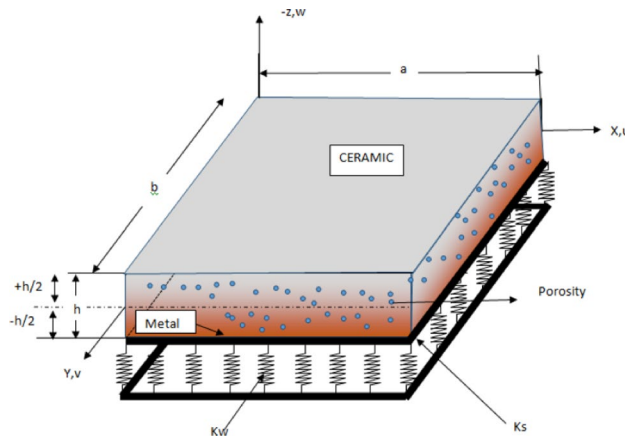


Fig. 71 The schematic of FGM plate with a rectangular geometry and porosity inside the coordinate system [331]

stiffness is supplementary visible at lower support stiffness levels. The impact of the support stiffness at one end on the essential frequency decreases as the stiffness of the support at the other end increases. It specifies that if the right side end at the nanorod have no traction, the left support stiffness on the basic f of the nanostructure extends the maximum value.

A linear FV analysis of FG-CNT of plates structure with elliptical geometry has been performed by using the MLS meshfree method with FSDT and HP [348]. The outcomes

shows that the vibration characteristics can be remarkably improved by the thickness direction of the FG-CNT. Additionally, the ND NF is decreased by rising the aspect ratio. High stability in the plates can be guaranteed by increasing the CNT VF, it also guarantees higher values of ND fundamental frequencies. Figure 78 illustrated the first nine mode of vibration.

Jankowski et al. [349] examined the FV of FGM sandwich nanobeam structure as presented in Fig. 79, which is SS by employing the Differential Quadrature Method (DQM) meshfree method. For the purpose of employing the NSGT with the basic Reddy TSDT for beam modeling assumption for developing a vibration base piezo electrically actuated smart nanoactuator model. The results of distributing the porosity in combination with external electric potential shows that increasing the L/H parameter will increase DL natural frequencies. Reducing l/t ratio will increase the DL natural frequencies.

Mohammadimehr et al. [350] investigated the viscoelastic double bonded polymeric (DBP) nanocomposites plate reinforced by FG-CNT's with a base design by viscoelastic foundation on MSGT to define the FV as shown in Fig. 80, by the MLS meshfree method with Navier's to define the NF of the nanocomposites. Furthermore, different dispersal of SWCNTs were examined for instance; FG-O, FG-V, FG-X and UD. The obtained results show that, due to the fact that the distribution of FG-X SWCNTs were discrete steadily in all the territories of the polymeric nanocomposite plate as presented in Fig. 81. It recorded the highest non-dimensional natural frequency (NDNF), and the lowest value of the NDNF in the FG-O. Additionally, increasing the aspect ratio of a/b will reduce the NDNF. Another remarkable outcome was that the nanocomposite was gradually converted to beam model with decrease in its rigidity, by increasing in a/b .

The RKPM has been applied to define the natural flexural frequency of nanotubes, to obtain the mechanical performance of the double walled carbon nanotubes (DWCNTs) for sensing the nanoparticles at various BCs [351]. For all BCs sets that have been considered, the deviation rate of first NDNF of the nanosensor in expression of the entire number of RKPM's particles seems to reduce. As the quantity of RKPM particles rises, the predicted results derived from different NLC technique combine to the specified values for each set BCs rise. Furthermore, a free flexural vibration study of the DWCNTs with random BCs by RKPM meshfree method has been performed [352]. It has been observed that in small scale parameters the natural frequencies decrease, especially at high mode of vibration. Also, at all various kinds of applied BCs, the natural frequencies express an improvement through the surrounding matrix lateral stiffness. Additionally, by adding the clamped-free (CF) BCs, the highest enhancement of the surrounding matrix

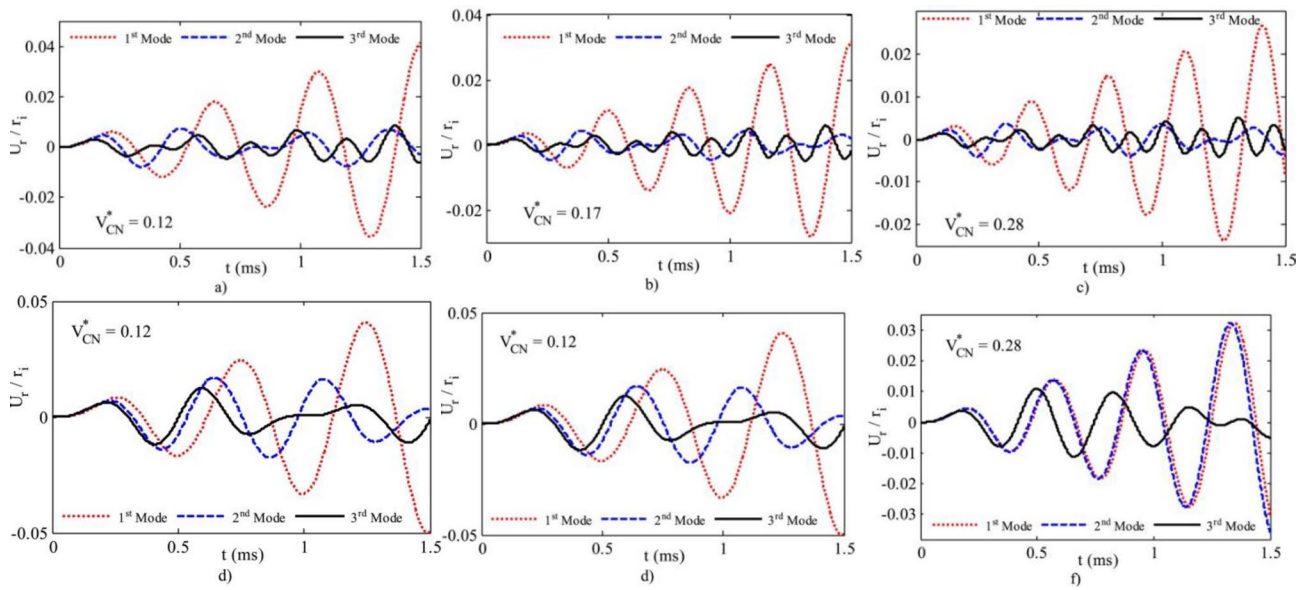


Fig. 72 Three first modes of radial vibration of the X-CNTRC cylinders with $r_i=0.1$, $r_o=0.2$, $L=0.4$ m, $AR=1000$ for **a–c** $w=0$ and **d–f** 0.425 at mid radius [340]

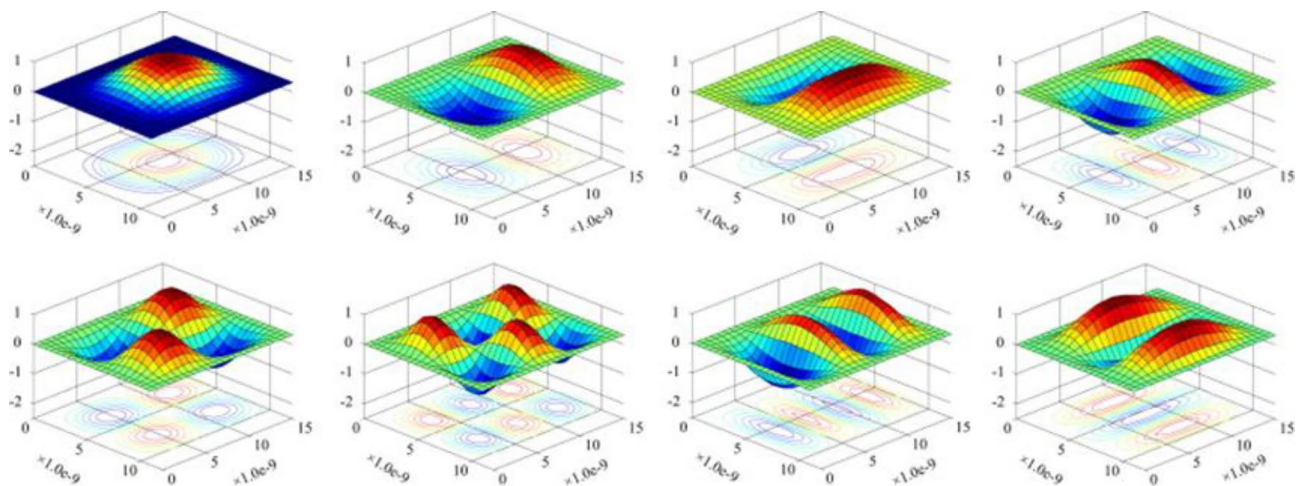


Fig. 73 The first eight vibration mode shapes of SLGS @ CCCC BCs [342]

rotational stiffness on the first natural vibration variations were obtained. For analyzing the FV performance of the FG nanoplates with diverse geometries, the NLC strain gradient meshfree method founded on the NSGT and HSST was developed. Furthermore, the MK meshfree approach was used to define the natural frequencies [268]. The results show that the natural frequencies decreased when l/t increase. For the n , as strain gradient parameter and the NLC parameter increases, the natural frequencies remains the same with these changes. Alshenawy et al. [353] developed a meshfree collocation technique to discretize the NL GEs using an amalgamated of polynomial and multiquadric basis functions (MQBF), in order to evade any potential

singularity in a bridge form of an energy harvester nanobeam alongside SS and CC BCs as shown in Fig. 82. The obtained results shows that the implementation of nanoscale energy harvesters improves the magnitude of surface stress impacts on acquired voltage from 24.77 to 25.59% for SS BCs and from 26.86 to 27.38% for CC BCs. Furthermore, a greater cluster volume proportion leads to rise the required period of time. As a result, the time for the SS energy harvester at nanostructures increases from 34.50 to 35.21 μ s founded on the classical model, as well as from 32.98 to 33.61 s based on the surface elastic-based model. The total required period for the CC energy harvester at nanostructures increases from

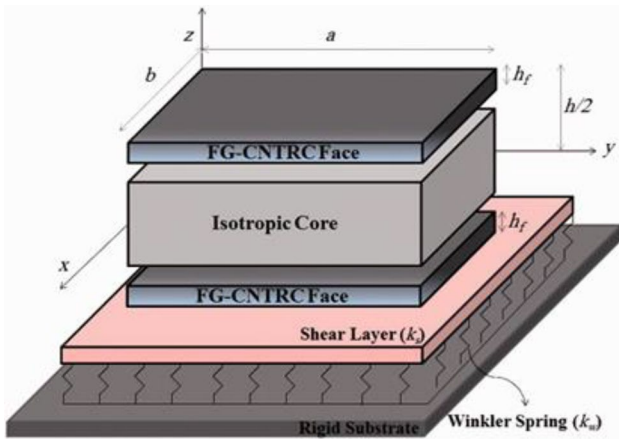


Fig. 74 The sandwich plate structure with 2 FG-CNTRC face sheets with the elastic basis [345]

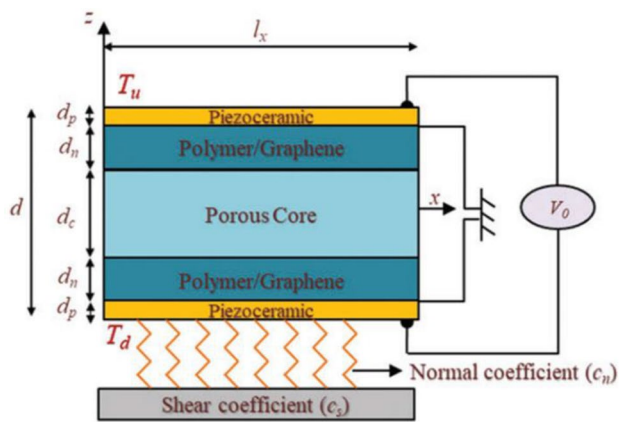


Fig. 75 The arrangement of the layers of the smart multifunctional sandwich plate structure [346]

32.88 to 33.46 s using the classical model, and from 31.54 to 32.08 s using the surface elastic-based model.

Sobhani et al. [354] investigated the FV of combined shells (hemispherical-cylindrical-conical) made of a hybrid porous nanocomposites (nanoscale 3D Gr foams, epoxy matrix as well as macroscale carbon fiber) as shown in Fig. 83. The GDQM has been employed in order to define the governing differential equations, and HP has been used to determine the governing equation of motion. The obtained results shows that in all patterns, rising the porosity factor will leads to reduce the NF. Besides, for all she thickness' values the hemispherical part meridional angle increments' enhanced the NF of the combined structure under CC and FC BCs. Sobhani et al. [355] accomplished a vibrational analysis of joined conical-conical-cylindrical shell (JCCCS) by presenting 30 different geometries all made of Gr nanoplatelet (GNP) as a nanocomposite (GNPN) as illustrated in Fig. 84. The purpose of using the GNPN is to influence the vibrational behavior of the JCCCS. The study has been accomplished by implementing a variety of methods where the Donnell's simplification and FSDT were employed for accessing the core relationships related with the JCCCS, and HP to define the differential motion equations (DMEs). To verify the mechanical marks; the HT combined with rule of mixture hypotheses were implemented. While the GDQM has been utilized for discretizing the DMEs. The outcomes of that study shows that, in all cases the highest NF values were recorded in the structures which has PX patterns dispersal of GNP, while the PO patterns dispersal has the minimum values of NF. Also, at greater modes the influence of GNP dispersal on the NFs is more significant. The researchers who are interested in ocean engineering generally are recommend to check the article for more details. The same methodologies GDQM, Donnell's simplification, FSDT and HP were employed by, Sobhani et al. [356] also for FV analysis but in this article the authors were interested

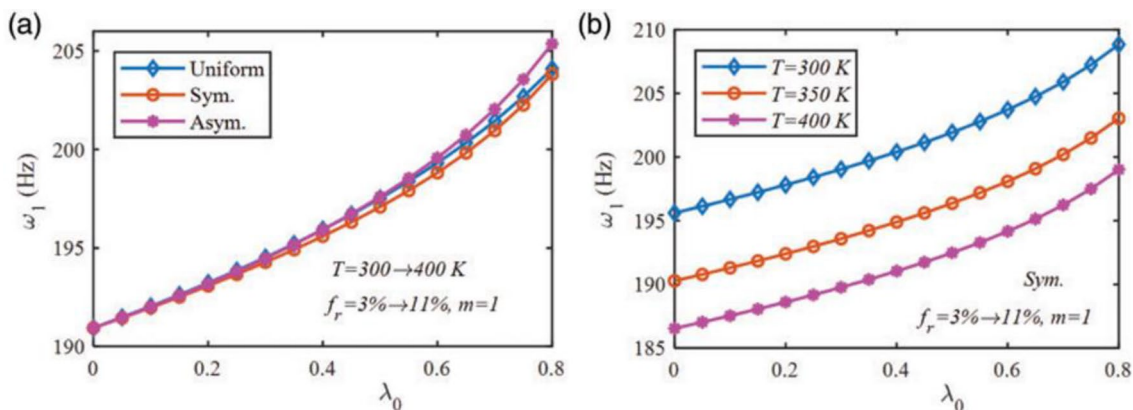


Fig. 76 The relation between the essential frequency of SMSP with porosity volume for **a** porosity dispersions and **b** environment temperatures [346]

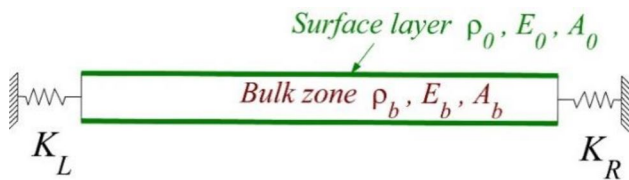


Fig. 77 The schematic of the elastically nanorod with fixed-fixed BCs [347]

on studying the FG-GNP as well as FG-CNT sandwich composite JCCCS. The enhancement of various BCs sets, several geometrical parameters and material conditions on NFs were considered. Sobhani [357], performed a recent study for the purpose of investigating the vibrational performance of a marine structure in which two various full-spheroidal and semi-spheroidal shells were connected to a conical shell.

Sobhani and Safaei [358], employed the GDQM for discretizing the equation of motion of a nanocomposite conical shells structure made of Gr oxide powder (GOP) based on Winkler as well as Winkler-Pasternak EF as shown in Fig. 85. Also, the HT and the rule of mixture techniques were utilized for discovering the nanocomposites' operative values. While for defining the essential connections of the structure the FSDT combined with Donnell's shell theory were used. Additionally, the equation of motion has been defined by HP. It has been observed that increasing the parameters of Winkler stiffness caused an increase in all presented models responses. Also, in case of using the Winkler-Pasternak the shell models' responses raised owing to the fact that Pasternak layer support a hardening condition. However the hardening condition play a major

Fig. 78 The first 9 mode shapes of FG-CNT elliptical plate SS; where $a/b=2$, $b/h=100$ and $V_{cn}^* = 0.17$ and FGX [348]

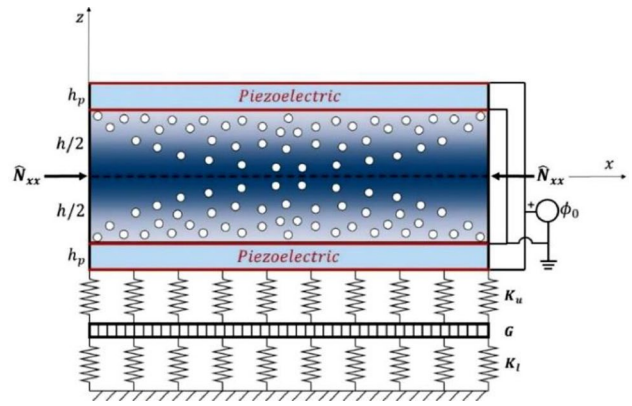
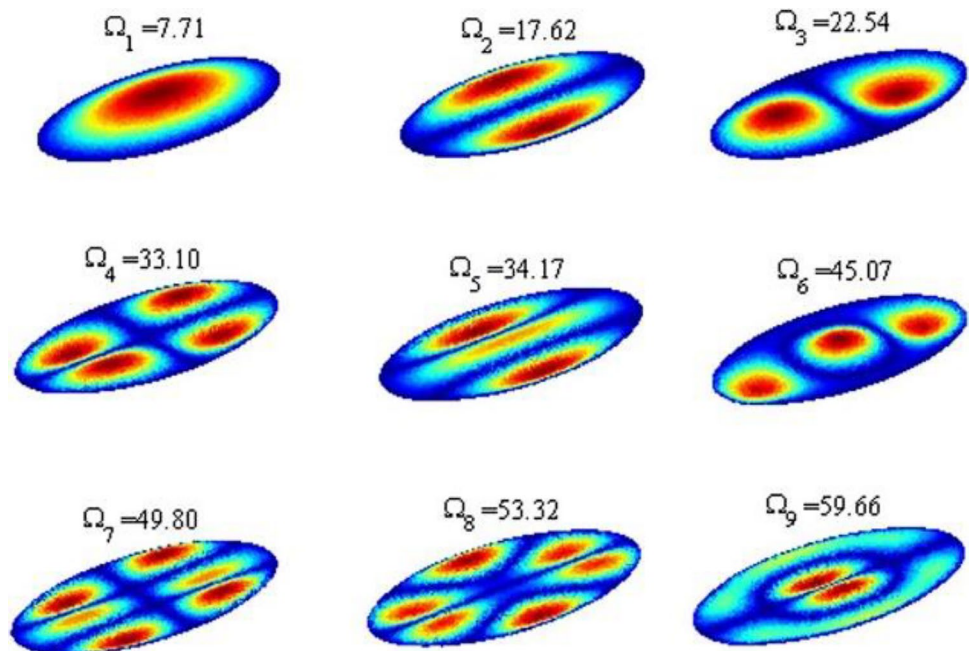


Fig. 79 The schematic of porous FGM sandwich nanobeam subjected to axial in-plane forces and external electric potential [349]

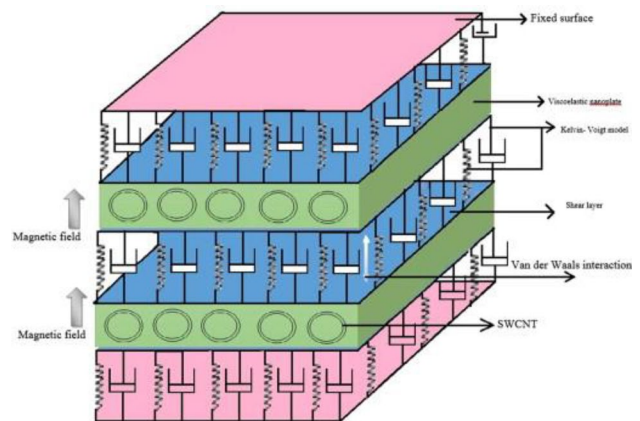


Fig. 80 The schematic of the BDP viscoelastic (nanocomposite plate structure) implanted in the visco-Pasternak foundation [350]

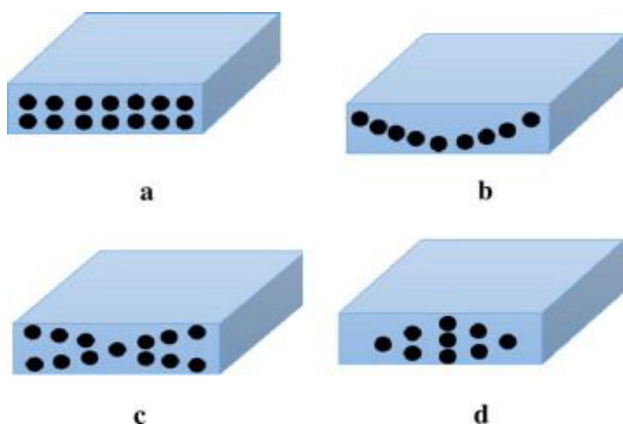


Fig. 81 Different distributions of SWCNTs in the nanocomposite plate structure; **a** UD **b** FG-V **c** FG-X **d** FG-O [350]

role in the effect of Pasternak on the system response. Additionally it is observed that even the minimum values of NFs dropped down by changing the BCs to FF. In another recent study for the same authors, Sobhani and Safaei [359] the same methods were employed for investigating the NF of a porous nanocomposite by embedding CNT and coupled hemispherical-cylindrical marine shell-system.

3.1.2 Free Vibration in Microscale

A FV analysis for (homogeneous square, isotropic FG square, sandwich FG square) microplate have been done by

Thai et al. [280]. The observation shows that in homogeneous square microplate, the maximum value of the first NDNF were recorded at $l/h = 1.0$ as well as $a/h = 100$ and it reached 13.6470. While for isotropic FG square, a close enough value = 13.5617 were recorded at the same l/h ratio but with different $a/h = 20$ and $n = 0$. However, for sandwich FG square the maximum value of NDNF was much more smaller compared to the other two geometrical structure were it reached 3.9325 at $a/h = 10$, $l/h = 1.0$ and $n = 0.5$. Figure 86 illustrates the first six modes shape of dynamic performance of this geometry at the same a/h and l/h values but $n = 1$.

To investigate the FV behavior of microtubules founded on an atomistic-continuum model Xiang and, Liew [371] applied a meshfree numerical scheme method with a higher-order gradient continuum constitutive. Figure 87, illustrates the microtubules structure. The effect of various length and BCs on the microtubules NF were examined, and showed that by increasing the vibration mode the predicting natural frequencies were increasing. Sahmani and Safaei [372], employed the Galerkin mesh-free technique collective with the basic of GDQM and the pseudo-arc-length continuation approach, for generating a numerical solution. For the purpose of investigating the NL FV of a micro/nano-beams made of bi-directional functionally graded materials (2D-FGM) as illustrated in Fig. 88. The SS and CC BCs were considered. Figure 89 illustrates the NDNF deflection response of the 2D-FGM micro/nano-beams effected by the NLC size effect. The obtained results shows that the NL frequency to linear

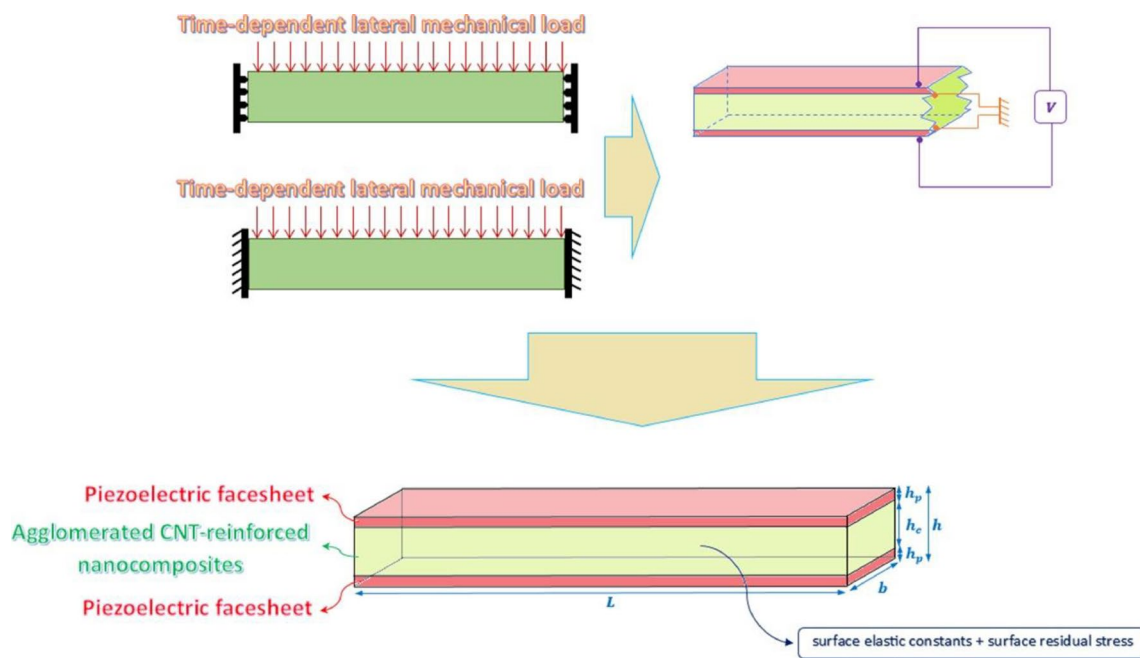


Fig. 82 The schematic of nanobeam-energy harvester subjected to time-dependent mechanical load [353]

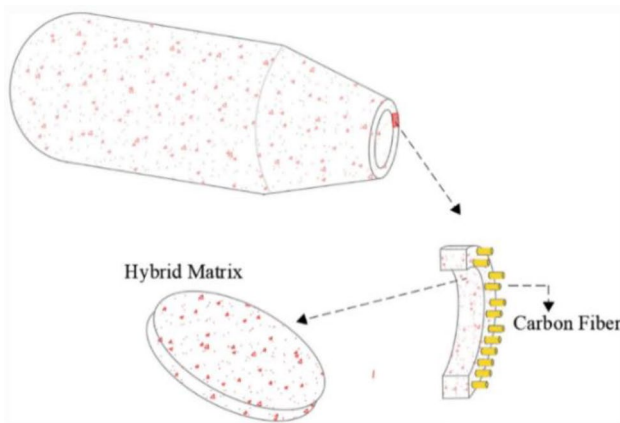
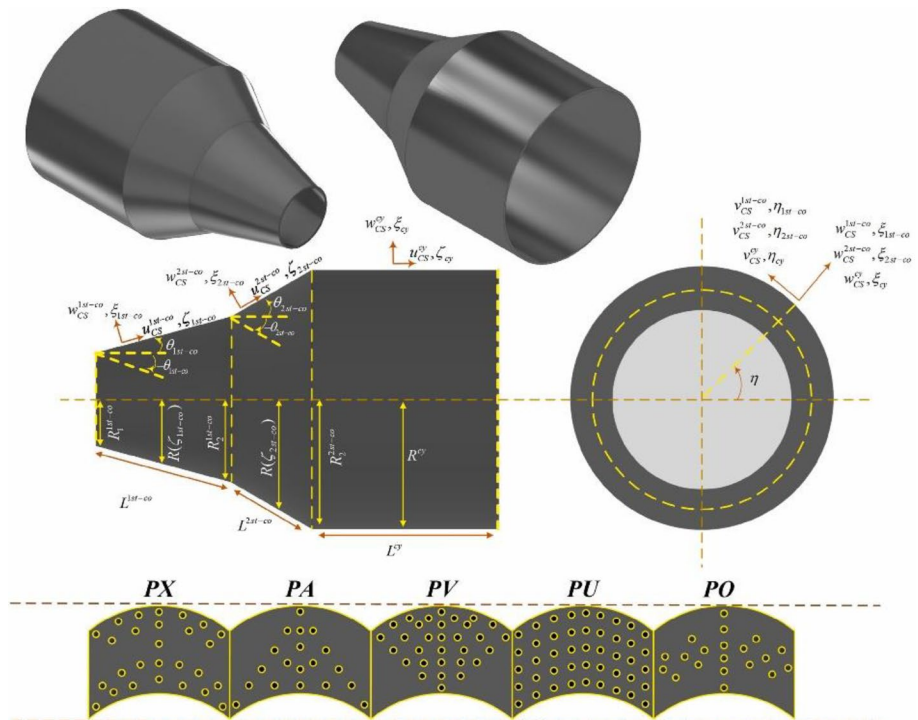


Fig. 83 The hybrid matrix carbon fiber nano-composite combined (hemispherical-cylindrical-conical) schematic shell structure [354]

frequency (W_{NL}/W_L) ratio increased at an extreme specific value of the deflection by the NLC size effect. Although (W_{NL}/W_L) ratio decrease by the small scale effect of the strain gradient. This configuration considered as more noticeable for greater amount of the maximum deflection. Yuan et al. [373] published an extensive study for a NL FV analysis of a conical microshells made of FGM in-plane with composite material in micro/nanoscale as shown in Fig. 90. The Galerikin method combined with the GDQM were used to obtain a mathematical model for obtaining the NL modified couple stress-based on the frequency of the structure.

Fig. 84 The concept of the GNPN-JCCCS schematic with its geometrical features [355]

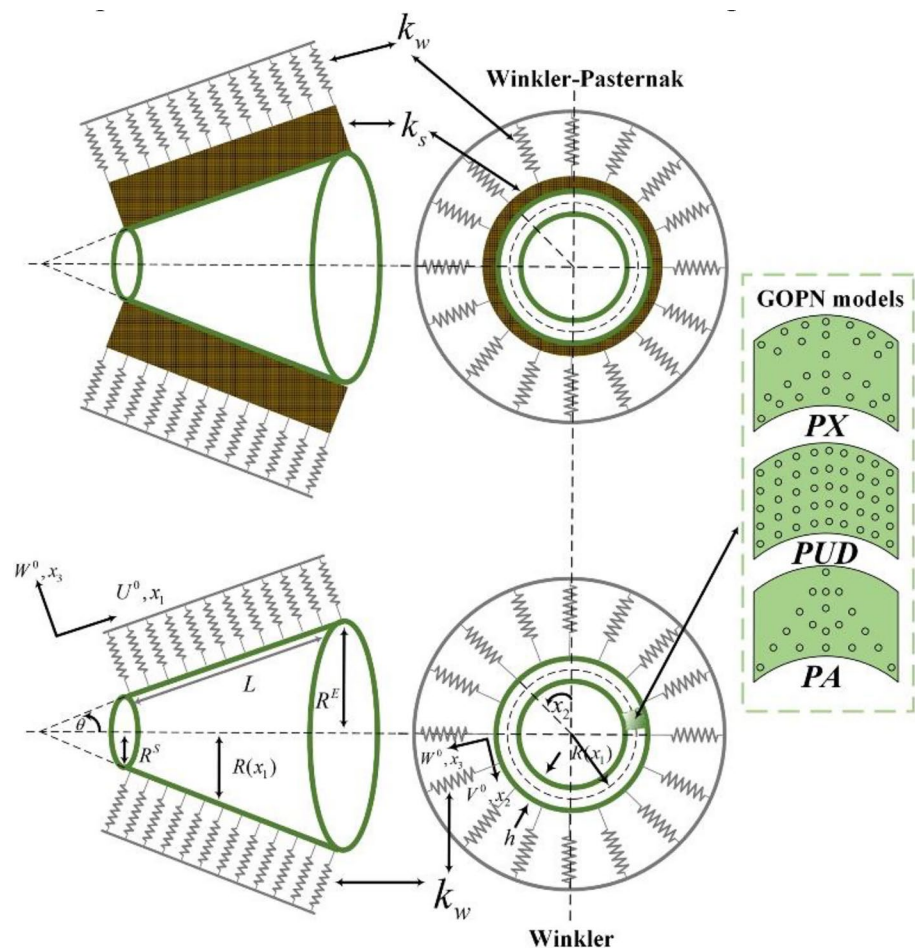


3.1.3 Free Vibration in Macroscale

According to Liew et al. [334], the RKPM with FSDT of the Mindlin/Reissner type have been exposed to be an exact and effective tool for finding the arithmetical solutions for FV of plates with diverse geometrical shapes and BCs. The lower order vibration modal shapes of a CC circular Mindlin/Reissner plate are presented in Fig. 91.

The goal of Zheng et al. [379] was identify the FV continuum structures with the EFG and SIMP and to maximize the essential eigenvalue while taking the nodal density into consideration as a design variable. Gong et al. [380] have used the modal topology optimization method to maximize the first order NF by applying the EFG with SIMP technique. Wu and Chiu [381] established RMVT-based MC and EFG methods for quasi-3D FV analysis of multilayered composite and FGM plates. The essential field parameters were interpolated utilizing DRK interpolants, which was generated using uniformly or NU distributed nodes, in these approaches. The exhibited examples show that the present MC and EFG solutions converge faster and have a high correlation with the earlier published approximate and precise 3D solutions of FGM sandwich plates. Where the highest order of basic functions (n) is suggested to be $n = 3$, the number of uniformly distributed nodes (N_p) is suggested to be $N_p = 21$, as well as the radius of the influence zone (a) is suggested to be (a) is assumed to be 3.1 times the distance among the adjacent nodes. The impact of aspect ratio, shear deformations, layer thickness ratios, and material characteristics

Fig. 85 The schematic of GOP nanocomposites shell based on Winkler-Pasternak EF [358]



gradient indices on frequency characteristics and their associated through-thickness dispersion of various modal field variables are investigated using a parametric approach. Additionally, the illustrative examples demonstrate that as the material characteristic gradient index grows, the variations of the through-thickness dispersion of different variables between FGM plates ($k_p \neq 0$) and homogeneous plates ($k_p = 0$) becomes progressively important. Likewise, the free-traction conditions on the sandwich plate's lateral surfaces, in addition to the displacement and transverse stress continuity conditions at the interfaces among neighboring layers, were precisely achieved. Figure 92 demonstrates the varying through-thickness dispersals of several modal field parameters with the material characteristics index, k_p , where $k_p = 0, 1$, and 10. It is demonstrated that the dispersals of in-plane and out-of-plane variables for the homogeneous plate, where $k_p = 0$, are higher-order polynomial fluctuations across the thickness coordinate, whereas there are higher-order polynomial variations for the FGM sandwich plate, where $k_p = 1$ and 10. Also, The free-traction features of the sandwich plate's lateral surfaces, in addition to the displacement as well as transverse stress continuity constraints at the interfaces between nearby layers, were perfectly met.

Ferreira et al. [382] have used the MQRBF to examine the symmetric laminated composite plates' FVs. The set of motion equations for the FSDT define an eigen-problem that can be solved using a variety of methods. The output results are in excellent agreement when compared to previously published results of FEM or meshfree techniques. The results for CC skew plates are always greater than those for supported plates because; of the collocation technique around the plate corners. This approach is a straightforward yet effective substitute for conventional meshless or FEM for analyzing the laminated composite plates for FV.

The meshless local collocation technique founded on a thin plate spline RBF has been employed by Xiang and Kang [383], to evaluate the FV behavior of laminated composite plates. The FSDT GEs and BCs have been discretized utilizing the local thin plate spline collocation approach. The MRPC technique has been used for developing a mathematical model as well as examining the FV of isotropic plates (square, circular). However, the results illustrate that at $n=9$, the highest amount of ND frequencies were gained at mode 8 for square and circular with $h/b=0.1$, and equal to 10.9057 and 125.45 respectively [384]. These method provides an

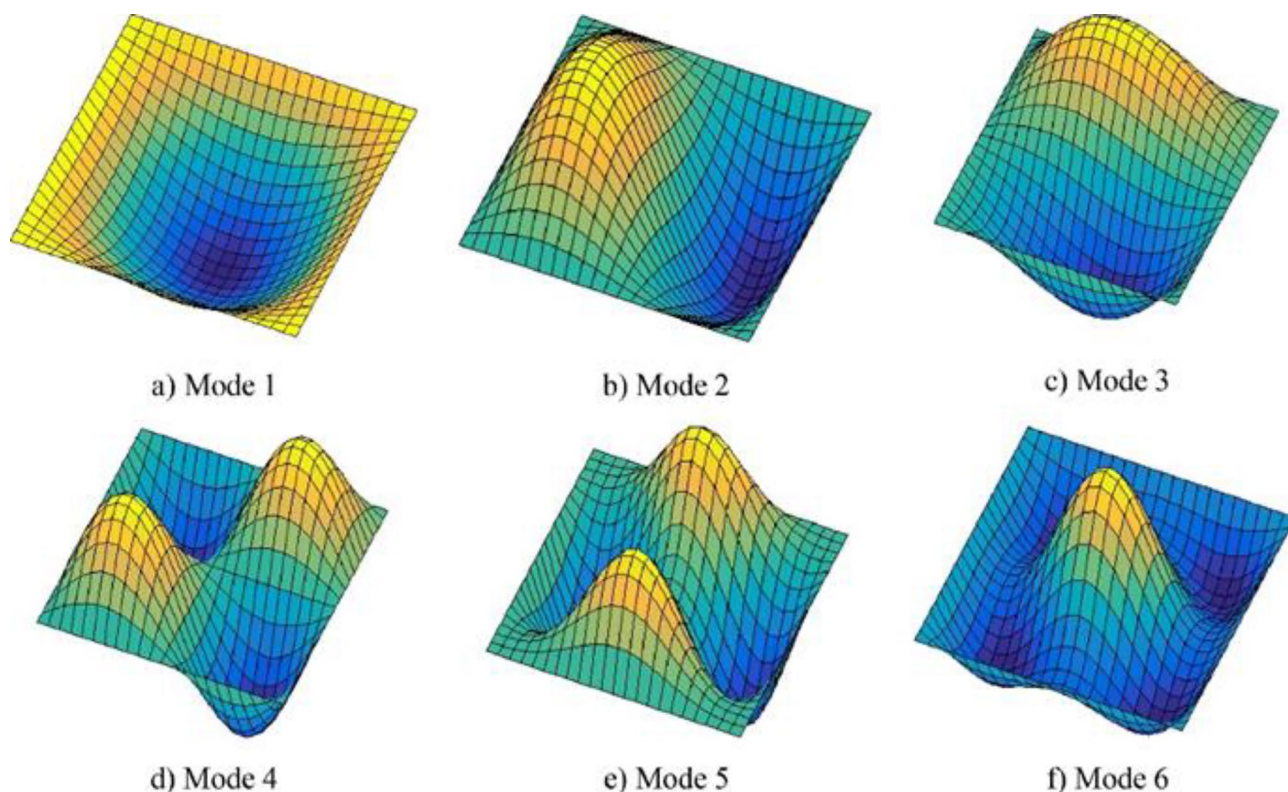


Fig. 86 The sandwich FG square microplate first six modes shape of dynamic response of this geometry at the same a/h and l/h values but $n=1$ [280]

opportunity to investigate with the optimum order number to estimate the structural issue less than inquiry and absence of any shear correction factor. Moreover, the FV analysis of symmetric composite plates by meshless MQRBF and trigonometric layerwise deformation theory discretized have performed. Besides, exceptionally solutions for the FV of composite and sandwich plates was provided [68]. The frequency analysis for five different thin plate's geometry were processed by using EFG with MLS meshfree methods [289]. A high efficiency analysis with significant convergence were observed. Additionally, the maximum value of NF of lateral FV in all different shapes of plates were recorded at the 10th mode. Dai et al. [290], used the HSDT with EFG to investigate the NF and static deflection of thin and thick laminated composite plates. A penalty technique execute fundamental BCs by numerous arithmetical models for laminates with diverse a/h , material coefficients, BCs or ply angles. The outcomes shows that the first three frequencies corresponding to the rigid displacements were $=0.0$, for the thick laminates CPT constantly over predicting natural frequencies [290].

It has been discovered that the superposition-Galerkin approach can be employed to accurately analyze the FV of a rectangular plate that is totally free. A general analysis of

all probable modes of the totally free plate is conceivable by coupling the given sets of building blocks with related sets driven along the edges $\eta=0$ and $\xi=0$. To obtain the extension in capabilities as most of the components of the larger eigenvalue matrix linked to the described problem, some additional research is required. One might be concerned about the requirement that pairs of building blocks can be used instead of individual ones in the new method for thin plates. On the condition of the Mindlin plate, a set of three blocks was used in place of the earlier procedure's individual blocks [385]. For the FV analysis of composite laminates with complex plate shapes, the EFG approach has been developed. Several numerical examples were provided and compared to previous findings to demonstrate the efficacy of this method in determining the natural frequencies of laminates. A good convergence for the EFG can be observed. For plates with regular shapes, there have been some significant agreements with other numerical results. Besides, it was investigated to show how the fiber orientation affected the frequencies for laminates with various forms and BCs. The outcomes shows that the EFG technique is reliable for the purpose of evaluating the FVs of laminated composite plates with complex shape [386].

Jayakumar et al. [387] have investigated the NL FV analysis of plate structure (SS piezo-laminated) with material

Fig. 87 **a** The microtubules structure and its subunits and **b** the homogenized model of protofilaments fraction [371]

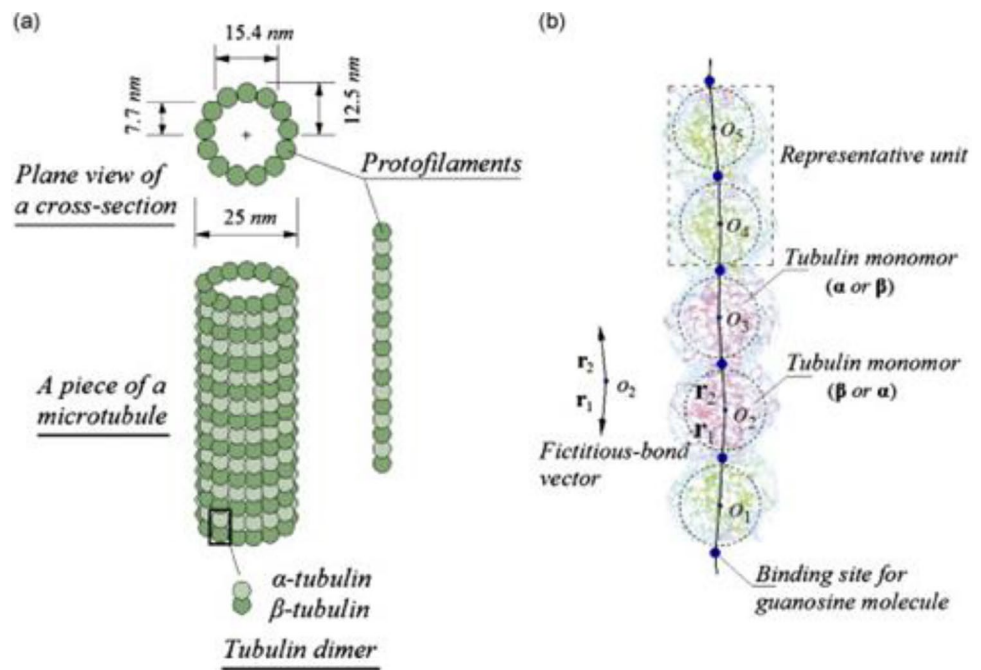
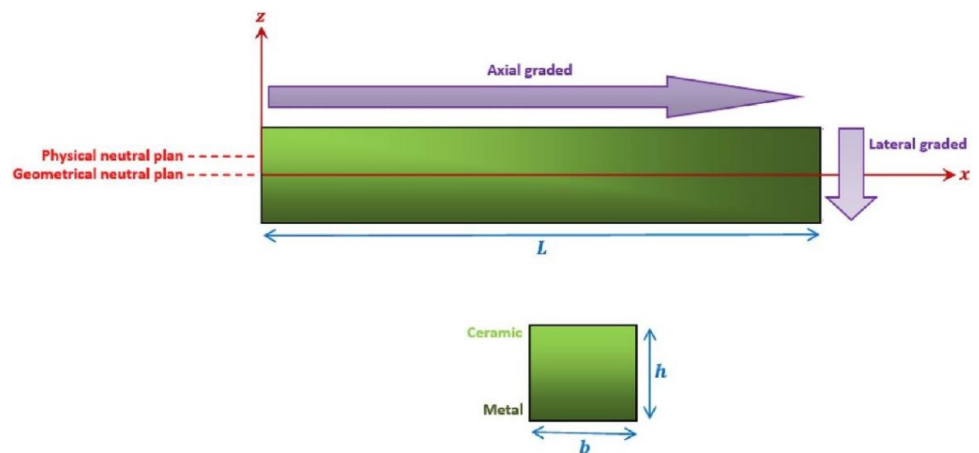


Fig. 88 The schematic of a 2D-FGM micro/nano-beam [372]



properties and arbitrary actuation electric potential difference by using the Galerkin meshfree method. Furthermore the same methodology was utilized for determining the linear/NL FVs for plates made of composite and fiber metal laminated in a close form solution [388]. Besides, Morozov et al. [389] applied the same technique to analyze the vibrations for fully CC sandwich plate. The arithmetical solution, analytical approach, as well as FEA were used to investigate the impact of panel size, elastic characteristics, and face and core densities on the basic frequency. The research reveals that the critical solution presented in that work can calculate the first NF with appropriate precision. A novel plate structure made of sandwich panels with geometry of square honeycomb cores have been analyzed in a purpose of studying FV, bending and buckling. Also, the HP parallel with Galerkin method were performed [390]. The meshless MLPG has

been applied with the HSDT as well as normal deformable plate theory to examine the force and FV of a thick plates structure with rectangular shapes by Qian et al. [391].

The same structure has been used by Safaei et al. [392], to investigate the FV response by MLS under steady state thermal gradient loads. Figure 93, presents the impact of cluster volume and CNTs fraction exponent to the sandwich plate frequency at thermal gradient loads of $T_t = 400$ K and $T_b = 300$ K. As a consequence of rising the volume exponent of CNTs to $n = 1$, an instantaneous increase in (FPs) was noticed, followed by dramatically decrease. Furthermore, the schematic is shown in Fig. 94.

Gu and Liu [310] examined the FV of a thin beam by applying the LPIM and Euler–Bernoulli (EB) beam as an analytical solution. FV analysis was performed with diverse BCs (pined–pined, fixed–fixed, fixed–free, and fixed–pined)

Fig. 89 The DL NL frequency-deflection response of the 2D-FGM micro/nano-beams effected by the NLC size effect [372]

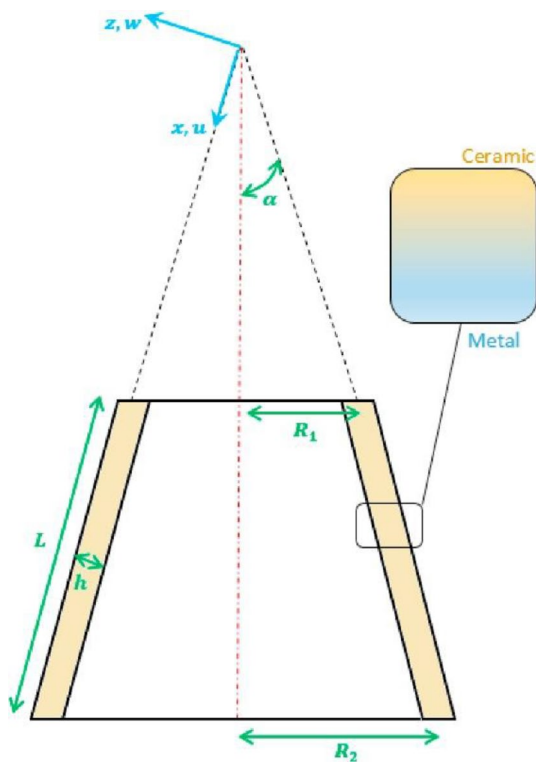
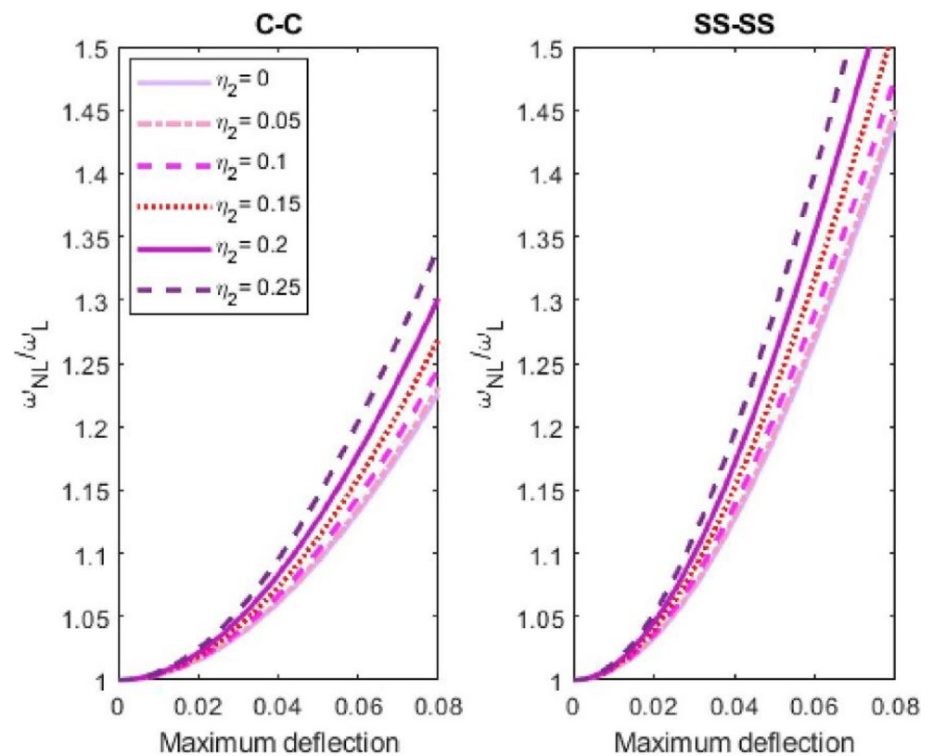


Fig. 90 The schematic of a FG composite conical microshell and the associated geometrical parameters [373]

at 21 uniformly distributed nodes as presented in Fig. 95. In addition, the time step and error % were considered in the force vibration analysis.

The local radial point interpolation (LRPIM) has been utilized by Liu and Gu [393], to study the boundary value problems for FV analysis purpose in 2D solids beam. The results show that these method is capable for use in both cases of regular and irregular nodal distributions. According to Liu et al. [394], it is recommended to use $\alpha=2$ in huge local support domains. Have used the point PI method which is a part of LRPIM meshfree approach to study the mode shape frequency and the static load of a 2D piezoelectric structure (disk and beam). However, a set of scattered nodes have been utilized to represent the problem boundaries and domain. Besides, the shape functions were derived founded on the PI approach. Both cases of ordinary and unordinary nodal distributions show good results. A FV analysis for a highly skewed plates have been investigated by Wu et al. [395], by applying the least-squares finite difference method (LSFD). Zhu and Liew [396] performed the FV analysis of moderately thick graded plates, by applying the local Kriging meshfree method. Zhang et al. [397] investigated the FV of a triangular CNT reinforced composite plates under plane stresses by employing the FSDT element-free technique. The various BCs and angles α for the mode shapes of the composite plate's reinforcement with FG-X-CNT were calculated and are shown in Fig. 96. Dastjerdi et al. [398] accomplished dynamic analysis (FV and stress wave), by subjecting the

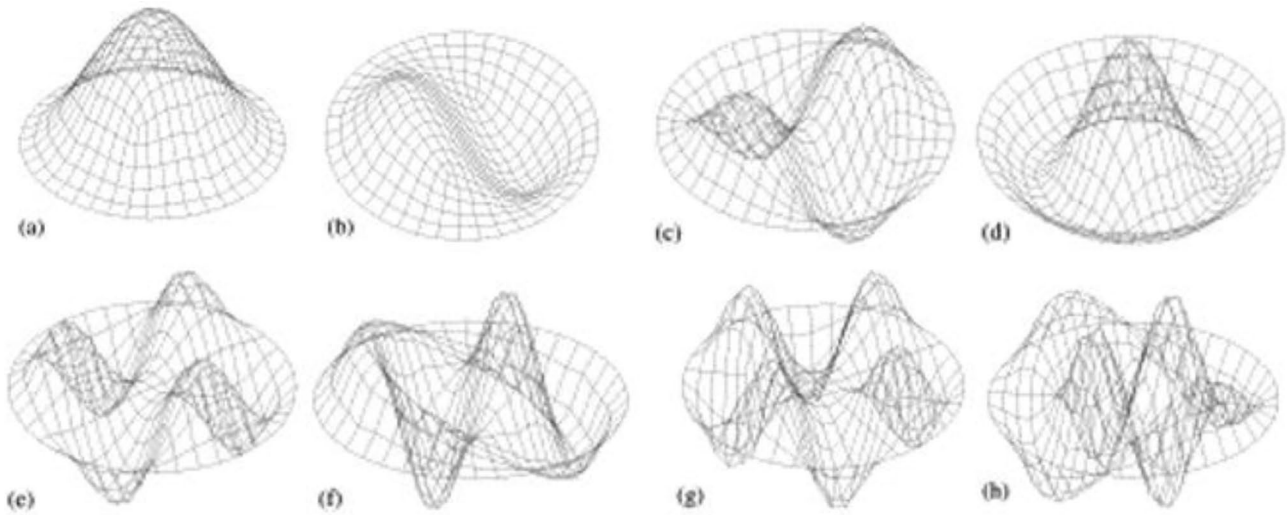


Fig. 91 FV modal shapes of a CC circular Mindlin/Reissner plate. **a** first Mode; **b** second Mode; **c** fourth Mode; **d** sixth Mode; **e** seventh Mode; **f** ninth Mode; **g** eleventh Mode; **h** thirteenth Mode; **i** fifteenth Mode; **j** seventeenth Mode [334]

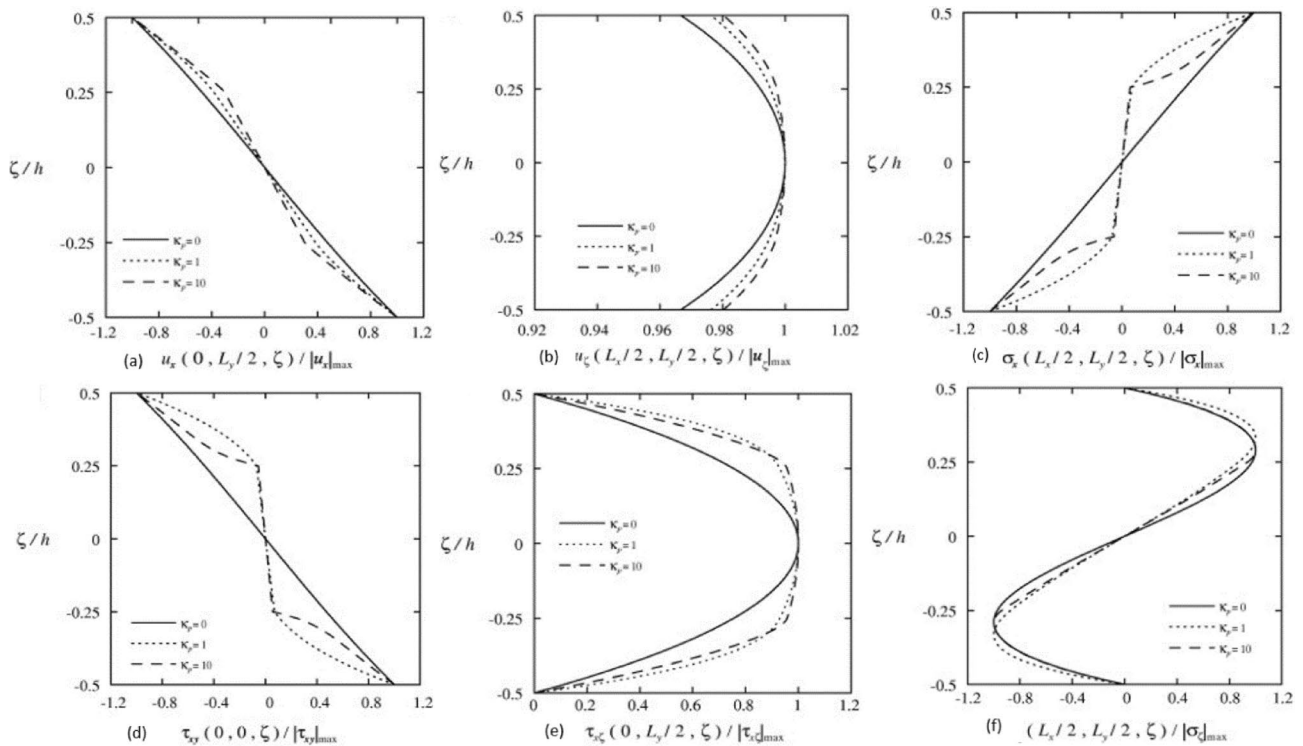


Fig. 92 The various modal field variables of the FGM sandwich plates' through-thickness distributions [381]

SWCNTs to impact case load using MLS. The NF characterization and stress wave propagation behavior caused by the improvement of type of dispersal and VFs of CNT and cylinder thickness. Figure 97 demonstrated that the velocity of stress wave propagation is nearly identical for diverse forms of CNT dispersion. The stress amplitudes in the FG-V and FG-X kinds are larger compared to the other

types. It has been shown that the UD and FG-X types act almost identically, yet the amplitude of axial and shear stresses rises in the FG type.

Liu [329] used the RPIM based on radial basis functions to analyze shear deformable laminated plates subjected to various BCs for FV. The natural frequencies was determined using TSDT. Based on a set of distributed nodes in

the problem territory, the technique approximates field variables. The enhancement of the aspect ratio, $(E1/E2)$, a/h , and the BCs, on NF were studied. The results indicate the FFs rises as the a/h rises. Additionally, it is observed that as the a/h of laminates increases, the disparity between the natural frequencies identified by CLPT, FSDT, and TSDT drops. The stabilization and vibrational persistent integration have been demonstrated to be crucial for achieving optimal alignment for nodal integration, which is an intriguing outcome recorded by Hillman and Chen [332]. Also, the eigenvalue evaluation demonstrated that the addition of vibrational consistent test functions did not sacrifice stability, and CPU time measurements demonstrated that the addition of vibrational consistent integration did not significantly reduce efficiency. The effectiveness of the suggested strategy in offering stable solutions for significant deformation problems was also demonstrated in a number of examples. For the purpose of developing accelerated, convergent and stable nodal integration for RKPM of plate and beam structures by RKPM. Figure 98 shows the eigenvalues of stiffness matrices. Figure 98a illustrates that the first lowest 30 modes in both cases fully integrated FEM agrees fairly well. However, when the initial smallest 200 modes were considered, VC-NSNI exhibits significantly greater agreement as in Fig. 98b.

A FV simulation for the nano clay-reinforced plates with piezoelectric layer has been performed by employing the MLS meshfree method. A substantial rise in amplitude of vibration has been noticed by reducing the nanocomposites core thickness. Furthermore, the vibrational amplitude decreases by increasing the thickness of piezoelectric layer. However, there is no evidence that changing the thickness structure will affect vibrational frequency [293]. Figure 99 illustrates the behavior of transvers vibration besides time history of the generated voltage effected by layer. Givli et al. [399] considered the FV for a sandwich panels (delaminated unidirectional with transvers flexible core). The numerical analysis was based on HP and HSDT. The results of NF were validated with previous data found by Galerkin meshfree method and found to be almost identical. Wang et al. [400] applied the MLS and Kp-Ritz meshfree methods for multiscale NL vibrational analysis of FG-base PMMA/CNT composites plate as presented in Fig. 100. The macroscale simulation reveals that the placement of CNTs have a substantial impact on the NL vibration behavior of FG-based composite plates. The established multiscale technique offers an effective framework for exploring the macroscopic performance of composite structures while taking mechanical response from microscopic constituents into consideration.

Ferreira et al. [295] employed the RBF collocation with two higher order Zig-Zag theories for analyzing the FV NF of the $[0^\circ/90^\circ/90^\circ/0^\circ]$ square cross-ply laminates SS. The obtained results shows that at all different grid values the z^3 -ZZ formulation is more efficient than

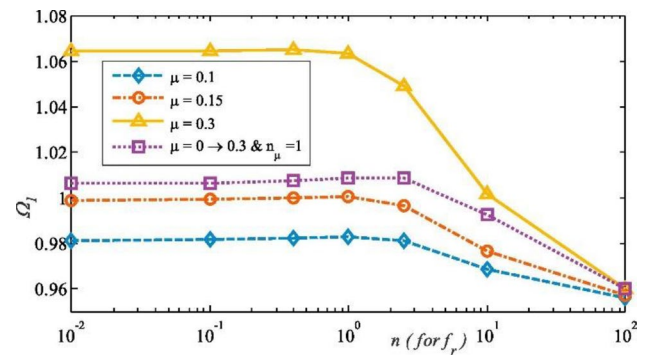


Fig. 93 The central point timeline vibrations of sandwich plates with $n=1$, $\mu=\eta=1$ (fully-scattered), $h/a=0.1$, $h_f/h=0.1$ and $k_s=k_w=0$ for $\mathbf{a} f_{rmax}=0.02$ and $\mathbf{b} f_{rmax}=0.05$ [392]

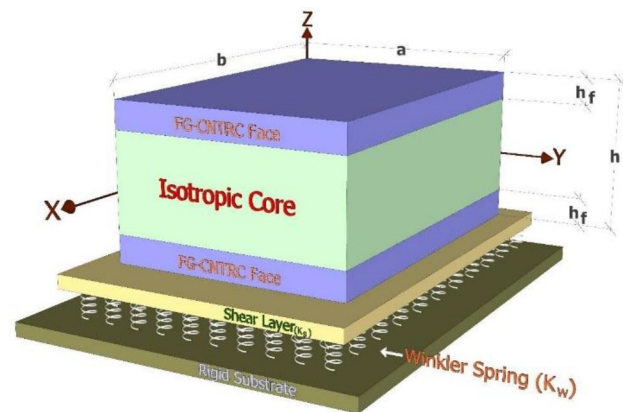


Fig. 94 The schematic of sandwich plate on 2-parameter EF [392]

SINUS-ZZ formulation for $v_{23}=0.25$ and more close to previous studies by exact and other meshfree methods. Neves et al. [298], implemented the quasi-three dimensional SSDT with developed implementation of CUF and the base of collocation RBF in order to solve the thickness stretching difficulty on static analysis of FGM plates. The FV analysis was performed on isotropic FGMs SS. For the purpose of achieving a comparable material properties, the Mori–Tanaka scheme was employed to compare the results. The obtained results shows good agreement with previous available results found by other meshfree methods and analytical solution. At $\epsilon_{zz} \neq 0$ results noticed to match the exact solution. This model considered as a comprehensive model to be considered in both static and vibration analysis of thin and thick FGM plates for BCs and equation of motion equations. Ferreira et al. [296] implemented the SSDT and the RBF collocation, for analyzing the FV behavior of the laminated spherical and cylindrical shells. The ND natural frequencies were found for various cross-ply spherical shells and compared with previous analytical solution results with excellent

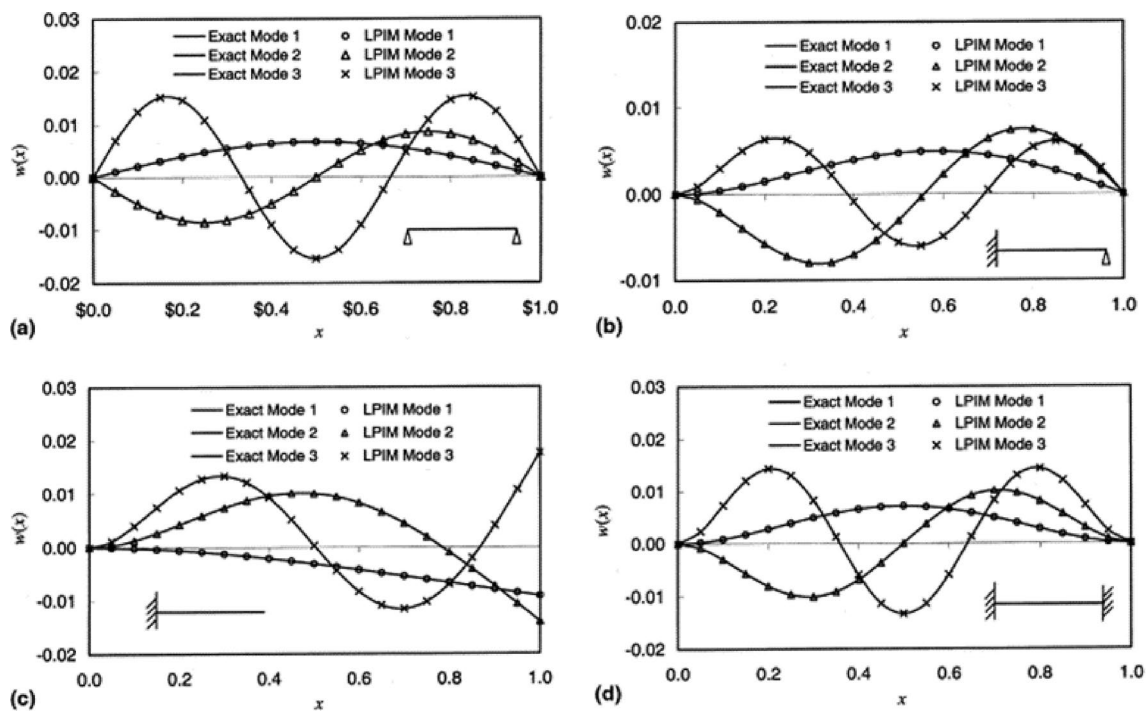


Fig. 95 FV modes of thin beams with different BCs: **a** pinned–pinned; **b** fixed–pinned; **c** fixed–free; **d** fixed–fixed [310]

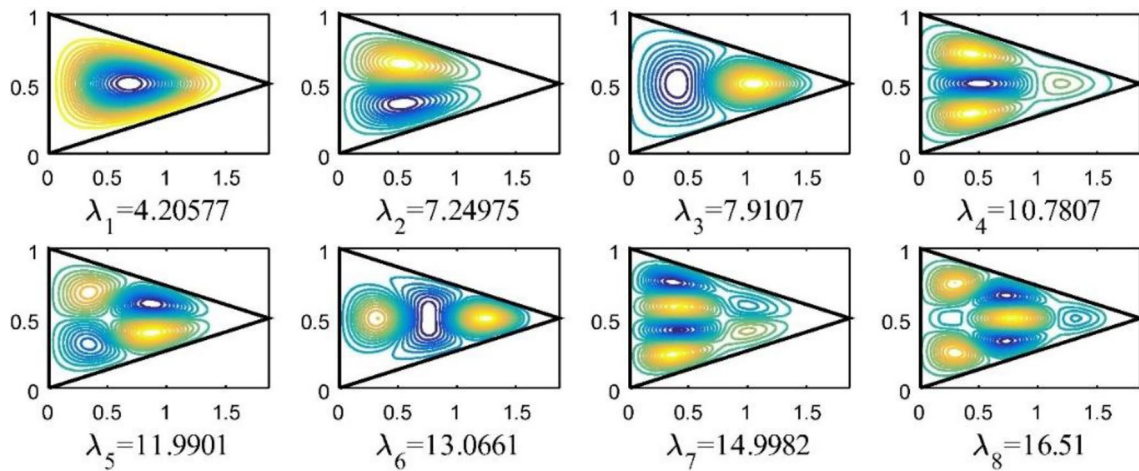


Fig. 96 The vibrational mode shapes of FG-X CNT-reinforced composite triangular plate with $t/b=0.01$, $\alpha=30^\circ$ and $k/k_{cr}=-0.5$ @ boundary condition CCC [397]

agreement. Tornabene et al. [401] used the RBF mesh-free approach on a general higher-order equivalent single layer (GHESL) formulation to explore the FV behavior of a doubly-curved laminated composite in panels and shells. The various geometrical structures were defined by using the differential geometry (DG) for singly-curved, degenerate shells, and doubly-curved. RBF and the placement of points on the provided computational domain influence the shape parameters. Nonetheless, changing

the placements of the points will modify the shape parameters. Furthermore, after the shape parameters have been set for a specific grid distribution, they can be rounded off and utilized for any type of construction. This is an important aspect because when a fixed parameter is utilized, the RBF methodology transforms into a "parameter free" numerical method. Besides, the maximum natural frequencies were recorded at the 10th mode in all methods which have been applied and it is strongly agreed

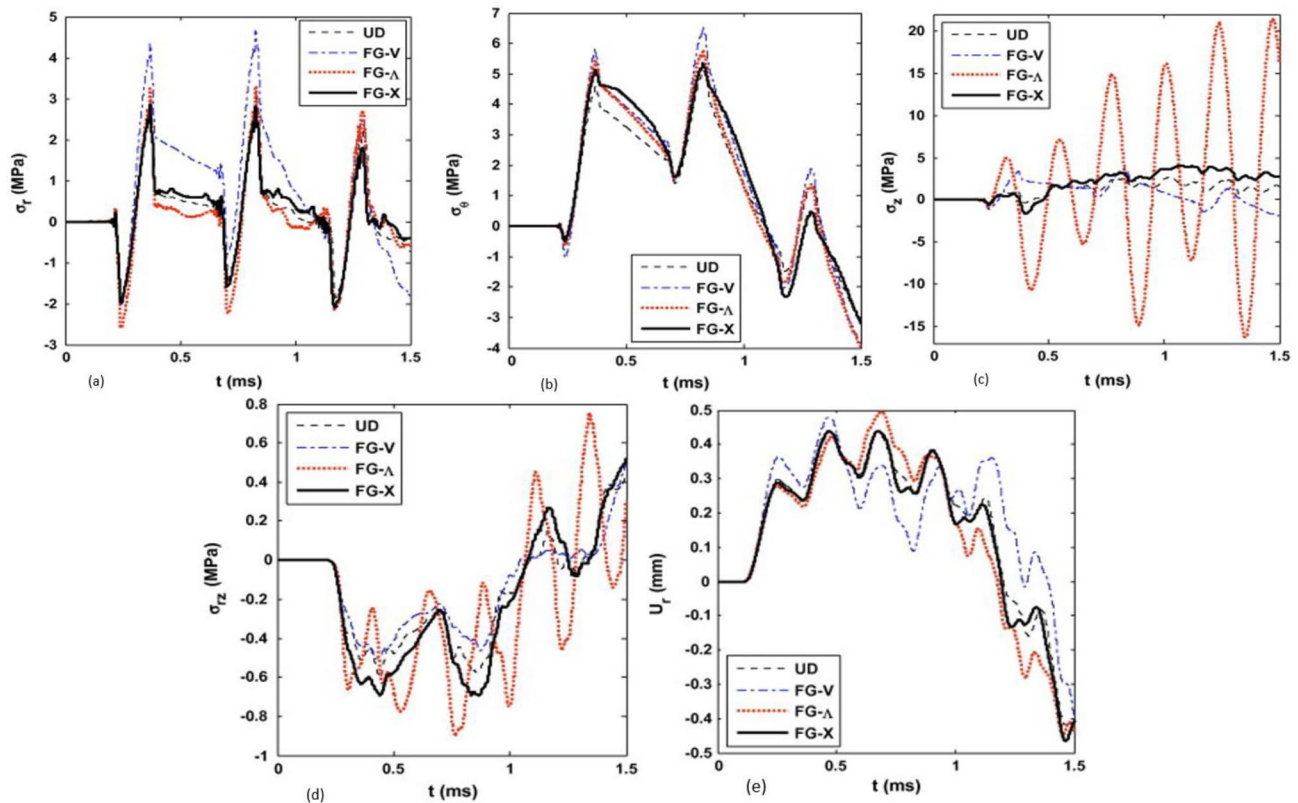


Fig. 97 The Time history of **a** Radial stress, **b** hoop stress, **c** axial stress, **d** shear stress and **e** radial vibration at inner radius of first model of CNTRC cylinders for different kind of CNT distribution [398]

with compared data. The schematic description of the doubly-curved shell and the co-ordinate system is presented in Figs. 101 and 102 illustrates the various shell and panel analyzed structures and the relative RBF discretization for computer applications.

Ferreira et al. [402] investigated the FV performance of the symmetric laminated composite plates (rectangular and square), by an advanced numerical scheme by combining the PS methods with the collocation RBF, where the enhancement of various t/l , thickness to side ratio (h/a) on NDNF were concerned. An earlier convergence observed at CC BCs at high t/b ratio regardless of a/b ratios. The outcomes indicated that increasing the a/h , will reduce the (FPs). These statistics additionally demonstrate that increasing the thickness ratio leads to a reduction in (FPs). The reason of this phenomena is that; the shear deformation as well as rotating inertia. These impacts are greater in higher modes. More significant frequencies were obtained with CCC borders similarly, to what was expected because stronger constraints result in higher frequencies. Ferreira et al. [301] considered the natural frequencies of a composites laminated plate $[0^\circ/90^\circ/90^\circ/0^\circ]$ and isotropic plate.

Both plates were square shape and SS. The analysis was established by employing the meshfree MQRBF combined with the layerwise deformation theory. The obtained results prove that the presented method is significant in predicting the NF when compared with the 3D method and with superior formulations. Additionally, the layerwise formulations may handle the deformation behavior of some laminates, specifically sandwich laminates with very diverse core and skin materials more significantly. Ferreira et al. [302] implemented the RBF meshfree technique founded on the layerwise deformation theory to investigate the FV behavior of laminated cross-ply cylindrical and spherical shells orientated as $[0^\circ/90^\circ/0^\circ]$ and $[0^\circ/90^\circ/90^\circ/0^\circ]$. The NF results were compared with HSDT and FSDT and noticed to have outstanding agreement with analytical solution. Kumar et al. [331], the MQRBF meshfree method has been employed for discretization in an analysis of FV behavior of porous FGM plate on the basis. By investigating the enhancement of number of nodes, and a/h of the FGM-2 plate with SS BCs on the NF parameter were $a=b=n=1$. It has been observed that increasing a/h to result in decreasing the NF parameters with in 1, 2, and 3 dimension. As an

Fig. 98 Eigenvalues of stiffness matrices: **a** 30 lowest modes and **b** 200 lowest modes [332]

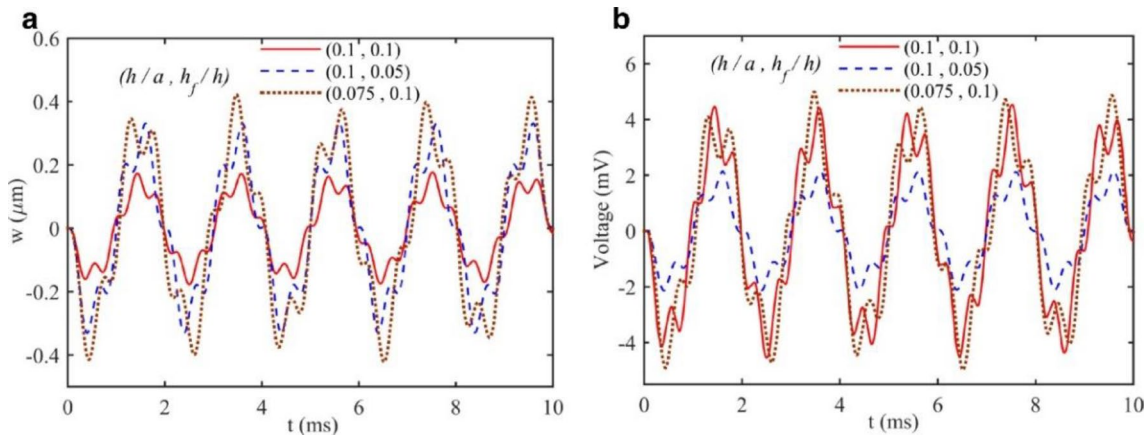
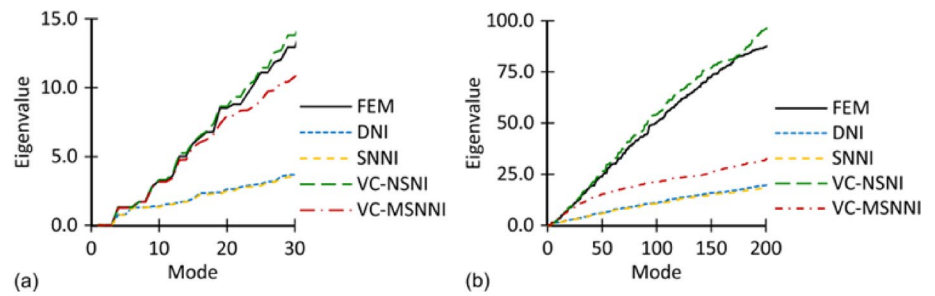
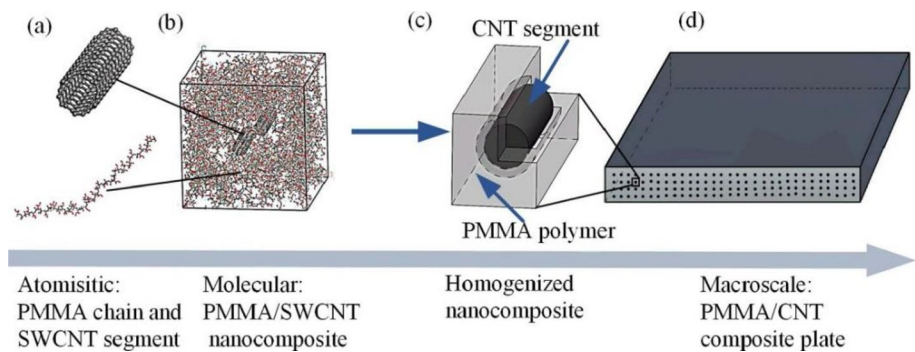


Fig. 99 Time history of central point **a** deflections **b** generated voltages of smart sandwich plates subjected to periodic mechanical load with $\omega_f = 500$ Hz [293]

Fig. 100 An Outline of the SWCN- reinforced PMMA composite at various length scales; **a** the atomistic models of the PMMA polymer chain and the SWCNT segment; **b** the molecular model of the PMMA/SWCNT nanocomposite; **c** the equivalent nanocomposite; and **d** the macroscale PMMA/CNT composite plate [400]



overall observation the maximum value of NF parameters in all different values of a/h were recorded at node distribution 9×9 . Besides, at $a/h = 50$ and $a/h = 100$ almost identical NF parameters were observed. Recently, Kim et al. [403], employed the meshfree shape function (MSF) which is categorized under the MLS method, in order to approximate the nodal displacement. The objective of this work was to inspect the FV behavior of a composite laminated double-plated system (CLDPS) as shown in Fig. 103 and it is considered as the first study of its type.

3.2 Force Vibration

3.2.1 Force Vibration in Nanoscale

Safaei et al. [412], investigate the force vibrational response by MLS under steady state thermal gradient loads. It is observed from Fig. 104, that the thermal gradient loads enhance the initial values of the vibrational (static deflection) along with the vibrational amplitudes of the sandwich plates. A significant improvement in the structure stiffness, increasing number of CNTs into the face sheets led to having slighter amount of vibrational amplitude. Moreover, the

schematic is shown in Fig. 105. Gu [310], investigated the force vibration of a thin beam by applying the LPIM and EB beam as an analytical solution, where the LPIM is usually used for analyzing the thin beam with pinned–pinned BCs forced vibration. The results after measuring the error shows great consistency with the systematic results, where significant LPIM stability was observed as well.

In order to increase the stiffness of CNTRC plates, it has been determined that reinforcements applied to the top and bottom of the structure are more durable in comparison to those placed in the mid-plane. Figure 106 display how the four sides of various types of CNTRC plates are fully CC while altering the plate aspect ratio ($\beta = a/b$) from 1.0 to 2.0. The CNT VF V_{CNT}^* is considered, and the plate width-to-thickness ratio (b/t) is specified to be $b/h = 10$. It is observed that when β of different types of FG-CNT and for UN-CNTRC plates rise, the ND FFs reduced. Also, variations in the plate aspect ratio enhance the distribution types of CNTs in the plate [338]. Sahmani and Safaei [413] employed GDQM combined with the Galerkin method to determine the surface elastic based NL frequencies of the conical nanoshell made by FG composites. The meshfree methods were employed after constructed the NC shell model by integrating the Gurtin–Murdoch elasticity theory into a HSDT of conical shell. It was established that decreasing shell thickness, thereby raising the surface to volume ratio, raises the gap in the middle of the surface elastic-based and classical FR, indicating that the increase in the gap becomes more important as the amplitude of the NL vibrations rises. Furthermore, raising the material characteristic gradient

indices increased the importance of surface stress impact on NL FV in the structure itself [414].

3.2.2 Force Vibration in Microscale

Sahmani and Safaei [419] implemented and solved the GDQM and Galerkin meshfree methods to obtain the amplitude respond related to NL primary resonance of the 2D-FGM micro/nano-beams, as well as the NL NLC strain gradient FR. Hence, for validation issue the strain gradient size dependency was ignored. Both SS and CC were considered as a BCs. Figure 107 depicts the effect of strain gradient size on the DL FR associated to the NL basic resonance of the 2D-FGM micro/nano-beams. It shows that the associated excitation frequency and the oscillation amplitude peak both increases by the locality. Nevertheless, the strain gradient size effect has a reverse impact and cause to reduce the associated excitation frequency and the oscillation amplitude peak. These remarks owing to the drop in the stiffness of the structure produced by the NL size influence, which results in greater geometrical NL. According to Yuan et al. [420] the GDQM and Galerkin meshfree methods can be combined and used to predict the NLC NST-based dynamic features of the FGM composite shortened conical microshell integrated by a magnetostrictive facesheet. Wang et al. [421] employed the meshfree Local Kriging method to investigate the behaviors of microelectromechanical system (MEMS) devices, exposed to a NL loading. The Kriging interpolation technique is used to attain the form function, which possesses partition of unity and delta function features. The GEs for

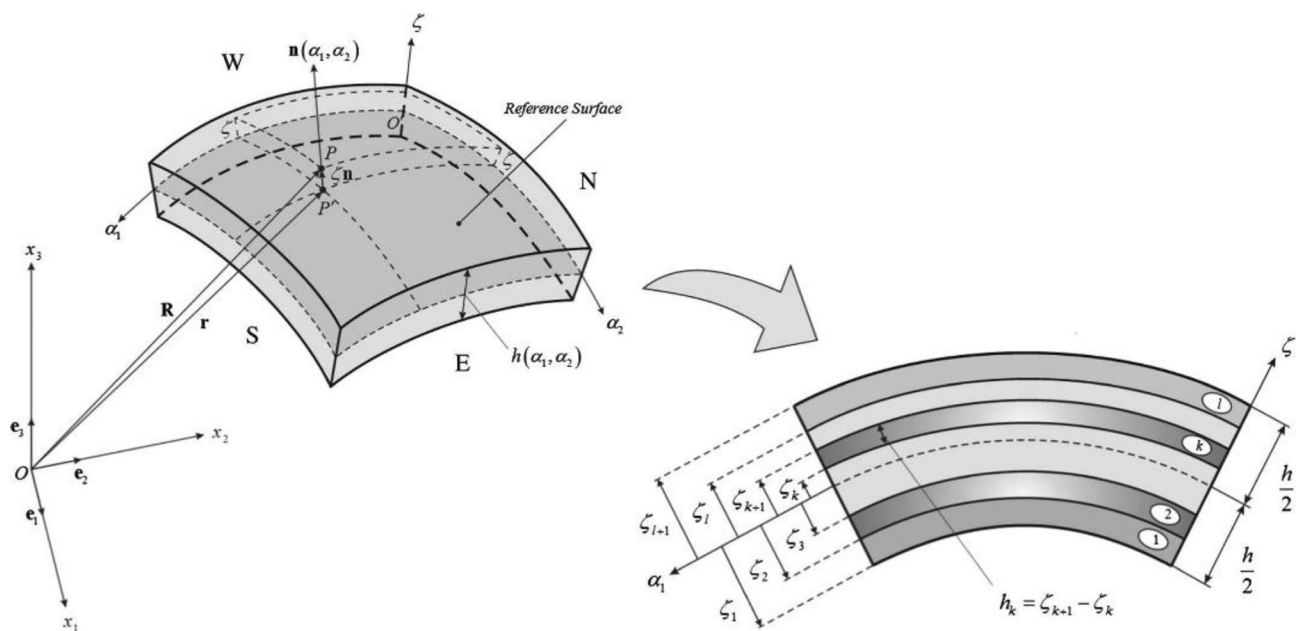
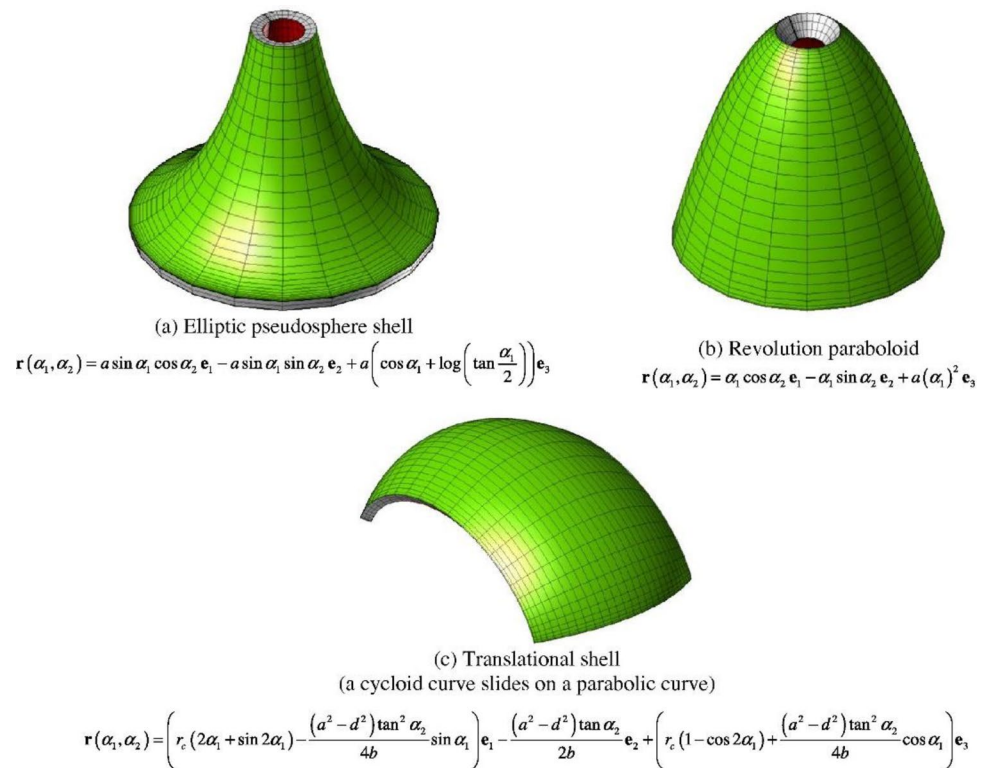


Fig. 101 The schematic description of the doubly-curved shell and the co-ordinate system [401]

Fig. 102 The various shell and panel analyzed structures and the relative RBF discretization for computer applications [401]



MEMS devices were derived in their local Petrov–Galerkin-WF. The Local Kriging method was designed to evaluate the performance of micro-switches and micro-tweezers, which are commonly employed in MEMS devices. Also, Wang et al. [422], shows interest in studying the MEMS, but in this study the analysis was accomplished by implementing the meshfree point weighted least-squares method (PWLS). Besides, the trial function has been generated based on the field nodes. However, the PWLS guaranty very high stability of the MEMS system. The Galerkin method has been employed by Rafiee et al. [315] for the purpose of linear/NL dynamic stability examination for plate structure exposing in-plane load harmonic applied voltage and thermal electrical loading. As a findings, the VF in CNTs increase the vibrational amplitude will reduce. Besides, the size of stability areas grows as the volume percentage of CNTs increases. It has been observed that the SWCNT distribution patterns have a considerable impact on the size of stability areas.

3.2.3 Force Vibration in Macroscale

Muthurajan et al. [423] studied the NL vibration analysis of primarily stressed thin laminated rectangular plates on EF by the EFG. Results of the CC square and SS were provided. Additionally, by applying the lateral and compressive in plane forces increasing the amplitude; will enhance the NL frequency. Chen et al. [424] have used the Galerkin technique to investigate the NL vibration of initially

stressed plates. The outcomes demonstrate that the NL vibration FR depend on; initial stress, Poisson ratio, vibration amplitude, and plate theory. According to the author’s findings, there are some unexpected discrepancies across the numerous plate theories, indicating that transverse normal strain, NU shear stress, as well as starting stress have a significant impact on how plates vibrate when subjected to NL vibration. Chen et al. [425] have performed a NL vibrational analysis for plates (orthotropic) through initial stresses that’s considered as an amalgamation of extensional stresses and pure bending stresses. The EF (Winkler and Pasternak) were examined with two parameters. It has been discovered that the NL foundation stiffness or compressive stress increase the frequency ratio value, while the EF stiffness or tensile stress decreases. The frequency ratio increases as the E1/E2 or biaxial stress ratio increases. A plate with initial compressive stress resting on a low stiffness basis and high E1/E2 exhibits NL vibration behavior. Under high foundation stiffness, increasing the bending stress ratio has a much smaller effect on the frequency ratio. Furthermore, the plate frequency ratio rises together with the vibration amplitude once the foundation stiffness seems to be low. A large foundation stiffness can minimize the plate’s NL vibration behaviors. The EFG method have been implemented for discretizing the equation of motion after obtaining the NL elastic region characterization in solid by performing the preisach-may-eroyz space (PM space), to investigate

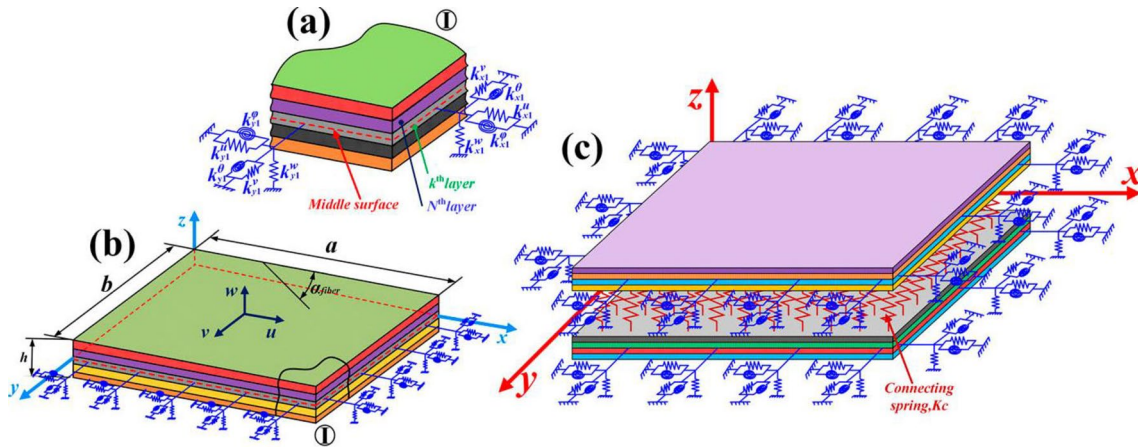


Fig. 103 The schematic of the CLDPS; **a** BCs of a single CLP, **b** geometry of single CLP, **c** CLDPS bonded by a number of elastic springs [403]

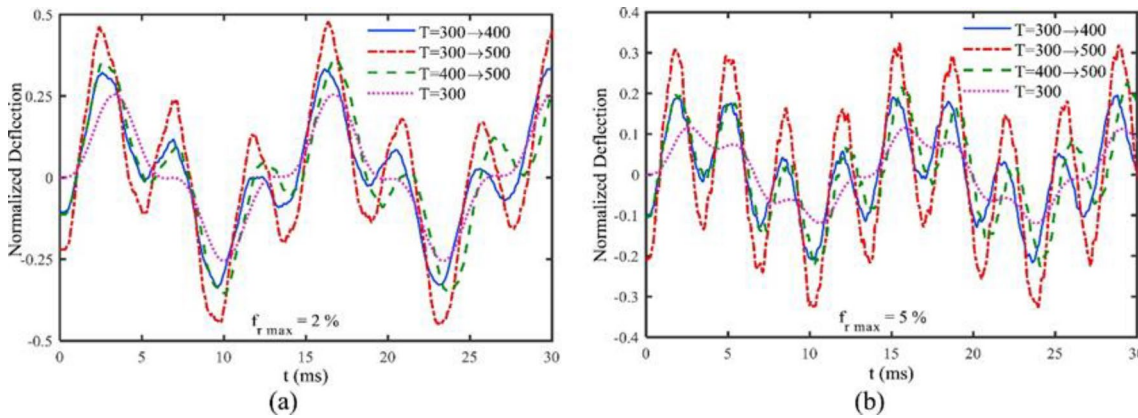
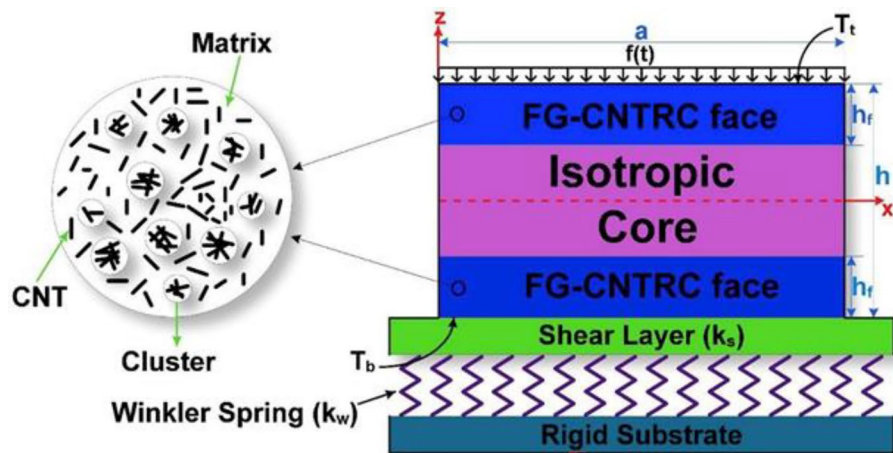


Fig. 104 The central point timeline vibrations of sandwich plates with $n=1, \mu=\eta=1$ (fully-scattered), $h/a=0.1, h_r/h=0.1$ and $k_s=k_w=0$ for **a** $f_{r\max}=0,02$ and **b** $f_{r\max}=0.05$ [412]

Fig. 105 The schematic of sandwich plate on 2 parameter EF with 2 nanocomposite face sheets reinforced with CNTs [412]



the NL wave propagation of a plate. It has been uniformly distributed and harmonic force with magnitude 3 kHz were observed. The elastic modulus shows a decrease

by increasing the harmonic load. While in plane stress case, the harmonic amplitude was observed to increase by increasing the fundamental amplitude acceleration [426].

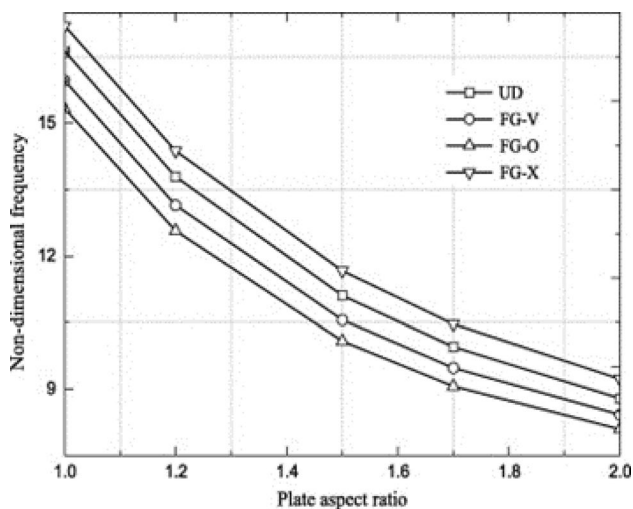


Fig. 106 The NDNF variation of various types of CNTRC plate's four edges fully CC versus plate aspect ratio [338]

Liu et al. [427] investigated the dynamic behavior of a corrugated cylindrical shells exposing NL low-velocity impact as shown in Fig. 108. An innovative computational technique for NL impact force in the local contact area has been utilized. In order to start, a novel comparable shell model for corrugated cylindrical shells was developed. The GEs were then constructed employing the Love thin shell theory and HP, subsequently converted into ordinary differential equations using the Galerkin method and for discretization, following a numerical solutions which was produced using the Duhamel integration and small-time increment technique. The findings show that this novel method agrees with results obtained previously. There was some variation due to the varied shell/plate theories and methodologies for calculating contact force. Besides, the convergence findings were received in all time histories when the wave numbers rise to $m = 50$ and $n = 50$, respectively. Hence, the shortened coefficients was used. Various corrugation types have a minor effect on contact time and extreme impact force. However, it is observed that the corrugation may overall improve shell stiffness, and the corrugated shell has a slighter transverse central displacement compared with the noncorrugated shell. Additionally, the radial displacement of the round corrugated cylindrical shell is least significant. This means that in all circumstances, the round corrugated cylindrical shell has a superior energy absorption effect and the greatest potential for enhancing impact resistance as shown in Fig. 109.

Bui et al. [410] applied the RPIM meshfree technique to investigate the frequency and the transverse response of the sandwich beam with inhomogeneous FG core subjected to dynamic load. The obtained results show that, increasing the core stiffness will enhance the NF to increase. As

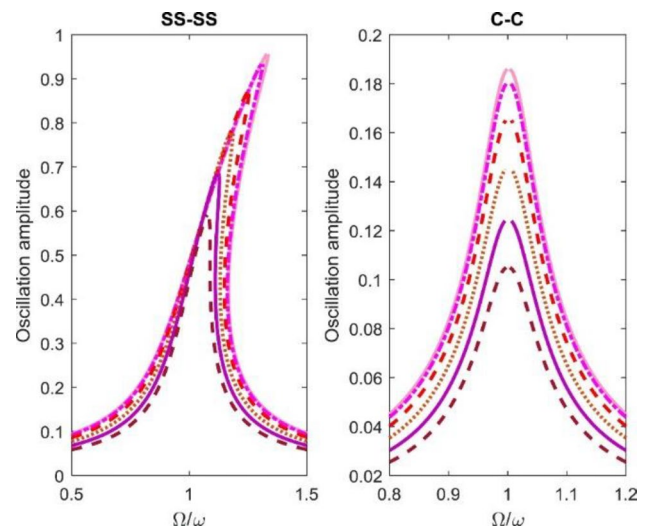


Fig. 107 The impact of the strain gradient size that influence the DL FR related to the NL primary resonance of the 2D-FGM micro/nano-beams [419]

long as a sufficiently small time steps were applied such as $\Delta t \leq 2 \times 10^{-4}$, stable results were guaranty additionally, when great time-steps are considered through time the displacement amplitude will decay. Moreover, in case of reducing number of nodes the obtained accuracy of the computed frequency is reduced.

3.3 Other Types of Dynamics Analysis

The vibration of a non-homogeneous (NH) visco-elastic rectangular plate with a linearly changeable thickness exposing a thermal gradient has been studied. Galerkin's technique has been utilized to solve the governing differential equation of motion. Time period, deflection, and logarithmic decrement at various points for a NH visco-elastic rectangular plate CC on two parallel edges and SS on the remaining two edges were calculated for various values of thermal gradients, NH constant, taper constant, and aspect ratio [428]. In a magnetic field, the vibrational response of bilayer graphene sheets (BLGSs) was investigated by Zhang et al. [429]. The kp-Ritz technique was used for the purpose of obtaining the PDE. The enhancement of aspect ratio, BCs, side length, magnetic parameters, and NLC parameters on vibrational behavior (frequency) were also investigated. Figure 110 depicts a schematic of BLGSs exposed to an in-plane magnetic field. The obtained results reveal that the magnetic field has a considerable effect on the second interlayer vibrational mode frequency, and as a result, at high magnetic fields, the first interlayer vibration mode frequency will eventually become asymptotic to the second interlayer vibration mode frequency. Besides, the NLC parameters, aspect ratio, BCs

and the side length were found to have no influence on the second interlayer vibration mode frequency.

The same method has been used by the same author in a further study to investigate the Impact of powder size on the crystallization response through laser solid forming $Zr_{55}Cu_{30}Al_{10}Ni_5$ bulk amorphous alloy [430]. Lei et al. [431] applied the kp-Ritz to perform elastodynamic analysis for CNT reinforced FGPs. The influence of CNT b/t, VF, aspect ratio, type of load type of distribution of CNT, and BCs on the dynamic responses of CNTR-FG-plates were investigated. Figure 111 presents the VF of CNTs as $V_{CNT}=0.17$ for the center vertical displacement time-profile curves of several types of FG-CNTR plates exposed to a transverse abrupt dynamic load. The results reveal that the CNTR plate's stiffness is excellent at high CNT VFs, and rising the CNT VF for UD and the other three FG-CNTR plates reduced the central vertical displacement.

Furthermore, the Galerkin technique was employed by Li et al. [432], to examine the the dynamic shear propagation behavior in plates under symmetric impact loads. The results show that by increasing the impact velocity, the characterization of the dynamic shear band will variate. In addition, the front region of shear band tip express to have high strain rate region. Medyanik et al. [433], presented an analysis of initiation and the propagation of the dynamic adiabatic shear bands (ASBs) for 4340 steel and OFHC copper. To examine and to confirm the suggested criterion by investigating the propagation, formation and the post bifurcation of the ASBs, large scale meshfree simulations were conducted. Kiani et al. [434], have employed the RKPM method parallel with HP to find the SWCNT-based sensor discrete form of the equation of motion. The study has focused on analyzing the potential application of the SWCNT as a nano-sensors with various BCs. The schematic of equivalent continuum structure (ECS) is presented in Fig. 112.

Recently Almasi et al. [435], implement the ISPH to examine the behaviors of various multi-phase flow system. Dastjerdi and Behdinin [436], employed the MLS for solving dynamic equation of the bridge type of the piezoelectric energy harvesters (PEH) with a multifunctional nanocomposite substrate. The schematic and cross sectional of the PEH bridge type are illustrated in Fig. 113. The results show that increasing the CNT volume will slightly have some effects on the dynamic responses, where the oscillation frequency will enhance and the amplitude will decrease. Liu et al. [437] employed the meshfree particle method (MP) to investigate the high velocity impact of micron particles at different speeds with different angles. Wu et al. [438] employed the strain-morphed NLC meshless method combined with interactive particle enrichment algorithm for the purpose of analyzing the dynamic ductile fracture. To analyze the behavior of an active constrained layered damping (ACLD) treatments on a smart laminated composite

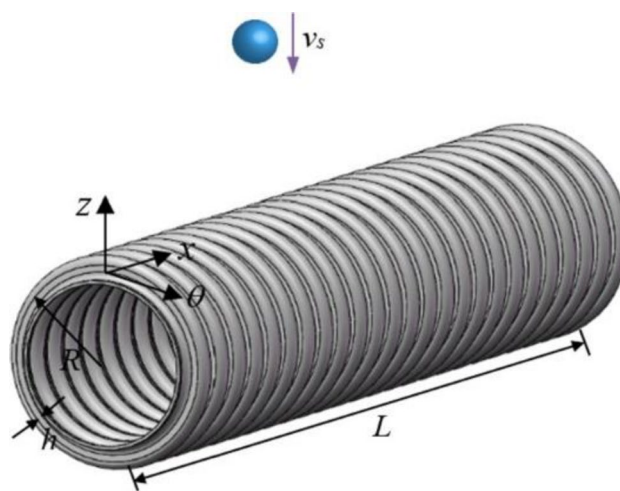


Fig. 108 The Schematic of a corrugated cylindrical shells exposed to NL low-velocity impact [427]

beams Sahoo and Ray [439], employed the EFG meshfree method to drive the meshless model of the system. Error analysis was carried out and the NF was determined. A further study has been performed by, Civalek [440] were the DQM combined with discrete singular convolution (DSC) have been employed to resolve the time wise integration in a NL dynamic as well as static responses of a shallow spherical shells with a Winkler-Pasternak EF as shown in Fig. 114. The obtained results shows that both static and dynamic response highly affected by the foundations' shear parameters. Besides, the shell curvature as well as the damping coefficient of the shell have a remarkable impact on the deflection results. Generally, increasing the foundation parameters will cause a reduction in the static as well as dynamic responses. That study prove that the combination of DSC-DQM counts as an accurate and effective approach for solving the NL static as well as dynamic analyses of the shell assembly.

4 Discussion

Meshfree or meshless methods are a group of method mainly based on Lagrange equation and have been developed to overcome the drawbacks of FEM and other traditional methods. The main concept of meshfree methods is that the functional evaluation is based on the nearby samples or nodes and it does not require net-mesh or remeshing where the nodes or points can be arranged uniformly or NU. These group of method can be utilized to solve and to handle the discretization of the linear and NL, partial differential equation (PDE), ordinary differential equation (ODE), local and NLC in many applications rather than dynamic and static analysis. The plate's structure in different geometry have

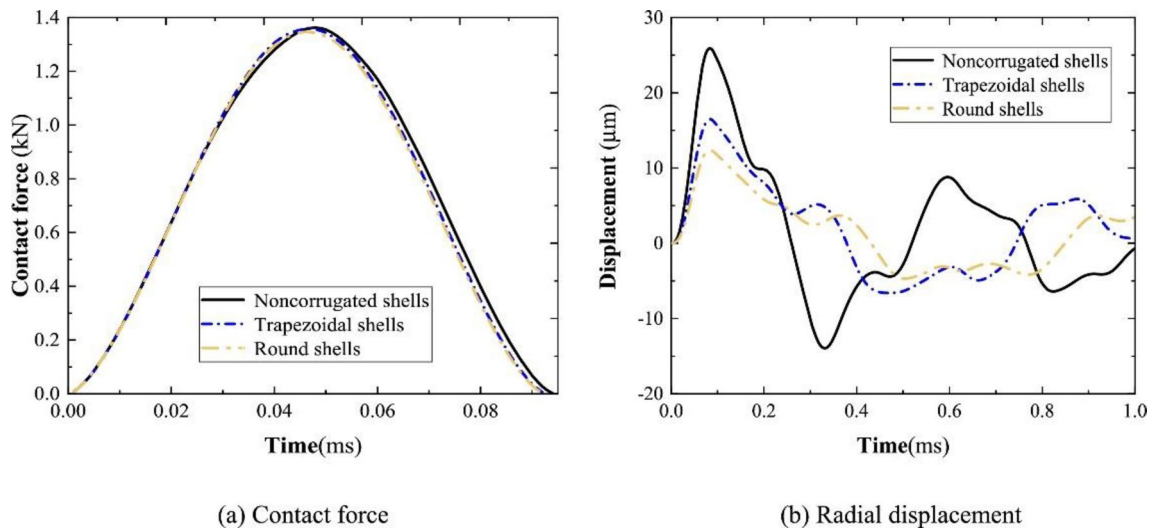


Fig. 109 The impact of corrugation type on impact response of the corrugated cylindrical shell [427]

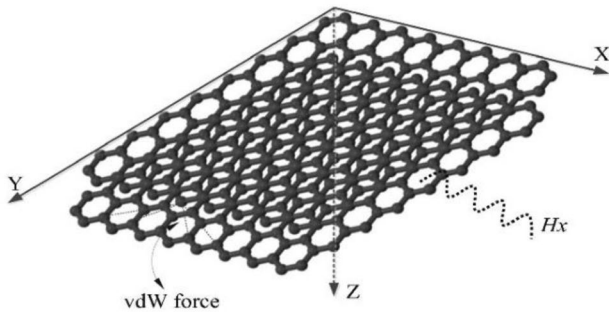


Fig. 110 The schematic of the BGSs subjected to in-plane magnetic field [429]

been favorable for studies and investigations in static and dynamic analysis. However, in theoretical terms, a meshfree method can be generated by combining function approximation, gradient approximation, and formulation techniques, resulting in a matrix that consist of a huge number of alternative methods.

Enforcement of essential BCs has been considered as a critical issue to investigate in many studies. Furthermore, meshfree modeling only requires a collection of unorganized points containing the domain of interest. Because of their simple topological data structures, meshfree particle techniques provide straightforward adaptable refinement, parallelization, and flexible interpolation in a deformed field. This class of methods has a high potential for meeting the requirements of modern software, such as error estimators, multiresolution analysis, HP adaptively, edge detection, and sampling approximations. Although great progress has been made in the last decade, there are still numerous

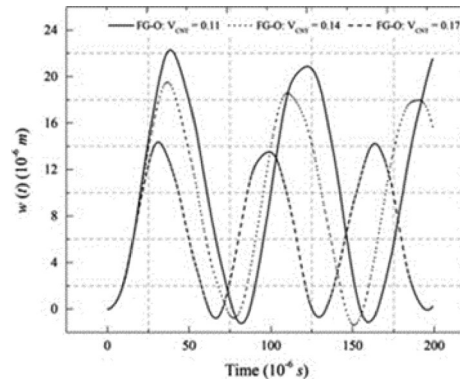


Fig. 111 The Central vertical displacement time-history for FG-O CNTR-FG plate with different CNT VFs [431]

responsibilities and challenges ahead, and optimizing the CPU is still considered a difficulty.

Among these challenges are the cost-effective meshfree Galerkin technique, scaled execution of important BCs, exact nodal integration strategies, and stabilization schemes that accommodate discretized WF and collocated strong form formulations. Although the essential for sensitivity filtering is implemented by employing the Galerkin based methods. Meshfree particle approaches are expected to play a large role in next generation computational meso-mechanics, or computational micro-mechanics, which is an integral part of nanotechnology and supercomputing technology. Nonetheless, most meshfree techniques have a significant computational cost, which makes large-scale investigations prohibitively expensive. Although the hybrid strategy combines the beneficial features of mesh based and meshfree systems, its high level of complexity

Fig. 112 The Schematic illustration of ECS with attached nanoparticles [434]

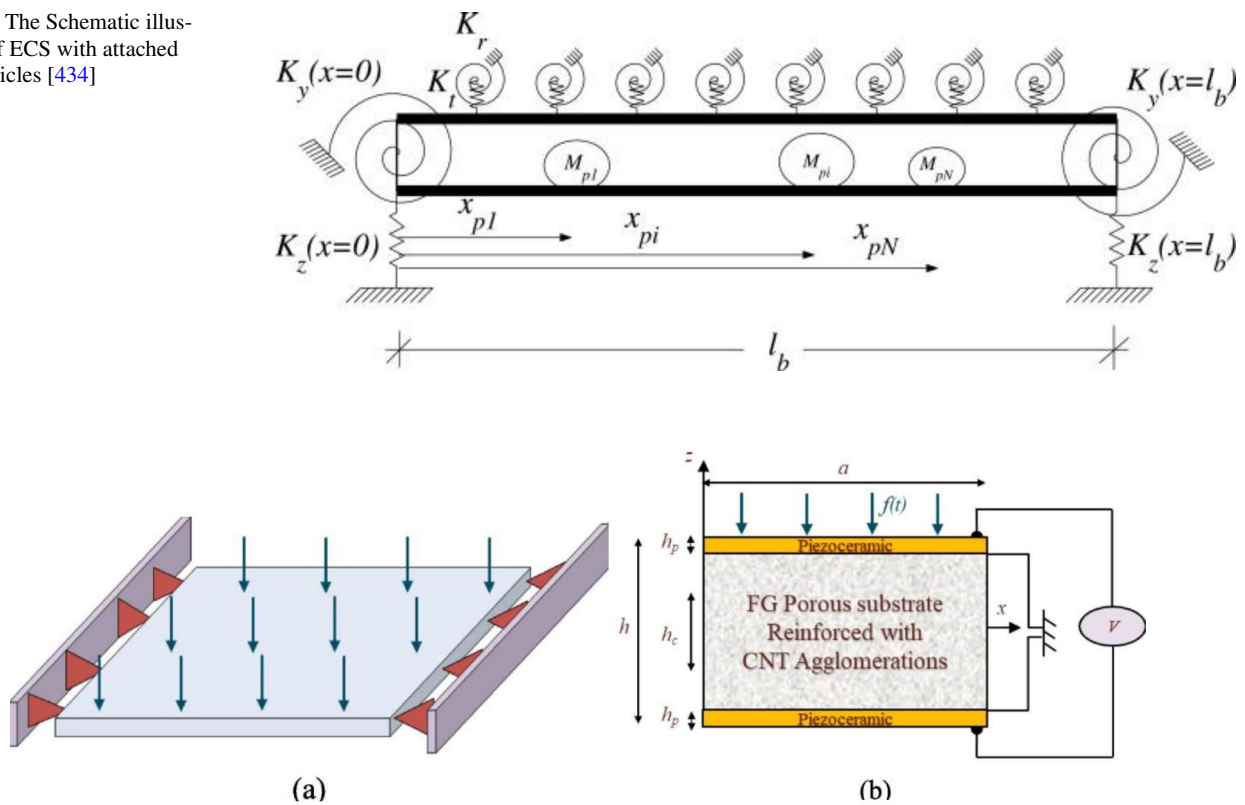


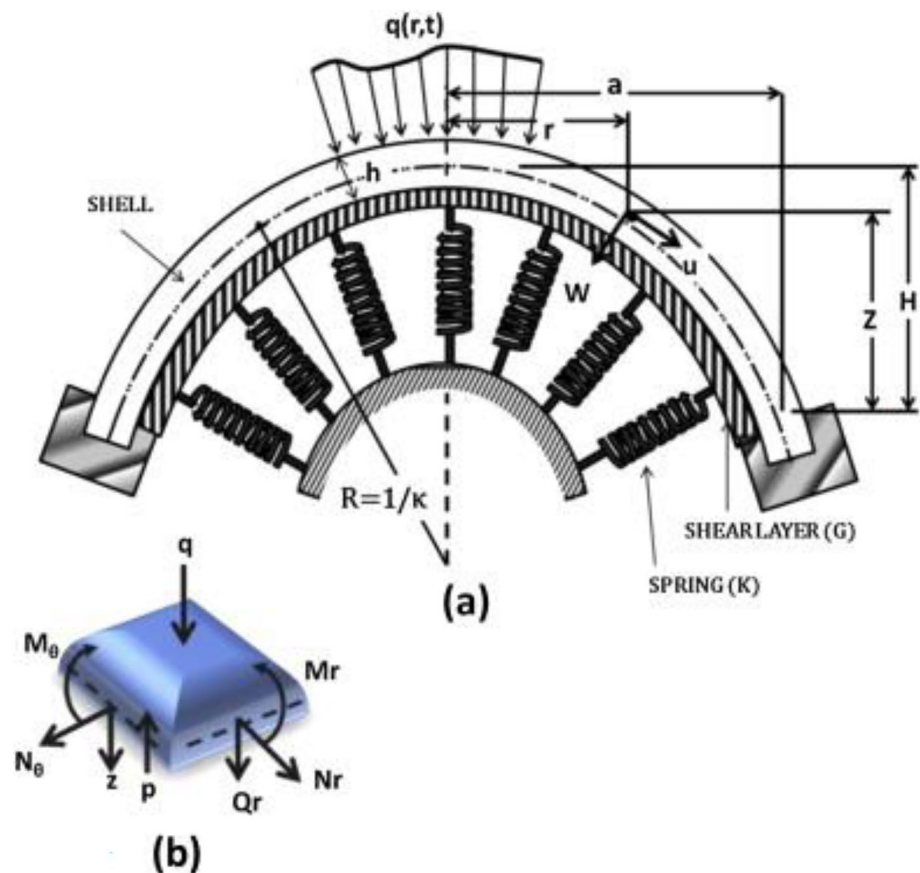
Fig. 113 The schematic and cross sectional (rectangular nanocomposite porous plate) of the PEH bridge type, with 2 SS edges and located between 2 piezoceramic faces [436]

and computational cost remain unresolved challenges. It is critical to examine the use of high performance computing (HPC) in the development of a multi-physics, multi-scale model. The MPM and SPH is able to overcome the huge mesh deformation. Due to this advantage both methods are considered as the most important methods. But there are still some restrictions on SPH method which inhibit its usage in indicating the rigid body motion accurately. To overcome this problem, researchers have developed a corrective kernel function, while keeping the original kernel. For the purpose of approximating the field variable, the EFG meshfree method uses the MLS meshfree method, while in discretizing an algebraic equation system, it follows the Galerkin-WF based method. Satisfying the BCs became much easier by developing the BMLS. As a result, it is capable to solve higher dimensional problems. Furthermore, the MK meshfree approach is capable to enforce the essential BCs straightly at the assigned node with the absence of any penalty method. The RBF has been developed in many studies based on various mathematical modeling.

The stabilizing conforming nodal integration approach is commonly used in static and dynamic analysis to predict bending stiffness, while the DNI strategy is used to avoid

shear locking. The first, third and fourth-orders shear deformation plate and shell theories were employed and combined with the meshfree methods in most studies. Furthermore, based on some literatures, there are many techniques to develop meshfree method by mathematical modeling and numerical method based on the aim to be accomplished in the study. Nevertheless, in static and dynamic analysis, researchers were interested in defining the influence of BCs, VF, and t/l ratio mainly on buckling strength, bending, and NF. Besides, some other parameters were considered due to some structural nature that needed investigation such as hole size and geometry in plates with holes. Based on some literature, it is important to highlight the error analysis to guaranty high performance and accuracy of the developed meshfree method no matter how the analysis was carried out. It has been observed that most of the studies were interested in investigating CNT, FGPs ceramic to metal composite, FGM, and polymeric composites. Another observation is that there are a quite large number of studies showing interest in investigating static analysis, especially dynamic analysis of the piezoelectric. However, these unique group of methods are not limited specifically on solid mechanics field (static and dynamic) analysis. Besides, it has many other various applications, especially in scientific fields and

Fig. 114 The schematic of shallow spherical shell with EF and its coordinate system [440]



mechanical engineering in particular such as thermal analysis which can be performed by Galerkin, fluid and particles analysis which can be investigated by SPH, for developing new material characterizations and properties the RBF method is employed, band structure and grain structure as well Quasi-brittle which can be examined by Galerkin, and Material defected crack failure microstructure changes and in civil engineering (concrete slab) which can be analyzed by kernel. Moreover, problems such as elasto-viscoplastic deformation, food engineering, biomedical, and temperature and heat transfer analysis also can be utilized by meshfree methods.

5 Conclusion

This is the first comprehensive review of meshfree methods, including traditional and developed meshless methods, that have been used to study static (bending, buckling/stability) and dynamic (FV, force vibration, and other types of dynamic analysis) for linear and NL analysis. For all different types of structures and geometries at various scales (nano, micro, and macroscales). In addition to the meshless approach, secondary methods and principles such as HP, FSDT, HSDT, Monte Carlo, local and

NLC theories, and others are highlighted. Likewise, some computational mechanics methods are discussed. The essential equations of meshfree methods are presented, as well as the error analysis. The basic mathematical equations of meshfree methods are illustrated. There is discussion of several sorts of schematics and structural size are addressed. Furthermore, this inclusive review is a significant resource for academics and researchers interested in the field of solid mechanics analysis at various scales utilizing meshfree techniques, as it addresses the secondary approaches used in conjunction with meshless methods, numerical and analytical analysis. Furthermore, several material types were described, as well as the enhancement of composite distribution and the impact of several variables on deformation, static and vibrational performance. The application of BCs and its effect as well as the implementation of FGM and other composite material for system which are examined by meshfree approaches are clarified.

Meshfree methods demonstrates excessive possibility to come across the demands of modern software, error estimators and various types of analysis. Meshfree technique, considered in its individual form represent the impending generation of computational numerical developed methods. Meshfree modeling requires simply a set

of unstructured points that encompass the territory of interest. Meshfree particle approaches enable easy adaptive refinement, parallelism, and flexible interpolation in a deformable territory due to their simple topological data structures. Numerous complications that cannot currently be addressed by FEM or finite difference methods have been demonstrated to be tractable by meshfree approaches. Despite the fact that tremendous progress has been made over the last decade, there are still many responsibilities and challenges ahead. Among the issues to be addressed are the cost-effectiveness of the meshfree-Galerkin technique, scalable application of essential BCs, accurate nodal integration strategies, and stabilization procedures for both discretized WF and SF. Meshfree particle methods are expected to play a key role in the future generation of computational meso-mechanics. Also known as computational micro-mechanics that is an integrated aspect of nanotechnology and computer systems technology. The high benefits and the unique characterizations of the RBF method makes it possible to be combined with a variety of different methods, therefore making its application limitless, especially in FG composite material structure for NL analysis. It is highly important to estimate the error in each study for the purpose of validating the developed mathematical method as well as for comparing the accuracy of the founded data with the data that have been published earlier.

Most of the research works carried out investigations in nanoscales structure in both static and dynamic analysis. Regarding dynamic analysis, most focused on FV analysis rather than forced vibration analysis. However, for static analysis it has been observed that in thermomechanical and electromechanical simulations, the authors were considering the buckling analysis and not bending analysis. The gap in literature is that a few studies focused on investigating force vibration. Also, absence of applying meshfree methods for analyzing pico-scale system. Besides, there is limitation in recorded data about applying the meshfree methods on examining the impact. Else, a few studies investigated the Gr copared with FGM and CNT. The limitation of this study that it discussed the fracture mechanics briefly so as a future work a comprehensive review about implementation of meshfree methodologies for studying cracks and failure caused by porosity may be accomplished.

References

- Nguyen VP, Rabczuk T, Bordas S, Duflot M (2008) Meshless methods: a review and computer implementation aspects. *Math Comput Simul* 79:763–813. <https://doi.org/10.1016/J.MATCOM.2008.01.003>
- Belytschko T, Krongauz Y, Organ D, Fleming M, Krysl P (1996) Meshless methods: an overview and recent developments. *Comput Methods Appl Mech Eng* 139:3–47. [https://doi.org/10.1016/S0045-7825\(96\)01078-X](https://doi.org/10.1016/S0045-7825(96)01078-X)
- Qiao P, Asce F, Yang M, Bobaru F (2008) Impact mechanics and high-energy absorbing materials: review. *J Aerosp Eng* 21:235–248. [https://doi.org/10.1061/\(ASCE\)0893-1321\(2008\)21:4\(235\)](https://doi.org/10.1061/(ASCE)0893-1321(2008)21:4(235))
- Lian H, Kerfriden P, Bordas SPA (2016) Implementation of regularized isogeometric boundary element methods for gradient-based shape optimization in two-dimensional linear elasticity. *Int J Numer Methods Eng* 106:972–1017. <https://doi.org/10.1002/NME.5149>
- Ma H, Chen J, Deng J (2023) Convergence analysis of the element-free Galerkin method for plate bending problem. *Comput Math Appl* 136:71–79. <https://doi.org/10.1016/J.CAMWA.2023.02.001>
- Belytschko T, Lu YY, Gu L (1994) Element-free Galerkin methods. *Int J Numer Methods Eng* 37:229–256. <https://doi.org/10.1002/NME.1620370205>
- Yoon YC, Schaefferkoetter P, Rabczuk T, Song JH (2019) New strong formulation for material nonlinear problems based on the particle difference method. *Eng Anal Bound Elem* 98:310–327. <https://doi.org/10.1016/J.ENGANABOUND.2018.10.015>
- Jafari N, Azhari M (2017) Buckling of moderately thick arbitrarily shaped plates with intermediate point supports using a simple hp-cloud method. *Appl Math Comput* 313:196–208. <https://doi.org/10.1016/J.AMC.2017.05.079>
- Liszka TJ, Duarte CAM, Tworzydło WW (1996) hp-Meshless cloud method. *Comput Methods Appl Mech Eng* 139:263–288. [https://doi.org/10.1016/S0045-7825\(96\)01086-9](https://doi.org/10.1016/S0045-7825(96)01086-9)
- Li X (2016) Error estimates for the moving least-square approximation and the element-free Galerkin method in n-dimensional spaces. *Appl Numer Math* 99:77–97. <https://doi.org/10.1016/J.APNUM.2015.07.006>
- Neofytou A, Huang TH, Kambampati S, Picelli R, Chen JS, Kim HA (2021) Level set topology optimization with nodally integrated reproducing kernel particle method. *Comput Methods Appl Mech Eng* 385:114016. <https://doi.org/10.1016/j.cma.2021.114016>
- Liu WK, Jun S, Zhang YF (1995) Reproducing kernel particle methods. *Int J Numer Methods Fluids* 20:1081–1106. <https://doi.org/10.1002/FLD.1650200824>
- Li S, Liu WK, Qian D, Guduru PR, Rosakis AJ (2001) Dynamic shear band propagation and micro-structure of adiabatic shear band. *Comput Methods Appl Mech Eng* 191:73–92. [https://doi.org/10.1016/S0045-7825\(01\)00245-6](https://doi.org/10.1016/S0045-7825(01)00245-6)
- Blank M, Nair P, Pöschel T (2023) Modeling surface tension in Smoothed Particle Hydrodynamics using Young-Laplace pressure boundary condition. *Comput Methods Appl Mech Eng* 406:115907. <https://doi.org/10.1016/J.CMA.2023.115907>
- Gingold RA, Monaghan JJ (1977) Smoothed particle hydrodynamics: theory and application to non-spherical stars. *Mon Not R Astron Soc* 181:375–389. <https://doi.org/10.1093/MNRAS/181.3.375>
- Russell MA, Souto-Iglesias A, Zohdi TI (2018) Numerical simulation of Laser Fusion Additive Manufacturing processes using the SPH method. *Comput Methods Appl Mech Eng* 341:163–187. <https://doi.org/10.1016/J.CMA.2018.06.033>
- Fernandes CM, Miranda G, Davim JP, Sridhar P, Manuel J, Prieto R et al (2022) Modeling grinding processes and mesh or mesh-free methods, 2D or 3D approach? *J Manuf Mater Process* 6:120. <https://doi.org/10.3390/JMMP6050120>
- Atluri SN, Zhu T (1998) A new Meshless Local Petrov-Galerkin (MLPG) approach in computational mechanics. *Comput Mech* 22:117–127. <https://doi.org/10.1007/S004660050346/METRICS>

19. Hosseininia M, Heydari MH, Razzaghi M (2022) Meshless local Petrov-Galerkin method for 2D fractional Fokker-Planck equation involved with the ABC fractional derivative. *Comput Math Appl* 125:176–192. <https://doi.org/10.1016/J.CAMWA.2022.08.040>
20. Dane TD, Sankar BV (2008) Meshless local Petrov-Galerkin micromechanical analysis of periodic composites including shear loadings. *C Comput Model Eng Sci* 26:169–187. <https://doi.org/10.3970/CMES.2008.026.169>
21. Wen PH, Aliabadi MH (2010) Elastic moduli of woven fabric composite by meshless local Petrov-Galerkin (MLPG) method. *C Comput Model Eng Sci* 61:133–154. <https://doi.org/10.3970/CMES.2010.061.133>
22. Kuzmin D, Quezada de Luna M, Kees CE (2019) A partition of unity approach to adaptivity and limiting in continuous finite element methods. *Comput Math Appl* 78:944–957. <https://doi.org/10.1016/J.CAMWA.2019.03.021>
23. Destuynder P, Hervella-Nieto L, López-Pérez PM, Orellana J, Prieto A (2022) A modal-based Partition of Unity Finite Element Method for elastic wave propagation problems in layered media. *Comput Struct* 265:106759. <https://doi.org/10.1016/J.COMPSTRUC.2022.106759>
24. Melenk JM, Babuška I (1996) The partition of unity finite element method: basic theory and applications. *Comput Methods Appl Mech Eng* 139:289–314. [https://doi.org/10.1016/S0045-7825\(96\)01087-0](https://doi.org/10.1016/S0045-7825(96)01087-0)
25. Talat N, Mavrič B, Hatić V, Bajt S, Šarler B (2018) Phase field simulation of Rayleigh-Taylor instability with a meshless method. *Eng Anal Bound Elem* 87:78–89. <https://doi.org/10.1016/j.enganabound.2017.11.015>
26. Zhou X, Yao WW, Berto F (2021) Smoothed peridynamics for the extremely large deformation and cracking problems: unification of peridynamics and smoothed particle hydrodynamics. *Fatigue Fract Eng Mater Struct* 44:2444–2461. <https://doi.org/10.1111/FFE.13523>
27. Patra S, Ahmed H, Banerjee S (2018) Peri-elastodynamic simulations of guided ultrasonic waves in plate-like structure with surface mounted PZT. *Sensors* 18:1–16. <https://doi.org/10.3390/S18010274>
28. Safaei B, Moradi-Dastjerdi R, Qin Z, Behdina K, Chu F (2021) Determination of thermoelastic stress wave propagation in nano-composite sandwich plates reinforced by clusters of carbon nanotubes. *J Sandw Struct Mater* 23:884–905. <https://doi.org/10.1177/1099636219848282>
29. Zhang H, Dong X (2015) Physically based crystal plasticity FEM including geometrically necessary dislocations: numerical implementation and applications in micro-forming. *Comput Mater Sci* 110:308–320. <https://doi.org/10.1016/J.COMMATSCI.2015.08.046>
30. Gong SG, Du JX, Liu X, Xie GL, Zhang JP (2010) Study on topology optimization under multiple loading conditions and stress constraints based on EFG method. *Int J Comput Methods Eng Sci Mech* 11:328–336. <https://doi.org/10.1080/15502287.2010.516789>
31. Luo Z, Zhang N, Wang Y, Gao W (2013) Topology optimization of structures using meshless density variable approximants. *Int J Numer Methods Eng* 93:443–464. <https://doi.org/10.1002/NME.4394>
32. Vinogradov A, Estrin Y (2018) Analytical and numerical approaches to modelling severe plastic deformation. *Prog Mater Sci* 95:172–242. <https://doi.org/10.1016/J.PMATSCI.2018.02.001>
33. Wang HP, Wu CT, Chen JS (2014) A reproducing kernel smooth contact formulation for metal forming simulations. *Comput Mech* 54:151–169. <https://doi.org/10.1007/S00466-014-1015-3/FIGURES/23>
34. Ren B, Li S (2010) Meshfree simulations of plugging failures in high-speed impacts. *Comput Struct* 88:909–923. <https://doi.org/10.1016/J.COMPSTRUC.2010.05.003>
35. Belytschko T, Lu YY, Gu L, Tabbara M (1995) Element-free galerkin methods for static and dynamic fracture. *Int J Solids Struct* 32:2547–2570. [https://doi.org/10.1016/0020-7683\(94\)00282-2](https://doi.org/10.1016/0020-7683(94)00282-2)
36. Fleming M, Chur YA, Belytschko T (1996) Enriched element-free Galerkin methods for crack tip fields. *Int J Numer Methods Eng* 29:1483–1504. [https://doi.org/10.1002/\(SICI\)1097-0207\(19970430\)40:8](https://doi.org/10.1002/(SICI)1097-0207(19970430)40:8)
37. Rabczuk T, Song JH, Belytschko T (2009) Simulations of instability in dynamic fracture by the cracking particles method. *Eng Fract Mech* 76:730–741. <https://doi.org/10.1016/J.ENGFRACMECH.2008.06.002>
38. Bui TQ, Nguyen NT, Van LL, Nguyen MN, Truong TT (2018) Analysis of transient dynamic fracture parameters of cracked theoretically graded composites by improved meshfree methods. *Theor Appl Fract Mech* 96:642–657. <https://doi.org/10.1016/J.TAFMEC.2017.10.005>
39. Lu P, Zhao G, Guan Y, Wu X (2008) Bulk metal forming process simulation based on rigid-plastic/viscoplastic element free Galerkin method. *Mater Sci Eng A* 479:197–212. <https://doi.org/10.1016/J.MSEA.2007.06.059>
40. Guan Y, Zhao G, Lu P (2012) Numerical study of equal-channel angular pressing based on the element-free Galerkin method. *Int J Mater Res* 103:1361–1375. <https://doi.org/10.3139/146.110765/MACHINEREADABLECITATION/RIS>
41. Lemiale V, Nairn J, Hurman A (2010) Material point method simulation of equal channel angular pressing involving large plastic strain and contact through sharp corners. *C Comput Model Eng Sci* 70:41–66
42. Fagan T, Das R, Lemiale V, Estrin Y (2012) Modelling of equal channel angular pressing using a mesh-free method. *J Mater Sci* 47:4514–4519. <https://doi.org/10.1007/S10853-012-6296-3/FIGURES/9>
43. Liu GR, Gu YT (2001) A point interpolation method for two-dimensional solids. *Int J Numer Methods Eng* 50:937–951. <https://doi.org/10.1002/1097-0207>
44. Kazemi Z, Hematiyan MR, Vaghefi R (2017) Meshfree radial point interpolation method for analysis of viscoplastic problems. *Eng Anal Bound Elem* 82:172–184. <https://doi.org/10.1016/j.enganabound.2017.06.012>
45. Wang H, Guang Yao L, Zhi HZ (2007) Parallel point interpolation method for three-dimensional metal forming simulations. *Eng Anal Bound Elem* 31:326–342. <https://doi.org/10.1016/J.ENGANABOUND.2006.09.012>
46. Garg S, Pant M (2018) Meshfree methods: a comprehensive review of applications. *Int J Comput Methods* 15:1830001. <https://doi.org/10.1142/S0219876218300015>
47. Nguyen NT, Bui TQ, Zhang C, Truong TT (2014) Crack growth modeling in elastic solids by the extended meshfree Galerkin radial point interpolation method. *Eng Anal Bound Elem* 44:87–97. <https://doi.org/10.1016/J.ENGANABOUND.2014.04.021>
48. Ha YD, Bobaru F (2010) Studies of dynamic crack propagation and crack branching with peridynamics. *Int J Fract* 162:229–244. <https://doi.org/10.1007/S10704-010-9442-4>
49. Guimatsia I, Falzon BG, Davies GAO, Iannucci L (2009) Element-Free Galerkin modelling of composite damage. *Compos Sci Technol* 69:2640–2648. <https://doi.org/10.1016/J.COMPSCITECH.2009.08.005>
50. Yaghoobi A, Chorzepe MG (2017) Fracture analysis of fiber reinforced concrete structures in the micropolar peridynamic analysis framework. *Eng Fract Mech* 169:238–250. <https://doi.org/10.1016/J.ENGFRACMECH.2016.11.004>

51. Selim BA, Liu Z, Liew KM (2019) Active vibration control of functionally graded graphene nanoplatelets reinforced composite plates integrated with piezoelectric layers. *Thin-Walled Struct* 145:1–15. <https://doi.org/10.1016/j.tws.2019.106372>
52. Behdinan K, Moradi-Dastjerdi R, Safaei B, Qin Z, Chu F, Hui D (2020) Graphene and CNT impact on heat transfer response of nanocomposite cylinders. *Nanotechnol Rev* 9:41–52. <https://doi.org/10.1515/NTREV-2020-0004/MACHINEREADABLECITATION/RIS>
53. Abdollahi R, Boroomand B (2019) On using mesh-based and mesh-free methods in problems defined by Eringen's non-local integral model: issues and remedies. *Meccanica* 54:1801–1822. <https://doi.org/10.1007/S11012-019-01048-6/FIGURES/15>
54. Pan X (2017) A generalized approach for solution to image stresses of dislocations. *J Mech Phys Solids* 103:3–21. <https://doi.org/10.1016/J.JMPS.2017.03.002>
55. Chen J-S, Hillman M, Chi S-W (2017) Meshfree methods: progress made after 20 years. *J Eng Mech* 143:04017001. [https://doi.org/10.1061/\(ASCE\)JEM.1943-7889.0001176](https://doi.org/10.1061/(ASCE)JEM.1943-7889.0001176)
56. Li S, Liu WK (2002) Meshfree and particle methods and their applications. *Appl Mech Rev* 55:1–34. <https://doi.org/10.1115/1.1431547>
57. Liu GR (2016) An overview on meshfree methods: for computational solid mechanics. *Int J Comput Methods* 13:1630001. <https://doi.org/10.1142/S0219876216300014>
58. Alijani F, Amabili M (2014) Non-linear vibrations of shells: a literature review from 2003 to 2013. *Int J Non Linear Mech* 58:233–257. <https://doi.org/10.1016/J.IJNONLINMEC.2013.09.012>
59. Shapiro V, Tsukanov I, Grishin A (2011) Geometric issues in computer aided design/computer aided engineering integration. *J Comput Inf Sci Eng* 11:1–13. <https://doi.org/10.1115/1.3593416>
60. Wu CP, Liu YC (2016) A review of semi-analytical numerical methods for laminated composite and multilayered functionally graded elastic/piezoelectric plates and shells, vol 147. Elsevier, Amsterdam
61. Liew KM, Zhao X, Ferreira AJM (2011) A review of meshless methods for laminated and functionally graded plates and shells. *Compos Struct* 93:2031–2041. <https://doi.org/10.1016/J.COMPOSSTRUCT.2011.02.018>
62. Garg A, Chalak HD, Zenkour AM, Belarbi MO, Houari MSA (2022) A review of available theories and methodologies for the analysis of nano isotropic, nano functionally graded, and CNT reinforced nanocomposite structures. *Arch Comput Methods Eng* 29:2237. <https://doi.org/10.1007/s11831-021-09652-0>
63. Palacio-Betancur A, Gutierrez SM (2023) Recent advances in computational methodologies for real-time hybrid simulation of engineering structures. *Arch Comput Methods Eng* 30:1637. <https://doi.org/10.1007/s11831-022-09848-y>
64. Gupta V, Jameel A, Verma SK, Anand S, Anand Y (2023) An insight on NURBS based isogeometric analysis, its current status and involvement in mechanical applications. *Arch Comput Methods Eng* 30:1187. <https://doi.org/10.1007/s11831-022-09838-0>
65. Gu YT, Zhang LC (2006) A concurrent multiscale method based on the meshfree method and molecular dynamics analysis. *Multiscale Model Simul* 5:1128–1155. <https://doi.org/10.1137/060654232>
66. Seleson P (2014) Improved one-point quadrature algorithms for two-dimensional peridynamic models based on analytical calculations. *Comput Methods Appl Mech Eng* 282:184–217. <https://doi.org/10.1016/J.CMA.2014.06.016>
67. Sun F, Wang J, Wei Q, Wu Y (2023) An improved meshless method based on the dimension splitting moving least-squares method for elasticity problems. *Eng Anal Bound Elem* 150:374–384. <https://doi.org/10.1016/J.ENGANABOUND.2023.02.025>
68. Roque CMC, Ferreira AJM, Jorge RMN (2006) Free vibration analysis of composite and sandwich plates by a trigonometric Layerwise deformation theory and radial basis functions. *J Sandw Struct Mater* 8:497–515. <https://doi.org/10.1177/1099636206065873>
69. Shu C, Ding H, Yeo KS (2003) Local radial basis function-based differential quadrature method and its application to solve two-dimensional incompressible Navier-Stokes equations. *Comput Methods Appl Mech Eng* 192:941–954. [https://doi.org/10.1016/S0045-7825\(02\)00618-7](https://doi.org/10.1016/S0045-7825(02)00618-7)
70. Tolstykh AI, Shirobokov DA (2003) On using radial basis functions in a “finite difference mode” with applications to elasticity problems. *Comput Mech* 33:68–79. <https://doi.org/10.1007/S00466-003-0501-9/METRICK>
71. Ding H, Shu C, Yeo KS, Xu D (2006) Numerical computation of three-dimensional incompressible viscous flows in the primitive variable form by local multiquadric differential quadrature method. *Comput Methods Appl Mech Eng* 195:516–533. <https://doi.org/10.1016/J.CMA.2005.02.006>
72. Fantuzzi N, Baccocchi M, Tornabene F, Viola E, Ferreira AJM (2015) Radial basis functions based on differential quadrature method for the free vibration analysis of laminated composite arbitrarily shaped plates. *Compos Part B Eng* 78:65–78. <https://doi.org/10.1016/j.compositesb.2015.03.027>
73. Shu C, Ding H, Chen HQ, Wang TG (2005) An upwind local RBF-DQ method for simulation of inviscid compressible flows. *Comput Methods Appl Mech Eng* 194:2001–2017. <https://doi.org/10.1016/J.CMA.2004.07.008>
74. Wright GB, Fornberg B (2006) Scattered node compact finite difference-type formulas generated from radial basis functions. *J Comput Phys* 212:99–123. <https://doi.org/10.1016/J.JCP.2005.05.030>
75. Oruç Ö (2022) A strong-form local meshless approach based on radial basis function-finite difference (RBF-FD) method for solving multi-dimensional coupled damped Schrödinger system appearing in Bose-Einstein condensates. *Commun Nonlinear Sci Numer Simul* 104:1–18. <https://doi.org/10.1016/J.CNSNS.2021.106042>
76. Tornabene F, Fantuzzi N, Baccocchi M, Neves AMA, Ferreira AJM (2016) MLS-DQ based on RBFs for the free vibrations of laminated composite doubly-curved shells. *Compos Part B Eng* 99:30–47. <https://doi.org/10.1016/J.COMPOSITESB.2016.05.049>
77. Ferreira AJM, Batra RC, Roque CMC, Qian LF, Jorge RMN (2006) Natural frequencies of functionally graded plates by a meshless method. *Compos Struct* 75:593–600. <https://doi.org/10.1016/J.COMPSTRUCT.2006.04.018>
78. Ferreira AJM, Batra RC, Roque CMC, Qian LF, Martins PALS (2005) Static analysis of functionally graded plates using third-order shear deformation theory and a meshless method. *Compos Struct* 69:449–457. <https://doi.org/10.1016/J.COMPSTRUCT.2004.08.003>
79. Ferreira AJM (2003) A formulation of the multiquadric radial basis function method for the analysis of laminated composite plates. *Compos Struct* 59:385–392. [https://doi.org/10.1016/S0263-8223\(02\)00239-8](https://doi.org/10.1016/S0263-8223(02)00239-8)
80. Ferreira AJM, Roque CMC, Martins PALS (2003) Analysis of composite plates using higher-order shear deformation theory and a finite point formulation based on the multiquadric radial basis function method. *Compos Part B Eng* 34:627–636. [https://doi.org/10.1016/S1359-8368\(03\)00083-0](https://doi.org/10.1016/S1359-8368(03)00083-0)
81. Ferreira AJM (2007) Analysis of composite plates using a layerwise theory and multiquadrics discretization. *Mech Adv Mater Struct* 12:99–112. <https://doi.org/10.1080/15376490490493952>
82. Ferreira AJM, Fasshauer GE (2006) Computation of natural frequencies of shear deformable beams and plates by an

- RBF-pseudospectral method. *Comput Methods Appl Mech Eng* 196:134–146. <https://doi.org/10.1016/J.CMA.2006.02.009>
83. Ferreira AJM, Fasshauer GE, Batra RC, Rodrigues JD (2008) Static deformations and vibration analysis of composite and sandwich plates using a layerwise theory and RBF-PS discretizations with optimal shape parameter. *Compos Struct* 86:328–343. <https://doi.org/10.1016/J.COMPSTRUCT.2008.07.025>
 84. Ho PLH, Le CV, Nguyen PH (2021) Kinematic yield design computational homogenization of micro-structures using the stabilized iRBF mesh-free method. *Appl Math Model* 91:322–334. <https://doi.org/10.1016/J.APM.2020.09.056>
 85. Xiang S, Jiang SX, Bi ZY, Jin YX, Yang MS (2011) A nth-order meshless generalization of Reddy's third-order shear deformation theory for the free vibration on laminated composite plates. *Compos Struct* 93:299–307. <https://doi.org/10.1016/J.COMPOSTRUCT.2010.09.015>
 86. Nie Y, Zhang W, Qi N, Li Y (2014) Parallel node placement method by bubble simulation. *Comput Phys Commun* 185:798–808. <https://doi.org/10.1016/J.CPC.2013.11.010>
 87. Rao BN, Rahman S (2003) Mesh-free analysis of cracks in isotropic functionally graded materials. *Eng Fract Mech* 70:1–27. [https://doi.org/10.1016/S0013-7944\(02\)00038-3](https://doi.org/10.1016/S0013-7944(02)00038-3)
 88. Racz D, Bui TQ (2012) Novel adaptive meshfree integration techniques in meshless methods. *Int J Numer Methods Eng* 90:1414–1434. <https://doi.org/10.1002/NME.4268>
 89. Liew KM, Cheng Y, Kitipornchai S (2005) Boundary element-free method (BEFM) for two-dimensional elastodynamic analysis using Laplace transform. *Int J Numer Methods Eng* 64:1610–1627. <https://doi.org/10.1002/NME.1417>
 90. Sansour C, Skatulla S (2008) A non-linear Cosserat continuum-based formulation and moving least square approximations in computations of size-scale effects in elasticity. *Comput Mater Sci* 41:589–601. <https://doi.org/10.1016/J.COMMATSCI.2007.05.024>
 91. Wang JG, Liu GR (2002) A point interpolation meshless method based on radial basis functions. *Int J Numer Methods Eng* 54:1623–1648. <https://doi.org/10.1002/NME.489>
 92. Rosca VE, Leitão VMA (2008) Quasi-Monte Carlo mesh-free integration for meshless weak formulations. *Eng Anal Bound Elem* 32:471–479. <https://doi.org/10.1016/J.ENGANABOUND.2007.10.015>
 93. Khosravifard A, Hematiyan MR (2010) A new method for meshless integration in 2D and 3D Galerkin meshfree methods. *Eng Anal Bound Elem* 34:30–40. <https://doi.org/10.1016/J.ENGANABOUND.2009.07.008>
 94. Fish J, Chen W, Li R (2007) Generalized mathematical homogenization of atomistic media at finite temperatures in three dimensions. *Comput Methods Appl Mech Eng* 196:908–922. <https://doi.org/10.1016/J.CMA.2006.08.001>
 95. Hematiyan MR (2008) Exact transformation of a wide variety of domain integrals into boundary integrals in boundary element method. *Commun Numer Methods Eng* 24:1497–1521. <https://doi.org/10.1002/CNM.1047>
 96. Monaghan JJ (1997) SPH and Riemann Solvers. *J Comput Phys* 136:298–307. <https://doi.org/10.1006/JCPH.1997.5732>
 97. Monaghan JJ, Implicit SPH (1997) Drag and dusty gas dynamics. *J Comput Phys* 138:801–820. <https://doi.org/10.1006/JCPH.1997.5846>
 98. Monaghan JJ (2000) SPH without a tensile instability. *J Comput Phys* 159:290–311. <https://doi.org/10.1006/JCPH.2000.6439>
 99. Dyka CT, Ingel RP (1995) An approach for tension instability in smoothed particle hydrodynamics (SPH). *Comput Struct* 57:573–580. [https://doi.org/10.1016/0045-7949\(95\)00059-P](https://doi.org/10.1016/0045-7949(95)00059-P)
 100. Belytschko T, Guo Y, Liu WK, Xiao SP (2000) A unified stability analysis of meshless particle methods. *Int J Numer Methods Eng* 48:1359–1400. [https://doi.org/10.1002/1097-0207\(2000730\)48:9%3c1359::AID-NME829%3e3.0.CO;2-U](https://doi.org/10.1002/1097-0207(2000730)48:9%3c1359::AID-NME829%3e3.0.CO;2-U)
 101. Vignjevic R, Campbell J, Libersky L (2000) A treatment of zero-energy modes in the smoothed particle hydrodynamics method. *Comput Methods Appl Mech Eng* 184:67–85. [https://doi.org/10.1016/S0045-7825\(99\)00441-7](https://doi.org/10.1016/S0045-7825(99)00441-7)
 102. Dilts GA (2000) Moving least-squares particle hydrodynamics II: conservation and boundaries. *Int J Numer Methods Eng* 48:1503–1524
 103. Morris JP, Fox PJ, Zhu Y (1997) Modeling low reynolds number incompressible flows using SPH. *J Comput Phys* 136:214–226. <https://doi.org/10.1006/JCPH.1997.5776>
 104. Khayyer A, Gotoh H, Falahaty H, Shimizu Y (2018) An enhanced ISPH–SPH coupled method for simulation of incompressible fluid–elastic structure interactions. *Comput Phys Commun* 232:139–164. <https://doi.org/10.1016/J.CPC.2018.05.012>
 105. Liu MB, Liu GR (2010) Smoothed particle hydrodynamics (SPH): an overview and recent developments. *Arch Comput Methods Eng* 17:25–76. <https://doi.org/10.1007/S11831-010-9040-7>
 106. Rahmat A, Barigou M, Alexiadis A (2019) Deformation and rupture of compound cells under shear: a discrete multiphysics study. *Phys Fluids* 31:1–14
 107. Silling SA, Askari E (2005) A meshfree method based on the peridynamic model of solid mechanics. *Comput Struct* 83:1526–1535. <https://doi.org/10.1016/J.COMPSTRUC.2004.11.026>
 108. Amiri F, Millán D, Shen Y, Rabczuk T, Arroyo M (2014) Phase-field modeling of fracture in linear thin shells. *Theor Appl Fract Mech* 69:102–109. <https://doi.org/10.1016/J.TAFMEC.2013.12.002>
 109. Zhang LW, Selim BA (2017) Vibration analysis of CNT-reinforced thick laminated composite plates based on Reddy's higher-order shear deformation theory. *Compos Struct* 160:689–705. <https://doi.org/10.1016/J.COMPSTRUCT.2016.10.102>
 110. Seleson P, Littlewood DJ (2016) Convergence studies in meshfree peridynamic simulations. *Comput Math Appl* 71:2432–2448. <https://doi.org/10.1016/J.CAMWA.2015.12.021>
 111. Fu Z, Chen W, Wen P, Zhang C (2018) Singular boundary method for wave propagation analysis in periodic structures. *J Sound Vib* 425:170–188. <https://doi.org/10.1016/J.JSV.2018.04.005>
 112. Lin J, Zhang C, Sun L, Lu J (2018) Simulation of seismic wave scattering by embedded cavities in an elastic half-plane using the novel singular boundary method. *Adv Appl Math Mech* 10:322–342. <https://doi.org/10.4208/AAMM.OA-2016-0187>
 113. Liu YJ, Mukherjee S, Nishimura N, Schanz M, Ye W, Sutradhar A et al (2011) Recent advances and emerging applications of the boundary element method. *Appl Mech Rev* 64:30802–30803. <https://doi.org/10.1115/1.4005491/370044>
 114. Shen S, Atluri SN (2004) Multiscale simulation based on the meshless local Petrov-Galerkin (MLPG) method. *C Comput Model Eng Sci* 5:235–255
 115. Tang Z, Shen S, Atluri SN (2003) Analysis of materials with strain-gradient effects: a meshless local Petrov-Galerkin (MLPG) approach, with nodal displacements only. *C Comput Model Eng Sci* 4:177–196. <https://doi.org/10.3970/cmescs.2003.004.177>
 116. Limkatanyu S, Sae-Long W, Rungamornrat J, Buachart C, Sukontasukkul P, Keawsawasvong S et al (2022) Bending, buckling and free vibration analyses of nanobeam-substrate medium systems. *Facta Univ Ser Mech Eng* 20:561. <https://doi.org/10.22190/FUME220506029L>
 117. Yvonnet J, Ryckelynck D, Lorong P, Chinesta F (2004) A new extension of the natural element method for non-convex and discontinuous problems: the constrained natural element method

- (C-NEM). *Int J Numer Methods Eng* 60:1451–1474. <https://doi.org/10.1002/NME.1016>
118. Bessa MA, Foster JT, Belytschko T, Liu WK (2014) A meshfree unification: reproducing kernel peridynamics. *Comput Mech* 53:1251–1264. <https://doi.org/10.1007/S00466-013-0969-X/TABLES/1>
 119. AlKhateab B, Tabrizi IE, Zanjani JSM, Rahimi MN, Poudesh LH, Kefal A et al (2020) Damage mechanisms in CFRP/HNT laminates under flexural and in-plane shear loadings using experimental and numerical methods. *Compos Part A Appl Sci Manuf* 136:1–16. <https://doi.org/10.1016/J.COMPOSITESA.2020.105962>
 120. Ren B, Li S, Qian J, Zeng X (2011) Meshfree simulations of spall fracture. *Comput Methods Appl Mech Eng* 200:797–811. <https://doi.org/10.1016/J.CMA.2010.10.003>
 121. Wright TW, Ramesh KT (2008) Dynamic void nucleation and growth in solids: a self-consistent statistical theory. *J Mech Phys Solids* 56:336–359. <https://doi.org/10.1016/J.JMPS.2007.05.012>
 122. Mishra A, Hemeda A, Torabi M, Palko J, Goyal S, Li D et al (2019) A simple analytical model of complex wall in multibody dissipative particle dynamics. *J Comput Phys* 396:416–426. <https://doi.org/10.1016/J.JCP.2019.06.075>
 123. Imai Y, Omori T, Shimogonya Y, Yamaguchi T, Ishikawa T (2016) Numerical methods for simulating blood flow at macro, micro, and multi scales. *J Biomech* 49:2221–2228. <https://doi.org/10.1016/J.JBIOMECH.2015.11.047>
 124. Karunasena HCP, Brown RJ, Gu YT, Senadeera W (2015) Application of meshfree methods to numerically simulate microscale deformations of different plant food materials during drying. *J Food Eng* 146:209–226. <https://doi.org/10.1016/J.JFOODENG.2014.09.011>
 125. Liu MB, Liu GR, Zhou LW, Chang JZ (2015) Dissipative particle dynamics (DPD): an overview and recent developments. *Arch Comput Methods Eng* 22:529–556. <https://doi.org/10.1007/S11831-014-9124-X>
 126. Huang Z, Lei D, Huang D, Lin J, Han Z (2019) Boundary moving least square method for 2D elasticity problems. *Eng Anal Bound Elem* 106:505–512. <https://doi.org/10.1016/J.ENGANABOUND.2019.06.005>
 127. Chen F, Qiang H, Zhang H, Gao W (2017) A coupled SDPH–FVM method for gas-particle multiphase flow: Methodology. *Int J Numer Methods Eng* 109:73–101. <https://doi.org/10.1002/NME.5279>
 128. Millán D, Rosolen A, Arroyo M (2013) Nonlinear manifold learning for meshfree finite deformation thin-shell analysis. *Int J Numer Methods Eng* 93:685–713. <https://doi.org/10.1002/nme.4403>
 129. Thai CH, Kulasegaram S, Tran LV, Nguyen-Xuan H (2014) Generalized shear deformation theory for functionally graded isotropic and sandwich plates based on isogeometric approach. *Comput Struct* 141:94–112. <https://doi.org/10.1016/J.COMPS TRUC.2014.04.003>
 130. Faghidian SA, Žur KK, Pan E, Kim J (2022) On the analytical and meshless numerical approaches to mixture stress gradient functionally graded nano-bar in tension. *Eng Anal Bound Elem* 134:571–580. <https://doi.org/10.1016/J.ENGANABOUND.2021.11.010>
 131. Chen JS, Pan C, Wu CT, Liu WK (1996) Reproducing Kernel Particle Methods for large deformation analysis of non-linear structures. *Comput Methods Appl Mech Eng* 139:195–227. [https://doi.org/10.1016/S0045-7825\(96\)01083-3](https://doi.org/10.1016/S0045-7825(96)01083-3)
 132. Breitkopf P, Rassineux A, Villon P (2002) An introduction to moving least squares meshfree methods. *Rev Eur Des Éléments Finis* 11:825–867. <https://doi.org/10.3166/REEF.11.825-867>
 133. Kamil Žur K, Faghidian SA (2021) Analytical and meshless numerical approaches to unified gradient elasticity theory. *Eng Anal Bound Elem* 130:238–248. <https://doi.org/10.1016/J.ENGANABOUND.2021.05.022>
 134. Faghidian SA, Tounsi A (2022) Dynamic characteristics of mixture unified gradient elastic nanobeams. *Facta Univ Ser Mech Eng* 20:539. <https://doi.org/10.22190/FUME220703035F>
 135. Sladek J, Sladek V, Repka M, Bishay PL (2016) Static and dynamic behavior of porous elastic materials based on micro-dilatation theory: a numerical study using the MLPG method. *Int J Solids Struct* 96:126–135. <https://doi.org/10.1016/J.IJSOL STR.2016.06.016>
 136. Kwak S, Kim K, Jong G, Cha J, Juhyok U (2021) A mesh-free approach for free vibration analysis of ply drop-off laminated conical, cylindrical shells and annular plates. *Acta Mech* 232:4775–4800. <https://doi.org/10.1007/S00707-021-03084-4/FIGURES/11>
 137. Lucy LB (1977) A numerical approach to the testing of the fission hypothesis. *Astron J* 82:1013. <https://doi.org/10.1086/112164>
 138. Strouboulis T, Copps K, Babuška I (2000) The generalized finite element method: an example of its implementation and illustration of its performance. *Int J Numer Methods Eng* 47:1401–1417. [https://doi.org/10.1002/\(SICI\)1097-0207\(20000320\)47:8%3c1401::AID-NME835%3e3.0.CO;2-8](https://doi.org/10.1002/(SICI)1097-0207(20000320)47:8%3c1401::AID-NME835%3e3.0.CO;2-8)
 139. Duarte CA, Oden JT (1996) H-p clouds: an h-p meshless method. *Numer Methods Partial Differ Equ* 12:673–705. [https://doi.org/10.1002/\(SICI\)1098-2426\(199611\)12:6](https://doi.org/10.1002/(SICI)1098-2426(199611)12:6)
 140. Fleming M, Chu YA, Moran B, Belytschko T (1997) Enriched element-free galerkin methods for crack tip fields. *Int J Numer Methods Eng* 40:1483–1504. [https://doi.org/10.1002/\(SICI\)1097-0207\(19970430\)40:8%3c1483::AID-NME123%3e3.0.CO;2-6](https://doi.org/10.1002/(SICI)1097-0207(19970430)40:8%3c1483::AID-NME123%3e3.0.CO;2-6)
 141. Gavete L, Gavete ML, Alonso B, Martín AJ, Martā AJ (2003) A posteriori error approximation in EFG method. *Int J Numer Methods Eng* 58:2239–2263
 142. Lu H, Chen J-S (2003) *Adaptive Galerkin particle method*. Springer, Berlin, pp 251–265
 143. Chung HJ, Belytschko T (1998) An error estimate in the EFG method. *Comput Mech* 21:91–100. <https://doi.org/10.1007/S004660050286/METRICS>
 144. Duarte CA, Oden JT (1996) An h-p adaptive method using clouds. *Comput Methods Appl Mech Eng* 139:237–262. [https://doi.org/10.1016/S0045-7825\(96\)01085-7](https://doi.org/10.1016/S0045-7825(96)01085-7)
 145. Duffot M, Nguyen-Dang H (2002) Dual analysis by a meshless method. *Commun Numer Methods Eng* 18:621–631. <https://doi.org/10.1002/CNM.521>
 146. Krongauzr Y, Belytschko T (1996) EFG approximation with discontinuous derivatives. *Int J Numer Methods Eng* 41:1215–1233. [https://doi.org/10.1002/\(SICI\)1097-0207\(19980415\)41:7](https://doi.org/10.1002/(SICI)1097-0207(19980415)41:7)
 147. Bordas S, Duffot M (2007) Derivative recovery and a posteriori error estimate for extended finite elements. *Comput Methods Appl Mech Eng* 196:3381–3399. <https://doi.org/10.1016/J.CMA.2007.03.011>
 148. Bordas S, Duffot M, Le P (2008) A simple error estimator for extended finite elements. *Commun Numer Methods Eng* 24:961–971. <https://doi.org/10.1002/CNM.1001>
 149. Duffot M, Bordas S (2008) A posteriori error estimation for extended finite elements by an extended global recovery. *Int J Numer Methods Eng* 76:1123–1138. <https://doi.org/10.1002/NME.2332>
 150. Häussler-Combe U, Korn C (1998) An adaptive approach with the element-free-Galerkin method. *Comput Methods Appl Mech Eng* 162:203–222. [https://doi.org/10.1016/S0045-7825\(97\)00344-7](https://doi.org/10.1016/S0045-7825(97)00344-7)

151. You Y, Chen JS, Lu H (2003) Filters, reproducing kernel, and adaptive meshfree method. *Comput Mech* 31:316–326. <https://doi.org/10.1007/S00466-003-0434-3/METRICS>
152. Zhang Y, Dang S, Li W, Chai Y (2022) Performance of the radial point interpolation method (RPIM) with implicit time integration scheme for transient wave propagation dynamics. *Comput Math Appl* 114:95–111. <https://doi.org/10.1016/J.CAMWA.2022.03.031>
153. Rabczuk T, Belytschko T (2005) Adaptivity for structured meshfree particle methods in 2D and 3D. *Int J Numer Methods Eng* 63:1559–1582. <https://doi.org/10.1002/nme.1326>
154. Bayona V, Moscoso M, Kindelan M (2011) Optimal constant shape parameter for multiquadric based RBF-FD method. *J Comput Phys* 230:7384–7399. <https://doi.org/10.1016/J.JCP.2011.06.005>
155. Duan Q, Li X, Zhang H, Belytschko T (2012) Second-order accurate derivatives and integration schemes for meshfree methods. *Int J Numer Methods Eng* 92:399–424. <https://doi.org/10.1002/NME.4359>
156. Hou D, Wang L, Yan J, Liew KM (2022) Vibration analysis of a strain gradient plate model via a mesh-free moving Kriging Interpolation Method. *Eng Anal Bound Elem* 135:156–166. <https://doi.org/10.1016/J.ENGANABOUND.2021.11.014>
157. Fu ZJ, Chen W, Yang HT (2013) Boundary particle method for Laplace transformed time fractional diffusion equations. *J Comput Phys* 235:52–66. <https://doi.org/10.1016/J.JCP.2012.10.018>
158. Iliopoulos A, Michopoulos JG (2013) Direct strain tensor approximation for full-field strain measurement methods. *Int J Numer Methods Eng* 95:313–330. <https://doi.org/10.1002/NME.4509>
159. Wu CT, Guo Y, Askari E (2013) Numerical modeling of composite solids using an immersed meshfree Galerkin method. *Compos Part B Eng* 45:1397–1413. <https://doi.org/10.1016/j.compositesb.2012.09.061>
160. Dehghan M, Najafi M (2016) Numerical solution of a non-classical two-phase Stefan problem via radial basis function (RBF) collocation methods. *Eng Anal Bound Elem* 72:111–127. <https://doi.org/10.1016/J.ENGANABOUND.2016.07.015>
161. Roque CMC, Ferreira AJM, Jorge RMN (2007) A radial basis function approach for the free vibration analysis of functionally graded plates using a refined theory. *J Sound Vib* 300:1048–1070. <https://doi.org/10.1016/J.JSV.2006.08.037>
162. Ferreira AJM (2010) Thick composite beam analysis using a global meshless approximation based on radial basis functions. *Mech Adv Mater Struct* 10:271–284. <https://doi.org/10.1080/15376490306743>
163. Civalek Ö (2008) Analysis of thick rectangular plates with symmetric cross-ply laminates based on first-order shear deformation theory. *J Compos Mater* 42:2853. <https://doi.org/10.1177/0021998308096952>
164. Nian Y, Wan S, Wang X, Zhou P, Avcar M, Li M (2023) Study on crashworthiness of nature-inspired functionally graded lattice metamaterials for bridge pier protection against ship collision. *Eng Struct* 277:115404. <https://doi.org/10.1016/j.engstruct.2022.115404>
165. Mellal F, Bennai R, Avcar M, Nebab M, Atmane HA (2023) On the vibration and buckling behaviors of porous FG beams resting on variable elastic foundation utilizing higher-order shear deformation theory. *Acta Mech* 2023:1–23. <https://doi.org/10.1007/S00707-023-03603-5/FIGURES/1>
166. Hadji L, Avcar M (2021) Nonlocal free vibration analysis of porous FG nanobeams using hyperbolic shear deformation beam theory. *Adv Nano Res* 10:281. <https://doi.org/10.12989/anr.2021.10.3.281>
167. Mercan K, Demir Ç, Civalek Ö (2016) Vibration analysis of FG cylindrical shells with power-law index using discrete singular convolution technique. *Curved Layer Struct*. <https://doi.org/10.1515/cls-2016-0007>
168. Civalek Ö (2006) The determination of frequencies of laminated conical shells via the discrete singular convolution method. *J Mech Mater Struct* 1:163. <https://doi.org/10.2140/jomms.2006.1.163>
169. Civalek Ö (2006) Free vibration analysis of composite conical shells using the discrete singular convolution algorithm. *Steel Compos Struct* 6:353. <https://doi.org/10.12989/scs.2006.6.4.353>
170. Van Vinh P, Belarbi MO, Avcar M, Civalek Ö (2023) An improved first-order mixed plate element for static bending and free vibration analysis of functionally graded sandwich plates. *Arch Appl Mech* 93:1841. <https://doi.org/10.1007/s00419-022-02359-z>
171. Hadji L, Avcar M, Civalek Ö (2022) Free vibration of carbon nanotube-reinforced composite beams under the various boundary conditions. *Adv Compos Mater Struct*. <https://doi.org/10.1201/9781003158813-6>
172. Hadji L, Avcar M, Civalek Ö (2021) An analytical solution for the free vibration of FG nanoplates. *J Braz Soc Mech Sci Eng*. <https://doi.org/10.1007/s40430-021-03134-x>
173. Rizov V (2023) Delamination analysis of multilayered functionally graded beams which exhibit non-linear creep behavior. *J Appl Comput Mech* 9:935–944. <https://doi.org/10.22055/jacm.2023.42743.3969>
174. Ersoy H, Mercan K, Civalek Ö (2018) Frequencies of FGM shells and annular plates by the methods of discrete singular convolution and differential quadrature methods. *Compos Struct* 183:7–20. <https://doi.org/10.1016/j.compstruct.2016.11.051>
175. Avcar M, Hadji L, Civalek O (2023) The influence of non-linear carbon nanotube reinforcement on the natural frequencies of composite beams. *Adv Nano Res* 14:421–433. <https://doi.org/10.12989/anr.2023.14.5.421>
176. Alibar MY, Safaei B, Asmael M, Zeeshan Q (2022) Effect of carbon nanotubes and porosity on vibrational behavior of nanocomposite structures: a review. *Arch Comput Methods Eng* 29:2621. <https://doi.org/10.1007/s11831-021-09669-5>
177. Nuhu AA, Safaei B (2022) State-of-the-art of vibration analysis of small-sized structures by using nonclassical continuum theories of elasticity. *Arch Comput Methods Eng* 29:4959. <https://doi.org/10.1007/s11831-022-09754-3>
178. Chakraborty S, Singh V, Dey T, Rajesh K (2023) Influence of carbon nanotubes on stability and vibration characteristics of plates and panels in thermal environment: a review. *Arch Comput Methods Eng* 2023(1):1–32. <https://doi.org/10.1007/S11831-023-09976-Z>
179. Kim H, Qaiser N, Hwang B (2023) Electro-mechanical response of stretchable PDMS composites with a hybrid filler system. *Facta Univ Ser Mech Eng* 21:51–61. <https://doi.org/10.22190/FUME221205002K>
180. Jankowski P (2022) Detection of nonlocal calibration parameters and range interaction for dynamics of FGM porous nanobeams under electro-mechanical loads. *Facta Univ Ser Mech Eng* 20:457. <https://doi.org/10.22190/FUME210207007J>
181. Kurpa L, Shmatko T, Awrejcewicz J, Timchenko G, Morachkovska I (2023) Analysis of free vibration of porous power-law and sigmoid functionally graded sandwich plates by the R-functions method. *J Appl Comput Mech* 9:1144–1155. <https://doi.org/10.22055/jacm.2023.43435.4082>
182. Rezaiee-Pajand M, Masoodi AR (2016) Exact natural frequencies and buckling load of functionally graded material tapered beam-columns considering semi-rigid connections. *J Vib Control* 24:1787–1808. <https://doi.org/10.1177/1077546316668932>

183. Rezaiee-Pajand M, Masoodi AR, Mokhtari M (2018) Static analysis of functionally graded non-prismatic sandwich beams. *Adv Comput Des*. <https://doi.org/10.12989/acd.2018.3.2.165>
184. Fantuzzi N, Tornabene F, Baccocchi M, Dimitri R (2017) Free vibration analysis of arbitrarily shaped Functionally Graded Carbon Nanotube-reinforced plates. *Compos Part B Eng* 115:384–408. <https://doi.org/10.1016/J.COMPOSITESB.2016.09.021>
185. Arefi M, Mohammad-Rezaei Bidgoli E, Dimitri R, Tornabene F (2018) Free vibrations of functionally graded polymer composite nanoplates reinforced with graphene nanoplatelets. *Aerosp Sci Technol* 81:108–117. <https://doi.org/10.1016/J.AST.2018.07.036>
186. Arefi M, Mohammad-Rezaei Bidgoli E, Dimitri R, Baccocchi M, Tornabene F (2019) Nonlocal bending analysis of curved nanobeams reinforced by graphene nanoplatelets. *Compos Part B Eng* 166:1–12. <https://doi.org/10.1016/J.COMPOSITESB.2018.11.092>
187. Tornabene F, Baccocchi M, Fantuzzi N, Reddy JN (2019) Multiscale approach for three-phase CNT/polymer/fiber laminated nanocomposite structures. *Polym Compos* 40:E102–E126. <https://doi.org/10.1002/PC.24520>
188. Tornabene F, Fantuzzi N, Baccocchi M, Viola E (2016) Effect of agglomeration on the natural frequencies of functionally graded carbon nanotube-reinforced laminated composite doubly-curved shells. *Compos Part B Eng* 89:187. <https://doi.org/10.1016/j.compositesb.2015.11.016>
189. Tornabene F, Fantuzzi N, Baccocchi M (2017) Linear static response of nanocomposite plates and shells reinforced by agglomerated carbon nanotubes. *Compos Part B Eng* 115:449–476. <https://doi.org/10.1016/J.COMPOSITESB.2016.07.011>
190. Sobhani E, Safaei B (2023) Vibrational development of nanocomposite cylindrical shells by employing reduced graphene oxide (rGO) as a nanoscale strengthener. *Eng Anal Bound Elem* 155:920–934. <https://doi.org/10.1016/J.ENGANABOUND.2023.07.016>
191. Shokrieh MM, Moshrefzadeh-Sani H (2016) On the constant parameters of Halpin-Tsai equation. *Polymer (Guildf)* 106:14–20. <https://doi.org/10.1016/j.polymer.2016.10.049>
192. Xiao L, Mei G, Xi N, Piccialli F (2022) Julia language in computational mechanics: a new competitor. *Arch Comput Methods Eng* 29:1713. <https://doi.org/10.1007/s11831-021-09636-0>
193. Zeng W, Liu GR (2018) Smoothed finite element methods (S-FEM): an overview and recent developments. *Arch Comput Methods Eng* 25:397–435. <https://doi.org/10.1007/s11831-016-9202-3>
194. Safaei B, Onyibo EC, Goren M, Kotrasova K, Yang Z, Arman S et al (2023) Free vibration investigation on rve of proposed honeycomb sandwich beam and material selection optimization. *Facta Univ Ser Mech Eng* 21:031. <https://doi.org/10.22190/FUME220806042S>
195. Safaei B, Onyibo EC, Hurdoganoglu D (2022) Effect of static and harmonic loading on the honeycomb sandwich beam by using finite element method. *Facta Univ Ser Mech Eng* 20:279. <https://doi.org/10.22190/FUME220201009S>
196. Sheikh T, Behdinan K (2023) Insight of discrete scale and multiscale methods for characterization of composite and nanocomposite materials. *Arch Comput Methods Eng* 30:1231. <https://doi.org/10.1007/s11831-022-09840-6>
197. Ramekte PM, Panda SK (2023) Computational modelling and experimental challenges of linear and nonlinear analysis of porous graded structure: a comprehensive review. *Arch Comput Methods Eng* 30:3437. <https://doi.org/10.1007/s11831-023-09908-x>
198. Gierden C, Kochmann J, Waimann J, Svendsen B, Reese S (2022) A review of FE-FFT-based two-scale methods for computational modeling of microstructure evolution and macroscopic material behavior. *Arch Comput Methods Eng* 29:4115. <https://doi.org/10.1007/s11831-022-09735-6>
199. Geers MGD, Kouznetsova VG, Brekelmans WAM (2010) Multi-scale computational homogenization: trends and challenges. *J Comput Appl Math* 234:2175. <https://doi.org/10.1016/j.cam.2009.08.077>
200. Cueto E, Sukumar N, Calvo B, Martínez MA, Cegoñino J, Doblaré M (2003) Overview and recent advances in natural neighbour Galerkin methods. *Arch Comput Methods Eng* 10:307. <https://doi.org/10.1007/BF02736253>
201. Lorong P, Yvonnet J, Coffignal G, Cohen S (2006) Contribution of computational mechanics in numerical simulation of machining and blanking: State-of-the-art. *Arch Comput Methods Eng* 13:45. <https://doi.org/10.1007/BF02905931>
202. Abdulle A, Weinan E (2003) Finite difference heterogeneous multi-scale method for homogenization problems. *J Comput Phys* 191:18–39. [https://doi.org/10.1016/S0021-9991\(03\)00303-6](https://doi.org/10.1016/S0021-9991(03)00303-6)
203. Rafiei S, Hossain KMA, Lachemi M, Behdinan K (2015) Profiled sandwich composite wall with high performance concrete subjected to monotonic shear. *J Constr Steel Res* 107:124–136. <https://doi.org/10.1016/j.jcsr.2015.01.015>
204. Rafiei S, Hossain KMA, Lachemi M, Behdinan K, Anwar MS (2013) Finite element modeling of double skin profiled composite shear wall system under in-plane loadings. *Eng Struct* 56:46–57. <https://doi.org/10.1016/J.ENGSTRUCT.2013.04.014>
205. Artioli E, Marfia S, Sacco E (2018) High-order virtual element method for the homogenization of long fiber nonlinear composites. *Comput Methods Appl Mech Eng* 341:571. <https://doi.org/10.1016/j.cma.2018.07.012>
206. Marino M, Hudobivnik B, Wriggers P (2019) Computational homogenization of polycrystalline materials with the Virtual Element Method. *Comput Methods Appl Mech Eng* 355:349. <https://doi.org/10.1016/j.cma.2019.06.004>
207. He C, Gao J, Li H, Ge J, Chen Y, Liu J et al (2020) A data-driven self-consistent clustering analysis for the progressive damage behavior of 3D braided composites. *Compos Struct* 249:112471. <https://doi.org/10.1016/j.compstruct.2020.112471>
208. He C, Ge J, Lian Y, Geng L, Chen Y, Fang D (2022) A concurrent three-scale scheme FE-SCA2 for the nonlinear mechanical behavior of braided composites. *Comput Methods Appl Mech Eng* 393:114827. <https://doi.org/10.1016/j.cma.2022.114827>
209. Civalek Ö, Akgöz B (2013) Vibration analysis of micro-scaled sector shaped graphene surrounded by an elastic matrix. *Comput Mater Sci* 77:295. <https://doi.org/10.1016/j.commatsci.2013.04.055>
210. Civalek Ö (2007) Free vibration and buckling analyses of composite plates with straight-sided quadrilateral domain based on DSC approach. *Finite Elem Anal Des* 43:1013. <https://doi.org/10.1016/j.finel.2007.06.014>
211. Civalek Ö (2009) A four-node discrete singular convolution for geometric transformation and its application to numerical solution of vibration problem of arbitrary straight-sided quadrilateral plates. *Appl Math Model* 33:300–314. <https://doi.org/10.1016/j.apm.2007.11.003>
212. Civalek Ö, Ülker M (2004) Harmonic differential quadrature (HDQ) for axisymmetric bending analysis of thin isotropic circular plates. *Struct Eng Mech* 17:1–14. <https://doi.org/10.12989/sem.2004.17.1.001>
213. Civalek Ö (2006) Harmonic differential quadrature-finite differences coupled approaches for geometrically nonlinear static and dynamic analysis of rectangular plates on elastic foundation. *J Sound Vib* 294:966. <https://doi.org/10.1016/j.jsv.2005.12.041>
214. Akgöz B, Civalek Ö (2011) Application of strain gradient elasticity theory for buckling analysis of protein microtubules. *Curr Appl Phys* 11:1133. <https://doi.org/10.1016/j.cap.2011.02.006>

215. Jalaei MH, Thai HT, Civalek (2022) On viscoelastic transient response of magnetically imperfect functionally graded nanobeams. *Int J Eng Sci* 172:103629. <https://doi.org/10.1016/j.jengsci.2022.103629>
216. Spahn J, Andrä H, Kabel M, Müller R (2014) A multiscale approach for modeling progressive damage of composite materials using fast Fourier transforms. *Comput Methods Appl Mech Eng* 268:871. <https://doi.org/10.1016/j.cma.2013.10.017>
217. Numanoglu HM, Ersoy H, Akgöz B, Civalek Ö (2022) A new eigenvalue problem solver for thermo-mechanical vibration of Timoshenko nanobeams by an innovative nonlocal finite element method. *Math Methods Appl Sci* 45:2592. <https://doi.org/10.1002/mma.7942>
218. Suchde P, Jacquemin T, Davydov O (2023) Point cloud generation for meshfree methods: an overview. *Arch Comput Methods Eng* 30:889. <https://doi.org/10.1007/s11831-022-09820-w>
219. Safaei B, Onyibo EC, Hurdoganoglu D (2022) Thermal buckling and bending analyses of carbon foam beams sandwiched by composite faces under axial compression. *Facta Univ Ser Mech Eng* 20:589. <https://doi.org/10.22190/FUME220404027S>
220. Balokhonov R, Romanova V, Schwab E, Zemlianov A, Evtushenko E (2021) Computational microstructure-based analysis of residual stress evolution in metal-matrix composite materials during thermomechanical loading. *Facta Univ Ser Mech Eng* 19:241. <https://doi.org/10.22190/FUME201228011B>
221. Asmael M, Memarzadeh A (2023) A review on recent achievements and challenges in electrochemical machining of tungsten carbide. *Arch Adv Eng Sci* 2023:1–23. <https://doi.org/10.47852/bonviewaees3202915>
222. Fallahi N, Viglietti A, Carrera E, Pagani A, Zappino E (2020) Original scientific paper- effect of fiber orientation path on the buckling, free vibration and static analyses of variable angle tow panels. *FACTA Univ Ser Mech Eng* 18:165–188. <https://doi.org/10.22190/FUME200615026F>
223. Zhan JM, Yao XH, Han F (2020) An approach of peridynamic modeling associated with molecular dynamics for fracture simulation of particle reinforced metal matrix composites. *Compos Struct* 250:112613. <https://doi.org/10.1016/j.compstruct.2020.112613>
224. Takari A, Ghasemi AR, Hamadani M, Sarafrazi M, Najafidoust A (2021) Molecular dynamics simulation and thermo-mechanical characterization for optimization of three-phase epoxy/TiO₂/SiO₂ nano-composites. *Polym Test* 93:106890. <https://doi.org/10.1016/j.polymertesting.2020.106890>
225. Qian WM, Vahid MH, Sun YL, Heidari A, Barbaz-Isfahani R, Saber-Samandari S et al (2021) Investigation on the effect of functionalization of single-walled carbon nanotubes on the mechanical properties of epoxy glass composites: experimental and molecular dynamics simulation. *J Mater Res Technol* 12:1931. <https://doi.org/10.1016/j.jmrt.2021.03.104>
226. Motamedi M, Naghdi AH, Jalali SK (2020) Effect of temperature on properties of aluminum/single-walled carbon nanotube nanocomposite by molecular dynamics simulation. *Proc Inst Mech Eng Part C J Mech Eng Sci* 234:635. <https://doi.org/10.1177/09554406219878760>
227. Min B, Wang P, Li S, Wang Z (2022) Mechanical influence of graphene oxide in the interface between calcium silicate hydrate and quartz: a molecular dynamics study. *Constr Build Mater* 325:126597. <https://doi.org/10.1016/j.conbuildmat.2022.126597>
228. Zhao L, Hou D, Wang P, Guo X, Zhang Y, Liu J et al (2020) Experimental and molecular dynamics studies on the durability of sustainable cement-based composites: reinforced by graphene. *Constr Build Mater* 257:119566. <https://doi.org/10.1016/j.conbuildmat.2020.119566>
229. Li H, Xu F, Li B, Sun T, Huang X, Zhu J et al (2022) Investigation on mechanical properties of excess-sulfate phosphogypsum slag cement: From experiments to molecular dynamics simulation. *Constr Build Mater* 315:125685. <https://doi.org/10.1016/j.conbuildmat.2021.125685>
230. Komarov PV, Khalatur PG, Khokhlov AR (2021) Magnetoresponsive smart nanocomposites with highly cross-linked polymer matrix. *Polym Adv Technol* 32:3922. <https://doi.org/10.1002/pat.5354>
231. Ketkaew R, Tantirungrotechai Y (2018) Dissipative particle dynamics study of SWCNT reinforced natural rubber composite system: an important role of self-avoiding model on mechanical properties. *Macromol Theory Simulations* 27:1700093. <https://doi.org/10.1002/mats.201700093>
232. Rezaiee-Pajand M, Arabi E, Masoodi AR (2019) Nonlinear analysis of FG-sandwich plates and shells. *Aerosp Sci Technol* 87:178–189. <https://doi.org/10.1016/J.AST.2019.02.017>
233. Milić P, Marinković D, Čojbašić Ž (2023) Geometrically nonlinear analysis of piezoelectric active laminated shells by means of isogeometric Fe formulation. *Facta Univ Ser Mech Eng* 2023:1–19. <https://doi.org/10.22190/FUME050123059M>
234. Milić P, Marinković D, Klinge S, Čojbašić Ž (2023) Reissner-mindlin based Isogeometric finite element formulation for piezoelectric active laminated shells. *Teh Vjesn.* <https://doi.org/10.17559/TV-20230128000280>
235. Fernández-Méndez S, Huerta A (2004) Imposing essential boundary conditions in mesh-free methods. *Comput Methods Appl Mech Eng* 193:1257. <https://doi.org/10.1016/j.cma.2003.12.019>
236. Tsiatas GC (2009) A new Kirchhoff plate model based on a modified couple stress theory. *Int J Solids Struct* 46:2757–2764. <https://doi.org/10.1016/J.IJSOLSTR.2009.03.004>
237. Liu GR, Zhao X, Dai KY, Zhong ZH, Li GY, Han X (2008) Static and free vibration analysis of laminated composite plates using the conforming radial point interpolation method. *Compos Sci Technol* 68:354–366. <https://doi.org/10.1016/J.COMPSCITECH.2007.07.014>
238. Fouaidi M, Jamal M, Belouaggadia N (2020) Nonlinear bending analysis of functionally graded porous beams using the multi-quadratic radial basis functions and a Taylor series-based continuation procedure. *Compos Struct* 252:1–12. <https://doi.org/10.1016/J.COMPSTRUCT.2020.112593>
239. Liu GR (2002) Mesh free methods: moving beyond the finite element method. *Appl Mech Rev* 56(2):B17. <https://doi.org/10.1299/jsmecmd.2003.16.937>
240. Lei ZX, Liew KM, Yu JL (2013) Buckling analysis of functionally graded carbon nanotube-reinforced composite plates using the element-free kp-Ritz method. *Compos Struct* 98:160–168. <https://doi.org/10.1016/J.COMPSTRUCT.2012.11.006>
241. Ren J, Liew KM (2002) Mesh-free method revisited: two new approaches for the treatment of essential boundary conditions. *Int J Comput Eng Sci* 03:219. <https://doi.org/10.1142/s1465876302000617>
242. Krysl P, Belytschko T (1996) Analysis of thin shells by the Element-Free Galerkin method. *Int J Solids Struct* 33:3057–3080. [https://doi.org/10.1016/0020-7683\(95\)00265-0](https://doi.org/10.1016/0020-7683(95)00265-0)
243. Chen JS, Wang HP (2000) New boundary condition treatments in meshfree computation of contact problems. *Comput Methods Appl Mech Eng* 187:441–468. [https://doi.org/10.1016/S0045-7825\(00\)80004-3](https://doi.org/10.1016/S0045-7825(00)80004-3)
244. Neves AMA, Ferreira AJM, Carrera E, Cinefra M, Roque CMC, Jorge RMN et al (2013) Static, free vibration and buckling analysis of isotropic and sandwich functionally graded plates using a quasi-3D higher-order shear deformation theory and a meshless

- technique. *Compos Part B Eng* 44:657–674. <https://doi.org/10.1016/J.COMPOSITESB.2012.01.089>
245. Wang JF, Cao SH, Zhang W (2021) Thermal vibration and buckling analysis of functionally graded carbon nanotube reinforced composite quadrilateral plate. *Eur J Mech A/Solids* 85:104105. <https://doi.org/10.1016/J.EUROMECHSOL.2020.104105>
 246. Ouakad HM, Kamil-Zür K (2022) On the snap-through buckling analysis of electrostatic shallow arch micro-actuator via meshless Galerkin decomposition technique. *Eng Anal Bound Elem* 134:388–397. <https://doi.org/10.1016/J.ENGANABOUND.2021.10.007>
 247. Karami G, Malekzadeh P (2003) An efficient differential quadrature methodology for free vibration analysis of arbitrary straight-sided quadrilateral thin plates. *J Sound Vib* 263:415–442. [https://doi.org/10.1016/S0022-460X\(02\)01062-3](https://doi.org/10.1016/S0022-460X(02)01062-3)
 248. Bert CW, Jang SK, Striz AG (1988) Two new approximate methods for analyzing free vibration of structural components. *AIAA J* 26:612. <https://doi.org/10.2514/3.9941>
 249. Jang SK, Bert CW, Striz AG (1989) Application of differential quadrature to static analysis of structural components. *Int J Numer Methods Eng* 28:561. <https://doi.org/10.1002/nme.1620280306>
 250. Wang X, Striz AG, Bert CW (1994) Buckling and vibration analysis of skew plates by the differential quadrature method. *AIAA J* 32:886. <https://doi.org/10.2514/3.12071>
 251. Noroozi AR, Malekzadeh P, Dimitri R, Tornabene F (2020) Meshfree radial point interpolation method for the vibration and buckling analysis of FG-GPLRC perforated plates under an in-plane loading. *Eng Struct* 221:1–20. <https://doi.org/10.1016/j.engstruct.2020.111000>
 252. Liew KM, Wang J, Tan MJ, Rajendran S (2006) Postbuckling analysis of laminated composite plates using the mesh-free kp-Ritz method. *Comput Methods Appl Mech Eng* 195:551–570. <https://doi.org/10.1016/j.cma.2005.02.004>
 253. Yang Z, Safaei B, Sahmani S, Zhang Y (2022) A couple-stress-based moving Kriging meshfree shell model for axial postbuckling analysis of random checkerboard composite cylindrical microshells. *Thin-Walled Struct* 170:1–16. <https://doi.org/10.1016/J.TWS.2021.108631>
 254. Artan R, Batra RC (2012) Free vibrations of a strain gradient beam by the method of initial values. *Acta Mech* 223:2393. <https://doi.org/10.1007/s00707-012-0709-x>
 255. Zhao J, Choe K, Xie F, Wang A, Shuai C, Wang Q (2018) Three-dimensional exact solution for vibration analysis of thick functionally graded porous (FGP) rectangular plates with arbitrary boundary conditions. *Compos Part B Eng* 155:369. <https://doi.org/10.1016/j.compositesb.2018.09.001>
 256. Zhao X, Lee YY, Liew KM (2009) Mechanical and thermal buckling analysis of functionally graded plates. *Compos Struct* 90:161–171. <https://doi.org/10.1016/J.COMPSTRUCT.2009.03.005>
 257. Chen XL, Liew KM (2004) Buckling of rectangular functionally graded material plates subjected to nonlinearly distributed in-plane edge loads. *Smart Mater Struct* 13:1430. <https://doi.org/10.1088/0964-1726/13/6/014>
 258. Ahmadi I (2022) Free vibration of multiple-nanobeam system with nonlocal Timoshenko beam theory for various boundary conditions. *Eng Anal Bound Elem* 143:719. <https://doi.org/10.1016/j.enganabound.2022.07.011>
 259. Pradhan SC, Loy CT, Lam KY, Reddy JN (2000) Vibration characteristics of functionally graded cylindrical shells under various boundary conditions. *Appl Acoust* 61:111. [https://doi.org/10.1016/S0003-682X\(99\)00063-8](https://doi.org/10.1016/S0003-682X(99)00063-8)
 260. Ansari R, Darvizeh M (2008) Prediction of dynamic behaviour of FGM shells under arbitrary boundary conditions. *Compos Struct* 85:284. <https://doi.org/10.1016/j.compstruct.2007.10.037>
 261. Barati MR, Zenkour AM (2018) Electro-thermoelastic vibration of plates made of porous functionally graded piezoelectric materials under various boundary conditions. *J Vib Control* 24:1910. <https://doi.org/10.1177/1077546316672788>
 262. Zhao X, Liew KM, Ng TY (2003) Vibration analysis of laminated composite cylindrical panels via a meshfree approach. *Int J Solids Struct* 40:161–180. [https://doi.org/10.1016/S0020-7683\(02\)00475-4](https://doi.org/10.1016/S0020-7683(02)00475-4)
 263. Natsuki T, Natsuki J (2019) Measurement of the elastic modulus of nanowires based on resonant frequency and boundary condition effects. *Phys E Low-Dimens Syst Nanostruct* 105:207. <https://doi.org/10.1016/j.physe.2018.09.003>
 264. Wang P, Wu N, Luo H, Sun Z (2021) Study on vibration response of a non-uniform beam with nonlinear boundary condition. *Facta Univ Ser Mech Eng* 19:781. <https://doi.org/10.22190/FUME210324045W>
 265. Moradi-Dastjerdi R, Behdinin K, Safaei B, Qin Z (2020) Static performance of agglomerated CNT-reinforced porous plates bonded with piezoceramic faces. *Int J Mech Sci* 188:105966. <https://doi.org/10.1016/J.IJMECS.2020.105966>
 266. Safaei B, Moradi-Dastjerdi R, Behdinin K, Qin Z, Chu F (2019) Thermoelastic behavior of sandwich plates with porous polymeric core and CNT clusters/polymer nanocomposite layers. *Compos Struct* 226:111209. <https://doi.org/10.1016/J.COMPSSTRUCT.2019.111209>
 267. Moradi-Dastjerdi R, Aghadavoudi F (2018) Static analysis of functionally graded nanocomposite sandwich plates reinforced by defected CNT. *Compos Struct* 200:839–848. <https://doi.org/10.1016/J.COMPSTRUCT.2018.05.122>
 268. Thai CH, Ferreira AJM, Nguyen-Xuan H, Phung-Van P (2021) A size dependent meshfree model for functionally graded plates based on the nonlocal strain gradient theory. *Compos Struct* 272:1–12. <https://doi.org/10.1016/J.COMPSTRUCT.2021.114169>
 269. Chinh TH, Tu TM, Duc DM, Hung TQ (2021) Static flexural analysis of sandwich beam with functionally graded face sheets and porous core via point interpolation meshfree method based on polynomial basic function. *Arch Appl Mech* 91:933–947. <https://doi.org/10.1007/S00419-020-01797-X/FIGURES/13>
 270. Thai CH, Tran TD, Phung-Van P (2020) A size-dependent moving Kriging meshfree model for deformation and free vibration analysis of functionally graded carbon nanotube-reinforced composite nanoplates. *Eng Anal Bound Elem* 115:52–63. <https://doi.org/10.1016/J.ENGANABOUND.2020.02.008>
 271. Sayyidmousavi A, Daneshmand F, Foroutan M, Fawaz Z (2018) A new meshfree method for modeling strain gradient microbeams. *J Braz Soc Mech Sci Eng* 40:1–9. <https://doi.org/10.1007/S40430-018-1305-3/FIGURES/7>
 272. Lei ZX, Liew KM, Yu JL (2013) Large deflection analysis of functionally graded carbon nanotube-reinforced composite plates by the element-free kp-Ritz method. *Comput Methods Appl Mech Eng* 256:189–199. <https://doi.org/10.1016/j.cma.2012.12.007>
 273. Liu GR, Dai KY, Nguyen TT (2007) A smoothed finite element method for mechanics problems. *Comput Mech* 39:859–877. <https://doi.org/10.1007/S00466-006-0075-4/METRICS>
 274. Roque CMC, Ferreira AJM, Reddy JN (2011) Analysis of Timoshenko nanobeams with a nonlocal formulation and meshless method. *Int J Eng Sci* 49:976–984. <https://doi.org/10.1016/J.IJENGSCI.2011.05.010>
 275. Moradi-Dastjerdi R, Payganeh G (2017) Thermoelastic dynamic analysis of wavy carbon nanotube reinforced cylinders under thermal loads. *Steel Compos Struct* 25:315–326. <https://doi.org/10.12989/scs.2017.25.3.315>

276. Moradi-Dastjerdi R, Foroutan M, Pourasghar A, Sotoudeh-Bahreini R (2013) Static analysis of functionally graded carbon nanotube-reinforced composite cylinders by a mesh-free method. *J Reinf Plast Compos* 32:593–601. <https://doi.org/10.1177/0731684413476353>
277. Roque CMC, Fidalgo DS, Ferreira AJM, Reddy JN (2013) A study of a microstructure-dependent composite laminated Timoshenko beam using a modified couple stress theory and a meshless method. *Compos Struct* 96:532–537. <https://doi.org/10.1016/J.COMPSTRUCT.2012.09.011>
278. Moradi-Dastjerdi R, Rashahmadi S, Meguid SA (2020) Electro-mechanical performance of smart piezoelectric nanocomposite plates reinforced by zinc oxide and gallium nitride nanowires. *Mech Based Des Struct Mach* 50:1954–1967. <https://doi.org/10.1080/15397734.2020.1766496>
279. Zhang LW, Lei ZX, Liew KM, Yu JL (2014) Large deflection geometrically nonlinear analysis of carbon nanotube-reinforced functionally graded cylindrical panels. *Comput Methods Appl Mech Eng* 273:1–18. <https://doi.org/10.1016/J.CMA.2014.01.024>
280. Thai CH, Ferreira AJM, Lee J, Nguyen-Xuan H (2018) An efficient size-dependent computational approach for functionally graded isotropic and sandwich microplates based on modified couple stress theory and moving Kriging-based meshfree method. *Int J Mech Sci* 142–143:322–338. <https://doi.org/10.1016/J.IJMECSCI.2018.04.040>
281. Roque CMC, Ferreira AJM, Reddy JN (2013) Analysis of Mindlin micro plates with a modified couple stress theory and a meshless method. *Appl Math Model* 37:4626. <https://doi.org/10.1016/j.apm.2012.09.063>
282. Sahmani S, Safaei B (2020) Influence of homogenization models on size-dependent nonlinear bending and postbuckling of bidirectional functionally graded micro/nano-beams. *Appl Math Model* 82:336–358. <https://doi.org/10.1016/J.APM.2020.01.051>
283. Sansour C, Skatulla S (2009) A strain gradient generalized continuum approach for modelling elastic scale effects. *Comput Methods Appl Mech Eng* 198:1401–1412. <https://doi.org/10.1016/J.CMA.2008.12.031>
284. Giunta G, Belouettar S, Ferreira AJM (2016) A static analysis of three-dimensional functionally graded beams by hierarchical modelling and a collocation meshless solution method. *Acta Mech* 227:969–991. <https://doi.org/10.1007/s00707-015-1503-3>
285. Li S, Hao W, Liu WK (2000) Mesh-free simulations of shear banding in large deformation. *Int J Solids Struct* 37:7185–7206. [https://doi.org/10.1016/S0020-7683\(00\)00195-5](https://doi.org/10.1016/S0020-7683(00)00195-5)
286. Li J, Guan Y, Wang G, Wang G, Zhang H, Lin J (2020) A meshless method for topology optimization of structures under multiple load cases. *Structures* 25:173–179. <https://doi.org/10.1016/J.ISTRUC.2020.03.005>
287. Krysl P, Belytschko T (1995) Analysis of thin plates by the element-free Galerkin method. *Comput Mech* 17:26–35. <https://doi.org/10.1007/BF00356476>
288. Long S (2001) A meshless local petrov-galerkin method for solving the bending problem of a thin plate. *Comput Model Eng Sci* 3:53
289. Liu GR, Chen XL (2001) A mesh-free method for static and free vibration analyses of thin plates of complicated shape. *J Sound Vib* 241:839–855. <https://doi.org/10.1006/JSVI.2000.3330>
290. Dai KY, Liu GR, Lim KM, Chen XL (2004) A mesh-free method for static and free vibration analysis of shear deformable laminated composite plates. *J Sound Vib* 269:633–652. [https://doi.org/10.1016/S0022-460X\(03\)00089-0](https://doi.org/10.1016/S0022-460X(03)00089-0)
291. Peng LX, Liew KM, Kitipornchai S (2011) Bending analysis of folded laminated plates by the FSDT meshfree method. *Procedia Eng* 14:2714–2721. <https://doi.org/10.1016/j.proeng.2011.07.341>
292. Liew KM, Ren J, Kitipornchai S (2004) Analysis of the pseudoelastic behavior of a SMA beam by the element-free Galerkin method. *Eng Anal Bound Elem* 28:497–507. [https://doi.org/10.1016/S0955-7997\(03\)00103-6](https://doi.org/10.1016/S0955-7997(03)00103-6)
293. Moradi-Dastjerdi R, Meguid SA, Rashahmadi S (2019) Electro-dynamic analysis of smart nanoclay-reinforced plates with integrated piezoelectric layers. *Appl Math Model* 75:267–278. <https://doi.org/10.1016/J.APM.2019.05.033>
294. Askes H, Alfantis EC (2002) Numerical modeling of size effects with gradient elasticity: formulation, meshless discretization and examples. *Int J Fract* 117:347–358. <https://doi.org/10.1023/A:1022225526483>
295. Ferreira AJM, Roque CMC, Carrera E, Cinefra M, Polit O (2011) Two higher order Zig-Zag theories for the accurate analysis of bending, vibration and buckling response of laminated plates by radial basis functions collocation and a unified formulation. *J Compos Mater* 45:2523–2536. https://doi.org/10.1177/0021998311401103/ASSET/IMAGES/LARGE/10.1177_0021998311401103-EQ19.JPG
296. Ferreira AJM, Carrera E, Cinefra M, Roque CMC, Polit O (2011) Analysis of laminated shells by a sinusoidal shear deformation theory and radial basis functions collocation, accounting for through-the-thickness deformations. *Compos Part B Eng* 42:1276–1284. <https://doi.org/10.1016/J.COMPOSITESB.2011.01.031>
297. Ferreira AJM, Roque CMC, Jorge RMN (2005) Analysis of composite plates by trigonometric shear deformation theory and multiquadrics. *Comput Struct* 83:2225–2237. <https://doi.org/10.1016/J.COMPSTRUC.2005.04.002>
298. Neves AMA, Ferreira AJM, Carrera E, Roque CMC, Cinefra M, Jorge RMN et al (2012) A quasi-3D sinusoidal shear deformation theory for the static and free vibration analysis of functionally graded plates. *Compos Part B Eng* 43:711–725. <https://doi.org/10.1016/j.compositesb.2011.08.009>
299. Ferreira AJM, Roque CMC, Martins PALS (2004) Radial basis functions and higher-order shear deformation theories in the analysis of laminated composite beams and plates. *Compos Struct* 66:287–293. <https://doi.org/10.1016/J.COMPSTRUCT.2004.04.050>
300. Neves AMA, Ferreira AJM, Carrera E, Roque CMC, Cinefra M, Jorge RMN et al (2011) Bending of FGM plates by a sinusoidal plate formulation and collocation with radial basis functions. *Mech Res Commun* 38:368–371. <https://doi.org/10.1016/J.MECHRESCOM.2011.04.011>
301. Ferreira AJM, Roque CMC, Jorge RMN, Kansa EJ (2005) Static deformations and vibration analysis of composite and sandwich plates using a layerwise theory and multiquadrics discretizations. *Eng Anal Bound Elem* 29:1104–1114. <https://doi.org/10.1016/J.ENGANABOUND.2005.07.004>
302. Ferreira AJM, Carrera E, Cinefra M, Roque CMC (2011) Analysis of laminated doubly-curved shells by a layerwise theory and radial basis functions collocation, accounting for through-the-thickness deformations. *Comput Mech* 48:13–25. <https://doi.org/10.1007/S00466-011-0579-4/METRICS>
303. Ferreira AJM, Roque CMC, Jorge RMN, Fasshauer GE, Batra RC (2007) Analysis of functionally graded plates by a robust meshless method. *Mech Adv Mater Struct* 14:577–587. <https://doi.org/10.1080/15376490701672732>
304. Zhao X, Liew KM (2009) Geometrically nonlinear analysis of functionally graded shells. *Int J Mech Sci* 51:131–144. <https://doi.org/10.1016/J.IJMECSCI.2008.12.004>
305. Van VuT, Nguyen NH, Khosravifard A, Hematiyan MR, Tanaka S, Bui TQ (2017) A simple FSDT-based meshfree method for analysis of functionally graded plates. *Eng Anal Bound Elem*

- 79:1–12. <https://doi.org/10.1016/J.ENGANABOUND.2017.03.002>
306. Karamanlı A (2017) Bending behaviour of two directional functionally graded sandwich beams by using a quasi-3d shear deformation theory. *Compos Struct* 174:70–86. <https://doi.org/10.1016/J.COMPSTRUCT.2017.04.046>
307. Qin X, Shen Y, Chen W, Yang J, Peng LX (2021) Bending and free vibration analyses of circular stiffened plates using the FSDT mesh-free method. *Int J Mech Sci* 202–203:1–13. <https://doi.org/10.1016/J.IJMECSCI.2021.106498>
308. Moradi-Dastjerdi R, Behdinin K (2020) Stability analysis of multifunctional smart sandwich plates with graphene nanocomposite and porous layers. *Int J Mech Sci* 167:105283. <https://doi.org/10.1016/J.IJMECSCI.2019.105283>
309. Yan JW, Liew KM, He LH (2012) A mesh-free computational framework for predicting buckling behaviors of single-walled carbon nanocones under axial compression based on the moving Kriging interpolation. *Comput Methods Appl Mech Eng* 247–248:103–112. <https://doi.org/10.1016/J.CMA.2012.08.010>
310. Gu YT, Liu GR (2001) A local point interpolation method for static and dynamic analysis of thin beams. *Comput Methods Appl Mech Eng* 190:5515–5528. [https://doi.org/10.1016/S0045-7825\(01\)00180-3](https://doi.org/10.1016/S0045-7825(01)00180-3)
311. Moradi-Dastjerdi R, Behdinin K, Safaei B, Qin Z (2020) Buckling behavior of porous CNT-reinforced plates integrated between active piezoelectric layers. *Eng Struct* 222:111141. <https://doi.org/10.1016/J.ENGSTRUCT.2020.111141>
312. Sun Y, Liew KM (2008) The buckling of single-walled carbon nanotubes upon bending: the higher order gradient continuum and mesh-free method. *Comput Methods Appl Mech Eng* 197:3001–3013. <https://doi.org/10.1016/J.CMA.2008.02.003>
313. Liew K, Peng L, Kitipornchai S (2006) Buckling analysis of corrugated plates using a mesh-free Galerkin method based on the first-order shear deformation theory. *Comput Mech* 38:61–75. <https://doi.org/10.1007/s00466-005-0721-2>
314. Safaei B, Moradi-Dastjerdi R, Behdinin K, Chu F (2019) Critical buckling temperature and force in porous sandwich plates with CNT-reinforced nanocomposite layers. *Aerosp Sci Technol* 91:175–185. <https://doi.org/10.1016/J.AST.2019.05.020>
315. Rafiee M, He XQ, Liew KM (2014) Non-linear dynamic stability of piezoelectric functionally graded carbon nanotube-reinforced composite plates with initial geometric imperfection. *Int J Non Linear Mech* 59:37–51. <https://doi.org/10.1016/J.IJNONLIN-MEC.2013.10.011>
316. Kiani K (2015) Column buckling of magnetically affected stocky nanowires carrying electric current. *J Phys Chem Solids* 83:140–151. <https://doi.org/10.1016/J.JPCS.2015.03.020>
317. Kiani K (2016) Column buckling of doubly parallel slender nanowires carrying electric current acted upon by a magnetic field. *J Phys Chem Solids* 95:89–97. <https://doi.org/10.1016/J.JPCS.2016.03.013>
318. Shahmohammadi MA, Abdollahi P, Salehipour H (2020) Geometrically nonlinear analysis of doubly curved imperfect shallow shells made of functionally graded carbon nanotube reinforced composite (FG_CNTRC). *Mech Based Des Struct Mach* 50:3796–3820. <https://doi.org/10.1080/15397734.2020.1822182>
319. Ipek C, Sofiyev AH, Fantuzzi N, Efendiyeva SP (2023) Buckling behavior of nanocomposite plates with functionally graded properties under compressive loads in elastic and thermal environments buckling behavior of nanocomposite plates with functionally graded properties under compressive loads in elastic and. *J Appl Comput Mech* 9:974–986. <https://doi.org/10.22055/JACM.2023.43091.4019>
320. Zhao J, Wang J, Sahmani S, Safaei B (2022) Probabilistic-based nonlinear stability analysis of randomly reinforced microshells under combined axial-lateral load using meshfree strain gradient formulations. *Eng Struct* 262:1–25. <https://doi.org/10.1016/J.ENGSTRUCT.2022.114344>
321. Alshenawy R, Sahmani S, Safaei B, Elmoghazy Y, Al-Alwan A, Nuwairan MA (2023) Three-dimensional nonlinear stability analysis of axial-thermal-electrical loaded FG piezoelectric microshells via MKM strain gradient formulations. *Appl Math Comput* 439:1–23. <https://doi.org/10.1016/J.AMC.2022.127623>
322. Yuan Y, Zhao K, Zhao Y, Sahmani S, Safaei B (2020) Couple stress-based nonlinear buckling analysis of hydrostatic pressurized functionally graded composite conical microshells. *Mech Mater* 148:103507. <https://doi.org/10.1016/J.MECHMAT.2020.103507>
323. Sun JH, Zhou ZD, Sahmani S, Safaei B (2021) Microstructural size dependency in nonlinear lateral stability of random reinforced microshells via meshfree-based applied mathematical modeling. *Int J Struct Stab Dyn*. <https://doi.org/10.1142/S0219455421501649>
324. Alshenawy R, Safaei B, Sahmani S, Elmoghazy Y, Al-Alwan A, Nuwairan MA (2022) Buckling mode transition in nonlinear strain gradient-based stability behavior of axial-thermal-electrical loaded FG piezoelectric cylindrical panels at microscale. *Eng Anal Bound Elem* 141:36–64. <https://doi.org/10.1016/J.ENGANABOUND.2022.04.010>
325. Liu H, Safaei B, Sahmani S (2022) Combined axial and lateral stability behavior of random checkerboard reinforced cylindrical microshells via a couple stress-based moving Kriging meshfree model. *Arch Civ Mech Eng* 22:1–20. <https://doi.org/10.1007/S43452-021-00338-9/FIGURES/16>
326. Liew KM, Lei ZX, Yu JL, Zhang LW (2014) Postbuckling of carbon nanotube-reinforced functionally graded cylindrical panels under axial compression using a meshless approach. *Comput Methods Appl Mech Eng* 268:1–17. <https://doi.org/10.1016/J.CMA.2013.09.001>
327. Wang BB, Lu C, Fan CY, Zhao MH (2021) A meshfree method with gradient smoothing for free vibration and buckling analysis of a strain gradient thin plate. *Eng Anal Bound Elem* 132:159–167. <https://doi.org/10.1016/J.ENGANABOUND.2021.07.014>
328. Liew KM, Chen XL, Reddy JN (2004) Mesh-free radial basis function method for buckling analysis of non-uniformly loaded arbitrarily shaped shear deformable plates. *Comput Methods Appl Mech Eng* 193:205–224. <https://doi.org/10.1016/J.CMA.2003.10.002>
329. Liu L, Chua LP, Ghista DN (2007) Mesh-free radial basis function method for static, free vibration and buckling analysis of shear deformable composite laminates. *Compos Struct* 78:58–69. <https://doi.org/10.1016/J.COMPSTRUCT.2005.08.010>
330. Ferreira AJM, Roque CMC, Neves AMA, Jorge RMN, Soares CMM, Reddy JN (2011) Buckling analysis of isotropic and laminated plates by radial basis functions according to a higher-order shear deformation theory. *Thin-Walled Struct* 49:804–811. <https://doi.org/10.1016/J.TWS.2011.02.005>
331. Kumar R, Lal A, Singh BN, Singh J (2019) Meshfree approach on buckling and free vibration analysis of porous FGM plate with proposed IHSDT resting on the foundation. *Curved Layer Struct* 6:192–211. <https://doi.org/10.1515/cls-2019-0017>
332. Hillman M, Chen JS (2016) An accelerated, convergent, and stable nodal integration in Galerkin meshfree methods for linear and nonlinear mechanics. *Int J Numer Methods Eng* 107:603–630. <https://doi.org/10.1002/NME.5183>
333. Peng LX, Liew KM, Kitipornchai S (2006) Buckling and free vibration analyses of stiffened plates using the FSDT mesh-free method. *J Sound Vib* 289:421–449. <https://doi.org/10.1016/J.JSV.2005.02.023>
334. Liew KM, Wang J, Ng TY, Tan MJ (2004) Free vibration and buckling analyses of shear-deformable plates based on FSDT

- meshfree method. *J Sound Vib* 276:997–1017. <https://doi.org/10.1016/J.JSV.2003.08.026>
335. Zhao X, Liew KM (2009) Geometrically nonlinear analysis of functionally graded plates using the element-free kp-Ritz method. *Comput Methods Appl Mech Eng* 198:2796–2811. <https://doi.org/10.1016/J.CMA.2009.04.005>
 336. Bi J, Zhou XP, Qian QH (2016) The 3D numerical simulation for the propagation process of multiple pre-existing flaws in rock-like materials subjected to biaxial compressive loads. *Rock Mech Rock Eng* 49:1611–1627. <https://doi.org/10.1007/S00603-015-0867-Y>
 337. Wu Y, Wang D, Wu CT (2014) Three dimensional fragmentation simulation of concrete structures with a nodally regularized meshfree method. *Theor Appl Fract Mech* 72:89–99. <https://doi.org/10.1016/J.TAFMEC.2014.04.006>
 338. Lei ZX, Liew KM, Yu JL (2013) Free vibration analysis of functionally graded carbon nanotube-reinforced composite plates using the element-free kp-Ritz method in thermal environment. *Compos Struct* 106:128–138. <https://doi.org/10.1016/J.COMPSTRUCT.2013.06.003>
 339. Moradi-Dastjerdi R, Momeni-Khabisi H, Moradi-Dastjerdi R, Momeni-Khabisi H (2016) Dynamic analysis of functionally graded nanocomposite plates reinforced by wavy carbon nanotube. *Steel Compos Struct* 22:277. <https://doi.org/10.12989/SCS.2016.22.2.277>
 340. Moradi-Dastjerdi R, Payganeh G, Tajdari M (2017) Resonance in functionally graded nanocomposite cylinders reinforced by wavy carbon nanotube. *Polym Compos*. <https://doi.org/10.1002/PC.24045>
 341. Ansari R, Faraji Oskouie M, Gholami R (2016) Size-dependent geometrically nonlinear free vibration analysis of fractional viscoelastic nanobeams based on the nonlocal elasticity theory. *Phys E Low-Dimens Syst Nanostruct* 75:266–271. <https://doi.org/10.1016/J.PHYSE.2015.09.022>
 342. Zhang Y, Lei ZX, Zhang LW, Liew KM, Yu JL (2015) Nonlocal continuum model for vibration of single-layered graphene sheets based on the element-free kp-Ritz method. *Eng Anal Bound Elem* 56:90–97. <https://doi.org/10.1016/J.ENGANABOUND.2015.01.020>
 343. Ghayoumizadeh H, Shahabian F, Hosseini SM (2013) Elastic wave propagation in a functionally graded nanocomposite reinforced by carbon nanotubes employing meshless local integral equations (LIEs). *Eng Anal Bound Elem* 37:1524–1531. <https://doi.org/10.1016/J.ENGANABOUND.2013.08.011>
 344. Ejabati SM, Fallah N (2021) Air drag effect on dynamic analysis of movingnanoparticle problems using meshfree finite volume method. *Eng Anal Bound Elem* 128:19–34. <https://doi.org/10.1016/j.enganabound.2021.03.011>
 345. Moradi-Dastjerdi R, Momeni-Khabisi H (2018) Vibrational behavior of sandwich plates with functionally graded wavy carbon nanotube-reinforced face sheets resting on Pasternak elastic foundation. *J Vib Control* 24:2327–2343. https://doi.org/10.1177/1077546316686227/ASSET/IMAGES/LARGE/10.1177_1077546316686227-FIG2.JPEG
 346. Moradi-Dastjerdi R, Behdinin K (2021) Temperature effect on free vibration response of a smart multifunctional sandwich plate. *J Sandw Struct Mater* 23:2399–2421. <https://doi.org/10.1177/1099636220908707>
 347. Kiani K (2016) Nonlocal-integro-differential modeling of vibration of elastically supported nanorods. *Phys E Low-Dimens Syst Nanostruct* 83:151–163. <https://doi.org/10.1016/J.PHYSE.2016.04.018>
 348. Ansari R, Torabi J, Hosein SA (2017) Vibration analysis of functionally graded carbon nanotube-reinforced composite elliptical plates using a numerical strategy. *Aerosp Sci Technol* 60:152–161. <https://doi.org/10.1016/j.ast.2016.11.004>
 349. Jankowski P, Žur KK, Farajpour A (2022) Analytical and meshless DQM approaches to free vibration analysis of symmetric FGM porous nanobeams with piezoelectric effect. *Eng Anal Bound Elem* 136:266–289. <https://doi.org/10.1016/J.ENGANABOUND.2022.01.007>
 350. Mohammadimehr M, Roustana Navi B, Ghorbanpour AA (2015) Free vibration of viscoelastic double-bonded polymeric nanocomposite plates reinforced by FG-SWCNTs using MSGT, sinusoidal shear deformation theory and meshless method. *Compos Struct* 131:654–671. <https://doi.org/10.1016/J.COMPSTRUCT.2015.05.077>
 351. Kiani K (2015) Nanomechanical sensors based on elastically supported double-walled carbon nanotubes. *Appl Math Comput* 270:216–241. <https://doi.org/10.1016/J.AMC.2015.07.114>
 352. Kiani K (2014) A nonlocal meshless solution for flexural vibrations of double-walled carbon nanotubes. *Appl Math Comput* 234:557–578. <https://doi.org/10.1016/J.AMC.2014.01.015>
 353. Alshenawy R, Sahmani S, Safaei B, Elmoghazy Y, Al-Alwan A, Nuwairan MA (2023) Surface stress effect on nonlinear dynamical performance of nanobeam-type piezoelectric energy harvesters via meshless collocation technique. *Eng Anal Bound Elem* 152:104–119. <https://doi.org/10.1016/J.ENGANABOUND.2023.04.003>
 354. Sobhani E, Arbabian A, Civalek Ö, Avcar M (2022) The free vibration analysis of hybrid porous nanocomposite joined hemispherical–cylindrical–conical shells. *Eng Comput* 38:3125. <https://doi.org/10.1007/s00366-021-01453-0>
 355. Sobhani E, Masoodi AR, Ahmadi-Pari AR (2022) Free-damped vibration analysis of graphene nano-platelet nanocomposite joined conical-conical-cylindrical Shell marine-like structures. *Ocean Eng* 261:112163. <https://doi.org/10.1016/J.OCEANENG.2022.112163>
 356. Sobhani E, Masoodi AR, Ahmadi-Pari AR (2021) Vibration of FG-CNT and FG-GNP sandwich composite coupled Conical-Cylindrical-Conical shell. *Compos Struct* 273:114281. <https://doi.org/10.1016/J.COMPSTRUCT.2021.114281>
 357. Sobhani E (2023) Vibrational characteristic simulations regarding connecting two different semi-spheroidal shells and a full-spheroidal shell with a conical shell categorized in underwater structures. *Ocean Eng* 276:114252. <https://doi.org/10.1016/j.oceaneng.2023.114252>
 358. Sobhani E, Safaei B (2023) Dynamic analysis of functionally graded embedded graphene oxide powder nanocomposite conical shells resting on flexible foundations. *Eng Anal Bound Elem* 152:757–773. <https://doi.org/10.1016/J.ENGANABOUND.2023.05.006>
 359. Sobhani E, Safaei B (2023) Vibrational characteristics of attached hemispherical-cylindrical ocean shell-structure reinforced by CNT nanocomposite with graded pores on two-parameter elastic foundations applicable in offshore components. *Ocean Eng* 285:115413. <https://doi.org/10.1016/J.OCEANENG.2023.115413>
 360. Moradi-Dastjerdi R, Pourasghar A, Foroutan M, Bidram M (2014) Vibration analysis of functionally graded nanocomposite cylinders reinforced by wavy carbon nanotube based on mesh-free method. *J Compos Mater* 48:1901–1913. https://doi.org/10.1177/0021998313491617/ASSET/IMAGES/LARGE/10.1177_0021998313491617-FIG2.JPEG
 361. Xiang S, Kang GW, Yang MS, Zhao Y (2013) Natural frequencies of sandwich plate with functionally graded face and homogeneous core. *Compos Struct* 96:226–231. <https://doi.org/10.1016/j.compstruct.2012.09.003>
 362. Moradi-Dastjerdi R, Behdinin K (2021) Free vibration response of smart sandwich plates with porous CNT-reinforced and piezoelectric layers. *Appl Math Model* 96:66–79. <https://doi.org/10.1016/J.APM.2021.03.013>

363. Zhang LW, Zhang Y, Liew KM (2017) Modeling of nonlinear vibration of graphene sheets using a meshfree method based on nonlocal elasticity theory. *Appl Math Model* 49:691–704. <https://doi.org/10.1016/J.APM.2017.02.053>
364. Bui TQ, Ngoc Nguyen M, Zhang C (2011) A moving Kriging interpolation-based element-free Galerkin method for structural dynamic analysis. *Comput Methods Appl Mech Eng* 200:1354–1366. <https://doi.org/10.1016/J.CMA.2010.12.017>
365. Zhao X, Liew KM (2011) Free vibration analysis of functionally graded conical shell panels by a meshless method. *Compos Struct* 93:649–664. <https://doi.org/10.1016/J.COMPSTRUCT.2010.08.014>
366. Yan JW, Liew KM, He LH (2013) Free vibration analysis of single-walled carbon nanotubes using a higher-order gradient theory. *J Sound Vib* 332:3740–3755. <https://doi.org/10.1016/J.JSV.2013.02.004>
367. Yan JW, Liew KM, He LH (2013) Ultra-sensitive analysis of a cantilevered single-walled carbon nanocone-based mass detector. *Nanotechnology* 24:1–13. <https://doi.org/10.1088/0957-4484/24/12/125703>
368. Lei ZX, Zhang LW, Liew KM (2016) Parametric analysis of frequency of rotating laminated CNT reinforced functionally graded cylindrical panels. *Compos Part B Eng* 90:251–266. <https://doi.org/10.1016/J.COMPOSITESB.2015.12.024>
369. Wang L, He X, Sun Y, Liew KM (2017) A mesh-free vibration analysis of strain gradient nano-beams. *Eng Anal Bound Elem* 84:231–236. <https://doi.org/10.1016/J.ENGANABOUND.2017.09.001>
370. Ahmadi I (2021) Vibration analysis of 2D-functionally graded nanobeams using the nonlocal theory and meshless method. *Eng Anal Bound Elem* 124:142–154. <https://doi.org/10.1016/J.ENGANABOUND.2020.12.010>
371. Xiang P, Liew KM (2012) Free vibration analysis of microtubules based on an atomistic-continuum model. *J Sound Vib* 331:213–230. <https://doi.org/10.1016/J.JSV.2011.08.024>
372. Sahmani S, Safaei B (2019) Nonlinear free vibrations of bi-directional functionally graded micro/nano-beams including nonlocal stress and microstructural strain gradient size effects. *Thin-Walled Struct* 140:342–356. <https://doi.org/10.1016/J.TWS.2019.03.045>
373. Yuan Y, Zhao K, Han Y, Sahmani S, Safaei B (2020) Nonlinear oscillations of composite conical microshells with in-plane heterogeneity based upon a couple stress-based shell model. *Thin-Walled Struct* 154:1–17. <https://doi.org/10.1016/j.tws.2020.106857>
374. Zhang QJ, Sainsbury MG (2000) The Galerkin element method applied to the vibration of rectangular damped sandwich plates. *Comput Struct* 74:717–730. [https://doi.org/10.1016/S0045-7949\(99\)00068-1](https://doi.org/10.1016/S0045-7949(99)00068-1)
375. Zhao X, Li Q, Liew KM, Ng TY (2006) The element-free kp-Ritz method for free vibration analysis of conical shell panels. *J Sound Vib* 295:906–922. <https://doi.org/10.1016/j.jsv.2006.01.045>
376. Liew KM, Ng TY, Zhao X, Reddy JN (2002) Harmonic reproducing kernel particle method for free vibration analysis of rotating cylindrical shells. *Comput Methods Appl Mech Eng* 191:4141–4157. [https://doi.org/10.1016/S0045-7825\(02\)00358-4](https://doi.org/10.1016/S0045-7825(02)00358-4)
377. Shivanian E, Ghadiri M, Shafiei N (2017) Influence of size effect on flapwise vibration behavior of rotary microbeam and its analysis through spectral meshless radial point interpolation. *Appl Phys A Mater Sci Process* 123:1–16. <https://doi.org/10.1007/S00339-017-0955-9>
378. Xiang P, Liew KM (2012) Dynamic behaviors of long and curved microtubules based on an atomistic-continuum model. *Comput Methods Appl Mech Eng* 223–224:123–132. <https://doi.org/10.1016/J.CMA.2012.02.023>
379. Zheng J, Long S, Li G (2012) Topology optimization of free vibrating continuum structures based on the element free Galerkin method. *Struct Multidiscip Optim* 45:119–127. <https://doi.org/10.1007/S00158-011-0667-2/TABLES/1>
380. Gong S, Chen M, Zhang J, He R (2012) Study on modal topology optimization method of continuum structure based on EFG method. *Int J Comput Methods* 9:1240005. <https://doi.org/10.1142/S0219876212400051>
381. Wu CP, Chiu KH (2011) RMVT-based meshless collocation and element-free Galerkin methods for the quasi-3D free vibration analysis of multilayered composite and FGM plates. *Compos Struct* 93:1433–1448. <https://doi.org/10.1016/J.COMPSTRUCT.2010.11.015>
382. Ferreira AJM, Roque CMC, Jorge RMN (2005) Free vibration analysis of symmetric laminated composite plates by FSDT and radial basis functions. *Comput Methods Appl Mech Eng* 194:4265–4278. <https://doi.org/10.1016/J.CMA.2004.11.004>
383. Xiang S, Kang GW (2012) Local thin plate spline collocation for free vibration analysis of laminated composite plates. *Eur J Mech A/Solids* 33:24–30. <https://doi.org/10.1016/J.EUROMECHSOL.2011.11.004>
384. Xiang S, Kang GW, Xing B (2012) A nth-order shear deformation theory for the free vibration analysis on the isotropic plates. *Meccanica* 47:1913–1921. <https://doi.org/10.1007/S11012-012-9563-0/TABLES/6>
385. Gorman DJ (2000) Free vibration analysis of completely free rectangular plates by the superposition–Galerkin method. *J Sound Vib* 237:901–914. <https://doi.org/10.1006/JSVI.2000.3151>
386. Chen XL, Liu GR, Lim SP (2003) An element free Galerkin method for the free vibration analysis of composite laminates of complicated shape. *Compos Struct* 59:279–289. [https://doi.org/10.1016/S0263-8223\(02\)00034-X](https://doi.org/10.1016/S0263-8223(02)00034-X)
387. Jayakumar K, Yadav D, Nageswara RB (2009) Nonlinear free vibration analysis of simply supported piezo-laminated plates with random actuation electric potential difference and material properties. *Commun Nonlinear Sci Numer Simul* 14:1646–1663. <https://doi.org/10.1016/J.CNSNS.2008.02.003>
388. Shooshtari A, Razavi S (2010) A closed form solution for linear and nonlinear free vibrations of composite and fiber metal laminated rectangular plates. *Compos Struct* 92:2663–2675. <https://doi.org/10.1016/j.compstruct.2010.04.001>
389. Morozov EV, Lopatin AV (2009) Fundamental frequency of fully clamped composite sandwich plate. *J Sandw Struct Mater* 12:591–619. <https://doi.org/10.1177/1099636209106366>
390. Liu J, Cheng YS, Li RF, Au FTK (2012) A semi-analytical method for bending, buckling, and free vibration analyses of sandwich panels with square-honeycomb cores. *Int J Struct Stab Dyn* 10:127–151. <https://doi.org/10.1142/S0219455410003361>
391. Qian LF, Batra RC, Chen LM (2003) Free and forced vibrations of thick rectangular plates using higher-order shear and normal deformable plate theory and Meshless Petrov-Galerkin (MLPG) method. *Comput Model Eng Sci* 4:519–534
392. Safaei B, Moradi-Dastjerdi R, Chu F (2018) Effect of thermal gradient load on thermo-elastic vibrational behavior of sandwich plates reinforced by carbon nanotube agglomerations. *Compos Struct* 192:28–37. <https://doi.org/10.1016/J.COMPSTRUCT.2018.02.022>
393. Liu GR, Gu YT (2001) A local radial point interpolation method (LRPIM) for free vibration analyses of 2-D solids. *J Sound Vib* 246:29–46. <https://doi.org/10.1006/JSVI.2000.3626>
394. Liu GR, Dai KY, Lim KM, Gu YT (2002) A point interpolation mesh free method for static and frequency analysis of two-dimensional piezoelectric structures. *Comput Mech* 29:510–519. <https://doi.org/10.1007/S00466-002-0360-9/METRICS>

395. Wu WX, Shu C, Wang CM, Xiang Y (2010) Free vibration and buckling analysis of highly skewed plates by least squares-based finite difference method. *Int J Struct Stab Dyn* 10:225–252. <https://doi.org/10.1142/S021945541000349X>
396. Zhu P, Liew KM (2011) Free vibration analysis of moderately thick functionally graded plates by local Kriging meshless method. *Compos Struct* 93:2925–2944. <https://doi.org/10.1016/j.compstruct.2011.05.011>
397. Zhang LW, Zhang Y, Zou GL, Liew KM (2016) Free vibration analysis of triangular CNT-reinforced composite plates subjected to in-plane stresses using FSDT element-free method. *Compos Struct* 149:247–260. <https://doi.org/10.1016/j.compstruct.2016.04.019>
398. Moradi-Dastjerdi R, Foroutan M, Pourasghar A (2013) Dynamic analysis of functionally graded nanocomposite cylinders reinforced by carbon nanotube by a mesh-free method. *Mater Des* 44:256–266. <https://doi.org/10.1016/J.MATDES.2012.07.069>
399. Schwarts-Givli H, Rabinovitch O, Frostig Y (2008) Free vibration of delaminated unidirectional sandwich panels with a transversely flexible core and general boundary conditions: a high-order approach. *J Sandw Struct Mater* 10:99–131. <https://doi.org/10.1177/1099636207076484>
400. Wang JF, Yang JP, Tam LH, Zhang W (2021) Molecular dynamics-based multiscale nonlinear vibrations of PMMA/CNT composite plates. *Mech Syst Signal Process* 153:1–19. <https://doi.org/10.1016/J.YMSSP.2020.107530>
401. Tornabene F, Fantuzzi N, Viola E, Ferreira AJM (2013) Radial basis function method applied to doubly-curved laminated composite shells and panels with a General Higher-order Equivalent Single Layer formulation. *Compos Part B Eng* 55:642–659. <https://doi.org/10.1016/J.COMPOSITESB.2013.07.026>
402. Ferreira AJM, Fasshauer GE (2007) Analysis of natural frequencies of composite plates by an RBF-pseudospectral method. *Compos Struct* 79:202–210. <https://doi.org/10.1016/J.COMPSTRUCT.2005.12.004>
403. Kim K, Kwak S, Jang P, Sok M, Jon S, Ri K (2021) Free vibration analysis of elastically connected composite laminated double-plate system with arbitrary boundary conditions by using meshfree method. *AIP Adv* 11:1–18. <https://doi.org/10.1063/5.0040270/990521>
404. Bui TQ, Nguyen MN, Zhang C (2011) An efficient meshfree method for vibration analysis of laminated composite plates. *Comput Mech* 48:175–193. <https://doi.org/10.1007/S00466-011-0591-8/METRICS>
405. Liew KM, Peng LX, Kitipornchai S (2009) Vibration analysis of corrugated Reissner-Mindlin plates using a mesh-free Galerkin method. *Int J Mech Sci* 51:642–652. <https://doi.org/10.1016/J.IJMECSCI.2009.06.005>
406. Peng LX, Kitipornchai S, Liew KM (2007) Free vibration analysis of folded plate structures by the FSDT mesh-free method. *Comput Mech* 39:799–814. <https://doi.org/10.1007/S00466-006-0070-9/METRICS>
407. Schwarts-Givli H, Rabinovitch O, Frostig Y (2007) Free vibrations of delaminated unidirectional sandwich panels with a transversely flexible core: a modified Galerkin approach. *J Sound Vib* 301:253–277. <https://doi.org/10.1016/J.JSV.2006.10.006>
408. Zhao X, Lee YY, Liew KM (2009) Free vibration analysis of functionally graded plates using the element-free kp-Ritz method. *J Sound Vib* 319:918–939. <https://doi.org/10.1016/J.JSV.2008.06.025>
409. Bui TQ, Nguyen MN (2011) A moving Kriging interpolation-based meshfree method for free vibration analysis of Kirchhoff plates. *Comput Struct* 89:380–394. <https://doi.org/10.1016/J.COMPSTRUC.2010.11.006>
410. Bui TQ, Khosravifard A, Zhang C, Hematiyan MR, Golub MV (2013) Dynamic analysis of sandwich beams with functionally graded core using a truly meshfree radial point interpolation method. *Eng Struct* 47:90–104. <https://doi.org/10.1016/J.ENGSTRUCT.2012.03.041>
411. Wang JF, Shi SQ, Yang JP, Zhang W (2021) Multiscale analysis on free vibration of functionally graded graphene reinforced PMMA composite plates. *Appl Math Model* 98:38–58. <https://doi.org/10.1016/J.APM.2021.04.023>
412. Safaei B, Moradi-Dastjerdi R, Qin Z, Chu F (2019) Frequency-dependent forced vibration analysis of nanocomposite sandwich plate under thermo-mechanical loads. *Compos Part B Eng* 161:44–54. <https://doi.org/10.1016/J.COMPOSITESB.2018.10.049>
413. Sahmani S, Safaei B (2021) Large-amplitude oscillations of composite conical nanoshells with in-plane heterogeneity including surface stress effect. *Appl Math Model* 89:1792–1813. <https://doi.org/10.1016/J.APM.2020.08.039>
414. Xie B, Sahmani S, Safaei B, Xu B (2021) Nonlinear secondary resonance of FG porous silicon nanobeams under periodic hard excitations based on surface elasticity theory. *Eng Comput* 37:1611–1634. <https://doi.org/10.1007/s00366-019-00931-w>
415. Der CR, Chen CS (2006) Nonlinear vibration of laminated plates on an elastic foundation. *Thin-Walled Struct* 44:852–860. <https://doi.org/10.1016/J.TWS.2006.08.016>
416. Chen CS, Fung CP, Der CR (2007) Nonlinear vibration of an initially stressed laminated plate according to a higher-order theory. *Compos Struct* 77:521–532. <https://doi.org/10.1016/J.COMPOSTRUCT.2005.08.004>
417. Lei ZX, Zhang LW, Liew KM, Yu JL (2014) Dynamic stability analysis of carbon nanotube-reinforced functionally graded cylindrical panels using the element-free kp-Ritz method. *Compos Struct* 113:328–338. <https://doi.org/10.1016/J.COMPOSTRUCT.2014.03.035>
418. Selim BA, Liu Z (2021) Impact analysis of functionally-graded graphene nanoplatelets-reinforced composite plates laying on Winkler-Pasternak elastic foundations applying a meshless approach. *Eng Struct* 241:112453. <https://doi.org/10.1016/J.ENGSTRUCT.2021.112453>
419. Sahmani S, Safaei B (2019) Nonlocal strain gradient nonlinear resonance of bi-directional functionally graded composite micro/nano-beams under periodic soft excitation. *Thin-Walled Struct* 143:1–18. <https://doi.org/10.1016/j.tws.2019.106226>
420. Yuan Y, Zhao X, Zhao Y, Sahmani S, Safaei B (2021) Dynamic stability of nonlocal strain gradient FGM truncated conical microshells integrated with magnetostrictive facesheets resting on a nonlinear viscoelastic foundation. *Thin-Walled Struct* 159:1–20. <https://doi.org/10.1016/j.tws.2020.107249>
421. Wang QX, Li H, Lam KY, Gu YT (2011) Analysis of microelectromechanical systems (mems) by meshless local kriging (lokriging) method. *J Chin Inst Eng* 27:573–583. <https://doi.org/10.1080/02533839.2004.9670905>
422. Wang QX, Li H, Lam KY (2007) Analysis of microelectromechanical systems (MEMS) devices by the meshless point weighted least-squares method. *Comput Mech* 40:1–11. <https://doi.org/10.1007/S00466-006-0077-2/METRICS>
423. Muthurajan KG, Sankaranarayanan K, Tiwari SB, Rao BN (2005) Nonlinear vibration analysis of initially stressed thin laminated rectangular plates on elastic foundations. *J Sound Vib* 282:949–969. <https://doi.org/10.1016/J.JSV.2004.03.047>
424. Chen CS, Fung CP, Der CR (2006) A further study on nonlinear vibration of initially stressed plates. *Appl Math Comput* 172:349–367. <https://doi.org/10.1016/J.AMC.2005.02.007>
425. Chen CS, Fung CP, Der CR (2006) Nonlinear vibration of orthotropic plates with initial stresses on a two-parameter elastic

- foundation. *J Reinf Plast Compos* 25:283–301. <https://doi.org/10.1177/0731684406058284>
426. Barbieri E, Meo M, Polimeno U (2009) Nonlinear wave propagation in damaged hysteretic materials using a frequency domain-based PM space formulation. *Int J Solids Struct* 46:165–180. <https://doi.org/10.1016/j.ijsolstr.2008.08.025>
427. Liu Y, Hu W, Zhu R, Safaei B, Qin Z, Chu F (2022) Dynamic responses of corrugated cylindrical shells subjected to nonlinear low-velocity impact. *Aerosp Sci Technol* 121:1–11. <https://doi.org/10.1016/j.ast.2021.107321>
428. Gupta AK, Kumar L (2008) Thermal effect on vibration of non-homogenous visco-elastic rectangular plate of linearly varying thickness. *Meccanica* 43:47–54. <https://doi.org/10.1007/S11012-007-9093-3/METRICS>
429. Zhang Y, Zhang LW, Liew KM, Yu JL (2016) Free vibration analysis of bilayer graphene sheets subjected to in-plane magnetic fields. *Compos Struct* 144:86–95. <https://doi.org/10.1016/j.compstruct.2016.02.041>
430. Zhang Y, Lin X, Wei L, Liu F, Huang W (2016) Influence of powder size on the crystallization behavior during laser solid forming Zr55Cu30Al10Ni5 bulk amorphous alloy. *Intermetallics* 76:1–9. <https://doi.org/10.1016/j.intermet.2016.06.006>
431. Lei ZX, Zhang LW, Liew KM (2015) Elastodynamic analysis of carbon nanotube-reinforced functionally graded plates. *Int J Mech Sci* 99:208–217. <https://doi.org/10.1016/j.ijmecsci.2015.05.014>
432. Li S, Liu WK, Rosakis AJ, Belytschko T, Hao W (2002) Mesh-free Galerkin simulations of dynamic shear band propagation and failure mode transition. *Int J Solids Struct* 39:1213–1240. [https://doi.org/10.1016/S0020-7683\(01\)00188-3](https://doi.org/10.1016/S0020-7683(01)00188-3)
433. Medyanik SN, Liu WK, Li S (2007) On criteria for dynamic adiabatic shear band propagation. *J Mech Phys Solids* 55:1439–1461. <https://doi.org/10.1016/j.jmps.2006.12.006>
434. Kiani K, Ghaffari H, Mehri B (2013) Application of elastically supported single-walled carbon nanotubes for sensing arbitrarily attached nano-objects. *Curr Appl Phys* 13:107–120. <https://doi.org/10.1016/j.cap.2012.06.023>
435. Almasi F, Shadloo MS, Hadjadj A, Ozbulut M, Tofighi N, Yildiz M (2021) Numerical simulations of multi-phase electro-hydrodynamics flows using a simple incompressible smoothed particle hydrodynamics method. *Comput Math Appl* 81:772–785. <https://doi.org/10.1016/j.camwa.2019.10.029>
436. Moradi-Dastjerdi R, Behdinin K (2021) Dynamic performance of piezoelectric energy harvesters with a multifunctional nanocomposite substrate. *Appl Energy* 293:1–11. <https://doi.org/10.1016/j.apenergy.2021.116947>
437. Liu P, Liu Y, Zhang X, Guan Y (2015) Investigation on high-velocity impact of micron particles using material point method. *Int J Impact Eng* 75:241–254. <https://doi.org/10.1016/j.ijimpeng.2014.09.001>
438. Wu CT, Ma N, Takada K, Okada H (2016) A meshfree continuous-discontinuous approach for the ductile fracture modeling in explicit dynamics analysis. *Comput Mech* 58:391–409. <https://doi.org/10.1007/S00466-016-1299-6/FIGURES/23>
439. Sahoo SR, Ray MC (2018) Analysis of smart damping of laminated composite beams using mesh free method. *Int J Mech Mater Des* 14:359–374. <https://doi.org/10.1007/S10999-017-9379-0/FIGURES/9>
440. Civalek Ö (2014) Geometrically nonlinear dynamic and static analysis of shallow spherical shell resting on two-parameters elastic foundations. *Int J Press Vessel Pip* 113:1–9. <https://doi.org/10.1016/j.ijpvp.2013.10.014>

Publisher's Note Springer Nature remains neutral with regard to jurisdictional claims in published maps and institutional affiliations.

Springer Nature or its licensor (e.g. a society or other partner) holds exclusive rights to this article under a publishing agreement with the author(s) or other rightsholder(s); author self-archiving of the accepted manuscript version of this article is solely governed by the terms of such publishing agreement and applicable law.